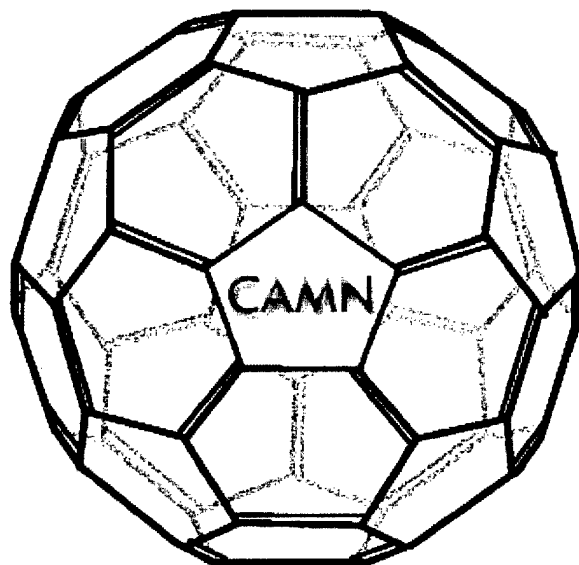# FINAL REPORT

Single Crystal Relaxor Ferroelectrics by Seeded Polycrystal Conversion

Professors M.P. Harmer (PI), H. M.Chan (Co-PI)
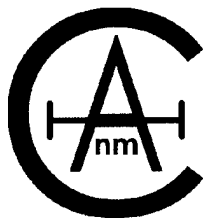Research Assistants E.P.Gorzkowski, P.T.King, D.J.Rockosi & A.M. Scotch

20030915 005

**CENTER FOR
ADVANCED MATERIALS
AND NANOTECHNOLOGY**

REPORT DOCUMENTATION PAGE

AFRL-SR-AR-TR-03-

0339

1. REPORT DATE *(DD-MM-YYYY)*	2. REPORT DATE	3. DATES COVERED *(From - To)*
7/15/03	Final Report	Oct 1999 – Apr 2003

4. TITLE AND SUBTITLE	5a. CONTRACT NUMBER
Single Crystal Relaxor Ferroelectrics by Seeded Polycrystal Conversion	F49620-99-1-0340
	5b. GRANT NUMBER
	5c. PROGRAM ELEMENT NUMBER

6. AUTHOR(S)	5d. PROJECT NUMBER
Harmer, M.P., Chan, H.M., Gorzkowski, E.P., King, P.T., Rockosi, D.J., and Scotch, A.M.	5e. TASK NUMBER
	5f. WORK UNIT NUMBER

7. PERFORMING ORGANIZATION NAME(S) AND ADDRESS(ES)	8. PERFORMING ORGANIZATION REPORT NUMBER
Center For Advanced Materials and Nanotechnology Lehigh University 5 East Packer Avenue Bethlehem, PA 18015	533051

9. SPONSORING/MONITORING AGENCY NAME(S) AND ADDRESS(ES)	10. SPONSOR/MONITOR'S ACRONYM(S)
	11. SPONSORING/MONITORING AGENCY REPORT NUMBER

12. DISTRIBUTION AVAILABILITY STATEMENT

Approved for public release. Distribution is unlimited

13. SUPPLEMENTARY NOTES

14. ABSTRACT

See attached report

15. SUBJECT TERMS
Single crystals, lead magnesium niobate: lead titanate, relaxor ferroelectrics, solid state conversion, grain growth, liquid phase sintering

16. SECURITY CLASSIFICATION OF:			17. LIMITATION OF ABSTRACT	18. NUMBER OF PAGES	19a. NAME OF RESPONSIBLE PERSON
a. REPORT	b. ABSTRACT	c. THIS PAGE			Martin P. Harmer
U	U	U	SAR	139	19b. TELEPONE NUMBER *(Include area code)* (610) 758-4227

1. PROGRESS SUMMARY

The group at Lehigh University has implemented the successful application of Seeded Polycrystal Conversion (SPC) to ferroelectric materials. Initial work at Lehigh established the feasibility of using the SPC process to grow single crystals of the relaxor-based ferroelectric $Pb(Mg_{1/3}Nb_{2/3})O_3$-35mol%$PbTiO_3$ (PMN-35PT) from seed crystals of the same composition.

However, much work was needed to refine this process. Maintaining single crystal growth until full conversion of the polycrystal can only be achieved with a fundamental understanding of the factors that influence the migrating boundary. The present work addressed, in particular, the roles of liquid phase content and chemistry, matrix grain size, and porosity, as previous results have indicated these to be key variables.

Some strides have been made in understanding the roles of each of the above key variables. In fact, over the past year, the Lehigh group has begun to model the effect of matrix grain size on single crystal growth. By improving this model, a better understanding of why single crystal growth slows can be achieved by pinpointing the mechanism of growth.

Additionally, great progress has been made in microscopic characterization of samples as Lehigh has acquired a dual-beam focused ion beam (FIB). This instrument allows for the TEM preparation of samples across specific boundary interfaces in the PMN-PT system, previously unattainable with traditional sample preparation techniques. This will help gain a better understanding of the liquid phase chemistry and its role in the SPC process.

2. ACCOMPLISHMENTS

(a) Recent work showed that by manipulating the chemistry of the liquid phase additives to PMN-PT materials, the mobility of the single crystal / polycrystal boundary can be tailored. Historically, PbO was used as a liquid phase, but now alternatives to PbO have been found, which have varying effects on single crystal growth.

(b) An existing model has been adapted and quantified to show the effects of starting matrix size and surface energy on the growth of PMN-PT single crystals by SPC. Increasing the starting particle size greatly reduces the amount of single crystal growth, indicating the necessity to control grain coarsening during the process. Furthermore, increasing the surface energy was found to increase the amount of single crystal growth.

(c) Using the work of Blendell *et al.*, it has been shown that there is a connection between abnormal grain growth in PMN-PT and coincident site lattice (CSL) boundaries. It appears that the majority of the abnormal grains are actually bi-crystals separated by $\Sigma 3$ boundaries, i.e. the twin orientation.

(d) Lehigh has acquired a dual-beam focused ion beam (FIB) that allows for TEM sample preparation of otherwise difficult microstructures. This instrument was set-up and TEM samples were prepared in just one month.

(e) The kinetics of {001} oriented $Pb(Mg_{1/3}Nb_{2/3})O_3$-35mol%$PbTiO_3$ [PMN-35PT] single crystals grown by Seeded Polycrystal Conversion (SPC) and the corresponding matrix grains were systematically quantified. Specifically, the kinetics were experimentally analyzed as a function of liquid phase (PbO) content. The average matrix grain size and single crystal growth were fitted to equations of the form G^n-G_0^n=kt and ΔL^n =kt, respectively, where G is the average grain size, L is the linear single crystal growth, n is a growth exponent, and k is the growth constant. Cubic growth laws (n=3) were observed for PbO contents from 0 to 5 vol.% for both the matrix grains and single crystals. At PbO volume fractions from 0 - 3 vol.%, both the matrix and single crystal growth rates increased with increasing PbO content, presumably due to an increase in pore mobility. For larger PbO volume fractions, single crystal growth was essentially independent of PbO content, indicating an interface reaction growth mechanism. The matrix grain growth decreased before beginning to level off, indicative of diffusion control. This suggests a possible transition from diffusion-controlled growth at lower PbO fractions to interface reaction-controlled growth at higher PbO fractions.

(f) Sintering in oxygen was necessary to obtain fully dense matrix microstructures, which, in turn, produced pore-free single crystals. The primary role of oxygen was to remove insoluble gases before densification began, then to reduce the internal pressure by diffusing out and allowing the pores to close from pressures derived from their own curvatures. The presence of a PbO liquid phase assisted this process by enhancing the densification rate in the early stages of sintering. In contrast, fully-dense, hot-pressed samples of PMN-35PT with

excess PbO underwent a de-densification process during the annealing treatments which was attributed to pore formation from internally evolved gases.

(g) Transparent single crystals with maximum strain values of 0.72% at 46 kV/cm, $d_{33} \sim$ 2180 pC/N, and a room temperature dielectric constant of ~5300 were obtained for poled <001> oriented crystals of PMN-30mol.%PT. The dielectric behavior of {001} oriented single crystals was found to be highly dependent on the initial orientation of the seed crystal. For example, {111} seeded crystals grown in oxygen yielded K_{max} values of ~33000, while {001} seeded crystals grown in oxygen had K_{max} values of ~25000. In addition, the T_{max} values were 3 to 5 °C higher for crystals grown from {001} seeds, compared to {111} seeds.

3. PROGRESS REPORTS

3.1 Effect of Liquid Phase Chemistry

Introduction and Background

Previous work showed that excess PbO had dramatic effects on the microstructure and single crystal growth of PMN-35PT by SPC. In fact, PbO has been used as a liquid phase additive for PMN-PT to promote sintering, grain growth, and single crystal growth. Later studies demonstrated that the amount of PbO liquid phase present had a significant effect on matrix grain growth in PMN-PT. This effect is shown in the plot in Figure 1. The corresponding microstructures are shown in Figure 2. It can be seen that an apparent maximum in grain size occurs at about 3 vol% excess PbO. It is believed that the grain growth rate decreases for PbO additions greater than 3 vol.% because the mechanism of grain growth shifts from reaction controlled to diffusion controlled. Therefore, as more liquid is added above 3 vol.%, the diffusion distance becomes larger and grain growth is reduced.

The situation is slightly different when discussing single crystal growth. As small amounts of PbO are added, growth of the single crystal correspondingly increases, as shown in Figure 3. However, qualitative observations suggest the amount of single crystal growth plateaus at around 1.5 vol.% PbO, where no additional growth is exhibited for increasing PbO contents. This is slightly different to the phenomenon seen for the matrix grains. Thus, future work will examine if the mechanism of growth is different for the matrix grains and the single crystal.

It is suspected that the observed change in kinetics of both the matrix grains and the single crystal is largely due to an increase in the boundary mobility with the presence of a liquid. Thus, it may be possible to control the boundary mobility and growth kinetics by adjusting the composition of the liquid phase. The composition can be changed in one of

two ways. First, a different PbO based liquid phase can be used to increase boundary mobility while lowering the volatility. Second, a non-PbO based composition can be found to serve the appropriate task. Both solutions may act to decrease the volatility of the liquid phase so that very long experimental heat treatments can be run without losing all of the liquid phase.

Progress over the past year has focussed mainly on two lead-based compositions. The first of these is lead germanate, $Pb_5Ge_2O_{11}$, which is a line compound with a melting point slightly below that of PbO. It is believed that the mobility of the liquid phase may be linked to the homologous temperature (T/T_m) of the liquid phase. As the homologous temperature increases, so does the fluidity. This may lead to a higher mobility, thus improving single crystal growth.

The second composition is the most promising to date. It is a eutectic composition of lead aluminate, $Pb_2Al_2O_5$ (P2A), and PbO, as shown on the PbO-Al_2O_3 phase diagram (Figure 4). The advantages of this compound are the low melting point and having alumina as a constituent. Alumina tends to lower the activity of PbO, which may be beneficial to this process.

Experimental Procedure

In this study, powder of PMN-35PT + x vol.% PbO + Al_2O_3 eutectic (P2A) were center-seeded with {100} PMN-35PT single crystal plates (Crystal Associates) and cold isostatically pressed at 340 MPa. The samples were then fired at 1150°C in static air for 1-10 hours so that both single crystal and matrix grain growth could be observed and compared to

samples containing excess PbO alone. All samples were fired in a double crucible arrangement with packing powder of the same activity, as done previously.

Results and Discussion

The samples with eutectic additions exhibited very large grain sizes (Figure 5). In fact, the average grain size was on the order of 35 μm, which is approximately10 μm larger than the samples with excess PbO alone (Figure 2). This suggests that the liquid phase chemistry does play a vital role in influencing the growth kinetics of the matrix. However, Figure 6 shows that there was an apparent decrease in single crystal growth for a seed embedded in PMN-35PT with 5 vol.% P_2A-PbO eutectic compared to a seed embedded in PMN-35PT with 5 vol.% PbO. The large matrix grain size of Figure 6(b) likely suppressed the migration of the single crystal boundary due to a decrease in driving force from curvature. In the future, more liquid phase compositions need to be examined in order to comment on the effect of homologous temperature. In the present work, the PbO-P_2A eutectic composition, possessing a higher homologous temperature than PbO, produced a larger average grain size. These results suggest that the increase in matrix grain growth may be linked to an increase in homologous temperature.
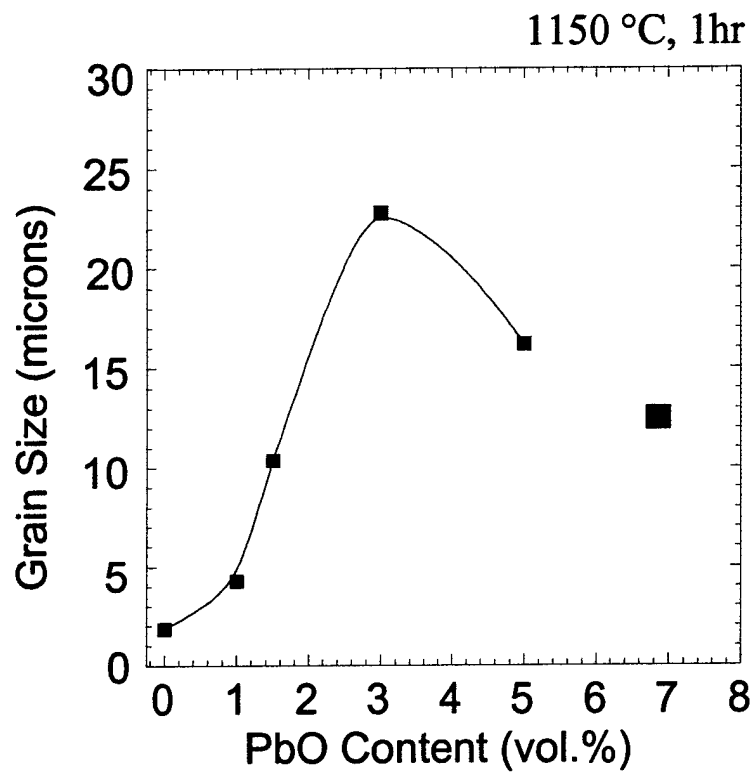
1150 °C, 1hr

Figure 1. PMN-PT matrix grain growth as a function of PbO.

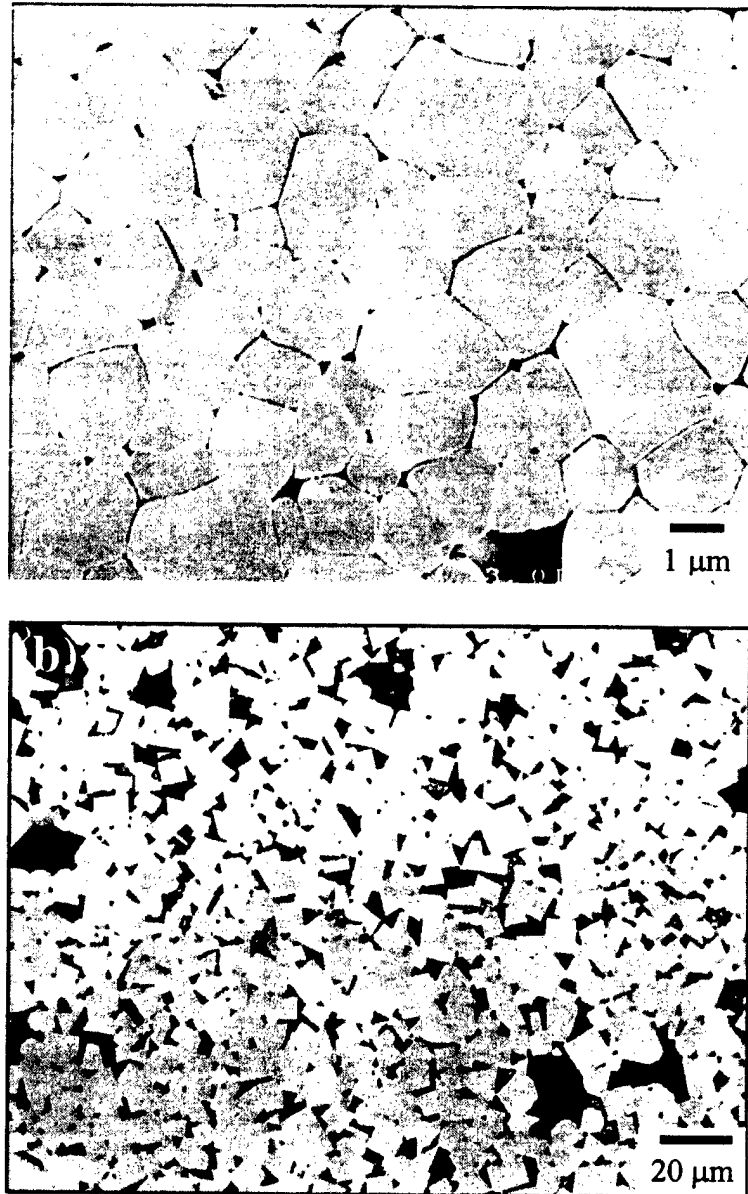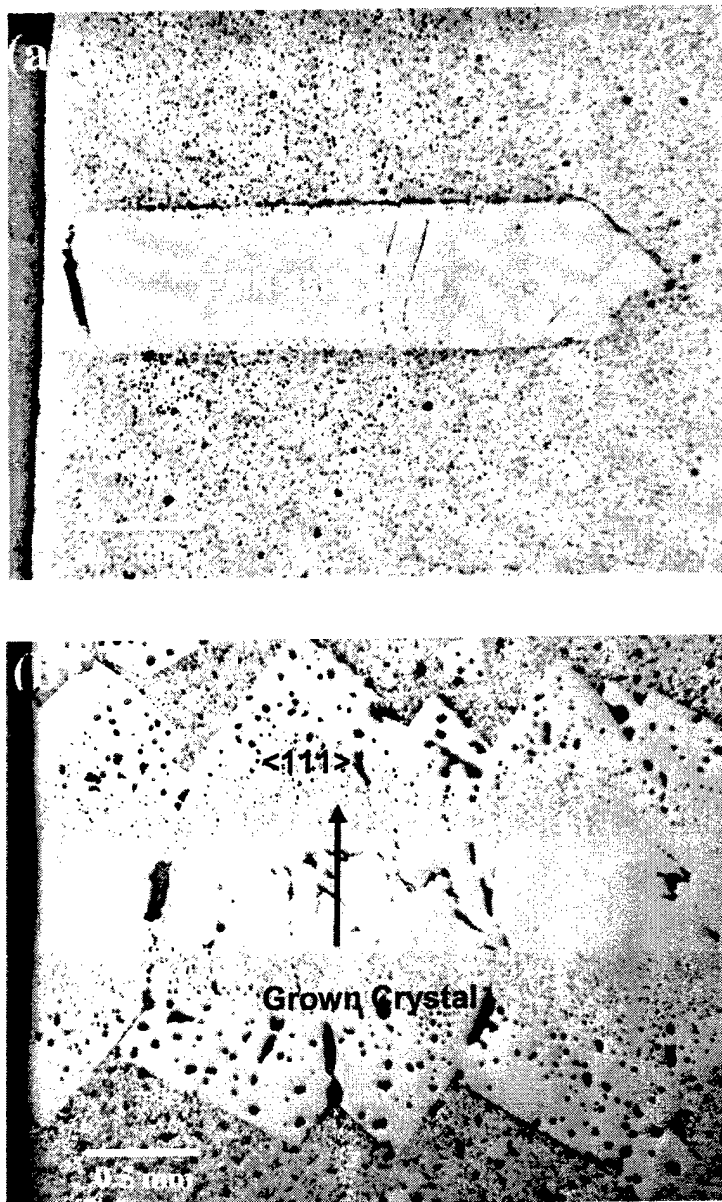**Figure 2.** Microstructures of PMN-35PT with (a.) 1 and (b.) 5 vol.% PbO additions.

Figure 3. (111) Single Crystal Growth of PMN-35PT with
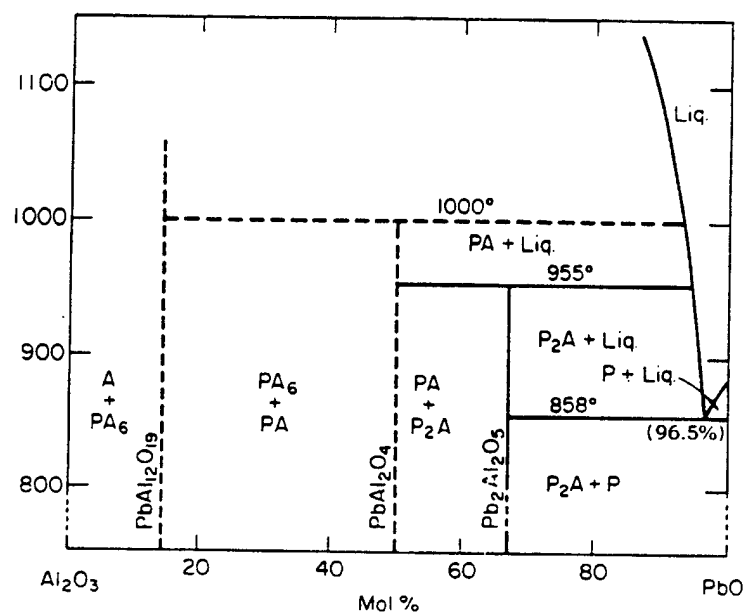(a) 1 and (b) 5 vol.% PbO additions.

A
+
PA6

PbAl$_{12}$O$_{19}$

PA6
+
PA

PbAl$_2$O$_4$

PA
+
P$_2$A

Pb$_2$Al$_2$O$_5$

1100

1000   1000°
PA + Liq.
955°

900   P$_2$A + Liq.
P + Liq.
858°
(96.5%)

P$_2$A + P

800

Liq.

20   40   60   80

Al$_2$O$_3$ Mol %   PbO

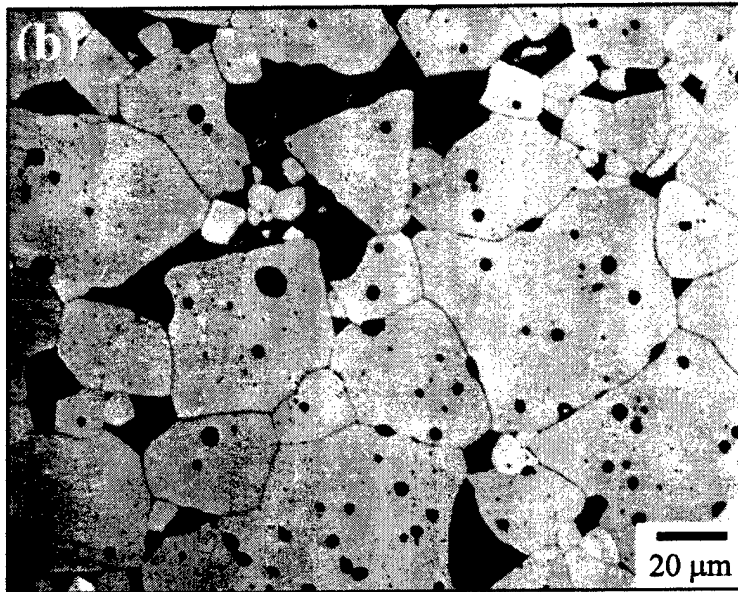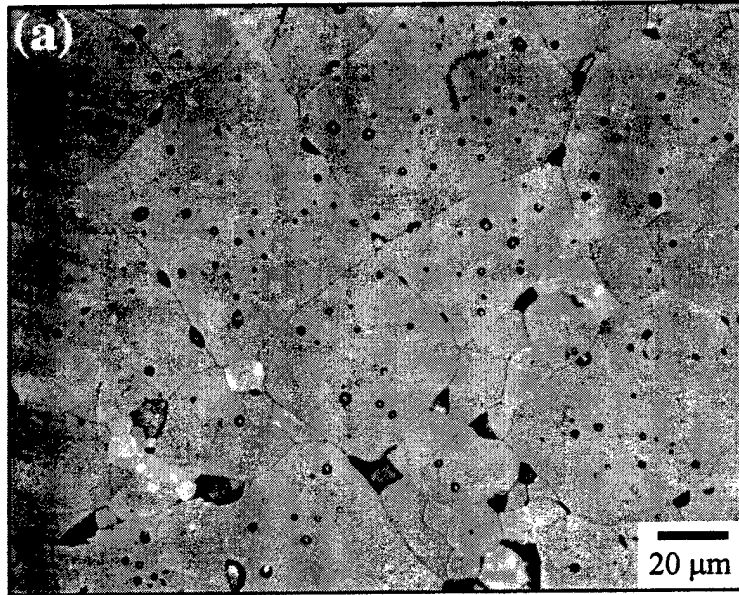**Figure 4.** Equilibrium Phase Diagram of PbO and Al$_2$O$_3$.

Figure 5. Microstructures of PMN-35PT with (a) 1 and (b) 5 vol.%
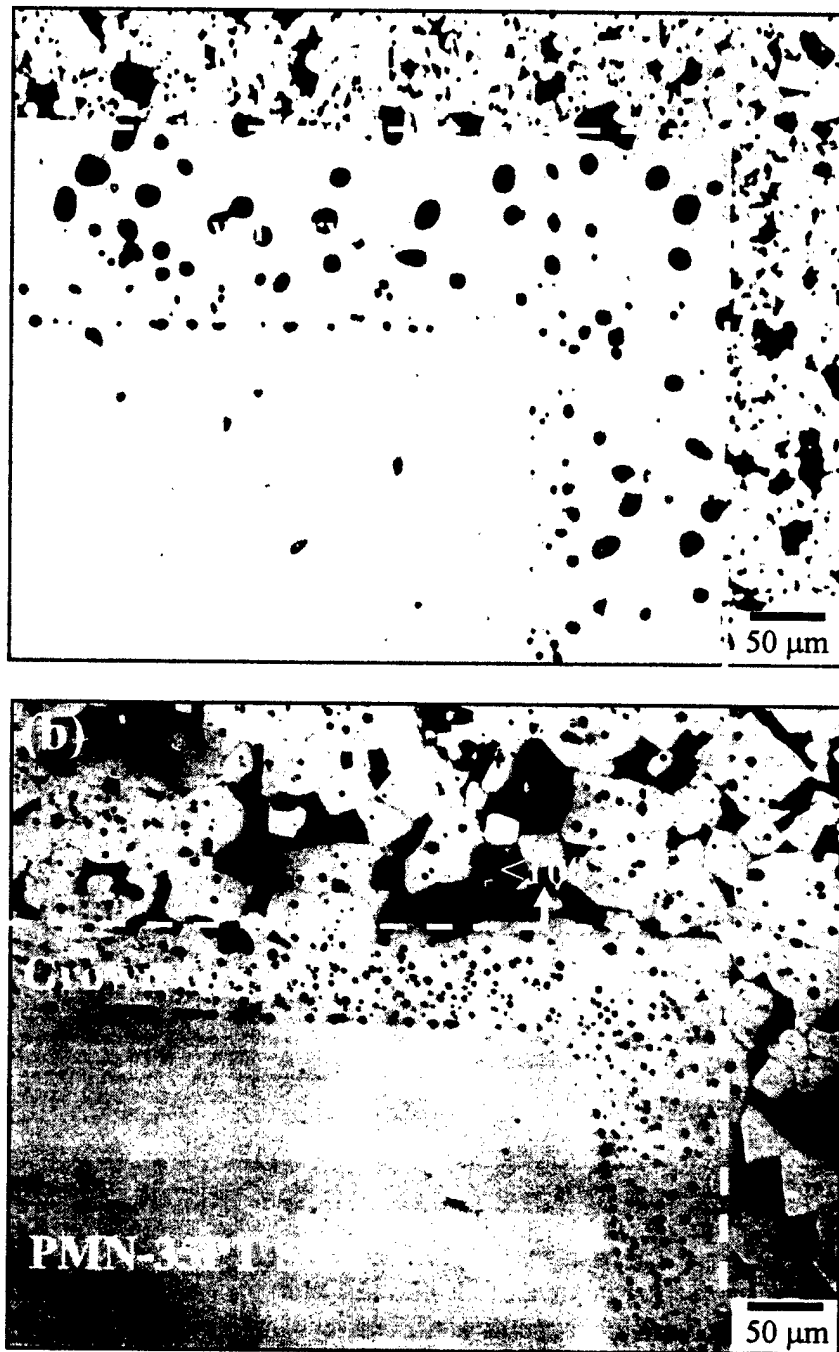P_2A-PbO eutectic additions.

Figure 6. Comparison of {100} single crystal growth in PMN-35PT with (a.) 5 vol.% PbO and (b.) 5 vol.% P$_2$A-PbO eutectic additions.

3.2 Interface Morphology of Single Crystals

To understand the role of seed orientation on crystal growth, PMN-PT seeds (Crystal Associates) of various orientations were embedded in PMN-35PT powder (TRS Ceramics) + 3.0 vol% PbO (Alfa Aesar). Samples were sintered using a double crucible arrangement (packed in powder of identical composition) at 1150°C for 10 hours in air. Figure 7 shows light optical micrographs of single crystals grown from {100}, {110}, and {111} oriented PMN-PT seeds. This figure clearly indicates that growth from {100} seeds is substantially less than that from the other two orientations.

The pyramidal growth from {110} and {111} seeds is due to the pseudo-cubic nature of PMN-35PT (rhombohedral crystal structure, $\alpha \sim 89.48°$). The preferential faceting indicates that {100} is the more stable and energetically favorable growth plane. Three-dimensional schematic diagrams of expected single crystal growth are shown in Figure 8. Crystals grown from {110} seeds facet into right-angle pyramids; crystals grown from {111} seeds facet into tetrahedral pyramids. Figure 9 shows SEM images of single crystals grown in a matrix of PMN-35PT + 3 vol% PbO. After heat treatment, the matrix was removed by ultrasonically agitating in a 30% HNO_3 solution to reveal the morphology of the grown crystal.

Though the single crystal interface appears planar in Figure 7, the interface is microscopically cusped due to curvature of adjacent grains. Figure 10 shows the effect of liquid phase on the local interface morphology of single crystals. Using the HNO_3 agitation process described above, single crystals were removed from matrix compositions of PMN-35PT with 1.5 and 5 vol% PbO additions.

In both samples, grain pockets were observed on the single crystal surface, indicating regions of prior contact with matrix grains. Higher fractions of liquid phase in the matrix

provide for a greater degree of grain boundary wetting, yielding a relatively smooth, flat interface morphology, as seen for the 5 vol.% PbO sample (Figure 10(b)). In addition, increasing the fraction of liquid phase from 1.5 to 5 vol.% enhances the amount of single crystal growth and produces a more macroscopically faceted pyramidal structure. The higher magnification images shown in the insets of Figure 10(a) and (b) reveal a transition in matrix morphology, from the classic tetrakaidecahedron grain shape (1.5 vol.% PbO) to faceted, cube-shaped grains (5 vol.% PbO).
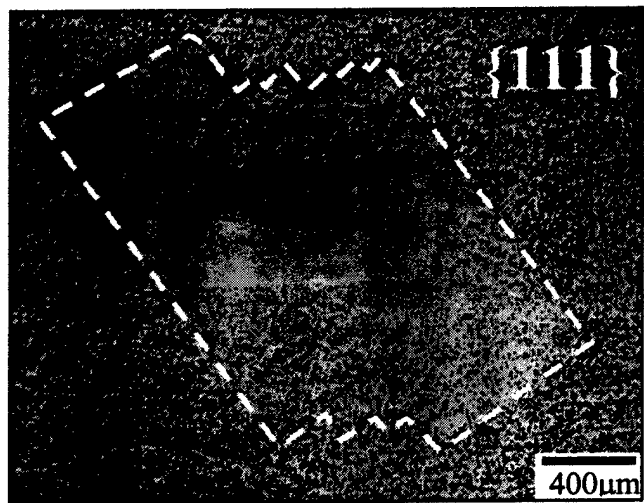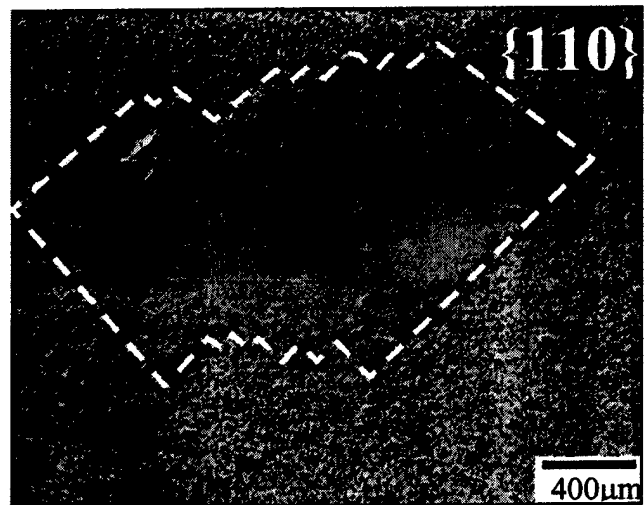
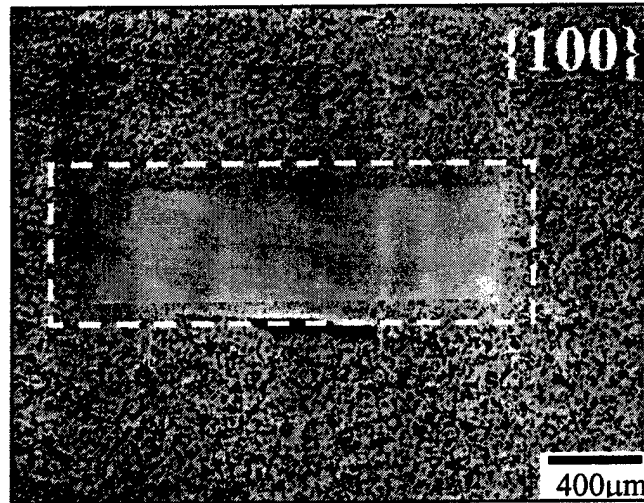**Figure 7.** Growth of single crystals from {100}, {110}, and {111} seeds into matrix compositions of PMN-35PT + 3vol% PbO.

{110}

Increased sintering time

{111}
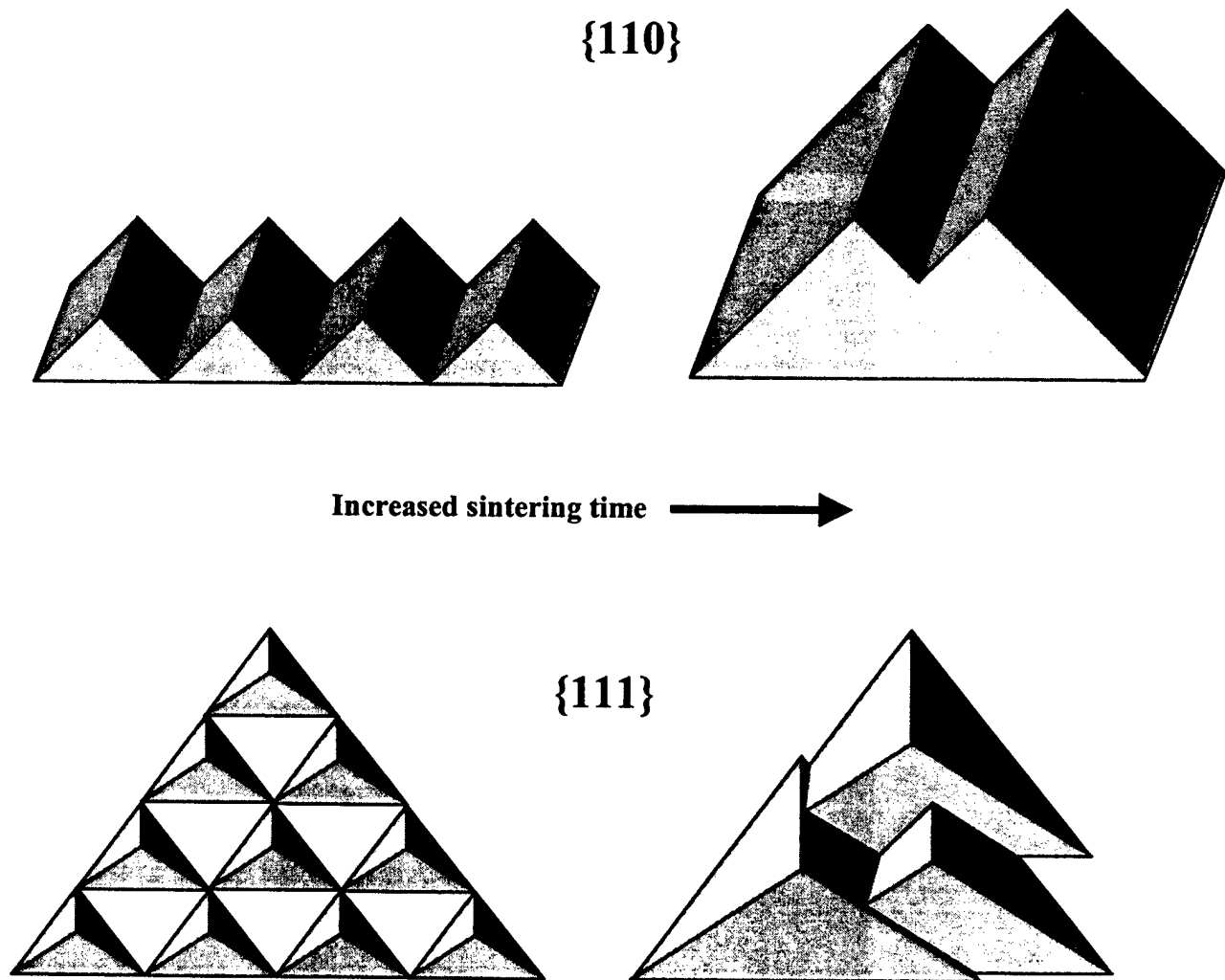
Figure 8. Schematic diagrams of growth and coalescence from {110} and {111} seeds.

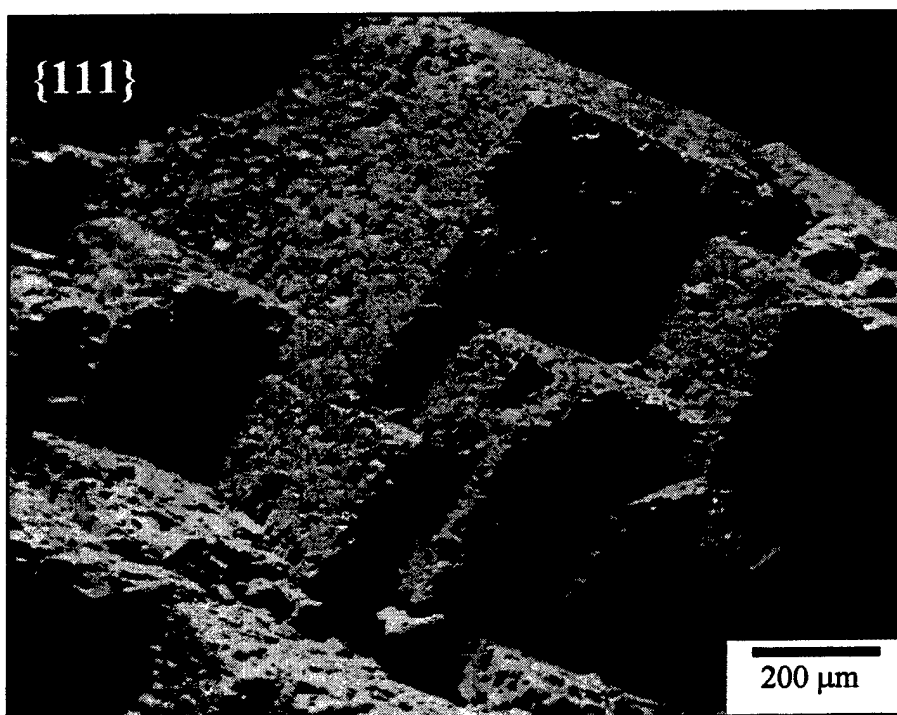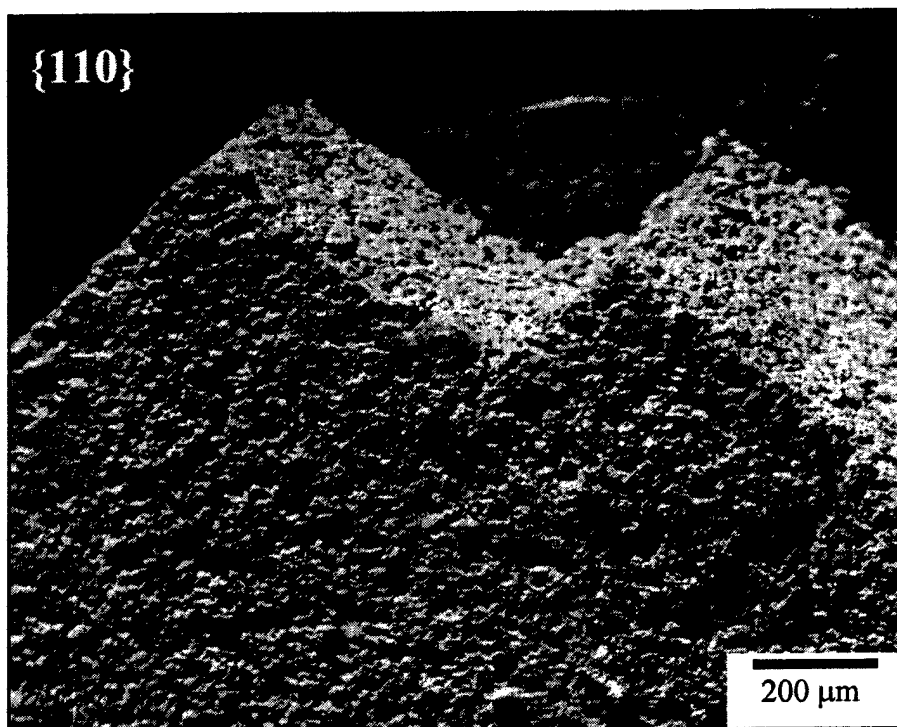**Figure 9.** Profiles of {100} and {111} single crystals grown in PMN-35PT + 3vol.% PbO; surfaces exposed by ultrasonic agitation in 30%HNO₃.
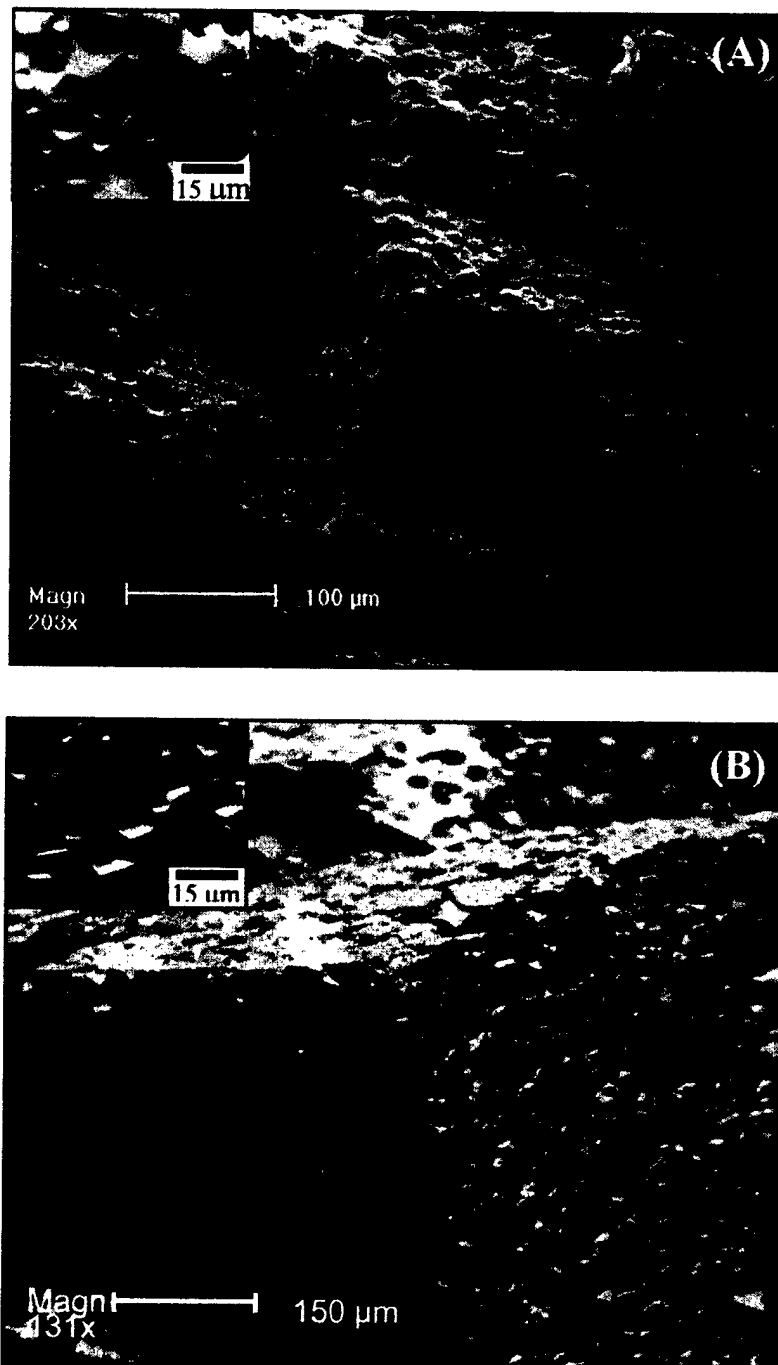
Figure 10. Local interface morphologies of {111} single crystals grown in PMN-35PT with (A) 1.5 vol% PbO and (B) 5 vol% PbO additions; surfaces revealed by ultrasonically agitating in 30%HNO₃.

3.3 Analytical Model for Single Crystal Growth

Leite *et al.* developed an analytical model that described a single crystal growing into a polycrystalline matrix. The model was based on earlier work by Thompson related to abnormal grain growth. In the present work, the Leite *et al.* model was further modified and adapted to quantitatively explain single crystal growth into a polycrystalline matrix with liquid phase additions. The effects of several parameters on the growth of PMN-35PT single crystals were studied. The following is a description of the modeled problem:

A {100} oriented single crystal seed is bonded to a dense polycrystalline matrix comprised of an array of tetrakaidecahedron or cubic grains with edge length l_p. The matrix morphology will be determined by the fraction of liquid phase in the matrix. Single crystal growth is assumed to occur only in the *x* direction, as shown schematically in Figure 11.

Driving Force

The driving force for grain boundary migration is evaluated by considering the grain boundary energy and surface energy anisotropy ($\Delta\gamma$). In this model, the $\Delta\gamma$ is defined as

$$\Delta\gamma = \gamma_a - \gamma_{min} \qquad (1),$$

where γ_a is the average surface energy per unit area and γ_{min} is the surface energy of the {100} oriented single crystal. The total grain boundary energy per unit volume (E) is given by

$$E = NA_{gb}\gamma_{gb} \qquad (2),$$

where N is the number of grains per unit volume, A_{gb} is the grain boundary area, and γ_{gb} is the surface energy of the grain boundary. After the growth process, the resultant single crystal will have dimensions *l* and *a* (Figure 11).

The initial energy before single crystal growth (E_i) and the final energy after single crystal growth (E_f) are defined as

$$E_i=[l^2\gamma_a + Nl^2aA_{gb}\gamma_{gb}]/l^2a \qquad (3),$$

$$E_f=[l^2\gamma_{min} + (l^2+4la)\gamma_{gb}]/l^2a \qquad (4),$$

Assuming $l >> a$, the energy variation during the single crystal growth process is

$$\Delta E= E_f - E_i = [-\Delta\gamma/a + \gamma_{gb}/a - NA_{gb}\gamma_{gb}] \qquad (5),$$

For a polycrystalline matrix composed entirely of tetrakaidecahedron grains of size l_p,

$$N=3/\sqrt{2}\cdot l_p^{3} \qquad (6),$$

and

$$A_{gb}=(6\sqrt{3} + 3)\cdot l_p^{2} \qquad (7),$$

with a corresponding average grain size, G

$$G=2\sqrt{2}\cdot l_p \qquad (8),$$

Similarly, for a matrix composed of cubic grains of size l_p, the geometric parameters are

$$N=l_p^{-3} \qquad (9),$$

$$A_{gb}=3\cdot l_p^{2} \qquad (10),$$

$$G= \sqrt{3}\cdot l_p \qquad (11),$$

Grain Boundary Migration

The motion of the grain boundary in the x direction can be written as

$$v_x=M_b\Delta E \qquad (12),$$

where v_x and M_b are the velocity and mobility of the migrating crystal, respectively. If it is assumed that the grain boundary velocity is proportional to the instantaneous rate of single

crystal growth (v_x=1/2 da/dt), inserting the geometric parameters of equations 6 through 11 into equation 5 gives

$$da/dt = 2M[-\Delta\gamma/a - 80.3\gamma_{gb}/G + \gamma_{gb}/a] \qquad (13),$$

for a tetrakaidecahedron matrix, and

$$da/dt = 2M[-\Delta\gamma/a - 3\sqrt{3}\cdot\gamma_{gb}/G + \gamma_{gb}/a] \qquad (14),$$

for a cubic matrix.

In the presence of a liquid phase, the migration of the single crystal is governed either by the diffusion through the liquid film or by the interface reaction (dissolution-reprecipitation process). If diffusion through the liquid film of thickness L is the rate-limiting step, the mobility (M_L) is defined as

$$M_L = D_L C_L \Omega / LkT \qquad (15),$$

where D_L is the diffusivity through the liquid film, C_L is the solubility of the grain in the liquid, Ω is the atomic volume, k is Boltzmann's constant, and T is temperature (K).

If the migration of the single crystal is controlled by the interface reaction, the mobility term is defined as

$$M_s = \Gamma\Omega/kT \qquad (16),$$

where Γ is a constant exponentially dependent on temperature.

Liquid Film Thickness

To apply the model to single crystal growth, it is necessary to develop a term for the liquid film thickness as a function of average grain size. For a fully dense matrix of tetrakaidecahedron grains with volumetric liquid fraction X, the total volume of the system (V_{sys}) can be described as

$$(1-X)V_{sys}=N \cdot 11.314 \cdot l_p^3 \qquad (17),$$

where $11.314 \cdot l_p^3$ is the volume of an individual tetrakaidecahedron grain. If a liquid film

layer t is assumed to encapsulate each grain ($2t$ is the distance between adjacent grains), then

$$V_{sys} = N \cdot 11.314 \left(l_p + \frac{2t\sqrt{3}}{3} \right)^3 \qquad (18),$$

Solving equations 17 and 18 simultaneously, and inserting the geometric value for

grain size, G, from equation 8, the liquid film thickness for a fully dense tetrakaidecahedron

matrix is given by

$$L=2t= \frac{3G(1-\sqrt[3]{1-X})}{2\sqrt{6} \sqrt[3]{1-X}} \qquad (19),$$

Similarly, for a fully dense cubic matrix, the liquid film thickness is

$$L=2t= \frac{G(1-\sqrt[3]{1-X})}{\sqrt{3} \sqrt[3]{1-X}} \qquad (20),$$

It is important to note from equations 12 and 13 that the liquid film thickness shows a

linear dependence on matrix grain size. Thus, given the mobility term in equation 15, it can

be seen that the mobility of the single crystal will decrease linearly with grain size, assuming

all other parameters remain constant.

Quantitative Analysis of Model

The model described above was applied to a matrix of PMN-35PT with small

additions of PbO as a liquid phase. The solubilities of PMN and PT in liquid PbO are

approximately 30mol % and 33mol%, respectively. The solubility of PMN-35PT in PbO was

therefore estimated as 31mol%. The atomic volume of PMN-35PT was calculated as

approximately 2.38 x 10^{-29} m³/atom. Surface energies were estimated to range from 0.2 to 1.0 J/m², commonly accepted values for oxides at high temperatures.

To the knowledge of the investigators, no numerical values exist in the literature for the diffusivity of PMN-35PT through PbO liquid. A value of 6 x 10^{-14} m²/s was estimated to give realistic values of single crystal growth in this model. As a result, the presented values of single crystal growth vs. time cannot be assumed to exactly predict the behavior of PMN-35PT. However, the intention was to investigate the effect of various parameters on single crystal growth, namely liquid fraction, starting grain size, matrix coarsening, surface energy, and surface energy anisotropy.

Prior work has shown that with increasing additions of PbO, a transition occurs in the matrix grain morphology from equiaxed (tetrakaidecahedron) grains to cubic grains. It was determined that the grains were equiaxed for 0 and 1 vol.% PbO additions, while they were cubic for PbO contents of 3 vol.% and greater. For PbO additions of 1.5 vol.%, a mixed microstructure of equiaxed and cubic grains was produced. Figure 19 shows the typical matrix morphologies of PMN-35PT with various PbO additions.

For simplicity, the present work investigated grain growth and single crystal growth behavior for a fixed PbO content of 3 vol.%. The growth of matrix grains was estimated from previously acquired data for growth of PMN-35PT with 3 vol.% PbO. This data was taken from samples that were initially hot pressed to full density and subsequently annealed in air. The measured grain growth constant was 2.7 x 10^{-16} m³/hr for 1150°C. Equations 14 and 20 were used to describe the instantaneous boundary velocity and liquid film thickness, respectively, for a cubic matrix.

Figure 13 shows a plot of single crystal growth and average matrix grain size vs. time for PMN-35PT + 3vol.% PbO at 1150°C. The surface energy and surface energy anisotropy are 0.2 and 0.1 J/m^2, respectively. The single crystal growth mechanism was assumed to be controlled by diffusion through the liquid, thus the mobility was evaluated using equation 15. Figure 13 clearly shows that the single crystal growth follows a trend similar to that of the matrix grains. Both curves follow a cubic growth law.

Figure 14 shows a plot of single crystal growth and change in grain size vs. initial grain size for PMN-35PT + 3vol.% PbO after 4 hours at 1150°C. The effect of starting grain size on the driving force for boundary migration can be seen in this plot. As the starting grain size is increased, the driving force for both the single crystal and the matrix decreases, resulting in substantially less growth in both cases. Both curves scale as G_0^3, where G_0 is the initial grain size of the matrix.

A plot of single crystal growth vs. surface energy can be seen in Figure 15 for PMN-35PT + 3 vol.% PbO after 4 hours at 1150°C with a surface energy anisotropy of 0.1 J/m^2. A linear dependence of single crystal growth on the surface energy can clearly be seen. Though not shown, the surface energy anisotropy was found to have little influence on the single crystal growth. Varying the surface energy anisotropy from 0.01 to 0.15 J/m^2 altered the single crystal growth by less than 0.5μm after 4 hours of growth. This will be examined in further detail in the future. Growth into matrices with other PbO contents will also be examined.
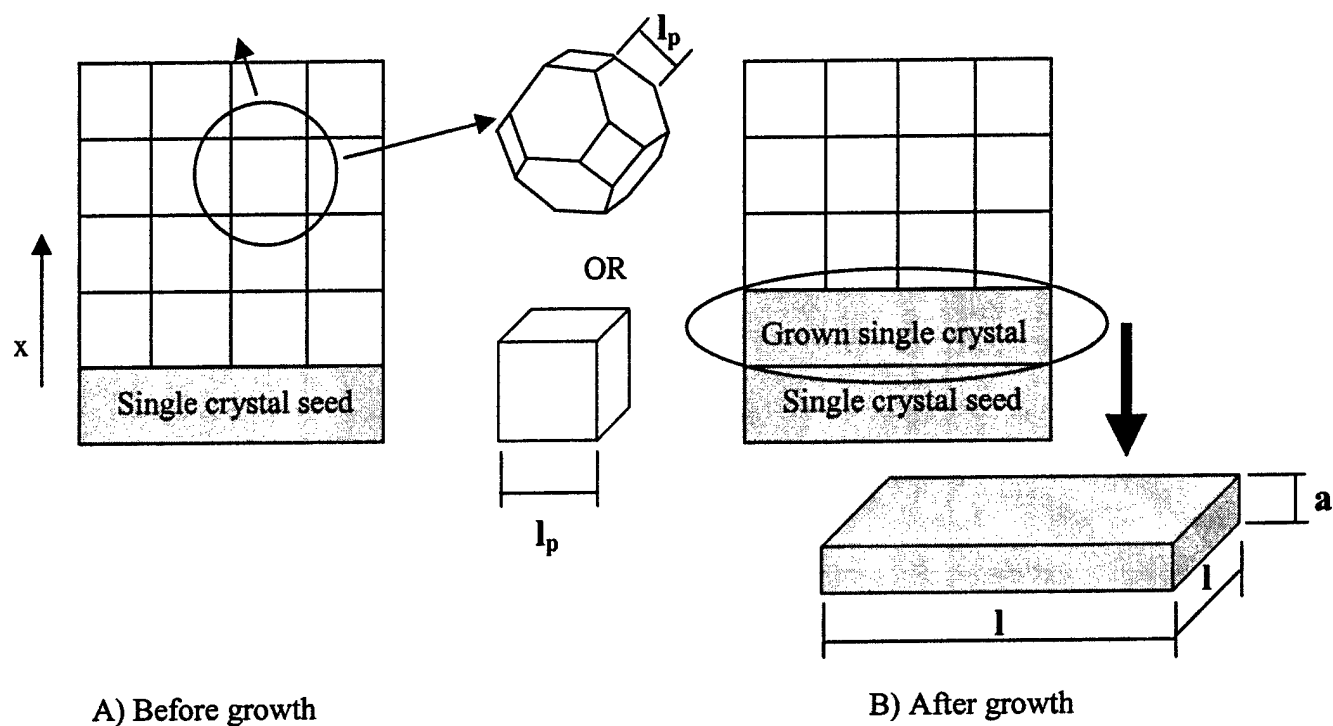
Polycrystalline matrix

X

Single crystal seed

l_p

OR

l_p

Grown single crystal

Single crystal seed

a

l

l

A) Before growth

B) After growth

Figure 11. Schematic diagram of the geometric model used in this study.
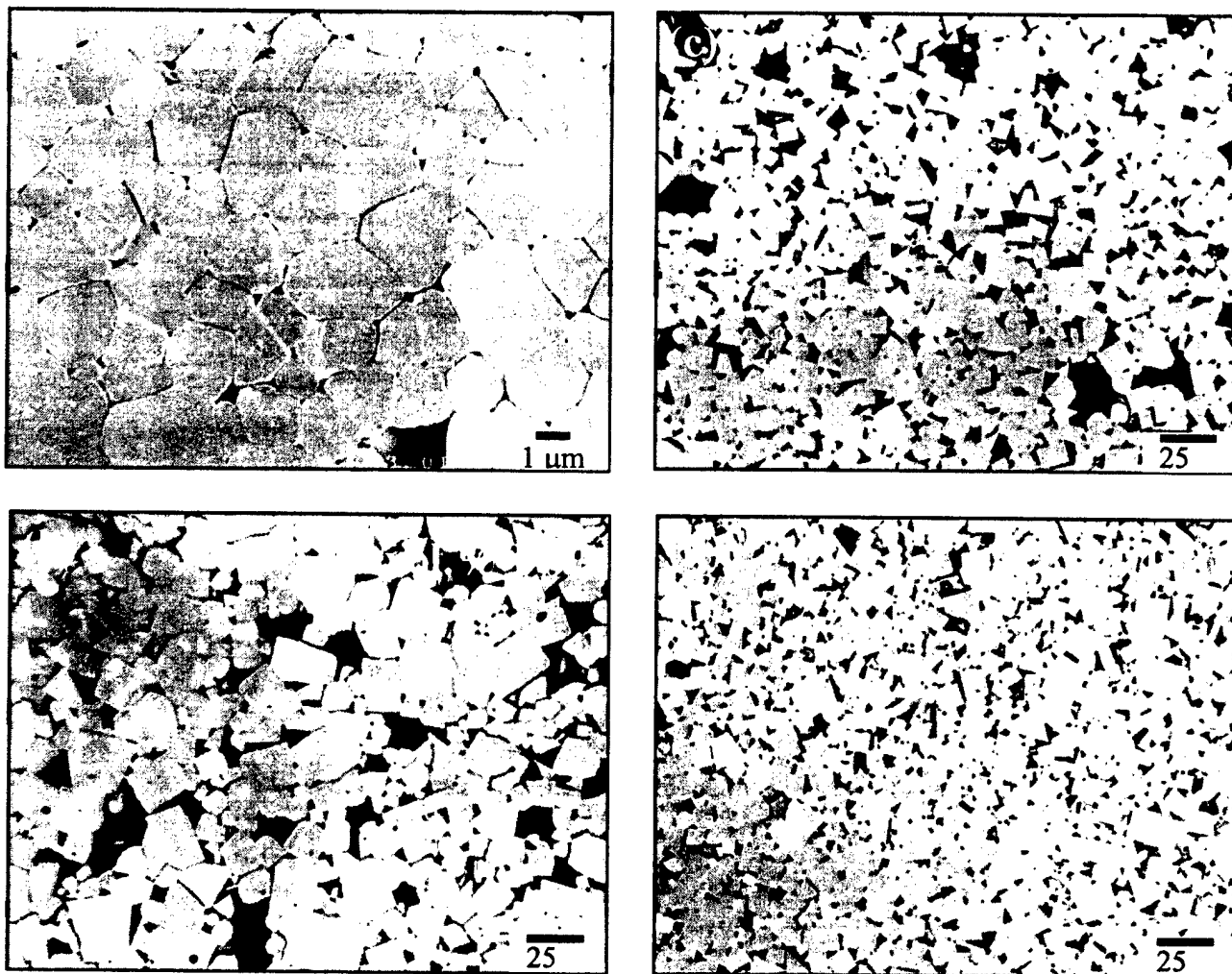
Figure 12. Typical microstructures of matrix grains in PMN-35PT with (a) 1, (b) 3, (c) 5, and (d) 7 vol% PbO.
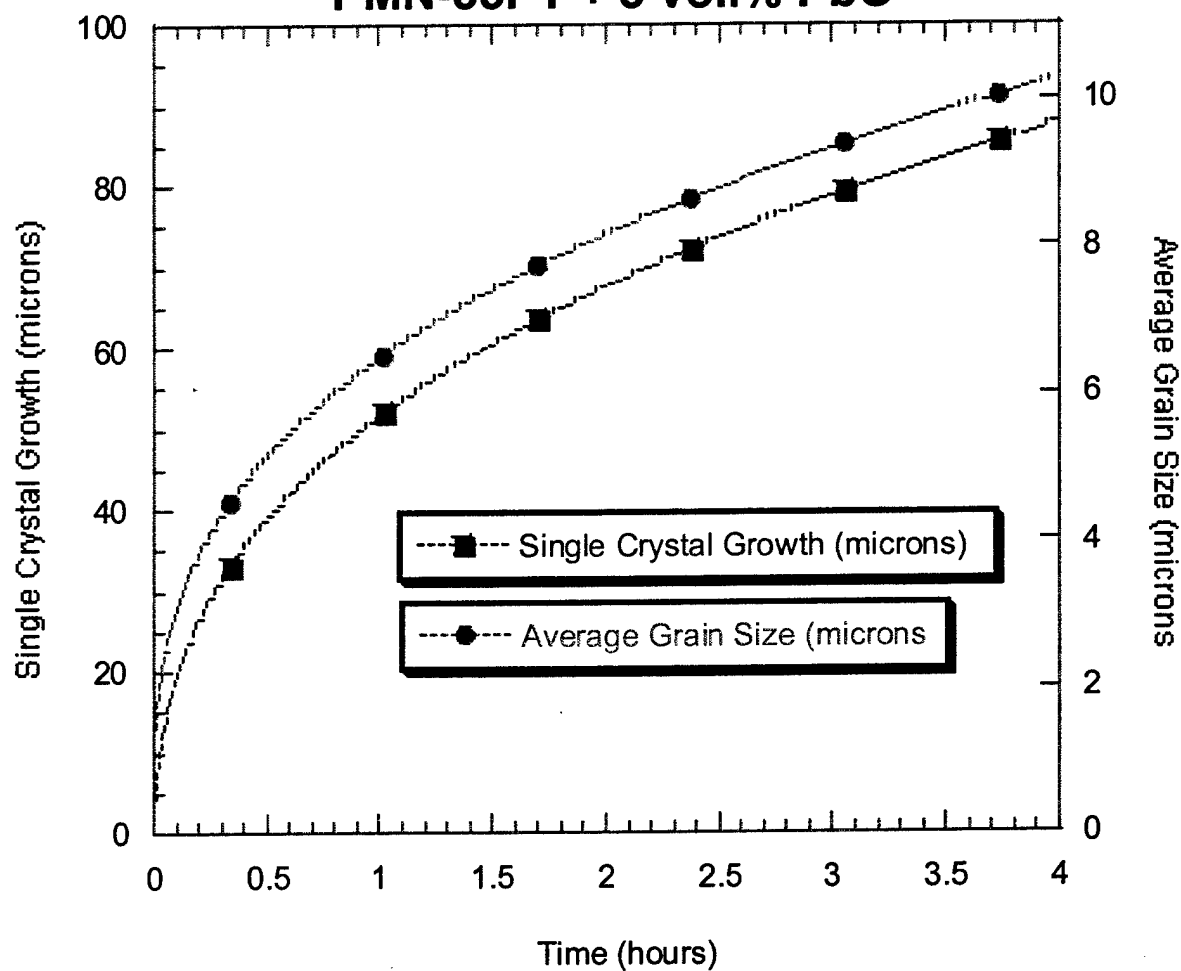
Figure 13. Model predictions of single crystal and matrix growth for
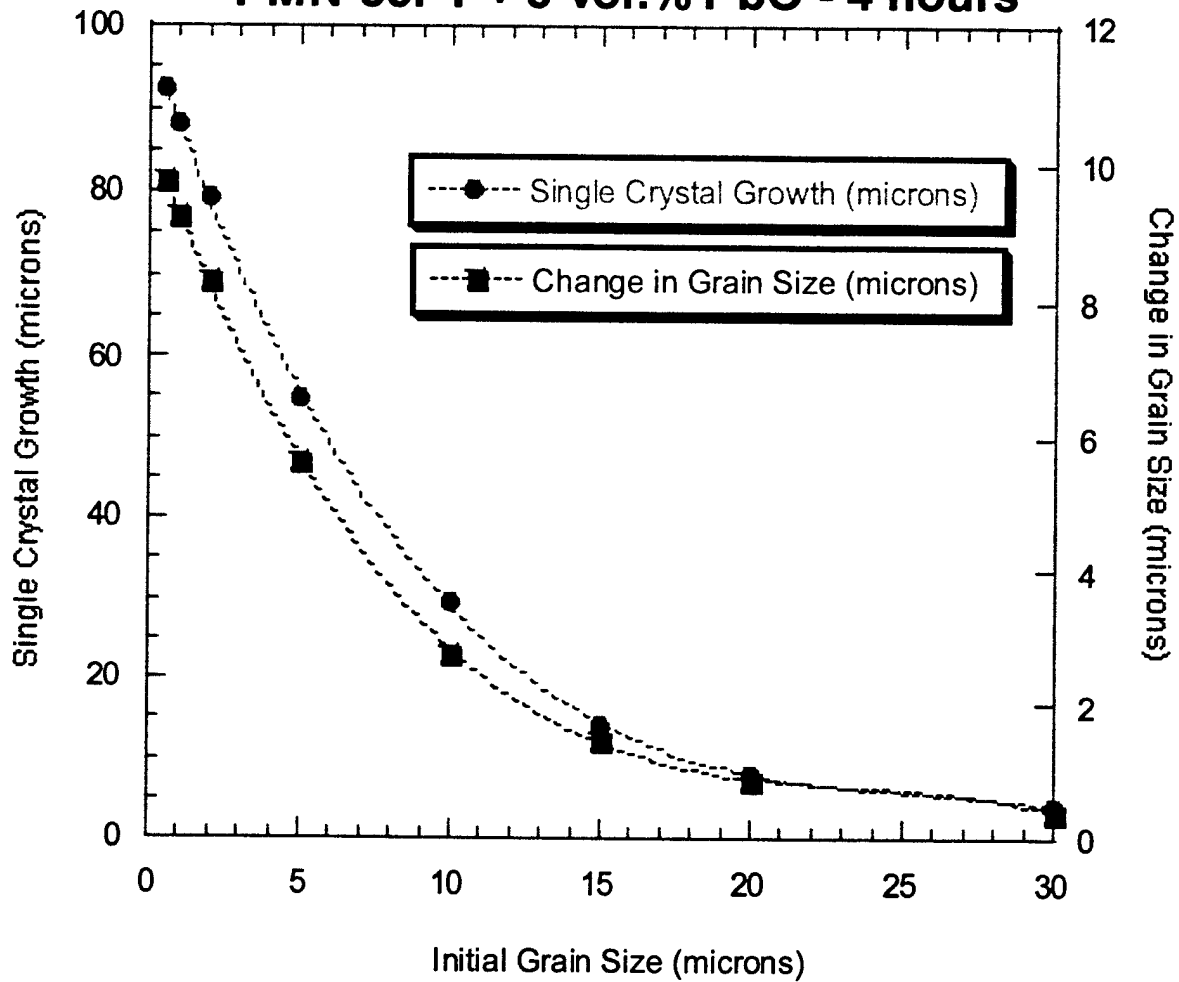PMN-35PT + 3vol.% PbO.

Figure 14. Model predictions of single crystal growth and change in grain size vs. initial grain size for PMN-35PT with 3 vol.% PbO.

Crystal Growth vs. Surface Energy
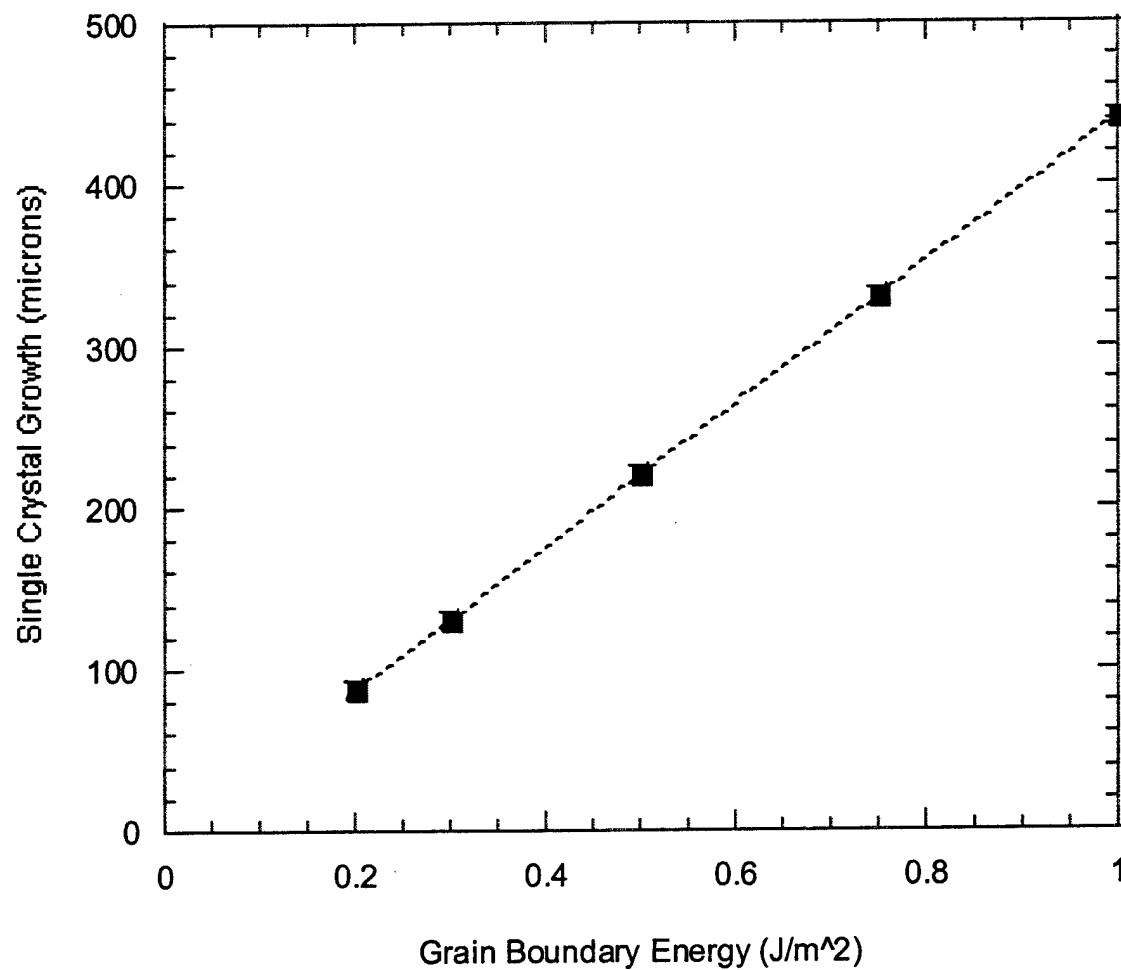## PMN-35PT + 3 vol.% PbO - 4 hours

Figure 15. Model predictions of single crystal growth as a function of grain boundary energy for 1 μm starting grain size.

3.4 Effect of Starting Particle Size on Crystal Growth

Introduction

In an effort to deduce the effect of grain coarsening on solid state conversion, single crystals of PMN-PT were grown into matrices of different starting grain sizes. Powders of different mean particle sizes were prepared by precoarsening PMN-PT powders and subsequently milling to the desired mean size.

Experimental Procedures

Samples were prepared according to the flow chart shown in Figure 16. The procedures are described in detail below.

Powder of PMN-35PT (TRS Ceramics, State College, PA) with 1.5 vol.% PbO (Alfa Aesar) was prepared and annealed at 1100°C for 1 hour in air. Figure 17 shows the microstructure of the annealed powder with an average grain size of 3-5 μm as characterized by SEM. The precoarsened powder was then milled for 2 hours to break up agglomerates and to mix in additional PbO. Half of the powder was set aside to be used as the coarse-grained matrix while the other half was milled for an additional 22 hours to obtain a fine, sub-micron particle size. The particle size distributions of the resultant powders were characterized by a Horiba LA-910 laser scattering particle analyzer and are shown in Figure 18. The powders were subsequently cold isostatically pressed (CIP) into bi-layer specimens which were seeded with (100) PMN-35PT single crystal seed plates (Crystal Associates), as shown in the schematic in Figure 19. The seeded, layered compacts were then sintered at 1150°C for 4 hours in an oxygen atmosphere.

Results and Discussion

According to the crystal growth model developed in section 3.3, the single crystal growth distance into the polycrystalline layer with the 0.6 μm initial average particle size should be 14% higher than the layer with a 1.8 μm particle size. Thus, a single crystal which grew 80 μm into a 0.6 μm average particle size matrix would be expected to grow 70 μm into a 1.8 μm average particle size matrix under identical conditions. Correspondingly, the polycrystalline matrix layers are expected to have an average final grain size of 9.1 μm.

Microstructures from polished cross-sections of the seeded, layered compacts are shown in Figures 20 and 21. The single crystal grew nearly equivalent amounts into the fine and coarse-grained layers, 80 ± 3.6 and 76 ± 3.5 μm, respectively, as shown in Figure 20. The final microstructures of the coarse and fine polycrystalline matrices are shown in Figure 21. The average final grain sizes for the coarse and fine matrices were measured to be 13.4 ± 1.3 μm and 14.8 ± 2.1 μm, respectively.

The discrepancy between the model and the experiment is likely due to the fact that the model assumes a fully dense, equiaxed microstructure, while the experiments employed porous, unsintered polycrystalline matrices. Furthermore, the fine and coarse-grained matrices had different starting green densities, which can significantly influence the densification rate and grain growth.

Future Work

In order to eliminate the effects of porosity and sintering, seeded layered compacts will be hot-pressed to full density prior to the annealing treatment. It is expected that the crystal growth and matrix grain growth behavior will follow more closely to the model predictions. The effect of much larger starting grain sizes (~10 μm) will also be examined.

Experimental Procedures

PMN-35PT → ← 1.5 vol.% PbO

→ Ball Mill
24 hrs in Ethanol

↓

Precoarsen powder

1.5 vol.% PbO →

↓

Ball Mill
2 hrs in Ethanol

→ Ball Mill
22 hrs in Ethanol

↓   ↓

Coarse-grained   Fine-grained

⬇

PMN-35PT + 1.5v% PbO
Seeded Bi-layer Sample
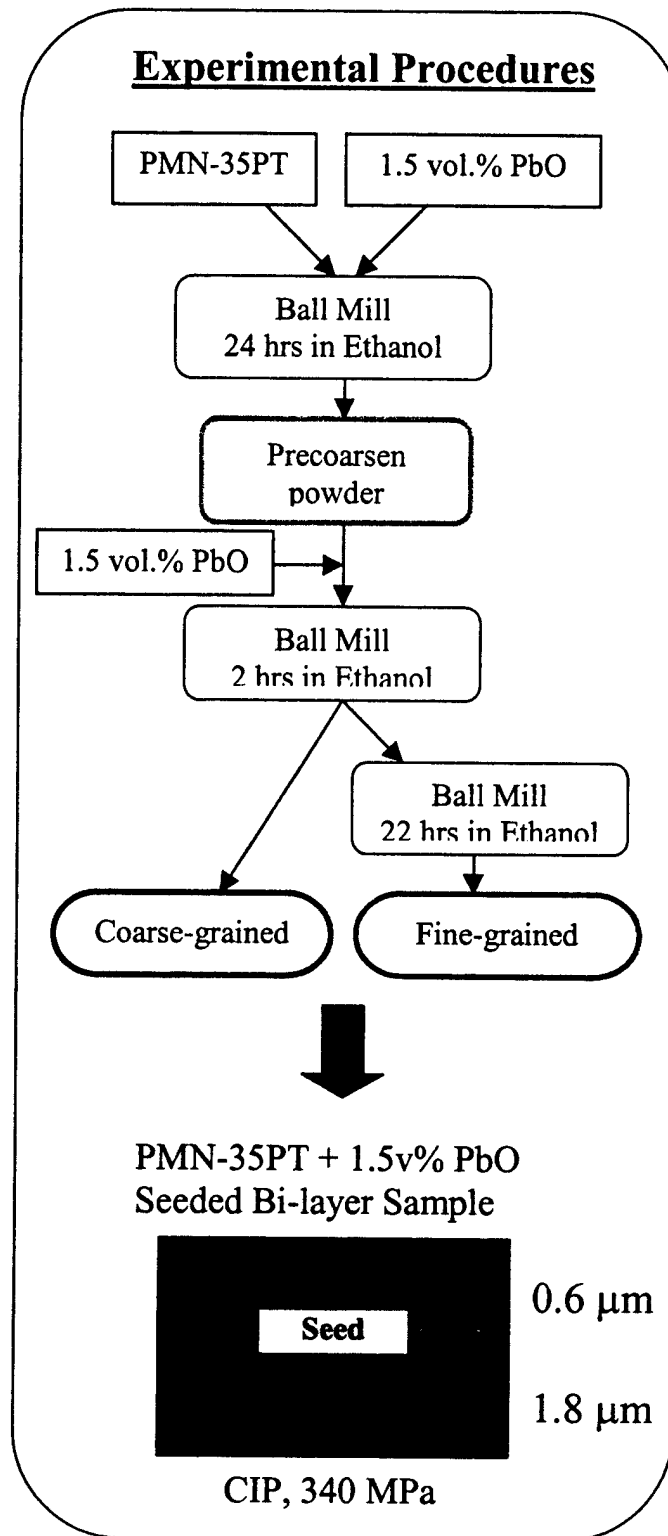
Seed

0.6 μm

1.8 μm

CIP, 340 MPa

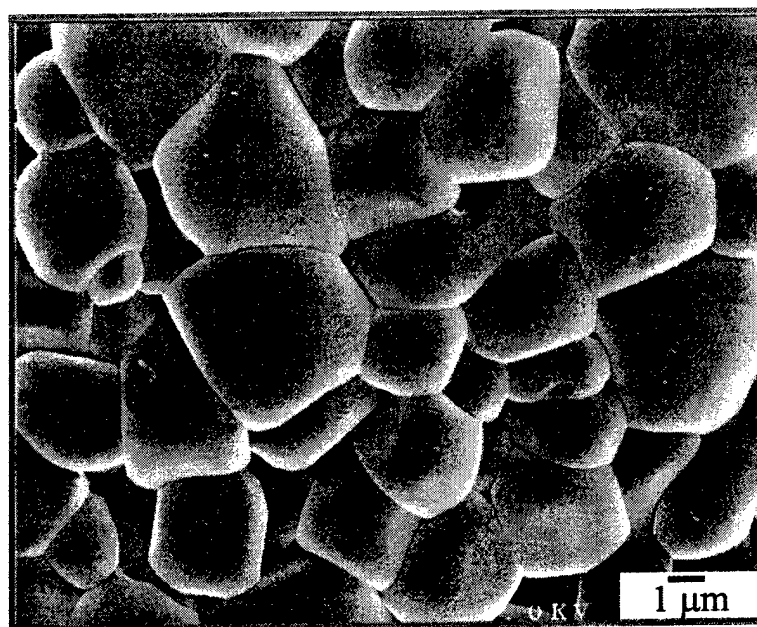**Figure 19.** Schematic diagram of experimental procedure for precoarsening experiment.

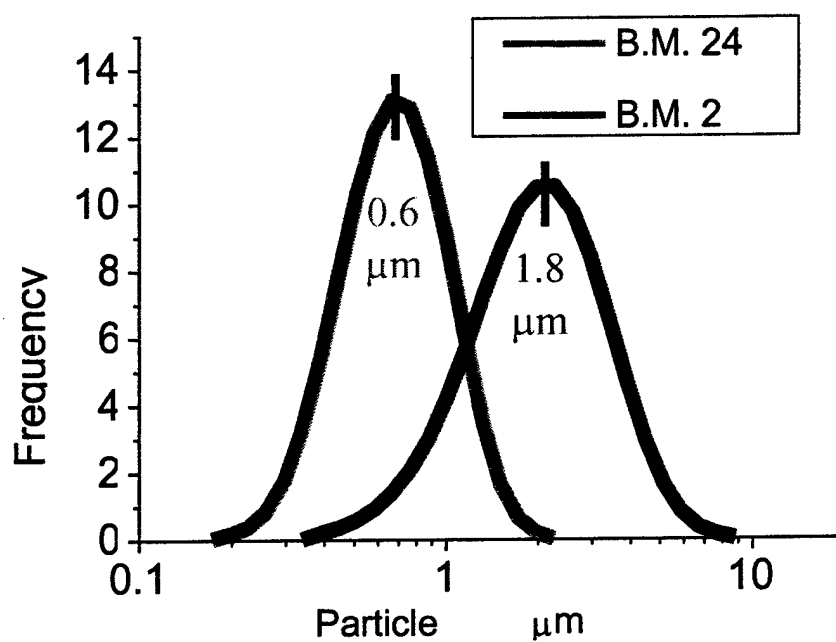**Figure 20.** SEM image of precoarsened PMN-35PT powder; grain size ~3-5µm.

Figure 21. Particle size distributions of precoarsened + ball-milled
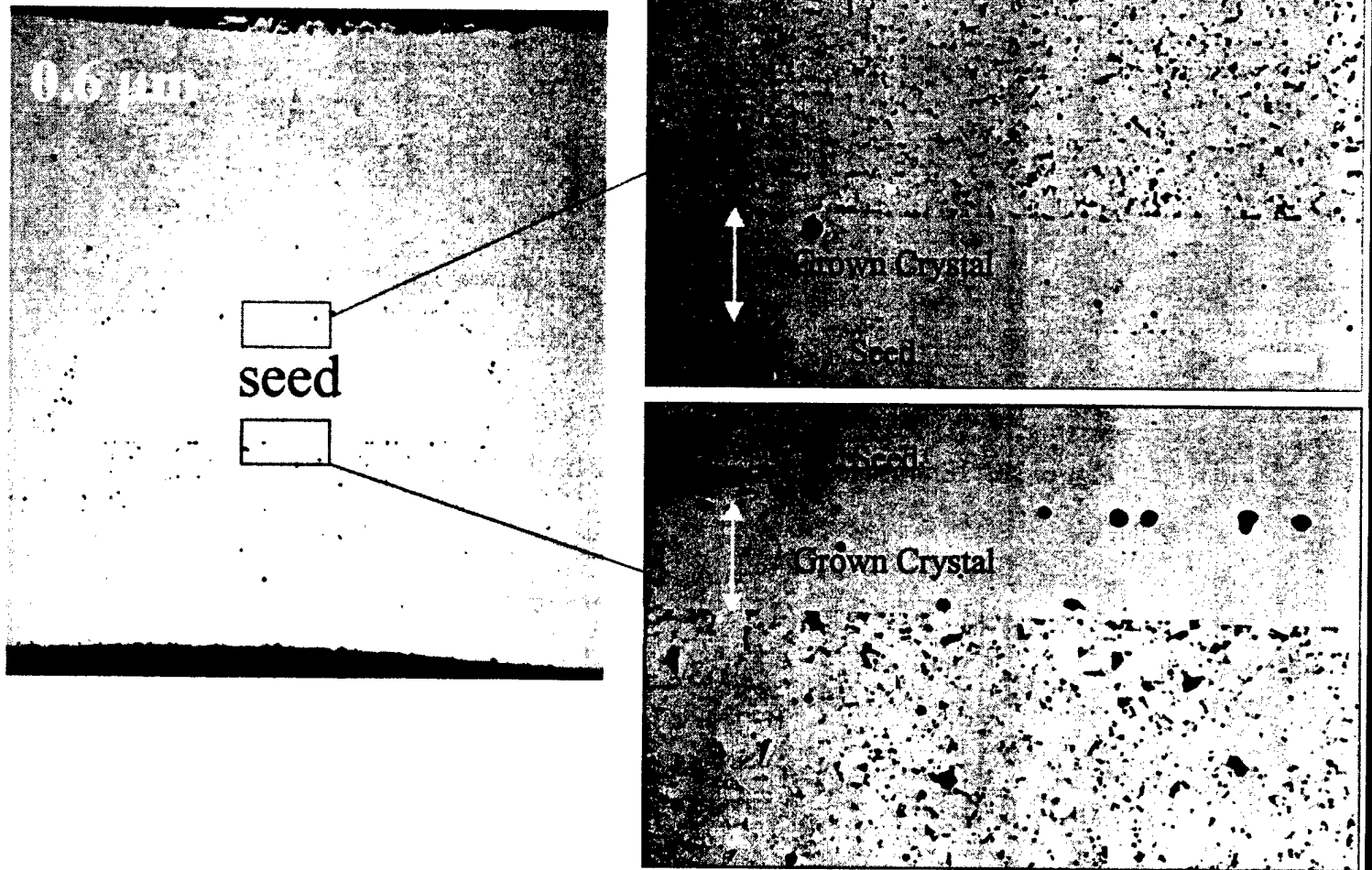PMN-35PT powders; median p.s. of 0.6 and 1.8 µm.

Figure 22. Optical micrographs of a layered compact sintered while embedded in powder of higher PbO content (PMN-35PT + 5vol.% PbO with PZ around crucible); nearly equivalent amounts of crystal growth were observed on both the fine and coarse-grained sides, 80 ± 3.6 and 76 ± 3.5 µm, respectively.
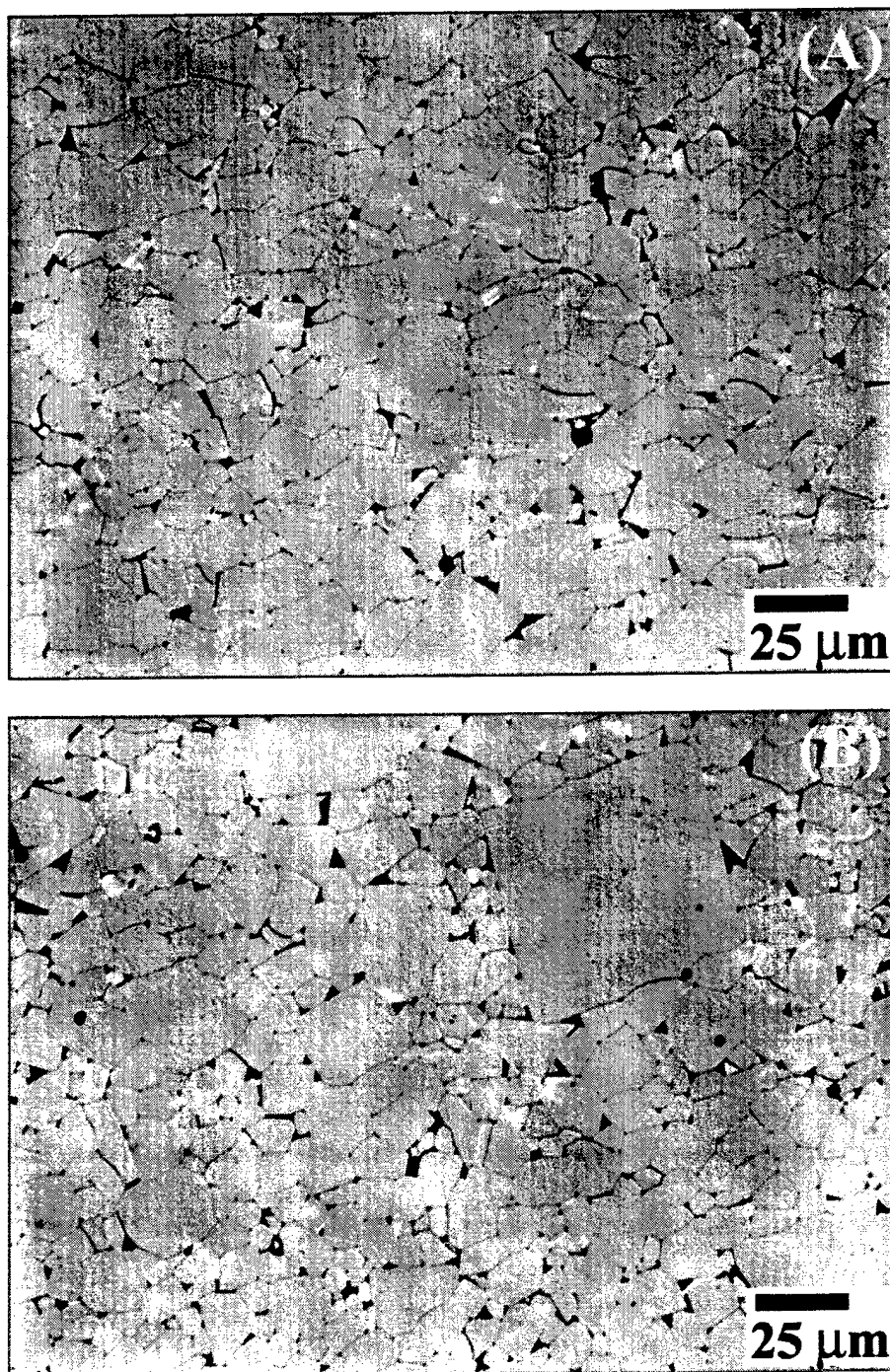
Figure 23. Optical micrographs of the sintered matrices of Figure 26. (A) Coarse (1.8 μm) and (B) Fine (0.6 μm) starting particle sizes; average final grain sizes were 13.4 ± 1.3 μm and 14.8 ± 2.1 μm for (A) and (B), respectively; the fine-grained side exhibited multiple abnormal grains.

3.5 Abnormal Grain Growth

Previous results have shown that a few large abnormal grains (>10 times average grain size) have been observed in PMN-35PT samples with greater than 1.5 vol% excess PbO. An example of a typical microstructure of PMN-35PT + 5 vol% PbO sintered at 1150°C for 4 hours can be found in Figure 24(a). Note the size of the abnormal grains approach 0.5-1mm. These sizes are consistent with abnormal grains found in all excess PbO samples.

Previously, the origin of these select grains in PMN-PT was not well understood. However, recent work by Blendell *et al.* showed that the abnormal grains in samples containing large amounts of excess PbO (10-60 vol%) were actually bicrystals. Furthermore, it was observed that the bicrystals were in a twin orientation, i.e. rotated 60° about the <111> with respect to each other. Preliminary evidence was also presented that indicated these bicrystals formed preferentially in the presence of excess MgO.

A close reexamination of all PMN-PT samples containing abnormal grains, from prior studies at Lehigh, indicated that many of the abnormal grains were bicrystals similar to that shown in Figure 24(b). In order to verify this, Orientation Imaging Microscopy was used to characterize multiple samples containing abnormal grains. Inverse pole figure maps, as shown in Figure 25, confirmed the abnormal grains to be bicrystals with $\Sigma 3$ boundaries, i.e. the twin orientation relationship. The twin boundary is denoted by a yellow line in the grain orientation map.
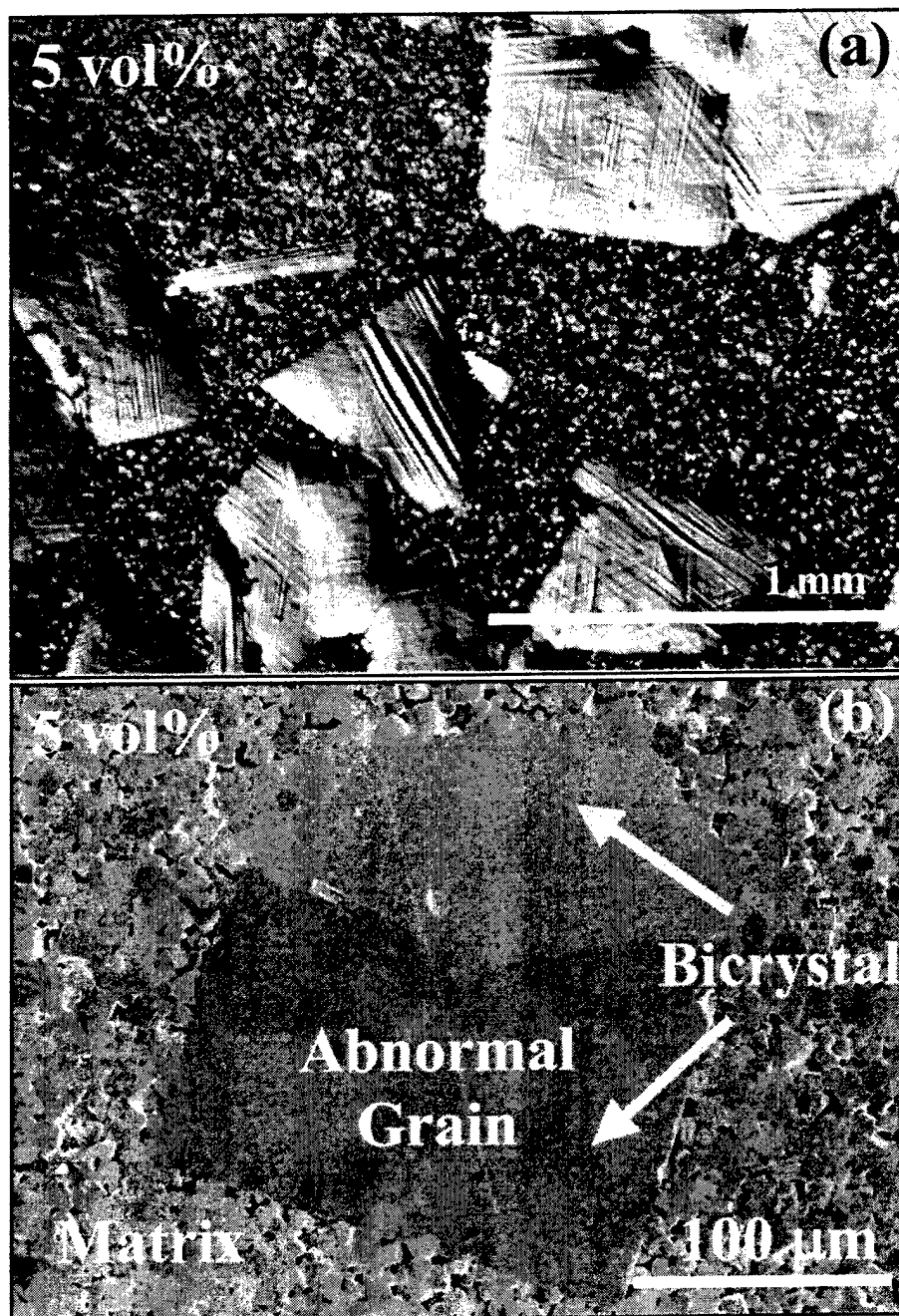
Figure 24. Abnormal grains in PMN-PT+ 5 vol% PbO matrix; after 1150°C for 4 hr. in O₂; (a) low mag and (b) high mag.
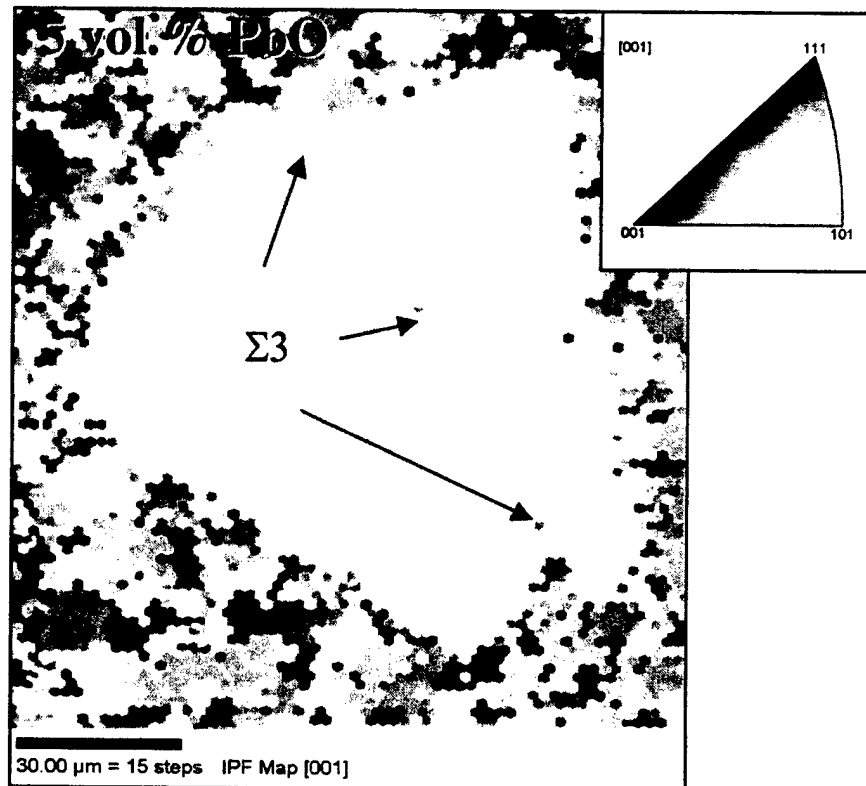
Figure 25. Orientation image map of large grains in samples with PbO; after 1150°C for 1 hr. in O₂.

3.6 Focused Ion Beam

The role of interfaces is a key issue in understanding the migration of single crystal boundaries. Important parameters such as interface morphology, crystallographic misorientation, defects, and liquid phase composition/distribution all require high resolution boundary characterization. To aid in specimen preparation for transmission electron microscopy (TEM), a dual-beam focused ion beam (FIB) can be used.

A dual-beam FIB offers the distinct advantage of being able to image with a scanning electron column and ion mill concurrently. Sample preparation includes deposition of a thin layer of platinum over the area of interest, followed by milling trenches on either side of the platinum layer. After subsequent thinning steps reduce the thickness to approximately 150nm, the TEM specimen is removed with a glass-rod extracting tool. This concept is shown schematically for a single crystal/polycrystal interface in Figure 26. The importance of this technique can be seen in Figure 27, which shows a sample that contains liquid phase at such an interface. This sample could not be fabricated using conventional TEM preparation due to the poor mechanical strength of the interface.
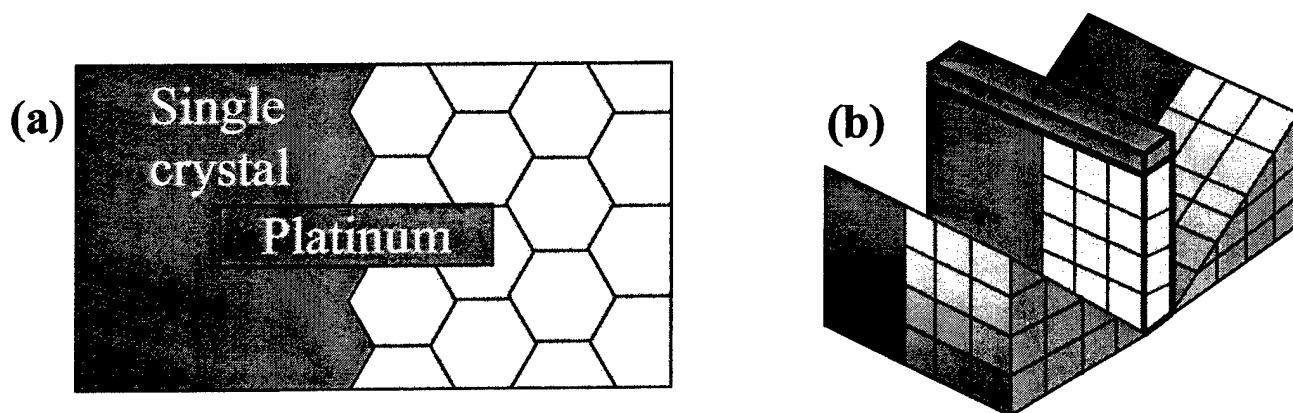

Figure 26. Schematic diagrams showing (a) platinum deposition and (b) trench milling with FIB to produce TEM sample across single crystal/polycrystal interface.
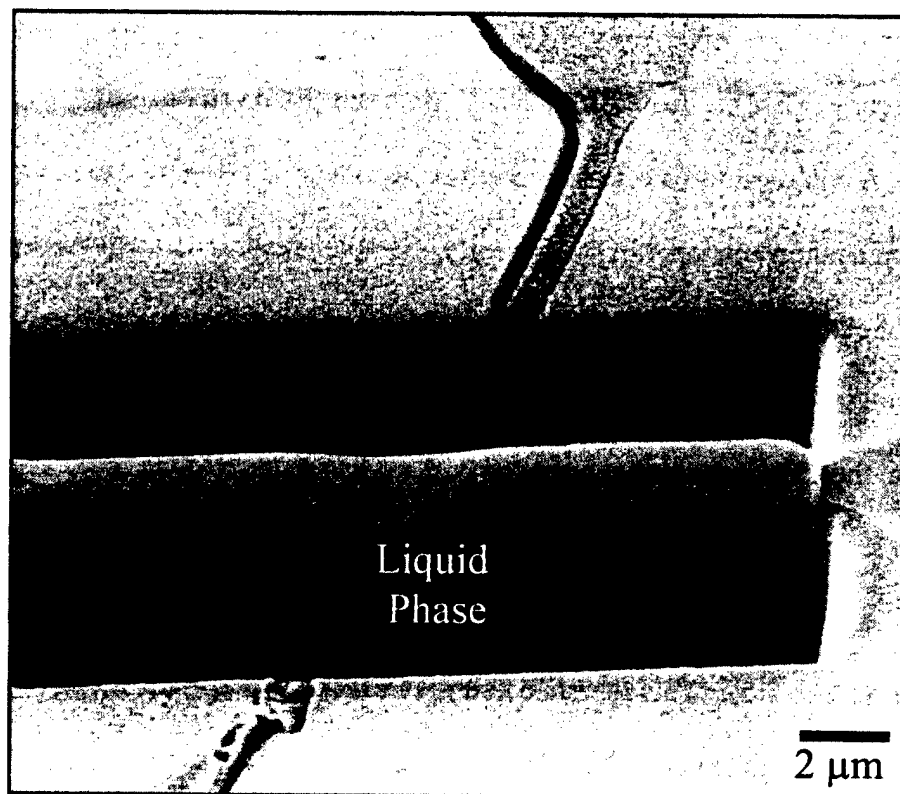
Figure 27. SEM image of PMN-35PT TEM sample produced with dual-beam FIB.

3.7 Kinetic Analysis of $Pb(Mg_{1/3}Nb_{2/3})O_3$-35mol%$PbTiO_3$ Single Crystals Grown by Seeded Polycrystal Conversion

Kinetic Analysis of Pb(Mg$_{1/3}$Nb$_{2/3}$)O$_3$-35mol%PbTiO$_3$ Single Crystals Grown by Seeded Polycrystal Conversion

by

Patrick Thomas King

A Thesis

Presented to the Graduate and Research Committee

of Lehigh University

in Candidacy for the Degree of

Master of Science

in

Materials Science and Engineering

Lehigh University

October 2002

CERTIFICATE OF APPROVAL

This thesis is accepted and approved in partial fulfillment of the requirements for the Master of Science.

_____

Date

_____

Dr. Martin P. Harmer, Advisor

_____

Dr. Helen M. Chan, Co-Advisor

_____

Dr. G. Slade Cargill, Dept. Chair

To my grandmothers

ACKNOWLEDGEMENTS

I would like to first thank my advisors, Drs. Martin Harmer and Helen Chan for their guidance and financial support over my graduate school years as well as during my senior project. It has been a privilege to conduct research under their guidance. I would also like to thank the generous financial support of DARPA, ONR, and AFOSR for funding the Seeded Polycrystal Conversion process over the last few years.

The support of my family has been instrumental over my collegiate years. I would like to thank my parents, Thomas and Michelle, my brother Chris, my sister Sherri, and my grandmothers and extended family for all of their encouragement. I would also like to thank my fiancée Lauren for all her love and support over the last few years – only she knows what I have been through on a daily basis.

I would like to thank my fellow bitter housemates for time well spent outside of Whitaker Lab: Phil (Oh yeah!) Anderson, Mario Epler, Derrick Rockosi, Dominik Zurakowsi, and Benjamin (Marlboro) Kiner. Special thanks to Phil, for never doing the dishes, to Derrick, whose purchase of Gamecube™ might have been the best idea ever, to Ben, for using my dinner trash as an ashtray, and to Mario, for just being bitter about everything. More recent shout outs go to Shen Dillon and Frank Gift – thanks guys, for the doing the dishes.

Thanks must also be given to the following members of the materials science & engineering staff for their respective assistance in research, graduate school debacles (and there were many), purchase orders, and of course making sure that I got a pay check twice a month: Arlan Benscoter/Dave Ackland, Maxine Mattie, Virginia

Newhard/Sue Stettler, and Deanne Hoenscheid. Very special thanks also to Professor S. Kenneth Tarby for help with my job search.

The tribulations of graduate school have been eased by the friendships and assistance of several senior members of the ceramic group. Specifically, my sincere gratitude is extended to Adam Scotch and Paul Martin Sheedy. Their assistance with the scientific specifics of my research, as well as with the finer things in life, helped make the last few years enjoyable, diversified, and a true learning experience. Only through their guidance was I able to learn to true meaning of the word sidetrack. Elephants are capable of swimming 20 miles.

I would also like to extend my appreciation to Ed Gorzkowski with help and guidance through the research project, as well as for co-founding the weekly run for the border. Honorary ceramic group member Steve Claves must be thanked for always suggesting that we play an afternoon round of golf, even though that nearly caused me to not finish my thesis. I would also like to recognize some other members of the ceramics group, past and present, whose time overlapped with my stay for their help and friendship: Derrick Rockosi, Dr. Gary (17 semesters – haha) Thompson, Chris Borradaile, Eduardo Lee, Peter Henderson, Dr. Suxing Wu, and Dr. (Shady) Lincoln Leatherland. I would also like to acknowledge the friendship and help of various other members of the department who helped but I have not mentioned above.

I'd like to mention the wonderful employees of Wawa for always putting my tomatoes outside of the sandwich, and for ripping my heart out by canceling the Boli.

As for the PhD – I think I'll take a *brodie* on that one.

TABLE OF CONTENTS

LIST OF FIGURES

(single headed arrow).

LIST OF TABLES

LIST OF SYMBOLS

G	average grain size at time t
G_0	average grain size at time t=0
k	kinetic growth constant
t	annealing time
v	boundary velocity
F_b	driving force
M	mobility of boundary
D_f	diffusivity through the liquid film
C_f	solubility of the grain in the liquid
Ω	atomic volume
k_B	Boltzmann's constant
T	annealing temperature
Γ	constant exponentially dependent on temperature
$\Delta\gamma$	surface energy anisotropy
γ_a	average surface energy per unit area
γ_{min}	surface energy of the {001} oriented single crystal
E	total grain boundary energy per unit volume
N	number of grains per unit volume
A_{gb}	grain boundary area
γ_{gb}	grain boundary energy
L	linear single crystal growth at time t

L_0 linear single crystal growth at time t=0

a   width of single crystal seed

l_p edge length of individual grain

Δw percentage change in sample weight

w_f final sample weight

w_o initial sample weight

W_{im} immersed sample weight

W_L dry weight of line for density measurement

W_W impregnated sample weight,

ρ density of the specimen

ρ_{H2O} theoretical density of water

ρ_{rel} percentage relative density

ρ_{theor} theoretical density of PMN-35PT

L_m measured (uncalibrated) single crystal growth

S   cross-sectional thickness of the seed crystal

V_f liquid volume fraction

X   volumetric liquid fraction

V_{sys} total volume of the system

f   liquid film thickness

i integer number of the time step

Δt time interval

ABSTRACT

The kinetics of {001} oriented $Pb(Mg_{1/3}Nb_{2/3})O_3$-35mol%PbTiO$_3$ [PMN-35PT] single crystals grown by Seeded Polycrystal Conversion (SPC) and the corresponding matrix grains were systematically quantified. In the SPC process, a small seed single crystal (several hundred microns thick) is embedded in a fine-grained powder compact with excess liquid phase, and the single crystal interface thermally migrates at the expense of the smaller matrix grains. Specifically, the kinetics were experimentally analyzed as a function of liquid phase (PbO) content. The average matrix grain size and single crystal growth were fitted to equations of the form $G^n-G_0^n=kt$ and $\Delta L^n =kt$, respectively, where G is the average grain size, L is the linear single crystal growth, n is a growth exponent, and k is the growth constant. Cubic growth laws (n=3) were observed for PbO contents from 0 to 5 vol.% for both the matrix grains and single crystals. At PbO volume fractions from 0 - 3 vol.%, both the matrix and single crystal growth rates increased with increasing PbO content, presumably due to an increase in pore mobility. For larger PbO volume fractions, single crystal growth was essentially independent of PbO content, indicating an interface reaction growth mechanism. The matrix grain growth decreased before beginning to level off, indicative of diffusion control. This suggests a possible transition from diffusion-controlled growth at lower PbO fractions to interface reaction-controlled growth at higher PbO fractions.

The growth behavior of {001} PMN-35PT single crystals grown by Seeded Polycrystal Conversion (SPC) has also been modeled. For this study, a preexisting analytical model of the SPC process has been modified and adapted to include the

1

experimental PMN-35PT matrix grain growth data. The results showed support of an effect of liquid phase chemistry on the single crystal growth behavior between 3 and 5 vol.% PbO. The model also revealed that a fine-grained matrix is necessary for the SPC to be effective, and the observed coarsening of the matrix grains may explain the cubic single crystal kinetics.

1. INTRODUCTION

Ferroelectric ceramics are dielectric materials that exhibit reversible polarization in the absence of an electric field, i.e. even after the applied voltage has been removed.[1] Studies conducted during recent years have shown that single crystals of certain ferroelectrics have vastly superior electromechanical properties compared to their polycrystalline counterparts. One such material is the relaxor $Pb(Mg_{1/3}Nb_{2/3})O_3$ (PMN) and its solid solution with $PbTiO_3$ (PT). Of particular interest are compositions near the morphotropic phase boundary, the boundary between the pseudo-cubic rhombohedral and tetragonal phases in the PMN-PT system. The PMN-PT system, which possesses the perovskite structure, has a morphotropic phase boundary which lies at approximately 32 mol.% $PbTiO_3$.[2] A schematic of Curie temperature vs. PT composition, analogous to a PMN-PT phase diagram, is shown in Figure 1.1.
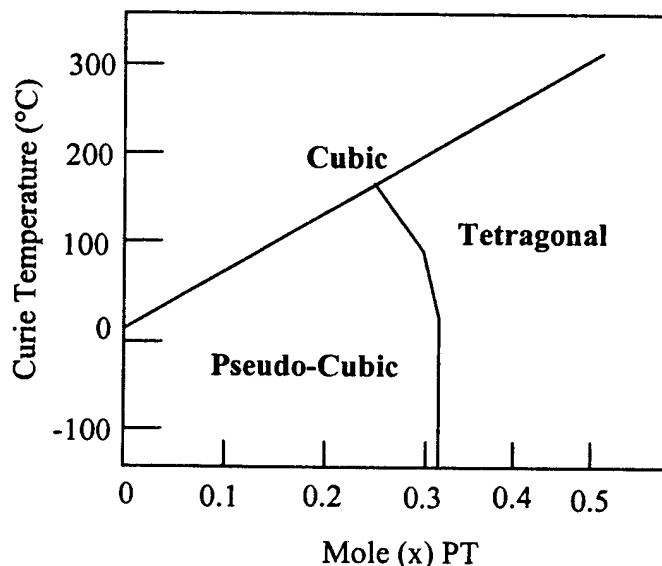
Figure 1.1. Plot of Curie temperature vs. mole fraction $PbTiO_3$ for the $Pb(Mg_{1/3}Nb_{2/3})O_3$- $PbTiO_3$ system (After Park and Fielding.[3])

3

Examples of electromechanical properties reported for ferroelectric single crystals include electric-field induced strains $\varepsilon_{33} > 0.7\%$, coupling coefficients $k_{33} > 90\%$, piezoelectric coefficients $d_{33} > 1200$ pC/N, and dielectric constants from 1000 to 5000.[4,5] These promising data have profound implications for the medical and military industries, where devices such as transducers and actuators rely heavily on the performance of such materials. In turn, these results have spearheaded the drive to find a viable method for producing high quality single crystals in a cost-efficient and time-effective manner.

Traditional methods of producing single crystals include the flux,[6] Bridgman,[7] and Czochralski[8] techniques. While the three methods are successful in growing bulk single crystals, they are fairly slow processes and cannot be readily and economically transferred to large-scale manufacturing. The flux method is a relatively inexpensive process, but is lacking in crystal quality and reproducibility. The Bridgman and Czochralski techniques produce high quality crystals, but both are very expensive processes which often produce crystals with chemical gradients. The novel Seeded Polycrystal Conversion (SPC) technique offers both a cost-effective and time-efficient method for producing quality ferroelectric single crystals.[9,10] A schematic diagram of the SPC process is shown below in Figure 1.2.
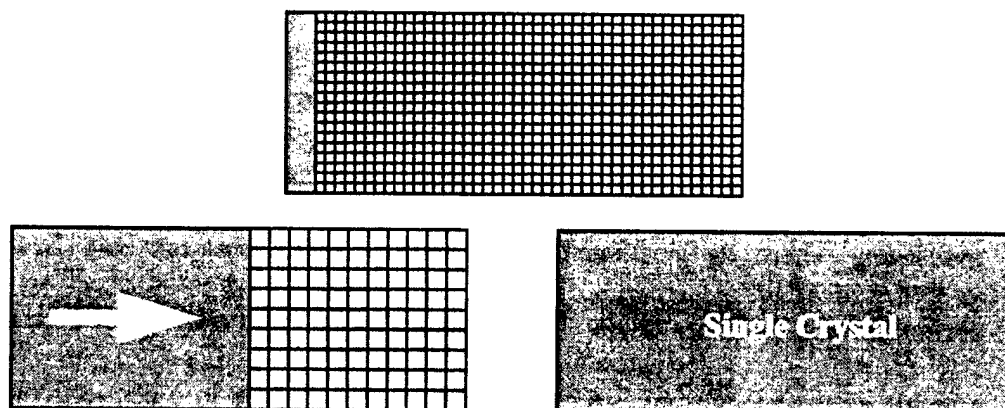
Figure 1.2. Schematic diagram of the Seeded Polycrystal Conversion (SPC) process showing the migration of the single crystal boundary at the expense of the small matrix grains. Note the accompaniment of matrix grain growth with single crystal growth.

The SPC process, similar to solid state demonstrations in Al_2O_3,[11] $BaTiO_3$,[12] and Mn-Zn ferrites,[13,14,15] has recently been proven feasible in the $Pb(Mg_{1/3}Nb_{2/3})O_3$-35mol%$PbTiO_3$ [PMN-35PT] system.[9,10] In this process, a single crystal seed is either bonded to, or embedded in, a polycrystalline matrix. A small amount of liquid phase (PbO) is added to the matrix to increase the mobility of the single crystal. During thermal treatment, the single crystal boundary migrates at the expense of the smaller matrix grains.

While the SPC process has been proven feasible in the PMN-35PT system, ongoing research has focussed on several factors controlling the process. Liquid phase content, annealing atmosphere, annealing temperature, and the starting matrix particle size have all been identified as key variables that may heavily influence the single crystal growth and resulting microsctructure.[9,16,17] A thorough understanding of these

5

variables is critical for the SPC process to be successfully implemented into wide-scale manufacturing of ferroelectric single crystals.

Among the key questions of how these factors influence the SPC process is their respective effect on the kinetics of the matrix grains and the migrating single crystal. Small additions of PbO to the matrix have qualitatively been shown to increase the single crystal growth,[16] but to date no systematic quantitative study has been conducted. While the SPC process has been successfully conducted with a variety of seed orientations,[9,18,19] the goal from a manufacturing standpoint has been to produce {001} oriented single crystals. This orientation has been shown to be electromechanically superior to other orientations such as {111}.[4] Presumably, {001} oriented single crystals could be extracted from a bulk single crystal of any orientation. However, as will be discussed in section 2.2.1, the faster growth velocities from non-{001} orientation seeds create excessive amounts of undesired trapped liquid phase and porosity.[18,19] In addition, the processing required to properly orient and section a {001} orientation from a bulk crystal would be costly in a manufacturing setting.

The aim of this research is therefore to quantitatively analyze and model the kinetics of PMN-35PT single crystals grown by the Seeded Polycrystal Conversion process from {001} oriented seeds.

2. BACKGROUND

2.1. Seeded Polycrystal Conversion (SPC)

Seeded Polycrystal Conversion (SPC) is a novel technique for producing ferroelectric single crystals in a cost-effective and time-efficient method. The process involves embedding a single crystal seed into a polycrystalline matrix and inducing boundary migration at the expense of the smaller matrix grains. This section will discuss various microstructural variables pertinent to the single crystal growth process as determined by previous studies.

2.1.1. Effect of PbO Content

Initial demonstrations of the SPC process on the PMN-PT system were performed using randomly oriented and {111} oriented PMN-PT and $SrTiO_3$ single crystal seeds.[9,19,20] In all instances, the single crystal growth exhibited macroscopic faceted morphologies with {001} cubic faces. Thermodynamically, this indicates that {001} faces are the most energetically favorable growth plane. A photomicrograph of PMN-35PT single crystal grown by Seeded Polycrystal Conversion at 1150°C for 140 hours under pressureless conditions is shown in Figure 2.1. The cubic facets are clearly visible at the single crystal growth front.
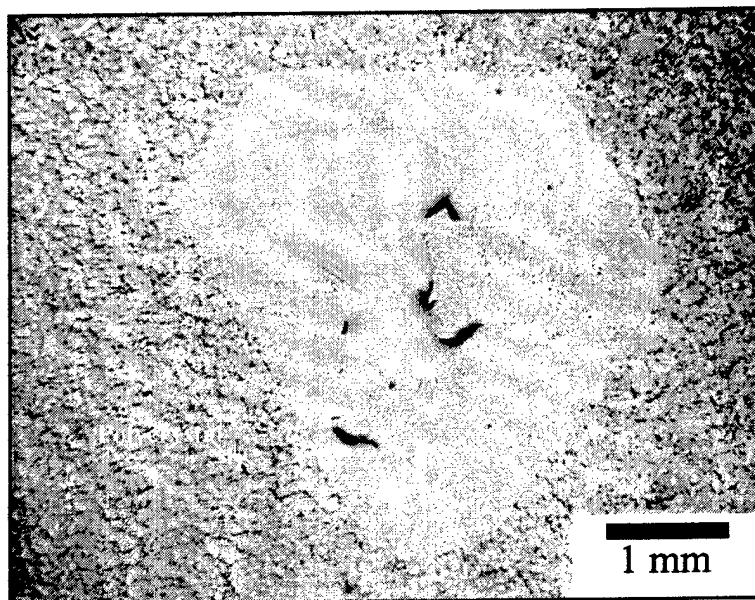
Figure 2.1. PMN-35PT single crystal grown by Seeded Polycrystal Conversion at 1150°C for 140 hours under pressureless conditions in air (image courtesy of Adam Scotch).

In the earlier stages of the process development, Seeded Polycrystal Conversion was considered a solid-state process since no liquid phase was intentionally added to the matrix. However, later results showed that PbO (melting temperature approximately 883°C),[21] was being transferred to the matrix, creating a secondary liquid phase that presumably increased the mobility of the migrating boundary. The source of the PbO was eventually linked to the presence of $PbZrO_3$, which was used as sacrificial packing powder to prevent volatilization in the sample.[20] Since this discovery, excess PbO has intentionally been added to the matrix to act as a liquid phase at the sintering temperatures and to enhance the single crystal mobility.

While the addition of PbO as a liquid phase increases the mobility of the single crystal, the boundary velocity also is dependent on the orientation of the seed. As shown in Figure 2.1, the single crystal facets to a cubic orientation with {001} faces.

8

Thus, <001> is inherently the slowest growth direction in the PMN-35PT system. Work conducted showing single crystal growth from different seed orientations is presented in the Appendix.
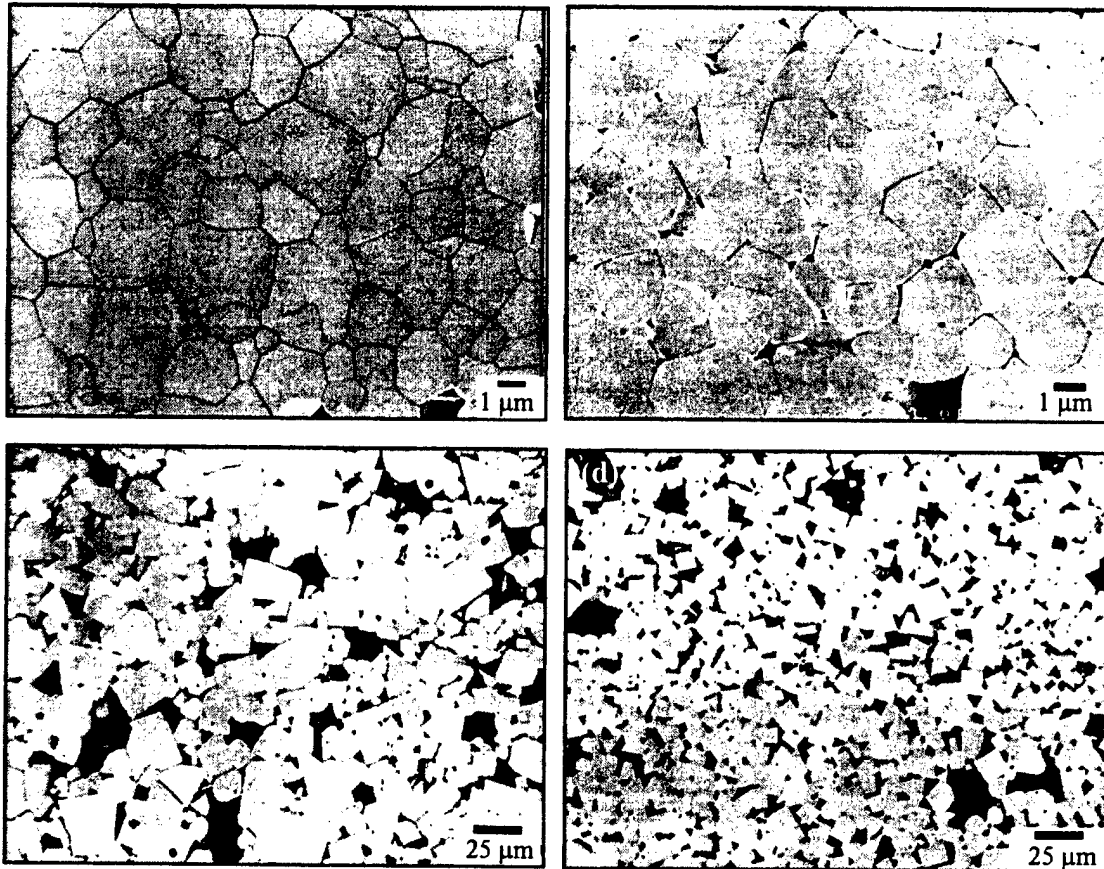
Figure 2.2. Transition in matrix grain morphologies in PMN-35PT with (a) 0 vol% PbO, (b) 1 vol% PbO additions, (c) 3 vol.% PbO, and (d) 5 vol.% PbO additions after sintering for 10 hours at 1150°C in air (images courtesy of Edward Gorzkowski).

The effect of PbO on the transition in matrix morphology can clearly be seen in Figure 2.2. It is also worthwhile to note the effect of PbO on the average matrix grain size. Qualitatively, the average grain size increases with PbO content up to 3 vol.%, but then appears to decrease with further liquid phase additions (5 vol.%). The initial increase in the grain size is most likely due to an increase in mobility from the presence

9

of the liquid phase. The cause of the sudden decrease in average grain size was attributed to a potential switch in grain growth mechanisms.[16] Section 2.2 will describe more in depth the different liquid phase sintering growth mechanisms that may be affecting the growth process in PMN-35PT.

The increase in matrix grain growth behavior was correlated with an increase in the amount of single crystal growth observed in Seeded Polycrystal Conversion of PMN-35PT.[16] Figure 2.3 shows single crystal growth from {111} oriented seeds into a matrix of PMN-35PT with 1 and 5 vol.% PbO. The amount of growth in the 1 vol.% PbO matrix was only about 50 μm, while growth on the order of several millimeters was observed in the 5 vol.% PbO sample. As in the matrix growth, the increase in the single crystal growth is likely due to an increase in the boundary mobility from the liquid phase. The theoretical aspects of boundary mobility will be discussed in section 2.2.
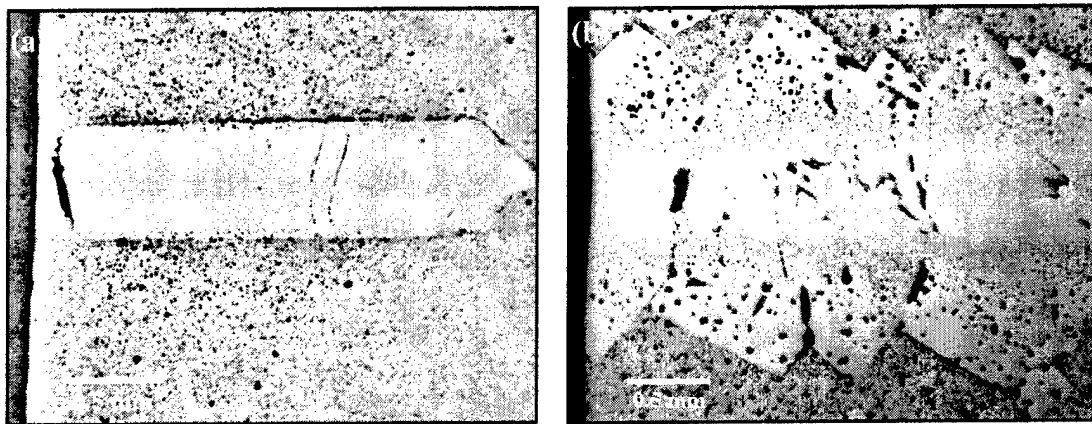
Figure 2.3. Single crystal growth from {111} oriented seeds into matrix compositions of PMN-35PT with (a) 1 vol.% PbO and (b) 5 vol.% PbO additions (images courtesy of Dr. Ajmal Khan).

2.1.2. Effect of Sintering Atmosphere

All of the microstructures shown in section 2.1.1 were sintered in air from the green state, or annealed in air after hot-pressing. Clearly, there are visible amounts of porosity in both the matrix and trapped within the grown single crystal. More recent results have shown that sintering a PMN-35PT sample from the green state in oxygen drastically reduces the amount of porosity in the sample, yielding a nearly full dense microstructure and single crystal.[17] Figure 2.4 shows a comparison of single crystals grown from {111} oriented seeds grown in a matrix of PMN-35PT + 5 vol.% PbO at 1150°C for 4 hours in different atmospheres. The amount of trapped porosity is clearly reduced in the sample sintered in oxygen.
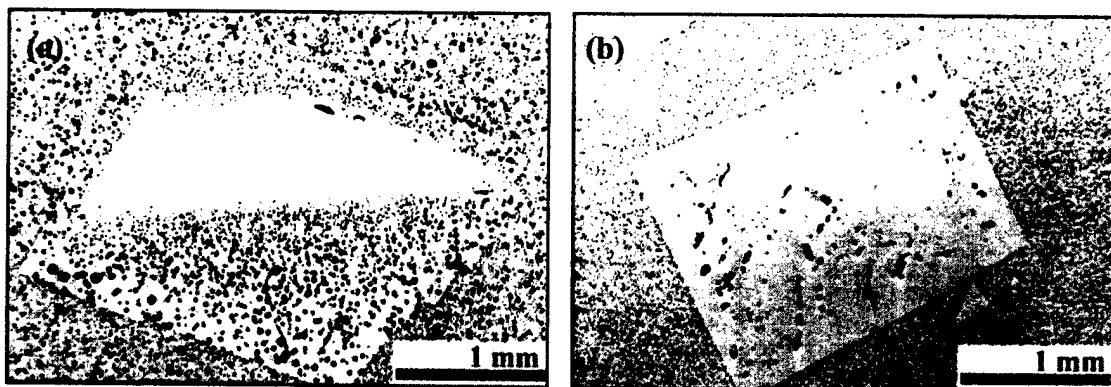
Figure 2.4. Comparison of single crystals grown from {111} oriented seeds into a matrix of PMN-35PT + 5 vol.% PbO after sintering from the green state for 4 hours at 1150°C in (a) air and (b) oxygen (images courtesy of Adam Scotch).

While sintering directly from the green-state in oxygen yields a fully dense sample, hot-pressing in air followed by annealing in oxygen produces a porous sample. In addition, a sample sintered in oxygen and subsequently annealed in air also produces porosity in the microstructure. Intergranular porosity likely developed during annealing due to trapped insoluble gases (N_2, CO, CO_2), the decomposition of PbO, and/or the

11

evolution of oxygen from non-stoichiometric PMN-35PT.[17] This porosity was then trapped in single crystal as it migrated through the matrix grains.

The possibility of trapped N_2 gas from annealing in air can likely be linked to the differences of p_{N2} in air ($\approx$ 0.2) and oxygen ($\approx$ 0.0). Organic-based gases such as CO and CO_2 can be attributed to the processing of the PMN-35PT-PbO powders in ethyl alcohol (see section 4.1.1). The potential decomposition of PbO is also ascribed to the processing of the PMN-35PT-PbO powders. Again referring to section 4.1.1, the organic residue is burned out at 450°C. However, at this temperature, PbO has been shown to transform to higher-level oxides, such as Pb_3O_4 and $Pb_{12}O_{19}$.[22,23] While hot-pressing allows the higher-level oxides to remain stable, pressureless annealing at temperatures between 1000 and 1200°C reverts oxides back to PbO. The result is a release of oxygen, which in turn can cause porosity formation in the matrix.[24]

2.1.3. Electromechanical Properties of SPC Grown Single Crystals

The ultimate goal of the Seeded Polycrystal Conversion process, of course, is to produce high quality ferroelectric single crystals. Figure 2.5 shows the mechanical strain-electric field behavior of (a) a grown single crystal compared to a polycrystalline matrix and (b) a single crystal grown in air compared to a single crystal grown in oxygen.
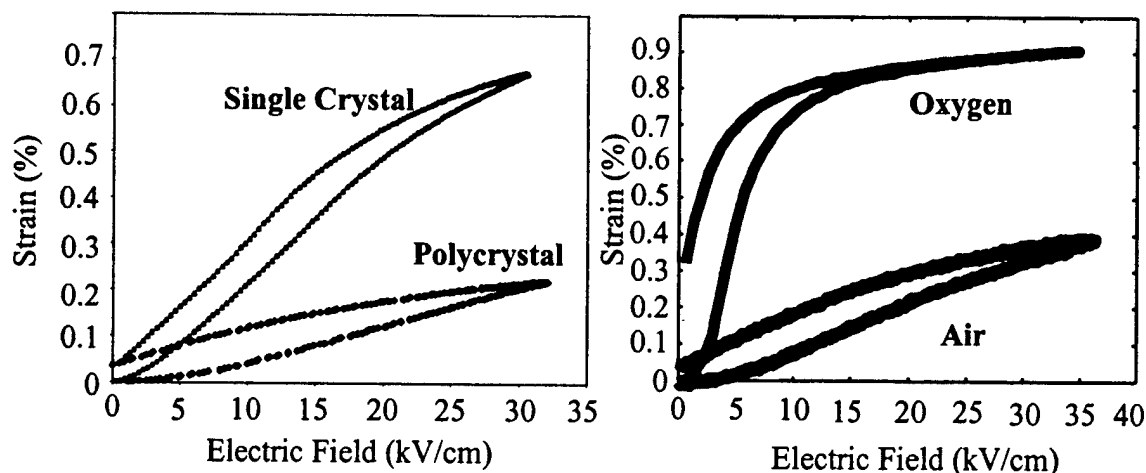
Figure 2.5. Plots of strain vs. electric field for PMN-35PT of (a) a grown single crystal compared to a polycrystalline matrix and (b) a single crystal grown in air compared to a single crystal grown in oxygen (plots courtesy of Adam Scotch).

The difference between the electromechanical properties of the single crystal and the polycrystalline matrix has been documented elsewhere.[4,5] However, the cause for the increased hysteresis and slightly higher strain behavior in the oxygen-sintered sample has been the focus of recent work. It is believed that the oxygen atmosphere slightly changes the stoichiometry of the grown crystal.[24] Referring to Figure 1.1, if the PbTiO$_3$ content is slightly increased in PMN-35PT single crystal, the properties exhibited will be characteristic of the tetragonal phase. The strain behavior reported in Figure 2.5 (b) is indeed representative of tetragonal PMN-PT single crystals, as reported elsewhere.[25]

It should be noted that the electromechanical properties of single crystals grown by the SPC process have matched or exceeded those grown by traditional methods discussed in section 1.1.[4,5,9] As mentioned in section 2.1.1, growth from {111} seeds causes excessive amounts of trapped PbO due to the fast migration rate. The properties reported in Figure 2.5 are from single crystals oriented in the <001> direction after

13

growth from {111} seeds. PbO is widely known to be deleterious to the electromechanical properties of PMN-PT.[26,2728] Therefore, it can be inferred that growth from {001} seeds, which traps less liquid phase, could potentially produce even more electromechanically superior single crystals.

2.1.4. Abnormal Grain Growth

The single crystal growth of PMN-35PT by Seeded Polycrystal Conversion discussed in the previous sections was mainly successful due to the large size disparity between the seed and matrix grains. However, one variable that could potentially hinder the single crystal growth process is the presence of abnormal grains. Abnormal grains, sometimes referred to as exaggerated grains, are typically classified as being several times larger than the size of the average matrix grain.[29] In the PMN-35PT system, abnormal grains have been shown to appear in samples with greater than 3 vol.% excess PbO sintered at temperatures higher than 1100°C.[17] Light optical micrographs showing the effect of PbO on the appearance of abnormal grains in PMN-35PT with 1.8 or 5 vol.% excess PbO after sintering for 4 hours at 1150° in oxygen are shown in Figure 2.6.
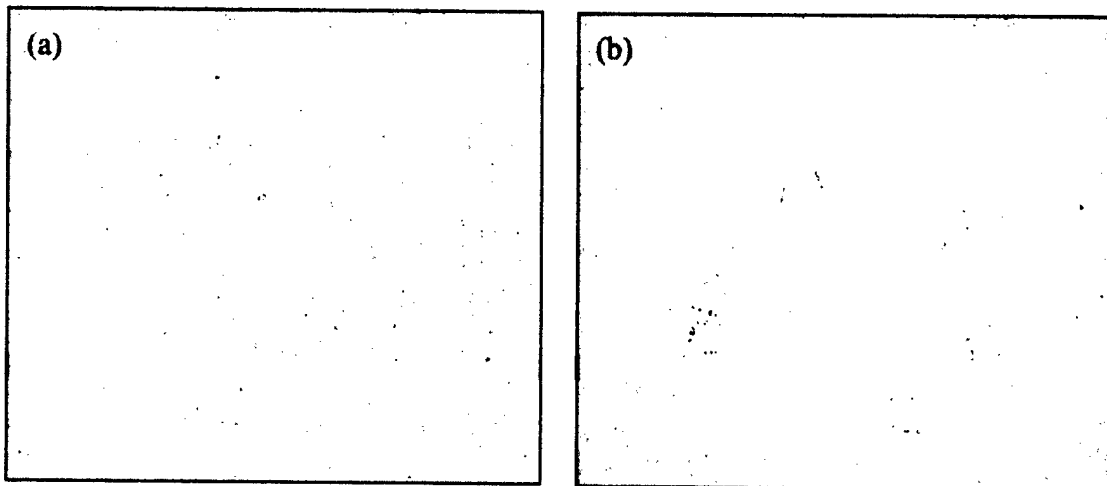
Figure 2.6. Light optical micrographs showing presence of abnormal grains dependence on PbO content in PMN-35PT with (a) 1.8 vol.% PbO and (b) 5 vol.% PbO after sintering for 4 hours at 1150° in oxygen (images courtesy of Adam Scotch).

It is clear from this study that the presence of abnormal grains has some dependence on the volume fraction of liquid phase present in the matrix. Recently, it has been shown that the abnormal grains in PMN-35PT are actually bi-crystals containing the $\Sigma 3$ boundary orientation.[17,30] Orientation imaging microscopy (OIM) was used to determine the orientation of both portions of the abnormal grain. As can be seen in Figure 2.7, the abnormal grain is composed of two different grains separated by a $\Sigma 3$ boundary.
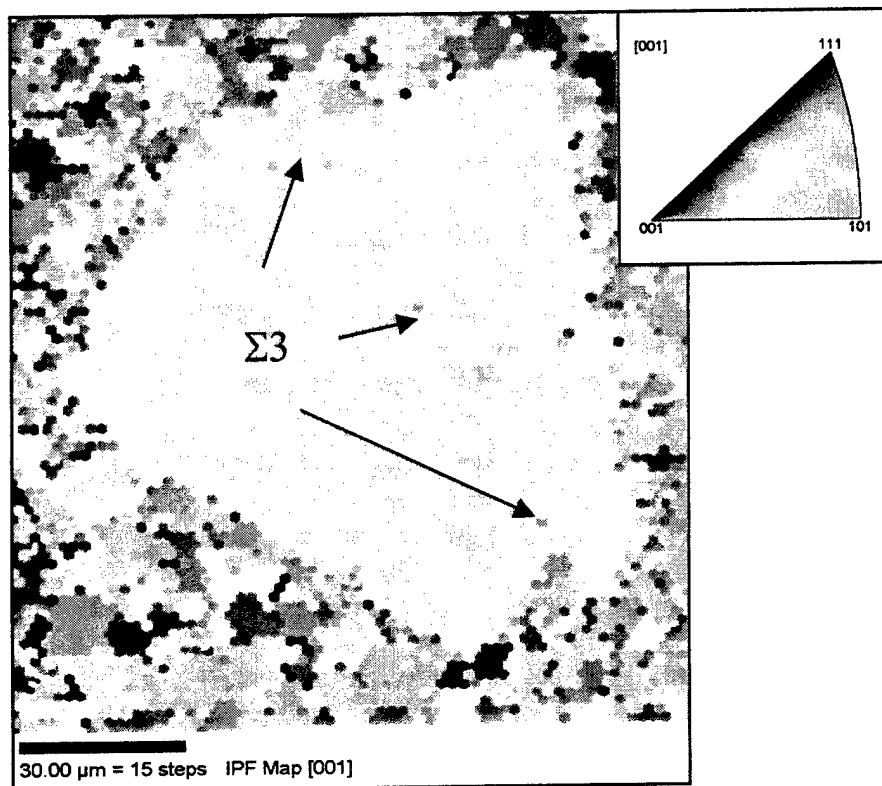
Figure 2.7. Orientation imaging microscopy (OIM) map showing the presence of a $\Sigma 3$ boundary in an abnormal grain in PMN-35PT + 5 vol.% PbO sintered for 1 hour at 1150°C in oxygen (image courtesy of Adam Scotch).

At the high sintering temperatures, there are presumably large amounts of grain rearrangement due to the presence of a liquid phase in the system. An increase in the volume fraction would aid this rearrangement process, thereby increasing the likelihood of two adjacent grains achieving this special boundary.[24] Once this orientation is achieved, the abnormal grains grow at the expense of the matrix grains. The bisecting angle between the two original grains is a <111> growing direction, which as shown in section 2.1.1, is the fastest growth direction for single crystal growth. This wedge orientation is retained throughout the sintering process, which was used to explain why abnormal grains continue initially grow at a fast rate.

16

Recent work, however, has actually shown that there appears to be no distinct advantage of abnormal grain growth compared to {001} single crystal growth.[31] In these studies, abnormal grains grown in PMN-35PT + 20 vol.% PbO were selectively etched out with HNO_3 as described in section 2.1.1. The abnormal grains were then reembedded in PMN-35PT + 3 vol.%, and the linear growth distances were quantified. The growth distances were roughly equivalent to those linear growth distances measured from 100 μm thick {001} single crystal seeds. While other studies have ascribed the presence of abnormal grains in PMN-35PT to a 2-D nucleation phenomenon,[32] it appears that the wedge shape of the bi-crystal may only have a size advantage at the early stages of growth.

Though no thorough analysis has been conducted, abnormal grains have been observed to impinge on the migration of the single crystal boundary. Figure 2.8 shows a single crystal grown from a {001} oriented seed into a matrix of PMN-35PT + 4 vol.% PbO that has been impinged by an abnormal grain. As mentioned in section 2.1.1, <001> is considered to be the slowest growth direction in the PMN-35PT system. The single crystal presumably has a lower driving force than the abnormal grain, which will grow at a faster rate than both the matrix and the single crystal. More on driving force and other related issues in liquid phase sintering will be discussed in section 2.2.

75 μm
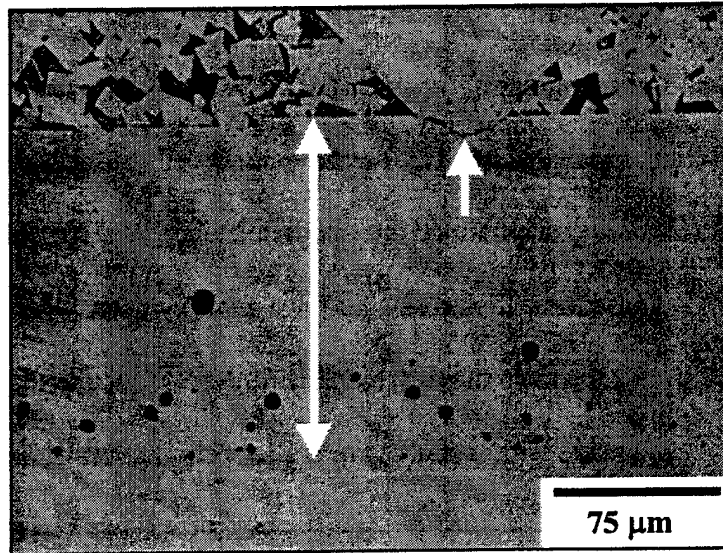
Figure 2.8. Light optical micrograph of {001}single crystal growth into PMN-35PT + 4 vol.% PbO matrix for 10 hours at 1150°C showing single crystal growth (double headed arrow) and boundary impingement by an abnormal grain (single headed arrow).

2.2. Liquid Phase Sintering

Liquid phase sintering is the process by which powder and sintering temperature are chosen such that a small amount of intergranular liquid is formed. The presence of a liquid phase provides for enhanced densification through: rearrangement of the grains and enhanced matter transport through the liquid.[33] For a successful sintering cycle, three main steps must be satisfied: (1) sufficient liquid must be present, (2) the solid must be at least partially soluble in the liquid, and (3) there is good wetting of the solid by the liquid phase.[34] In the Seeded Polycrystal Conversion process of PMN-35PT, PbO is added as the liquid phase. The PbO is assumed to be a persistent liquid phase, in that the volume of the liquid does not change appreciably with sintering (see section 4.1.5 for steps taken to ensure a persistent liquid phase). Sections 2.2.1 and 2.2.2 describe the three stages of liquid phase sintering and the phenomenon of grain growth, respectively.

18

2.2.1. Stages of Liquid Phase Sintering

Liquid phase sintering has classically been divided into three distinct stages of rate-controlling mechansims: (1) rearrangement of grains and liquid phase (initial stage), (2) solution-precipitation (intermediate stage), and (3) final pore removal (final stage).[35,36,37] These three distinct stages have actually been found to overlap in sintering practice. Figure 2.9 shows the approximate time scale for liquid phase sintering and the presence of each stage with respect to overall specimen density.
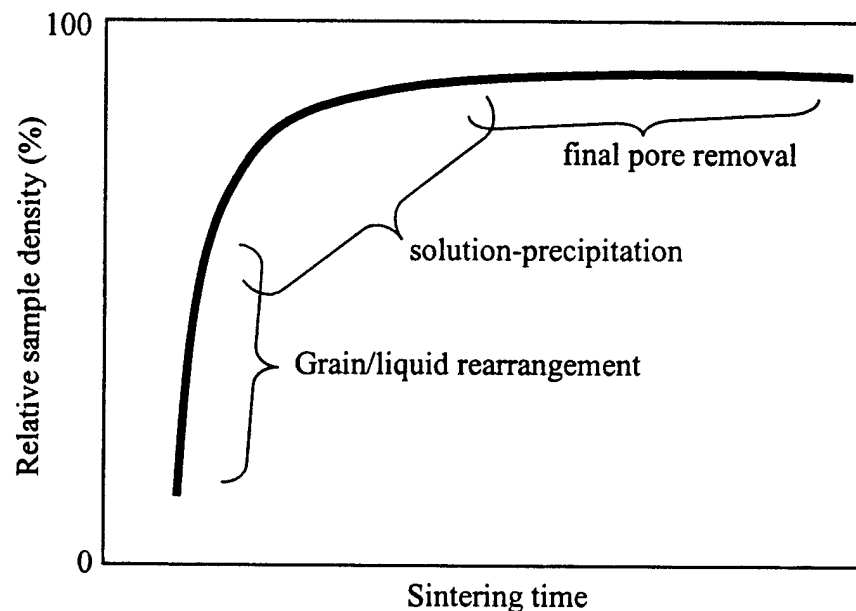
Figure 2.9. Approximate time scale for the three stages of liquid phase sintering. (After Huppmann[38]).

In the initial stage of liquid phase sintering, considerable rearrangement of both the matrix grains and the liquid phase takes place. There are two stages of rearrangement: primary rearrangement and secondary rearrangement.[39] In primary rearrangement, soon after the formation of the liquid phase at elevated temperatures, the liquid distributes itself between the grains and there is fragmentation of the polycrystalline particles. Secondary rearrangement involves the subsequent

19

rearrangement of these fragmented particles. Figure 2.10 shows the transition from liquid formation to primary arrangement to secondary arrangement.

primary rearrangement

penetration and fragmentation

secondary rearrangement
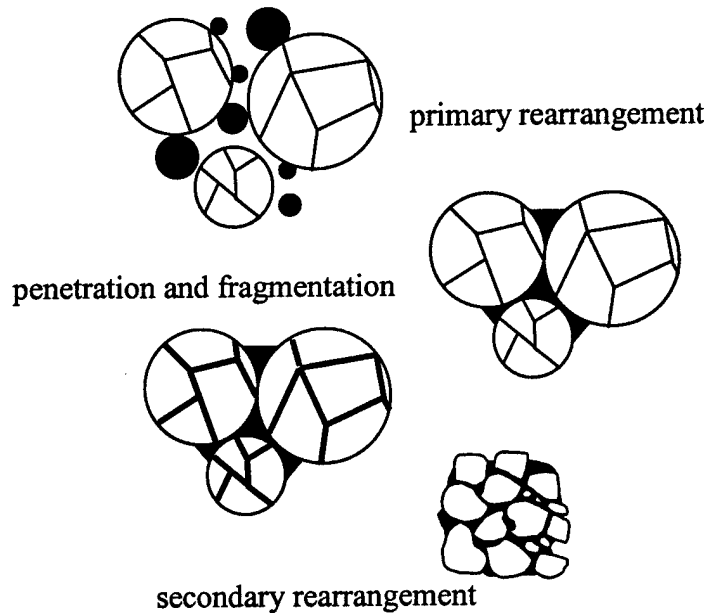
Figure 2.10. Schematic diagram showing the steps of rearrangement in liquid phase sintering. (After German.[39])

During the rearrangement stage, significant densification can occur, as can be seen in Figure 2.9. The capillary forces cause the liquid to redistribute into between the particles and into small pores, thereby increasing the density. Increasing amounts of liquid phase further increase the densification rate by enhancing the transport rate of the solid through the liquid.

The second stage of liquid phase sintering, solution-precipitation, overlaps with the end of the rearrangement stage. In this stage, densification continues to occur by either contact flattening or by Ostwald ripening. In contact flattening, the solubility at the contact points between two particles is higher than at any point on the surface of the solid. The result is a chemical potential gradient that leads to transportation of matter

away from the contact points, allowing the centers to approach one another.[40] Ostwald ripening involves the dissolution and precipitation of smaller grains onto larger grains.[41] This process occurs away from the contact points of two grains, thereby allowing for further densification. Schematic diagrams of the contact flattening and Ostwald ripening mechanisms are shown in Figures 2.11 and 2.12, respectively.
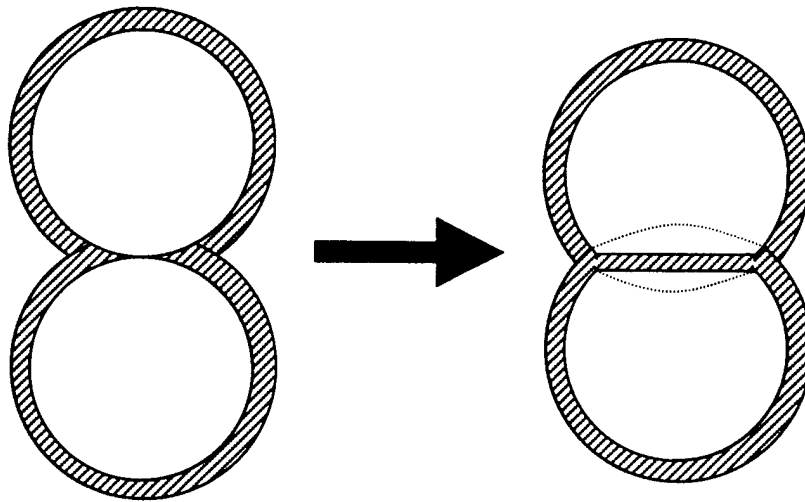
Figure 2.11. Schematic diagram of the contact flattening mechanism of solution-precipitation. (After Rahaman.[33])
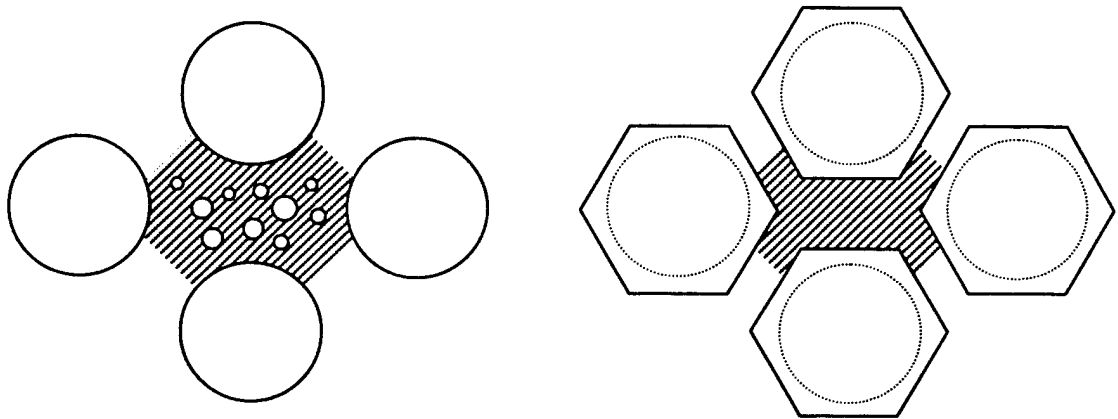
Figure 2.12. Schematic diagram of the Ostwald ripening mechanism of solution-precipitation. (After Rahaman.[33])

During the later stages of solution-precipitation, pore channels are pinched off to form isolated pores.[42,43] At this point, the last stage known as final pore removal begins. As the densification rate begins to slow, microstructural coarsening (grain growth) becomes the dominant rate-controlling mechanism and continues to dominate through the third stage of liquid phase sintering. Pore coarsening by Ostwald ripening has also been observed during this stage, and has been found to scale with grain growth.[35,44,45] The coarsening of pores is analogous to solution-precipitation controlled grain growth in that larger pores grow at the expense of smaller ones. The following section discusses more in depth the theories of grain growth.

2.2.2. Grain Growth

As mentioned in section 2.2.1, grain growth becomes significant during the final stage of liquid phase sintering. During this stage, two different processes can lead to coarsening: Ostwald ripening (Figure 2.12) and grain coalescence.

Ostwald ripening, as discussed in the previous section, occurs due to a distribution in grain sizes. The solubility of larger grains is less than that of smaller grains in the surrounding liquid. The resulting concentration gradient causes a transport of material from smaller grains to larger grains by diffusion. Thus, large grains grow at the expense of smaller matrix grains.

The kinetics of grain growth have been widely studied since the theoretical analysis proposed by Lifshitz, Slyozov, and Wagner, commonly referred to as the LSW theory.[46,47,48,49] The growth of the average grain size, G, with time, t, is given by

$$G^n - G_0^n = kt \qquad (2.1)$$

22

where G_0 is the average grain size at time t=0, n is the growth exponent, and k is a temperature-dependent parameter known as the growth constant. For most ceramic systems, a value of n=3 is typically observed. Theoretically, for the case of liquid phase sintering, a growth exponent of 2 is indicative of interface reaction-controlled grain growth, and an exponent of 3 indicates diffusion-controlled grain growth.

More exactly, the instantaneous grain growth rate dG/dt can be expressed by

$$\frac{dG}{dt} = 2v = 2MF_b \tag{2.2}$$

where v is the velocity of the migrating boundary, M is the mobility of the boundary, and F_b is the driving force dictated by the grain boundary curvature, r.

If diffusion through the liquid film of thickness f is the rate-limiting step for grain growth, the mobility (M_f) is defined as[50]

$$M_f = \frac{D_f C_f \Omega}{f k_B T} \tag{2.3}$$

where D_f is the diffusivity through the liquid film, C_f is the solubility of the grain in the liquid, Ω is the atomic volume, k_B is Boltzmann's constant, and T is temperature (K).

The driving force can be represented by

$$F_b = \frac{2\gamma}{r} \tag{2.4}$$

where γ is the interfacial surface energy and r is the grain boundary curvature. Assuming that the liquid film thickness is dependent on the average grain size, it is clear that integration of equation 2.2, after substituting equations 2.3 and 2.4 into equation 2.2, yields cubic (n=3) grain growth kinetics.

23

If the migration of the single crystal is controlled by interface reaction, the mobility term is defined as[50]

$$M_s = \frac{\Gamma \Omega}{k_B T} \qquad (2.5)$$

where Γ is a constant exponentially dependent on temperature, and the other parameters are identical to those described for equation 2.3. Integrating after substitution of equations 2.4 and 2.5 into equation 2.2 yields parabolic (n=2) grain growth kinetics.

Grain coalescence is a phenomenon that may also lead to grain growth. When two grains come together to a form a contact, the grains attempt to form the lowest energetic state by eliminating the interface. The interface between the grains can be thought of as a grain boundary. In this way, the boundary can be envisioned to migrate by solid-state diffusion. The driving force is thus the difference in the grain boundary curvature, r, and the larger grain will eventually overcome the smaller grain.[51]

2.3. Kinetic Model for Single Crystal Growth

Leite *et al.* developed a model that describes a single crystal growing into a polycrystalline matrix to analytically explain the growth behavior in the Seeded Polycrystal Conversion process.[52] The model was based on earlier work by Thompson related to abnormal grain growth in thin films.[53] This model is used as the basis for the calculated results presented in section 6.2, which discuss the effects of starting matrix particle size and PbO content on the migration of the single crystal. Following is a description of the modeled problem:

An oriented {001} single crystal seed is bonded to a dense polycrystalline matrix comprised of an array of tetrakaidecahedron or cubic grains with edge length l_p.

24

The matrix morphology will be determined by the fraction of liquid phase in the matrix. Single crystal growth is assumed to occur only in the x direction, as shown schematically in Figure 2.13.
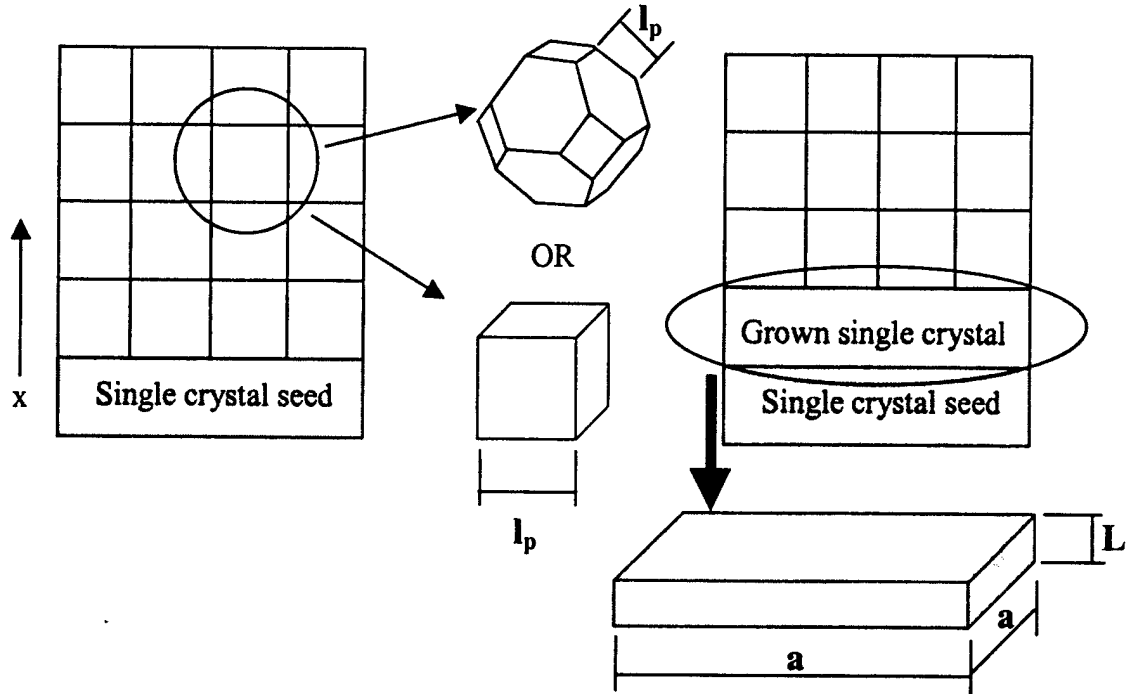
Figure 2.13. Schematic diagram of the modeled problem for single crystal growth into a polycrystalline matrix. (After Leite.[52])

2.3.1. Driving Force

The driving force for grain boundary migration is evaluated by considering the grain boundary energy and surface energy anisotropy ($\Delta\gamma$). In this model, $\Delta\gamma$ is defined as

$$\Delta\gamma=\gamma_a - \gamma_{min} \tag{2.6}$$

where γ_a is the average surface energy per unit area and γ_{min} is the surface energy of the {001} oriented single crystal. The total grain boundary energy per unit volume (E) is given by

25

$$E=NA_{gb}\gamma_{gb} \tag{2.7}$$

where N is the number of grains per unit volume, A_{gb} is the grain boundary area, and γ_{gb} is the surface energy of the grain boundary. After the growth process, the resulting single crystal will have dimensions a and L (Figure 2.13).

The initial energy before single crystal growth (E_i) and the final energy after single crystal growth (E_f) are defined as

$$E_i = \frac{a^2\gamma_a + Na^2LA_{gb}\gamma_{gb}}{a^2L} \tag{2.8}$$

$$E_f = \frac{a^2\gamma_{min} + (a^2 + 4aL)\gamma_{gb}}{a^2L} \tag{2.9}$$

Assuming a >> ΔL, the energy variation during the single crystal growth process is

$$\Delta E = E_f - E_i = -\frac{\Delta\gamma}{L} + \frac{\gamma_{gb}}{L} - NA_{gb}\gamma_{gb} \tag{2.10}$$

For a polycrystalline matrix composed entirely of tetrakaidecahedron grains of size l_p,

$$N = 3/\sqrt{2}\cdot l_p^3 \tag{2.11}$$

and

$$A_{gb} = (6\sqrt{3} + 3)\cdot l_p^2 \tag{2.12}$$

with a corresponding average grain size, G

$$G = 2\sqrt{2}\cdot l_p \tag{2.13}$$

Similarly, for a matrix composed of cubic grains of size l_p, the geometric parameters are

$$N = l_p^{-3} \tag{2.14}$$

$$A_{gb} = 3\cdot l_p^2 \tag{2.15}$$

$$G = l_p \qquad (2.16)$$

2.3.2. Single Crystal Migration

The motion of the single crystal boundary into the polycrystal can be written similar to that of grain boundary migration in equation 2.2 by

$$v_x = M_b \Delta E \qquad (2.17)$$

where v_x and M_b are the velocity and mobility of the migrating crystal, respectively. If it is assumed that the boundary velocity is proportional to the instantaneous rate of single crystal growth ($v_x = 1/2 \; dL/dt$), inserting the geometric parameters of equations 2.11 through 2.16 into equation 2.10 gives

$$\frac{dL}{dt} = 2M \left[\frac{-\Delta\gamma}{L} - \frac{80.3\gamma_{gb}}{G} + \frac{\gamma_{gb}}{L} \right] \qquad (2.18)$$

for a tetrakaidecahedron matrix, and

$$\frac{dL}{dt} = 2M \left[\frac{-\Delta\gamma}{L} - \frac{3\sqrt{3}\gamma_{gb}}{G} + \frac{\gamma_{gb}}{L} \right] \qquad (2.19)$$

for a cubic matrix.

In the presence of a liquid phase, the migration of the single crystal is governed either by the diffusion through the liquid film or by the interface reaction, as described in equations 2.3 and 2.5. These equations can subsequently be substituted into equations 2.18 or 2.19 to calculate the instantaneous rate of single crystal growth.

3. STATEMENT OF PURPOSE

The objective of this research is to quantitatively analyze the single crystal and matrix kinetics of $Pb(Mg_{1/3}Nb_{2/3})O_3$-35mol%$PbTiO_3$ (PMN-35PT) in the Seeded Polycrystal Conversion (SPC) process. Specifically, the effect of liquid phase (PbO) additions on the kinetics of both the matrix and the single crystal will be systematically evaluated. An existing kinetic model will be enhanced and adapted to assess the effects of PbO content and starting matrix particle size on the SPC process. By systematically evaluating the effects of these factors on the single crystal growth, the process can hopefully be optimized to produce high quality single crystals in the most time-efficient and cost-effective manner.

4. EXPERIMENTAL PROCEDURE

4.1. Processing

4.1.1. Powder Preparation

$Pb(Mg_{1/3}Nb_{2/3})O_3$-35mol%$PbTiO_3$ (PMN-35PT) powder (TRS Ceramics, State College, PA) was add-mixed with PbO[§] (Alfa Aesar, Ward Hill, MA) in various amounts from 0 to 5 vol.% PbO using a balance with 0.00001 g resolution (Mettler H-51, Hightstown, NJ). Prior to shipment from the manufacturer, the PMN-35PT powder was calcined. The PMN-35PT-PbO powders were milled in batches of 25 grams for 24 hours with a jar mill in ethanol using 100 grams of 3 mm diameter ZrO_2 milling media (Tosoh, Tokyo, Japan) in 125 mL polyethylene bottles (Nalge, Rochester, NY).

After milling, the powders were distilled under vacuum in a 2000 mL boiling flask (C.S. Glass, Malaga, NJ) using a rotoevaporator (Büchi R-124, Switzerland) in a waterbath (Büchi B-481, Switzerland) at approximately 68°C. The powders were subsequently placed in covered 10 cm diameter Al_2O_3 crucibles (Vesuvius, Beaver Falls, PA) and heated to 450°C for 4 hours in air using a standard box furnace (Carbolite, Sheffield, England) to remove any organic residue. Finally, the powders were ground using an agate mortar and pestle (Fisher Scientific, Pittsburgh, PA) and sieved with a 100-mesh sieve (VWR Scientific, West Chester, PA) using a sieve auto-shaker (CSC Scientific, Fairfax, VA). A total of 5 powder batches were produced using the methods described above. Excess PbO contents of 0, 1.5, 3, 4 and 5 vol.% PbO were added to PMN-35PT.

[§] purity > 99.999% (metals basis)

4.1.2. Powder Characterization

Upon receipt of the PMN-35PT powder, x-ray diffraction was conducted to ensure phase purity. A small amount of the starting PMN-35PT powder was chemically tested using inductively coupled plasma-optical emission spectroscopy (ICP-OES) using lithium borate fusion and dissolution (NSL Analytical Services, Inc., Cleveland, OH). The percentages of relevant elements compared to the respective theoretical stoichiometric ratios are shown in Table 4.1. It should be noted that all three of the non-lead cations (magnesium, niobium, and titanium) are present in levels lower than their respective theoretical compositions. This indicates that the starting powder may be somewhat more PbO-rich than the stoichiometric relation suggests. The implications of this effect will be discussed in depth in section 5.3. The average particle size of each powder batch was determined using a laser scattering particle size distribution analyzer (LA-910, Horiba, Tokyo, Japan). The mean particle sizes for all batches are listed in Table 4.2.

Table 4.1. ICP-OES elemental testing analysis results and comparison with the theoretical elemental composition of PMN-35PT.

Element	Testing Analysis (wt. %)	Theoretical (wt. %)
Mg	1.47	1.66
Nb	11.26	12.68
Ti	4.68	5.28

Table 4.2. Mean particle size for all processed powders as measured by a laser scattering particle size distribution analyzer.

PbO Content	Mean Particle Size (μm)
0.0	0.77 ± 0.04
1.5	0.81 ± 0.05
3.0	0.74 ± 0.04
4.0	0.75 ± 0.05
5.0	0.76 ± 0.06

4.1.3. Specimen Fabrication

Oriented {001} PMN-PT single crystal seeds (Crystal Associates, East Hanover, NJ) were sectioned into smaller seeds with approximate dimensions of 3 mm x 3 mm x 0.5 mm using a high speed diamond cut-off saw (Acutom, Struers, Cleveland, OH). Each seed was then embedded in approximately 3 grams of the PMN-35PT powders described in section 4.1.1. The powders were subsequently uniaxially pressed (Model M, Carver, Menomonee Falls, WI) at 10 MPa in an Al_2O_3 die to make pellets nominally 13 mm in diameter and 3 mm in height. These pellets were then vacuumed sealed in latex gloves (DGP-350, Microflex, Reno, NV) and cold isostatically pressed at 340 MPa for two minutes.

4.1.4. Hot-Pressing of Specimens

The cold isostatically pressed pellets were embedded in 3 grams of coarse Al_2O_3 release powder in a 13 mm diameter Al_2O_3 die. The pellets were subsequently pressed in a hot-press (Thermal Technologies, Santa Rosa, CA) at 20 MPa for 30 minutes. The hot pressing temperature for samples with 0 vol.% excess PbO was 900°C. This temperature was lowered to 880°C for all samples with excess PbO to reduce volatilization of the liquid phase.

After hot pressing, each specimen was sectioned into eight equivalent pie pieces using a high-speed diamond cut-off saw (Acutom, Struers, Cleveland, OH). Figure 4.1 shows a schematic diagram of seed orientation inside the final specimen. Once sectioned, each specimen piece was ultrasonically flushed in beakers of acetone, ethyl alcohol, and deionized water, respectively, for 30 minutes each.

Profile   Top view
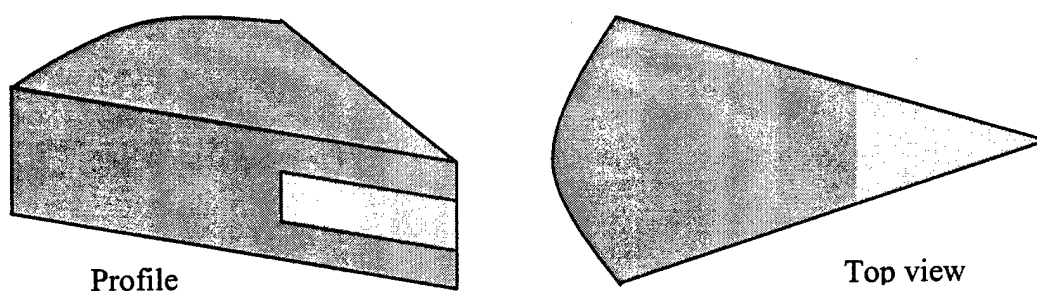
Figure 4.1. Schematic diagram showing orientation of {001} oriented single crystal seed within the polycrystalline wedge-shaped matrix.

4.1.5. Annealing of Specimens

Each specimen was weighed prior to annealing using a balance with 0.00001 g resolution (Mettler H-51, Hightstown, NJ). The specimen, wrapped in a 0.002 mm thick platinum foil pouch (VWR Scientific, West Chester, PA), was embedded in approximately 5 grams of PMN-35PT powder with 5 vol.% PbO excess over the amount of PbO in the specimen. The packing powder was selected so that the activity mimicked that of the nearly 100% dense sample, as done in previous studies.[16] For example, a specimen with a matrix composed of PMN-35PT + 3 vol.% PbO was embedded in PMN-35PT + 8 vol.% PbO. The sacrificial packing powder was used to

help the specimen maintain its weight throughout the annealing cycle. The packing powder was compacted manually to achieve a more dense green sample.

The specimen and packing powder were embedded in a double crucible arrangement. The 16 mm diameter inner Al_2O_3 crucible (CoorsTEK, Golden, CO) was inserted face down inside a covered outer Al_2O_3 crucible (CoorsTEK, Golden, CO). Figure 4.2 shows a schematic diagram of the double crucible arrangement used for all annealing treatments.
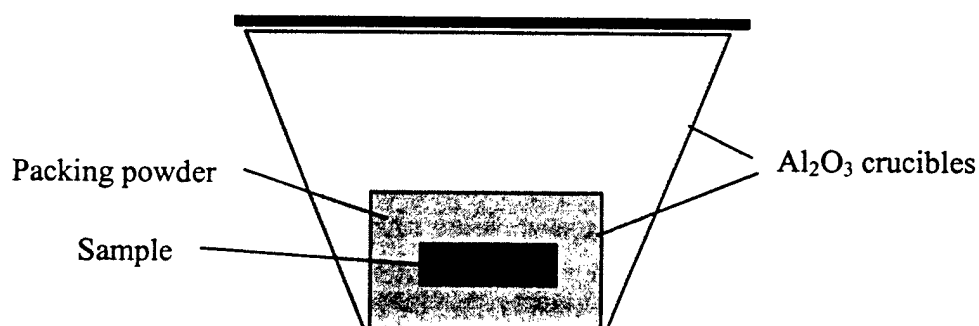
Figure 4.2. Schematic diagram showing double crucible arrangement used for all annealing treatments.

The specimens were then annealed for 0 to 10 hours (time at temperature) at 1150°C in an air atmosphere. The annealing treatments were conducted in a standard box furnace (Carbolite, Sheffield, England). After annealing, the weight of each specimen was again measured, and the percentage weight loss or weight gain was determined by

$$\Delta w = \frac{w_f - w_o}{w_o} \tag{4.1}$$

33

where Δw is the percentage change in weight, w_f is the final weight (grams), and w_o is the initial weight (grams). Only samples with weight changes of less than $\pm$ 0.5 wt.% were deemed acceptable for the experimental results presented in section 5.2.

4.2. Characterization

4.2.1. Density Measurements

The density of each hot pressed sample and annealed sample was determined by the Archimedes method. The dry weight of each specimen, W_D was measured using a balance with 0.00001 g resolution (Mettler H-51, Hightstown, NJ). Each specimen was then placed in a beaker of deionized water containing 0.01 wt.% wetting agent (Brij-35, Fisher Scientific, Pittsburgh, PA), and pumped in a desicator for 40 minutes and backfilled with air. Nylon fishing line was used to suspend the specimen in the beaker. The immersed weight, W_{im}, and the dry weight of the line, W_L, were also measured. Lastly, the surface of the specimen was dried with a damp paper towel, and the impregnated weight, W_W, was measured. Figure 4.3 is a schematic diagram showing the relevance of each of the measured weights. The density of each specimen was then calculated by

$$\rho = \frac{W_D - W_L}{(W_{im} - W_W)}\rho_{H2O} \tag{4.2}$$

where ρ is the density of the specimen (g/cm^3), and ρ_{H2O} is theoretical density of water at the temperature measured.[54] The percentage relative density of each specimen is

$$\rho_{rel} = \frac{\rho}{\rho_{theor}} \cdot 100 \tag{4.3}$$

34

where ρ_{rel} is the percentage relative density, ρ is the density of the specimen (g/cm^3),

and ρ_{theor} is the theoretical density of the PMN-35PT, 8.13 g/cm^3.
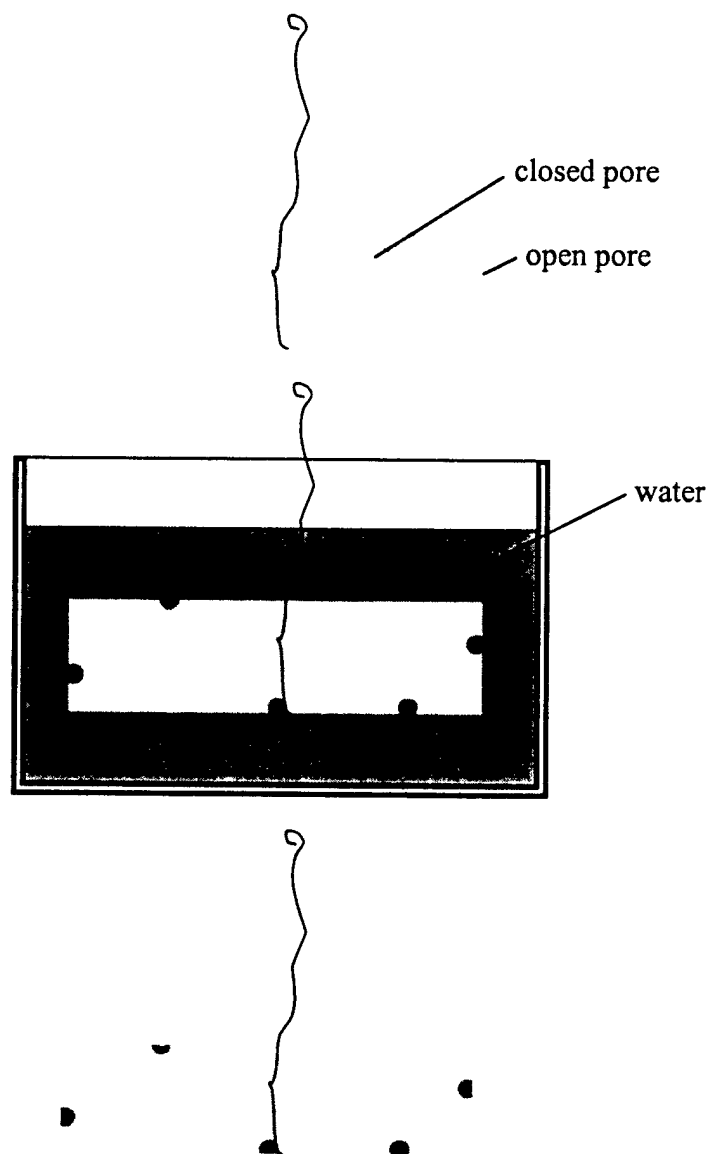
Figure 4.3. Schematic diagrams of different measurements for calculating density using the Archimedes method (After Dong.[34])

4.2.2. Microscopy

Each annealed specimen, and one hot pressed specimen from each powder composition, was mounted in epoxy resin (Leco, St. Joseph, MI). The specimens were then ground with 600 grit SiC paper (Struers, Cleveland, OH) using an automatic polisher (Abrapol, Struers, Cleveland, OH). The specimens were subsequently polished using 9, 3, and 1 μm diamond paste (Hyprex, Engis, Wheeling, IL) on a DAC polishing cloth (Struers, Cleveland, OH) using an oil lubricant (Hyprez W Lubricant, Engis, Wheeling, IL). The specimens were then vibratory polished with 1 μm diamond and 0.05 μm SiO_2 (Buehler, Lake Bluff, IL). When necessary, the specimens were chemically etched with Kroll's reagent (1% HF, 4 % HNO_3, 95% H_2O, % by volume) to reveal grain boundaries.

Photomicrographs of each hot-pressed and annealed specimen were recorded using either a light optical microscope (Reichert-Jung MeF3, Excel, Enfield, CT) or an environmental scanning electron microscope (Phillips XL-30, Hillsboro, OR). If deemed necessary, Nomarski techniques were used to provide visual distinction between the single crystal and the polycrystalline region in light optical micrographs. All images recorded with the scanning electron microscope were captured with uncoated specimens using a 20 kV accelerating voltage and a water vapor pressure of 0.3 torr.

4.2.3. Stereological Measurements

4.2.3.1. Average Matrix Grain Size Measurements

The average matrix grain size of each annealed sample was measured by the feret method using an automated image analysis system (Leco 3001, St. Joseph, MI). The feret method measures the perpendicular distance between two parallel lines drawn tangentially to the grain boundaries. Ten fields were recorded with a scanning electron microscope (Phillips XL-30, Hillsboro, OR) for each sample. The magnification of each field image was determined by using a non-traceable magnification standard (MRS-3, Geller Microanalytical, Topsfield, MA). The grain boundaries were subsequently traced and eight ferets were measured for each grain. The ferets were measured in increments of 22.5° in the range of 0 to 157.5° to obtain a feret average for each grain. Approximately 1000 grains for each specimen were analyzed. The average grain size for each specimen was calculated by multiplying the feret average mean by a conversion factor of 1.56 to convert from a two-dimensional planar value to a three-dimensional value.[55] The feret method was used because it allowed for easy exclusion of pores and prior liquid phase that were not part of the average matrix grain size.

4.2.3.2. Linear Single Crystal Growth Measurements

The average linear single crystal growth in each annealed specimen was measured using an automated image analysis system (Leco 3001, St. Joseph, MI). The measurements were calibrated using a stage micrometer (Olympus, Melville, NY). To eliminate any sectioning effects, each measurement was normalized by determining the

cross-sectional thickness of the seed with respect to the original seed thickness (500 μm) by

$$\Delta L = 500 \cdot \Delta L_m / S \tag{4.4}$$

where ΔL is the normalized single crystal growth (μm), ΔL_m is the measured single crystal growth (μm), and S is the cross-sectional thickness of the seed (μm).

The single crystal growth was assumed to be the distance between the first sign of porosity and the crystal/matrix interface. Annealing in air, as described in section 2.2.3, yields porosity in the grown crystal due to the transformation of PbO to higher oxides. A schematic diagram of the measured single crystal growth is shown in Figure 4.4. Since the crystallographic orientation of the seed "sides" may be different than the polished "top" and "bottom" surfaces, the single crystal growth was only measured from these two faces. Ten measurements were recorded for the top face and ten measurements were recorded for the bottom face.
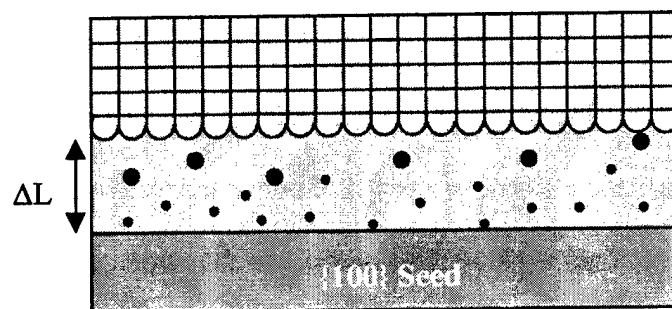
Figure 4.4. Schematic diagram showing the use of porosity in the grown single crystal to measure the growth distance (ΔL).

5. GROWTH KINETICS OF THE PMN-35PT SYSTEM

5.1. Introduction

The following sections present experimental results on the growth kinetics of the PMN-35PT system with PbO additions from 0 to 5 vol.%. Section 5.2.1 presents microstructural observations observed for the matrix grains for a variety of PbO contents. The kinetics of the grown single crystal and the corresponding matrix grains as a function of PbO content are presented in sections 5.2.2 and 5.2.4, respectively. Sections 5.2.3 and 5.2.5 describe quantitative results of the effect of annealing temperature on single crystal and matrix growth, respectively.

5.2. Results

5.2.1. Microstructural Observations

Microstructures of the PMN-35PT matrix grains after annealing for 5 hours at 1150°C are shown for various liquid phase contents in Figure 5.1. As the liquid phase fraction was increased, there was a noticeable transition from equiaxed to faceted matrix grains. These changes in grain morphology, which also increased with longer anneal times, were met by a greater amount of boundary wetting.

There is also a noticeable effect of PbO on the average matrix grain size. At 0 vol.%, the grains are very small, approximately 5 μm. A significant amount of grain growth occurs as the PbO content is increased to 3 vol.%, and there appears to be a decrease in the average grain size as the liquid fraction is increased to 5 vol.%.

Figure 5.2 shows the effect of PbO on PMN-35PT single crystal growth after annealing for 5 hours at 1150°C. Similar to the matrix microstructures in Figure 5.1,

39

there appears to be an increase in single crystal growth up to 3 vol.% PbO, before decreasing or leveling off when the liquid phase amount is increased to 5 vol.%. The growth front of the {001} oriented single crystal seed remained uniformly planar along the length of the seed. The larger porosity towards the edges of the grown single crystal growth is indicative of matrix coarsening during the annealing treatments. While it is possible that the porosity may have slightly hindered the single crystal migration, the presence of porosity was advantageous in this study, as it was used as a reference marker for the onset of single crystal growth.
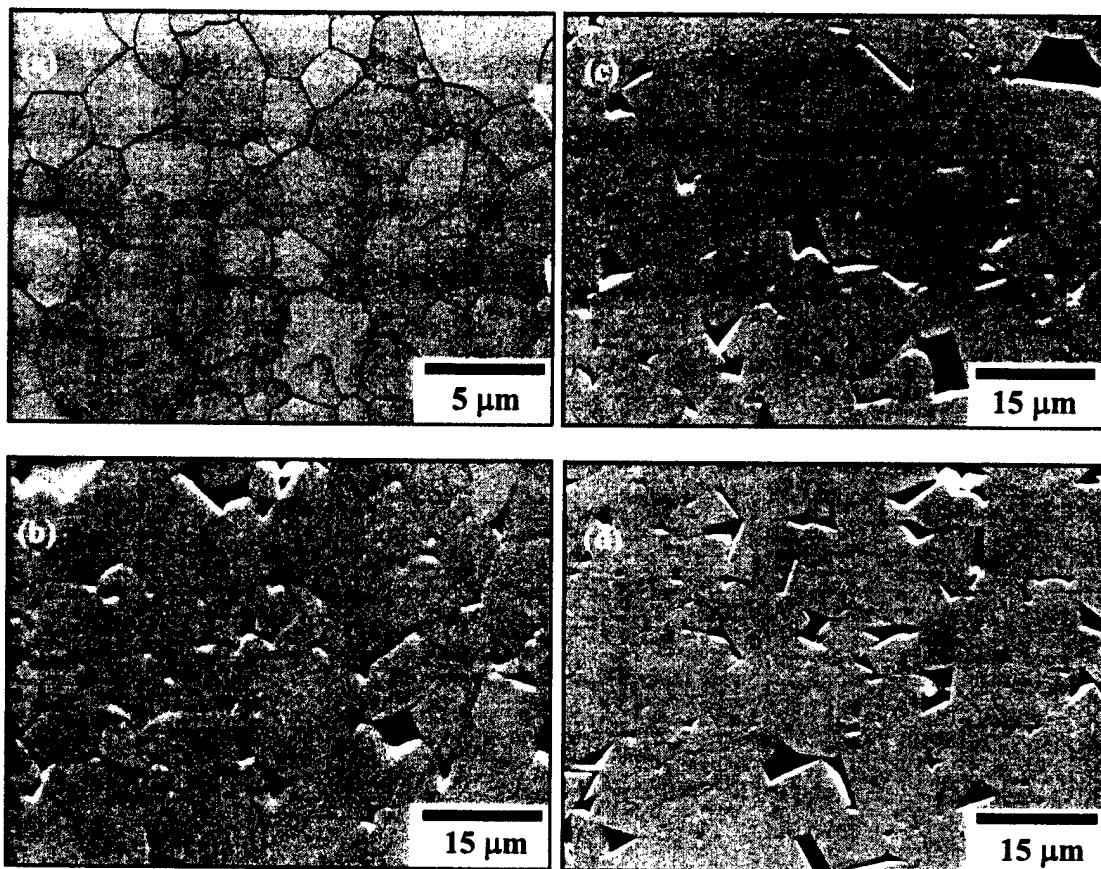
Figure 5.1. SEM micrographs of PMN-35PT matrix grains annealed for 5 hours at 1150°C for (a) 0.0 vol.%, (b) 1.5 vol.%, (c) 3.0 vol.%, and (d) 5.0 vol.% PbO additions.
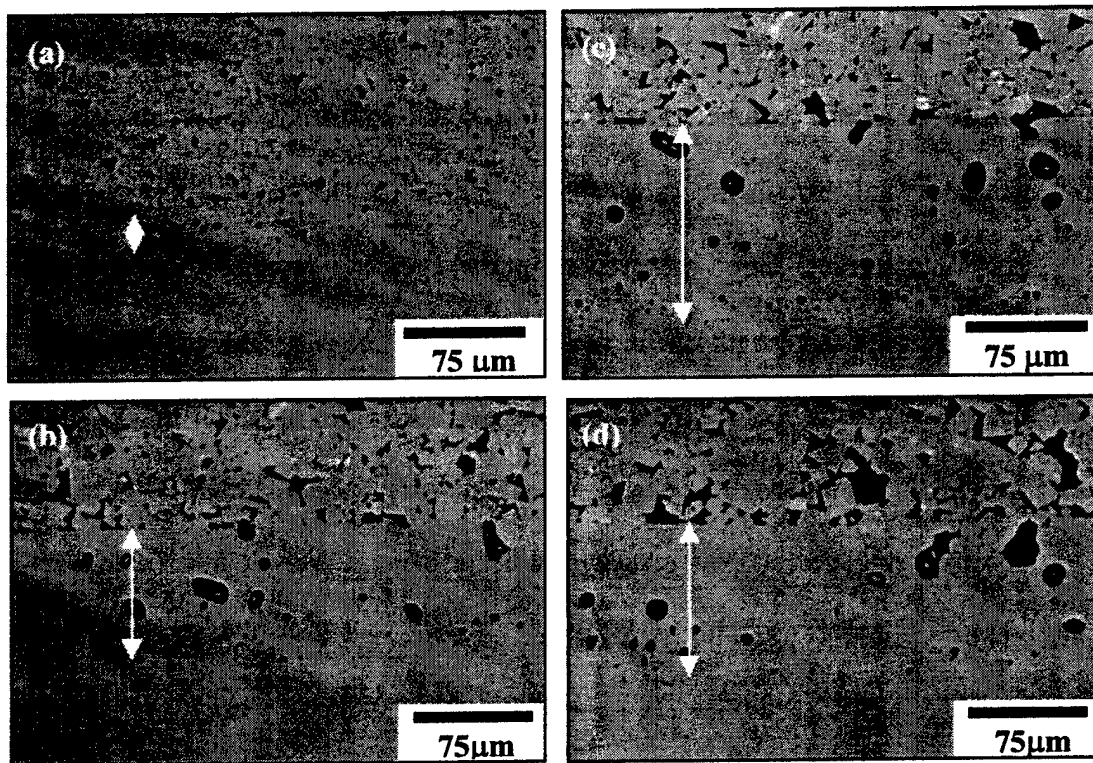
Figure 5.2. Light optical micrographs of PMN-35PT single crystal migration annealed for 5 hours at 1150°C for (a) 0.0 vol.%, (b) 1.5 vol.%, (c) 3.0 vol.%, and (d) 5.0 vol.% PbO additions.

5.2.2. Effect of Liquid Phase Fraction on Single Crystal Growth

Figure 5.3 shows plots of single crystal growth data for all of the studied compositions. These data were fitted to a crystal growth law of the form

$$\Delta L^n = kt \qquad (5.1)$$

where the kinetic parameters are identical to those in equation 2.1, and ΔL is the linear single crystal growth measured from the onset of porosity to the polycrystal/single crystal interface. Error bars represent the standard deviation of ten measurements recorded over the length of the single crystal. A cubic crystal-growth law $(n=3)$[e] was determined to fit best for all matrix compositions. An apparent maximum k value of 2.43×10^{-13} m^3/hr was also observed for PMN-35PT + 3 vol.% PbO. A summary of all observed single crystal and matrix growth constants is presented in Table 5.1.
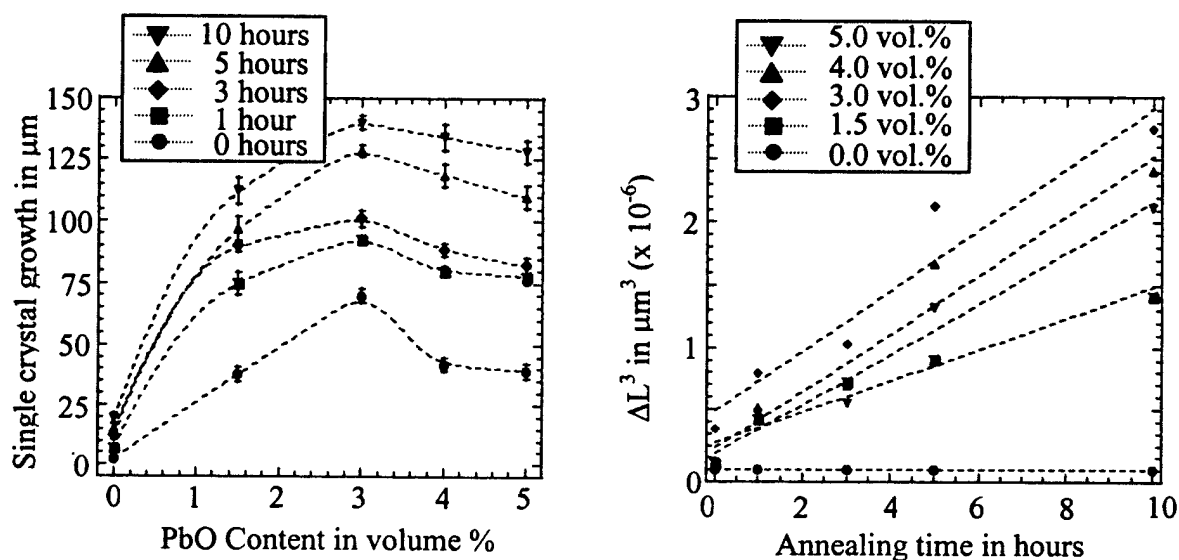
Figure 5.3. Single crystal kinetics of PMN-35PT with PbO additions from 0-5 vol.% annealed at 1150°C.

---

[e]Correlation factors for a cubic single crystal growth law were 0.99, 0.97, 0.96, 0.98, and 0.96 for 0.0, 1.5, 3.0, 4.0, and 5 vol.% PbO additions, respectively.

Table 5.1. Comparison of experimental growth constants for matrix and single crystal.

	Growth Constant, k (m^3/hr)	
Vol. % PbO	**Matrix**	**Single Crystal**
0.0	0.01 x 10^{-15}	0.73 x 10^{-13}
1.5	1.51 x 10^{-15}	1.25 x 10^{-13}
3.0	2.73 x 10^{-15}	2.43 x 10^{-13}
4.0	0.72 x 10^{-15}	2.33 x 10^{-13}
5.0	0.39 x 10^{-15}	2.02 x 10^{-13}

5.2.3. Effect of Liquid Phase Fraction on Matrix Grain Growth

Plots of average grain size versus anneal time at 1150°C for PbO contents from 0-5 vol.% are shown in Figure 5.4. These data were fitted to the grain-growth law of equation 2.1 where t is the annealing time in hours, n is the growth exponent, and k is the temperature-dependent growth constant in m^3/hr. Error bars presented in the plots were calculated from the standard deviation of each of the ten fields used for feret average measurement with respect to the overall grain size average. Once again, a cubic grain-growth law (n=3)[#] was determined to fit best for all matrix compositions studied. An apparent maximum k value of 2.73 x 10^{-15} m^3/hr was observed for PMN-35PT + 3 vol.% PbO.

In certain instances, particularly in matrix compositions > 3 vol.% PbO and annealing times longer than 5 hours, abnormal grain growth was observed. Recent

results have shown that these abnormal grains in PMN-35PT are actually two grains joined by a Σ3 boundary, as discussed in section 2.1.4.[17,30] The increased amount of boundary wetting from larger amounts of liquid phase is believed to enhance the probability of two grains achieving this special orientation. The abnormal grains were therefore excluded from average grain size calculations. Additionally, the penetration of any abnormal grains into the grown single crystal region was not included in the growth measurements presented in Figure 5.8.
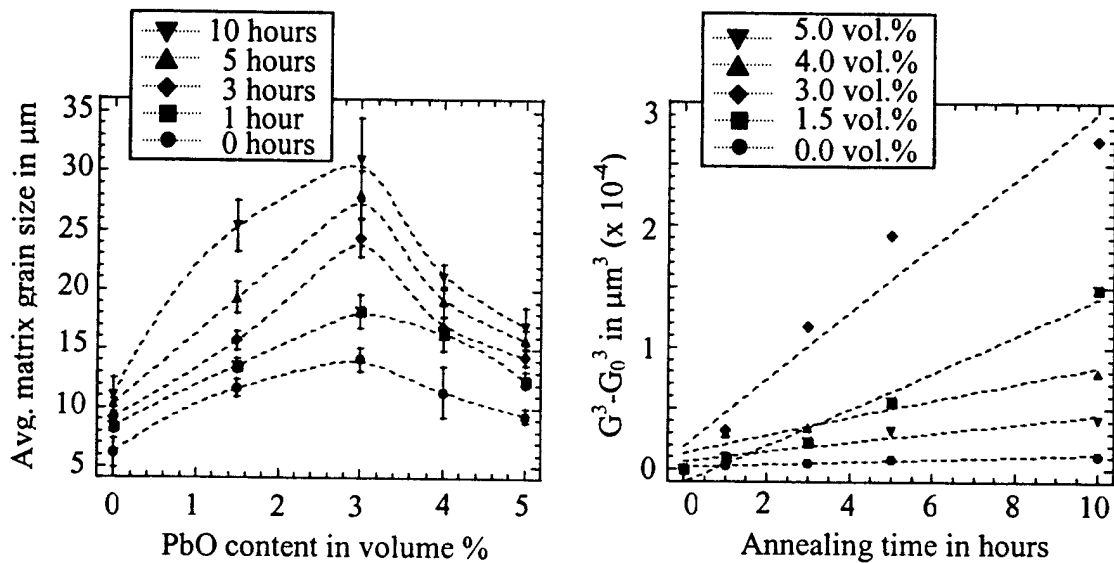
Figure 5.4. Grain-growth kinetics of PMN-35PT with PbO additions from 0-5 vol.% annealed at 1150°C.

5.3. Discussion

It is clear from Figure 5.1 that as the PbO volume fraction was increased, there was a marked transition from equiaxed to faceted matrix grains. Additionally, longer annealing times for the 3 and 4 vol.% PbO samples produced a more faceted

---

[#] Correlation factors for a cubic grain growth law were 0.95, 0.98, 0.97, 0.96, and 0.95 for 0.0, 1.5, 3.0, 4.0, and 5 vol.% PbO additions, respectively.

morphology. This implies that the matrix morphology has a strong dependence on the average liquid film thickness between grains at the annealing temperature. At larger grain sizes, the reduced surface area of the grains causes an increase in the average amount of liquid separating two grains. When a grain is completely surrounded by the liquid phase at the annealing temperature, it is believed that the solid-liquid surface energy dictates the faceted grain morphology in the PMN-35PT system.

Intergranular porosity developed during annealing due to trapped insoluble gases (N_2, CO, CO_2), the decomposition of PbO, and/or the evolution of oxygen from non-stoichiometric PMN-35PT.[17] Porosity was also entrapped in the grown single crystal during migration through the matrix grains (Figure 5.2). As there is no indication of pore drag in the grown single crystals, it is believed that the presence of the porosity most likely did not hinder the single crystal growth rate during the annealing process. The porosity, however, may help to explain the initial increase in both matrix and single crystal growth rates at low PbO volume fractions.

As can be seen in Table 5.1, the growth constants, k, increased with PbO content from 0 to 3 vol.%. While the samples were hot-pressed to essentially full theoretical density during processing, dedensification up to approximately 10% (Figure 5.7) occurred during the ramping stages of the annealing treatment (0 hours). Previous studies on the growth kinetics of porous Al_2O_3 and c-ZrO_2 in the presence of a liquid phase (anorthite) showed an increase in growth rate with an increase in liquid content for low liquid volume fractions.[56] The authors attributed the increase in growth rate to an increase in pore mobility for a system in which pore-drag inhibits grain growth. As the volume fraction of liquid was increased, it is believed that the pore surfaces became

46

coated with a very thin liquid film, thereby allowing for a faster atomic flux and increased pore mobility. The growth rate continued to increase with increasing film thickness (proportional to volume fraction) until an equilibrium thickness was reached, at which point the growth rate achieved a maximum value.

These grain growth data are slightly larger than those reported by Sabolsky et al. in a recent study of PMN-35PT.[57] In that study, grain growth behavior was found to be essentially *independent* of PbO content for the three compositions studied (1, 3, and 5 wt.%). The reasons for this discrepancy are not well understood. It can be speculated, however, that differences in processing conditions affected the grain growth behavior. In the current study, samples were hot-pressed prior to annealing, while in the work of Sabolsky et al., samples were sintered directly from the green state. Recent work has suggested that hot-pressing may induce phase changes in the PbO that would change the characteristics of the liquid phase and possibly the grain growth behavior.[19] Secondly, only one composition of packing powder (PMN-35PT + 7 wt.% PbO) was used for all samples in the work of Sabolsky et al. In the current experiment, it was found to be necessary to have increasingly more PbO in the packing powder as the level of PbO in the samples was increased.

The data presented in Table 5.1 clearly show the growth constant advantage of the migrating single crystal compared to that of the matrix grains when a liquid phase is present. When no liquid phase is added to the matrix, the growth constants of the matrix and the single crystal are within an order of magnitude of each other. However, when as little as 1.5 vol.% PbO is added to the matrix, the single crystal constant increases to nearly 100 times that of the matrix grains, clearly showing the effectiveness

of the SPC process. The difference in growth rates is assumed to be attributable to a size advantage of the seed over the matrix grains.

This size advantage has been supported by recent kinetic studies of abnormal grain growth in PMN-35PT with excess PbO.[31,58] These studies produced growth constant data very comparable to those data presented in Table 5.1. The $\Sigma 3$ boundary seems to play an important role in the nucleation of abnormal grains. However, once the abnormal grain has reached sufficient size, the abnormal grain continues to grow at the rate of {001} single crystals.

As mentioned in section 5.2.1, there is qualitative evidence in Figures 5.3 and 5.4 indicating that both the matrix and single crystal growth rates are decreasing with time. The data in Figures 5.3 and 5.4 showing the cubic kinetics (n=3) of the system lend quantitative support to this theory. While cubic kinetics were found to be the best statistical fit in both instances, parabolic (n=2) and quartic (n=4) kinetics also fit fairly well (correlation factors > 0.90). In either case, linear growth laws (n=1) did not fit very well (correlation factors < 0.85). Clearly, there is both visual and statistical evidence that the matrix and single crystal growth rates decrease at longer annealing times.

It is worthwhile to mention that while there is a clear influence of PbO on both matrix and single crystal growth, the amount of excess PbO in the samples may be slightly underestimated. Referring to Table 4.1, ICP-OES analysis showed that the starting PMN-35PT powder is actually slightly PbO-rich. The amount of excess PbO in the powder is likely less than 0.5 vol.%, however, and realistically should have no significant outcome on the generalizations made here about the effect of PbO on SPC.

48

The theory of Ostwald ripening, discussed in section 2.2.2, can be readily applied to the growth of matrix grains by examining the grain size distributions. From Figure 5.1, it is clear that there is a range of grain sizes that can easily result in the solution-precipitation process. Referring to Figure 2.15, the solubility of larger grains is less than that of smaller grains in the liquid. The resulting concentration gradient causes a transport of material from smaller grains to larger grains by diffusion. Large grains therefore grow at the expense of smaller matrix grains.

For additions of PbO to PMN-35PT greater than 3 vol.%, the growth constants for both the matrix grains and single crystal began to decrease or level off. A decrease in the growth constants with increasing liquid fractions usually is indicative of diffusion-controlled growth, while growth constants independent of liquid fraction typically are dominated by interface reaction.[50] Classic models propose that systems that follow cubic growth kinetics (n=3), as found to be the best fit in this study, are controlled by the rate of atomic diffusion through the liquid film. However, as in other studies, it is often difficult to unequivocally assign a particular growth mechanism based simply on the experimental growth exponent.[59]

Figures 5.3 and 5.4 suggest a slight difference between the effect of liquid volume fraction on the matrix and single crystal growth behavior above 3 vol.% PbO. The average matrix grain size decreases from about 31 μm at 3 vol.% to about 21 μm at 4 vol.% after 10 hours, a reduction of approximately 32%. Subsequently, a decrease from 21 to 17 μm, or approximately 20%, was observed between 4 and 5 vol.% for the same annealing time. Similar reductions were observed for samples annealed for 0, 1, 3, and 5 hours.

The decrease in grain growth as a function of liquid volume fraction (V_f) is consistent with a diffusion-controlled mechanism, in which the growth constant, k, is proportional to $V_f^{-1/3}$.[60,61] In previous studies, it has been observed that PMN-PT matrix grain growth is independent of PbO content for liquid contents greater than 10 vol.%.[50] Thus, it is believed that while diffusion limits grain growth between 3 and 5 vol.% PbO, interface reaction begins to dominate matrix growth at even larger PbO fractions.

The decreases observed in the average single crystal growth with increasing PbO volume fraction were less apparent than those of the matrix. Crystal growth decreased only 3 μm between 3 and 4 vol.%, and 6 μm between 4 and 5 vol.% for 10 hour annealing treatments. Similar trends were observed for the other annealing times. These decreases, only slightly greater than the experimental error of the measurements, appear to indicate that crystal growth is independent of V_f above a critical level. Additionally, qualitative studies have shown that the amount of single crystal growth in 7 vol.% is roughly equivalent to that observed in 5 vol.%.[62] This indicates that the single crystal growth is also dominated by an interface reaction-controlled growth mechanism at larger PbO fractions.

The reasons why the single crystal and matrix grains are controlled by interface reaction at different levels are currently not well known. However, it is reasonable to suspect that the advancing single crystal front may create a "snowplough" effect. In this situation, the liquid is pushed ahead of the single crystal, thereby increasing the effective film thickness at the crystal interface and reducing the PbO content necessary for interface reaction.

It was previously mentioned that it is usually difficult to unequivocally separate between diffusion-controlled growth and interface reaction-controlled growth simply based on the experimental growth exponent. However, it some instances, at the later stages of diffusion-controlled growth, it may be difficult to identify whether the growth constant follows a $V_f^{-1/3}$ relationship or is independent with liquid volume fraction within experimental reason. The schematic diagram shown in Figure 5.13 shows the dependence of growth constant on the two possible rate-limiting mechanisms on V_f. At low volume fractions, the slope dk/dV_f is very large. At larger liquid fractions, dk/dV_f is small, and within experimental error, it may be difficult to distinguish a $V_f^{-1/3}$ relationship from a straight line. Thus, although the experimental data indicate that a transition between diffusion-controlled growth and interface reaction-controlled growth is taking place, the critical liquid volume fraction at which this mechanism switch takes place is difficult to determine.
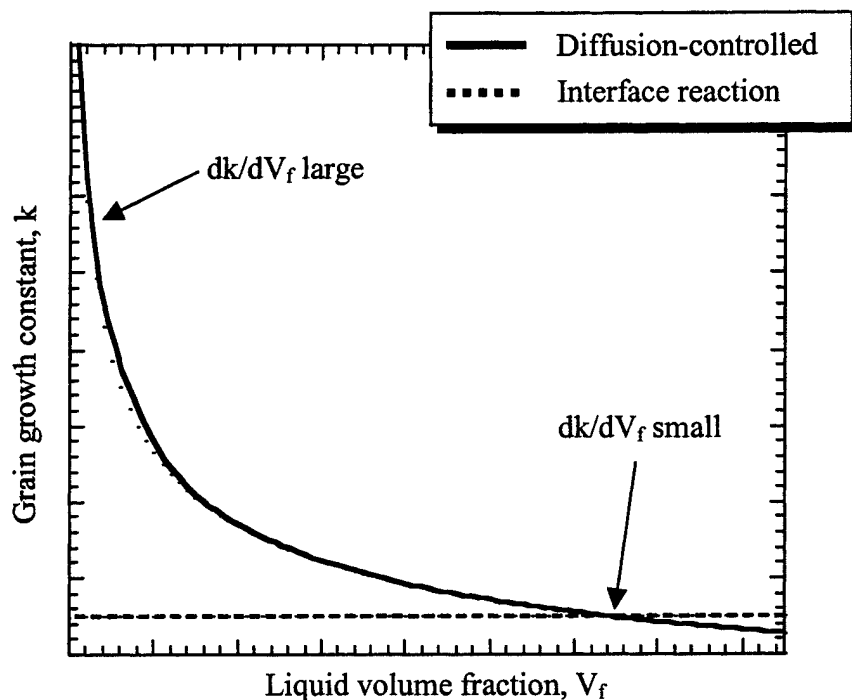
Figure 5.5. Schematic diagram of possible transition from diffusion-controlled growth to interface reaction controlled growth.

Figure 5.7 shows the effect of PbO content on density after samples were annealed at 1150°C. Prior to annealing, all samples were approximately 100% theoretically dense (8.13 g/cm³). The microstructures shown in Figures 5.1 and 5.2 clearly show the formation of intergranular porosity during annealing. This formation of intergranular porosity has been ascribed to trapped insoluble gases (N_2, CO, CO_2) and the decomposition of PbO, as discussed in section 2.1.2.[17] It is interesting to note that the samples which contained no excess PbO showed very little dedensification during the annealing process. Though all powders were processed in ethyl alcohol (section 4.1.1), it can be inferred that the presence of PbO acts as a catalyst for the evolution of organic gases such as CO and CO_2.[24]

5.4. Conclusions

The systematic study on the effect of PbO on Seeded Polycrystal Conversion revealed a transition in the dominating growth mechanism. At low PbO fractions (0 to 3 vol.%), the single crystal and matrix growth constants both increased with increasing PbO content due to pore mobility arguments. Beyond 3 vol.%, the growth constants decreased slightly before leveling off, indicating a transition from diffusion-controlled growth ($\alpha V_f^{-1/3}$) to interface reaction-controlled growth (independent of V_f). This mechanism transformation was paralleled with a morphological evolution in the matrix grains from equiaxed to faceted shapes. The difference in critical PbO content for an interface reaction mechanism to dominate may be due to a "snowplough effect." In this situation, the liquid is pushed ahead of the single crystal, thereby increasing the effective film thickness at the crystal interface and reducing the PbO content necessary for interface reaction.

Intergranular porosity, as well as trapped porosity in the grown single crystals, was observed in all samples containing excess PbO. This porosity formation was acribed to trapped insoluble gases (N_2, CO, CO_2) from and the decomposition of PbO. As a result, samples dedensified up to 10% during annealing from the approximately 100% theoretical densities achieved by hot-pressing. Samples without any PbO did not form this intergranular porosity during annealing, lending for support for the influence of PbO on dedensification.

Photomicrographs of the matrix grains and single crystal growth fronts revealed an apparent decrease in the growth rates at longer annealing times. Quantitative data

supported this argument, as the matrix and single crystal data were found to closely follow $G^3-G_0^3=kt$ and $L^3-L_0^3=kt$ growth laws, respectively.

6. MODELING THE EFFECTS OF MICROSTRUCTURAL VARIABLES ON THE SEEDED POLYCRYSTAL CONVERSION PROCESS

6.1. Introduction

The experimental results presented in section 5.2 provide excellent insight into the effects of PbO content and annealing temperature on the growth of PMN-35PT single crystals by the Seeded Polycrystal Conversion process. However, the amount of data that can be generated is always limited due to time constraints and experimental variations. The Leite kinetic model discussed in section 2.3 has been modified and applied to the single crystal growth of PMN-35PT with PbO additions. Section 6.2 discusses the steps taken to enhance the model. The method of solution for the kinetic equation is presented in section 6.3. Calculated results for the effects of liquid phase fraction, annealing temperature, and starting matrix particle size are presented in sections 6.4.1, 6.4.2, and 6.4.3, respectively.

6.2. Enhancement of Leite's Kinetic Model

To apply the Leite kinetic model to single crystal growth, it is necessary to develop a term for the liquid film thickness as a function of average grain size. For a fully dense matrix of tetrakaidecahedron grains with volumetric liquid fraction X, the total volume of the system (V_{sys}) can be described as

$$(1-X)V_{sys} = N \cdot 11.314 \cdot l_p^3 \qquad (6.1)$$

where $11.314 \cdot l_p^3$ is the volume of an individual tetrakaidecahedron grain. If a liquid film layer t is assumed to encapsulate each grain (2t is the distance between adjacent grains), then

$$V_{sys} = N \cdot 11.314 \left(l_p + \frac{2t\sqrt{3}}{3} \right)^3 \qquad (6.2)$$

Solving equations 6.1 and 6.2 simultaneously, and inserting the geometric value for grain size, G, from equation 2.13, the liquid film thickness for a fully dense tetrakaidecahedron matrix is given by

$$f = 2t = \frac{3G(1 - \sqrt[3]{1 - X})}{2\sqrt{6} \sqrt[3]{1 - X}} \qquad (6.3)$$

Similarly, from equation 2.16, for a fully dense cubic matrix, the liquid film thickness is

$$f = 2t = \frac{G(1 - \sqrt[3]{1 - X})}{\sqrt[3]{1 - X}} \qquad (6.4)$$

It is important to note from equations 6.3 and 6.4 that the liquid film thickness shows a linear dependence on matrix grain size. Thus, given the mobility term in equation 2.3, it can be seen that the mobility of the single crystal will decrease linearly with grain size, assuming all other parameters remain constant, if a diffusion-controlled mechanism dictates the rate of single crystal growth.

6.3. Method of Solution for the Kinetic Equation

The kinetic equations proposed by Leite (equations 2.18 and 2.19) are extremely difficult to integrate by traditional analytical methodology, even with computer software products such as MAPLE™ and Matlab.™ To solve the kinetic equations, a first-order Euler numerical integration was used to predict the linear single crystal growth distance, a, as a function of time. The details of the Euler method have been previously explained, so only a brief description is given below.[63]

It was assumed that the instantaneous rate of single crystal growth, dL/dt, could be well approximated by ΔL/Δt, as long as the time interval, Δt, was sufficiently small. The linear single crystal growth at the end of each succinct time interval was calculated using the formula

$$L_{i+1} \approx L_i + \Delta t \left(\frac{dL}{dt} \right)_i \qquad (6.5)$$

where i is the integer number of the time step. This equation was solved iteratively such that L_{i+1} (time i) becomes L_i at the subsequent time step (time $i+1$). The time step was set at 2 seconds. Reducing the time step to as little as 0.0001 sec. altered the predicted single crystal growth in PMN-35PT + 3 vol.% PbO only 2 μm over a 10 hour anneal at 1150°C, clearly less than the variances observed in section 5.2.

To apply the model summarized in section 2.3 to the growth of PMN-35PT single crystals into a polycrystalline matrix, certain critical assumptions had to be made. The theoretical solubility of PMN-35PT was determined based on the PMN-PbO[64] and TiO$_2$-PbO[65] phase diagrams, where the solubilities of PMN and PT in liquid PbO are approximately 30 mol.% and 33 mol.%, respectively. The solubility of PMN-35PT in PbO was therefore estimated as 31 mol.% based on the weighted average of the two solubilities. It was assumed that these solubility levels were not dependent on temperature over the range of temperatures investigated.

The atomic volume of PMN-35PT was calculated as approximately 14.33 cm^3/mol based on the atomic volumes of lead, magnesium, niobium, titanium, and oxygen, 18.27, 13.97, 10.84, 10.64, and 14.0, respectively, in cm^3/atom.[66]

Surface energy is a difficult parameter to directly measure. However, in the applied model, the most necessary assumption is that the surface energy of the

57

migrating {001} single crystal plane is temperature independent. Thus, surface energies were estimated to range from 0.2 to 1.0 J/m^2, commonly accepted values for oxides at high temperatures.[67] A value of 0.2 J/m^2 was used for the data presented in the following section.

A thorough search of the relevant literature yielded no numerical values for the diffusivity of PMN-35PT through PbO liquid. A value of 2.65×10^{-12} m^2/s was determined to give the most realistic values of single crystal growth in this model for PMN-35PT + 3 vol.% PbO. This value was subsequently used to predict single crystal growth for the other liquid volume fractions. It was assumed that the liquid volume fraction had no effect on the diffusivity of PMN-35PT through PbO.

As shown in section 5.2, with increasing additions of PbO, a transition occurs in the matrix grain morphology from equiaxed (tetrakaidecahedron) grains to cubic grains (Figure 5.1). It was determined that the grains were equiaxed for 0 and 1 vol.% PbO additions, while they were cubic for PbO contents of 4 vol.% and greater. For PbO additions of 1.5 vol.%, a mixed microstructure of equiaxed and cubic grains was produced. For the purposes of this model, it was assumed that the behavior of the liquid film was based on a 7:3 and 3:7 mixture of equiaxed to cubic grains in samples with 1.5 and 3 vol.% PbO, respectively. All other volume fractions were assumed to result in 100% characteristic liquid film behavior of their respective grain shapes described above.

6.4. Calculated Results and Discussion

6.4.1. Effect of Liquid Phase Fraction

The grain growth data used for modeling the single crystal growth were extracted from the data in section 5. While interface reaction was assumed to be the dominating factor in the experimental single crystal results, evaluation of equation 2.18, equation 2.19, and Figure 5.4 show that the single crystal growth must have some dependence on PbO content. The single crystal cannot be independent of PbO content if the matrix grain growth is dependent over the same liquid phase composition range. For this reason, the modeling calculations assume a diffusion-controlled growth mechanism for both the matrix and single crystal. Additionally, the experimental growth kinetics fit best to a $t^{1/3}$ dependence, which classically is related to diffusion control.

Figures 6.1 (a) and (b) show a comparison of modeled diffusion-controlled single crystal growth with and without PbO-dependent diffusion constant values, respectively. A PbO content of 3 vol.% was used as the basis for the modeling for plots without PbO-dependent diffusion constants. In each figure, the modeled single crystal growth is plotted with the experimental single crystal results of section 4. Figure 6.2 is a plot of the fitted diffusion constant values vs. PbO content from the data presented in Figure 6.1 (a).

The plot shown in Figure 6.1 (b) reveals that there is a strong effect of the diffusion constant on the single crystal growth. When the diffusion constant is assumed to be identical for all PbO levels, the matrix grain size dominates the kinetics (equations 2.18 and 2.19). The growth of the single crystal is reciprocal to that observed in the

59

matrix; when the matrix grains are small, the single crystal growth is large, and vice versa. This suggests a possible chemistry difference in the liquid phase for various PbO levels.
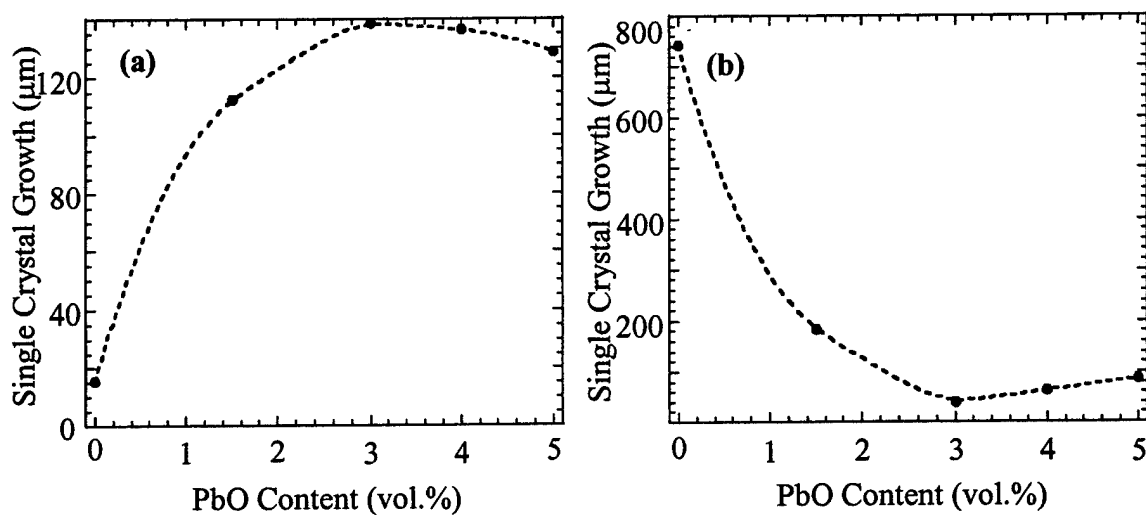
Figures 6.1. Comparison of modeled diffusion-controlled single crystal growth (a) with and (b) without PbO-dependent diffusion constant values.
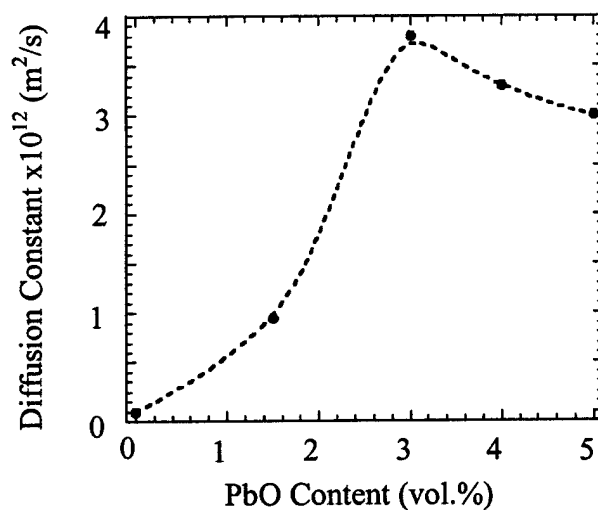

Figure 6.2. Plot of the fitted diffusion constant values vs. PbO content from the data presented in Figure 6.1 (a).

Recent microanalysis studies conducted by Gorzkowski et al. have verified that there is a chemistry change in the liquid for longer annealing times.[68] Both the matrix and the liquid had an increased $PbTiO_3$ level due to the thermodynamically favorable precipitation of MgO particles. It can be assumed that the intergranular liquid film thickness at long annealing times for low PbO contents approximates the film thickness at short annealing times for high PbO contents. The current work therefore suggests that the liquid chemistry can be linked to both the PbO content and the length of the annealing treatment.

6.4.2. Effect of Starting Matrix Grain Size

The experimental matrix grain growth data in section 5 was produced from samples with sub-micron starting grain sizes (after hot-pressing). The amount of matrix coarsening is evident, particularly at the early stages of the annealing treatment (the kinetics to fit best to a cubic growth law). For PMN-35PT with 3 vol.% excess PbO, the average matrix grain coarsened to about 13 μm after annealing at 1150°C for 0 hours. These large levels of coarsening may have an adverse effect on the amount of single crystal growth because of the strong influence of grain size that can be seen in equations 2.18 and 2.19.

Figure 6.3 shows a plot of the expected final single crystal growth after annealing a PMN-35PT + 3 vol.% PbO sample for 10 hours with various starting grain sizes. The starting grain sizes were assumed to be the average matrix grain size after annealing at 1150°C for 0 hours. For all the cases, the growth constant was assumed to be 2.73 x 10^{-15} m^3/hr, as dictated by Table 5.1. The kinetic variables were identical to

those used for the 3 vol.% PbO data shown in Figure 6.1 (a), with a diffusion constant of 2.65×10^{-12} m^2/s.
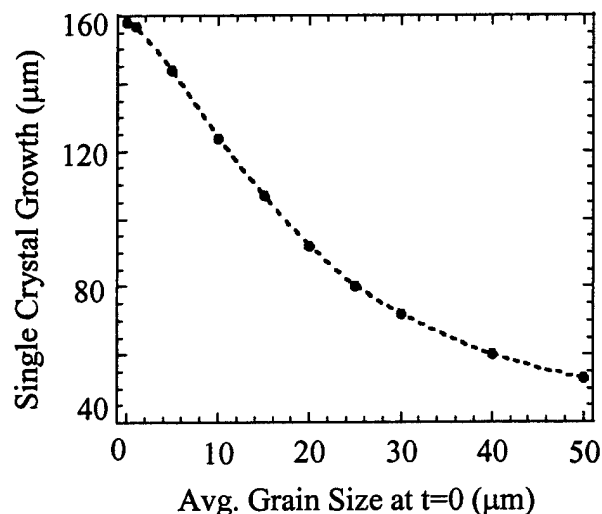

Figure 6.3. Plot of the expected final single crystal growth after annealing a PMN-35PT + 3 vol.% PbO sample for 10 hours with various starting grain sizes.

While the previous section revealed that the diffusion constant is strongly dependent on both PbO content and annealing time, Figure 6.3 shows that the single crystal growth is also strongly influenced by the matrix grain size. As the matrix grains coarsen, the amount of expected single crystal growth is also reduced. This may be validation as to why both the matrix and single crystal growth follow $t^{1/3}$ kinetics. The modeling also shows that refining the starting particle size to even the nanoscale level would not sufficiently increase the growth rate. The growth constant of 2.73×10^{-15} m^3/hr causes nano-sized grains to coarsen to several microns after only a brief time at the annealing temperature of 1150°C.

Further experimental evidence showing the effect of the matrix can be explained by the presence of abnormal grains at or near the single crystal. Abnormal grain

growth, which has been observed to occur in PMN-35PT samples with at least 3 vol.% excess PbO, is actually due to the coalescence and growth of two grains joined by a Σ3 boundary.[17,30] Though abnormal grain growth is a very different phenomenon than matrix coarsening, the growth of single crystals from SPC has nonetheless been observed to be severely slowed by the impingement of abnormal grains.[17,68,18] This is in agreement with equations 2.18 and 2.19, which show that the instantaneous rate of single crystal growth would be hampered by a matrix of extremely large grains.

6.5. Conclusions

The results suggested a possible effect of liquid phase chemistry that may cause a difference in the PbO-dependent growth behavior of the matrix grains and the single crystal. The single crystal growth data were modeled to fit those produced by experimental results, which produced calculated diffusion constant values that had a maximum value at 3 vol.% excess PbO. While excess PbO is clearly necessary for the process to work, modeling also revealed that coarsening of the matrix grains may be slowing the growth of the single crystal down at later annealing stages. This may also account for the reason why the single crystal and matrix grains both follow a $t^{1/3}$ growth dependence.

7. SUMMARY

- Both single crystal and matrix have apparent growth maxima at an excess PbO composition of 3 vol.%

- Single crystal and matrix growth rates increase with increase PbO content, indicating that both rates are governed by pore mobility, in the range of 0 to 3 vol.% excess PbO

- Above 3 vol.% excess PbO, single crystal growth is independent of PbO content, indicating that it is dominated by interface reaction

- Above 3 vol.% excess PbO, single crystal growth decreases with PbO content before leveling off, which most likely indicates a transition from diffusion control to interface reaction

- The difference in critical PbO content for interface reaction to dominate is possibly due to a plough effect, where the single crystal pushes the liquid ahead of the boundary, thereby increasing the effective film thickness

- Both the matrix grains and the single crystal growth follow cubic growth laws for 0 to 10 hours of annealing at 1150°C

- Modeling of the SPC process reveals that liquid phase chemistry may play a key role in the behavior of the single crystal growth between 3 and 5 vol.% excess PbO

- The coarsening of the matrix grains appears to be a main cause in why the single crystal growth follows cubic growth kinetics

- Refining the starting particle size of the matrix to the nanoscale will not achieve any significant increase in single crystal due to the rapid coarsening kinetics of the system

8. SUGGESTIONS FOR FUTURE WORK

- Sintering atmosphere (section 2.1.2) may play a significant role in explaining the matrix and single crystal growth behavior for liquid fractions between 0 and 3 vol.% (section 5.2.2 and 5.2.3). Sintering PMN-35PT-PbO from the green state in flowing oxygen has produced virtually pore-free microstructures and single crystals.[17]

- A systematic study conducted in oxygen parallel to the current work may help to provide more insight to the effect of porosity on the growth kinetics of the matrix grains and single crystal in PMN-35PT, especially at lower PbO fractions.

- Experimental verification of the calculated dependence of single crystal growth on starting matrix particle size (section 6.4.2) may help to answer the fundamental question of what microstructural variable is contributing most to the saturation of single crystal growth after a relatively short period of time

- A study on the experimental kinetics of {001} single crystal and matrix growth at extremely large PbO contents (20 + vol.%) would verify the theory that interface reaction dominates growth above a critical liquid content

- Modeling of the liquid phase chemistry as a function of annealing time and PbO content would give supporting evidence to the role of PbO on single crystal growth in the range of 3 to 5 vol.%

9. APPENDIX

Figure A.1 compares single crystal growth from various seed orientations in a matrix of PMN-35PT + 3 vol.% PbO at 1150°C for 10 hours. As expected, the least amount of growth is observed from {001} oriented single crystal seeds. The amount of porosity and trapped liquid phase is also drastically increased in the growth from non-{001} orientations.
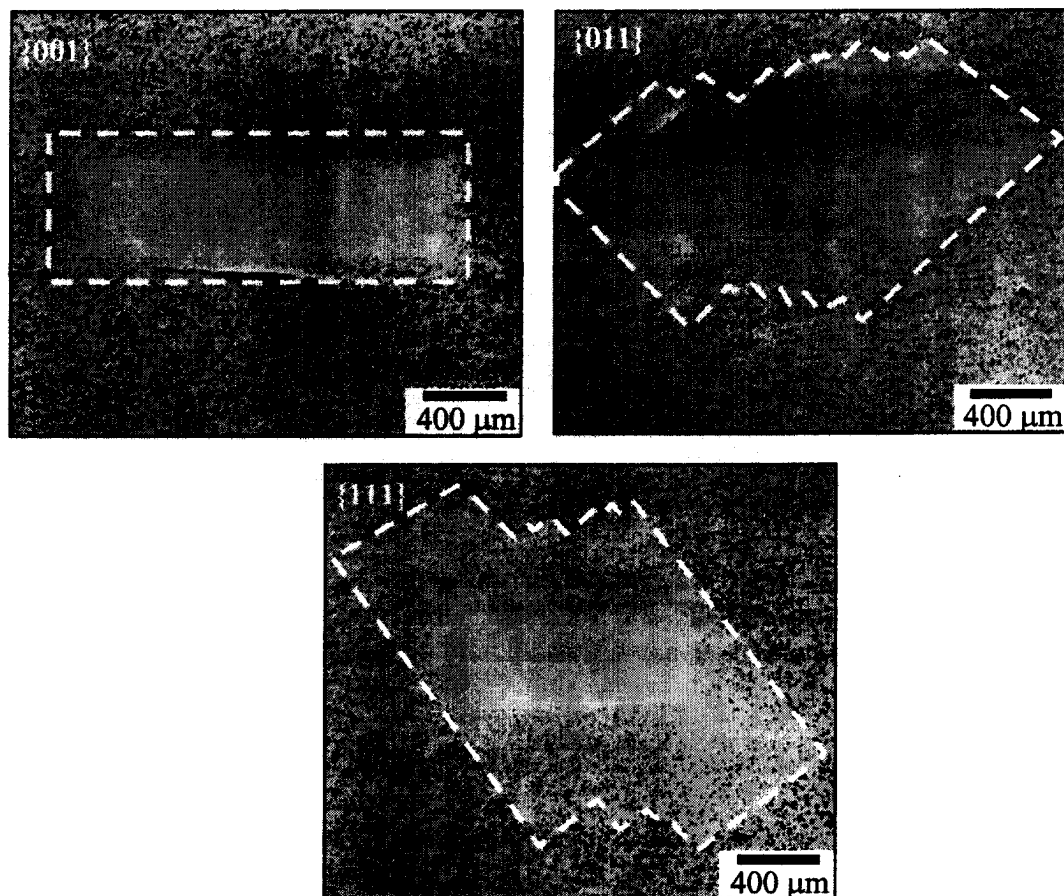

Figure A.1. Single crystal growth from various seed orientations into a matrix of PMN-35PT + 3 vol.% PbO for 10 hours at 1150°C in air, with growth areas outlined in white.

The facetted growth front from oriented {011} and {111} seeds was analyzed three-dimensionally by selectively leaching out the matrix with HNO_3.[69] After heat treatment, the matrix grains were removed by ultrasonically agitating in a 30% HNO_3. The resulting macroscopic single crystal morphologies were revealed by scanning electron microscopy (SEM) images shown in Figure A.2. Crystals grown from {011} seeds facet into right-angle pyramids, while crystals grown from {111} seeds facet into tetrahedral pyramids.

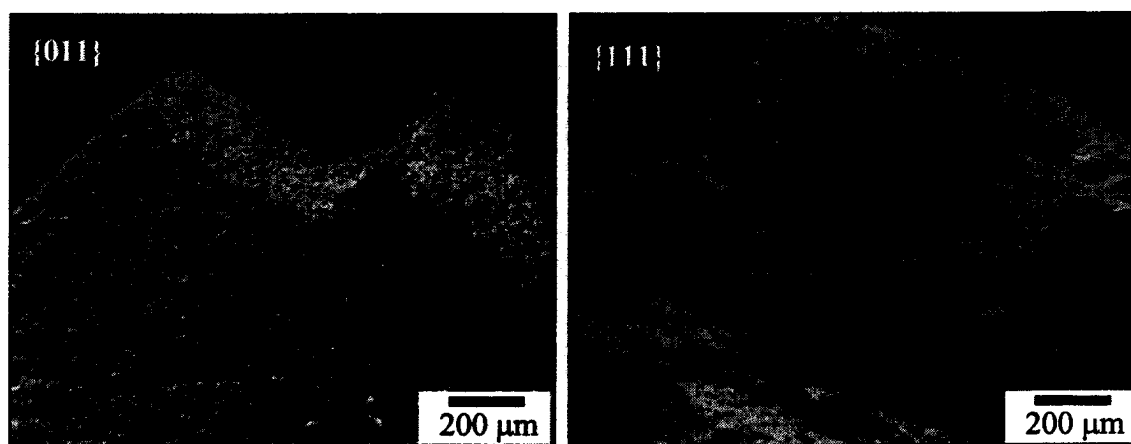**Figure A.2.** SEM image of single crystal growth morphologies from {011} and {111} oriented seeds in PMN-35PT + 3 vol.% PbO after sintering for 10 hours at 1150°C. Matrix grains removed by ultrasonically agitating in 30% HNO_3.

It is believed that the individual pyramids observed in Figure A.2 result from the nucleation and coalescence of even smaller pyramids. As the sintering time increases, the single crystal continues to grow at a high velocity until the pyramids have completely coalesced to form a cube. Once the single crystal has coalesced to a cube, the cubic facets allow for the single crystal to grow only in the slower <001> direction.

Closer analysis of single crystal morphologies grown from {111} seeds yields interesting insights to the microstructural characteristics of the matrix grains. Figure A.3 shows SEM images of single crystals grown from {111} seeds in PMN-35PT with 1.5 and 5 vol.% PbO additions with matrix grains removed with HNO_3 as described above. In both samples, grain pockets were observed on the single crystal surface, indicating regions of prior contact with matrix grains. Higher fractions of liquid phase in the matrix provide for a greater degree of grain boundary wetting, yielding a relatively smooth, flat interface morphology, as seen for the 5 vol.% PbO sample. In addition, increasing the fraction of liquid phase from 1.5 to 5 vol.% enhanced the amount of single crystal growth and produced a more macroscopically faceted pyramidal structure. The higher magnification images shown in the insets reveal a transition in matrix morphology, from the classic tetrakaidecahedron grain shape (1.5 vol.% PbO) to faceted, cube-shaped grains (5 vol.% PbO).
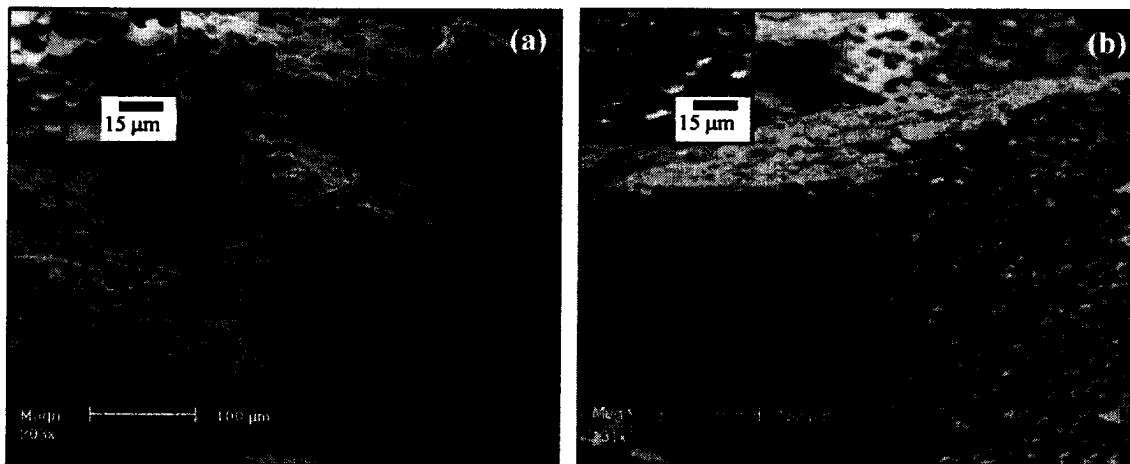

Figure A.3. Local interface morphologies of {111} single crystals grown in PMN-35PT with (a) 1.5 vol% PbO and (b) 5 vol% PbO additions for 10 hours at 1150°C in air; matrix grains removed by ultrasonically agitating in a 30% HNO_3 solution.

The transition in matrix morphology agrees well with previous results from a systematic analysis of the effect of PbO on matrix grain growth in PMN-35PT.[16] Figure 2.2 shows the relationship between matrix morphology and liquid volume fraction for additions between 0 and 5 vol.%. At low volume fractions (0 and 1 vol.% PbO), the matrix grains all had a tetrakaidecahedron (equiaxed) morphology. When the volume fraction is raised to 1.5 vol.%, the matrix grains had a relatively equal mixture of a faceted (cubic) and equiaxed morphologies. At even higher volume fractions of PbO, the matrix grains were composed entirely of a cubic morphology. This transition in matrix morphology was attributed to an increased amount of wetting over the grain boundaries due to the presence of more liquid phase.

REFERENCES

1. D. W. Richerson, "Moderm Ceramic Engineering," Marcel Dekker, New York, NY, (1992).

2. S. W. Choi, T. R. Shrout, S. J. Jang, A. S. Bhalla, "Dielectric and Pyroelectric Properties in the $Pb(Mg_{1/3}Nb_{2/3})O_3$-$PbTiO_3$ System," *Ferreoelectrics*, **100** 29-38 (1989).

3. T. R. Shrout and J. Fielding, Jr., "Relaxor Ferroelectric Materials," *IEEE Ultrasonics Symposium*, 711-20 (1990).

4. S. -E. Park and T. R. Shrout, "Characteristics of Relaxor-Based Piezoelectric Single Crystals for Ultrasonic Transducers," *IEEE Trans. Ultrason., Ferroelectr. Frequency Control*, Special Issue on Ultrasonic Transducers, **44** [5] 1140-47 (1997).

5. S.-E. Park and T. R. Shrout, "Relaxor-Based Ferroelectric Single Crystals for Electromechanical Actuators," *Mater. Res. Innovations*, 1 20-25 (1997).

6. N. Setter and L. E. Cross, "Flux Growth of Lead Scandium Tantalate $Pb(Sc_{0.5}Ta_{0.5})O_3$ and Lead Magnesium Niobate $Pb(Mg_{1/3}Nb_{2/3})O_3$ Single Crystals," *J. Cryst. Growth*, **50** 555-56 (1980).

7. K. Harada, S. Shimanuki, T. Kobayashi, S. Saitoh, and Y. Yamashita, "Crystal Growth and Electrical Properties of $Pb((Zn_{1/3}Nb_{2/3})_{0.91}Ti_{0.09}O_3$ Single Crystals Produced by Solution Bridgman Method," *J. Am. Ceram. Soc.*, **81** [11] 2785-88 (1998).

8. R. R. Neurgaonkar, M. H, Kalisher, T. C. Lim, E. J. Staples, and K. L. Keester, "Czochralski Single Crystal Growth of Strontium Barium Niobate $(Sr_{.61}Ba_{.39}Nb_2O_6)$ for Surface Acoustic Wave Applications," Mater. Res. Bull, 15 [9] 1235-40 (1980).

9. T. Li, A. M. Scotch, H. M. Chan, M. P. Harmer, S. -E. Park, T. R. Shrout, and J. R. Michael, "Single Crystals of $Pb(Mg_{1/3}Nb_{2/3})O_3$-35mol%$PbTiO_3$ from Polycrystalline Precursors," *J. Am. Ceram. Soc.*, **81** [1] 244-8 (1998).

10. M. P. Harmer, H. M. Chan, H.-Y. Lee, A. M. Scotch, T. Li, F. Meschke, and A. Khan, "Method for Growing Single Crystals from Polycrystalline Precursors," U.S. Pat. No. 6 048 394, 2000.

11. C. Scott, J. Strok, and L. Levinson, "Solid State Thermal Conversion of Polycrystalline Alumina to Sapphire using a Seed Crystal," US Pat. No. 5 549 746, 1996.

12. T. Yamamoto and T. Sakuma, "Fabrication of Barium Titanate Single Crystals by Solid-State Grain Growth," *J. Am. Ceram. Soc.*, 77 [4] 1107-09 (1994).

13. S. Matsuzama and S. Mase, "Method for Producing a Single Crystal Ferrite," U.S. Pat. No. 4 339 301, 1990.

14. N. Yamamoto and S. Matsuzama, "The Solid-Phase Epitaxial Growth Method," pp. 39-44 in *Fine Ceramics*. Edited by S. Saito. Elsevier, New York, 1988.

15. K. Kugimiya, K. Hirota, and K. Matsuyama, "Process for Producing Single Crystal Ceramics," U.S. Pat. No. 4 900 393, 1990.

16. A. Khan, E. P. Gorzkowski, A. M. Scotch, H. M. Chan, and M. P. Harmer, "Influence of Excess PbO Additions on the Growth of (111) $Pb(Mg_{1/3}Nb_{2/3})O_3$-35mol%$PbTiO_3$ Single Crystals by Seeded Polycrystal Conversion," to be submitted to *J. Am. Ceram. Soc.* (2002).

17. A. M. Scotch, H. M. Chan, and M. P. Harmer, "Effect of Sintering Atmosphere on the Growth of $Pb(Mg_{1/3}Nb_{2/3})O_3$-35mol%$PbTiO_3$ Single Crystals by Seeded Polycrystal Conversion," to be submitted to *J. Am. Ceram. Soc.* (2002).

18. P.T. King, H. M. Chan, and M. P. Harmer, unpublished work (2001).

19. A. Khan, F.A. Meschke, A. M. Scotch, T. Li, H. M. Chan, and M. P. Harmer, "Growth of $Pb(Mg_{1/3}Nb_{2/3})O_3$-35mol%$PbTiO_3$ Single Crystals from (111) Substrates by Seeded Polycrystal Conversion," *J. Am. Ceram. Soc.*, **82** [11] 2958-62 (1999).

20. T. Li, S. Wu, A. Khan, A. M. Scotch, H. M. Chan, and M. P. Harmer, "Hetero-Epitaxial Growth of Bulk Single Crystal $Pb(Mg_{1/3}Nb_{2/3})O_3$-35mol%$PbTiO_3$ from (111) SrTiO3," *J. Mater. Res.*, **14** [8] 3189-91 (1999).

21. M. Dong, Z.-G. Ye, "High temperature thermodynamic properties and pseudo-binary phase diagram of the $Pb(Zn_{1/3}Nb_{2/3})_{0.91}Ti_{0.09}O_3$-PbO system," *Jap. J. Appl. Phys.* **40** [7] 4604-4610 (2001).

22. D. Risold, "PbO Systems," *J. Phase. Equil.*, **19** [3] 213-15 (1998).

23. J. S. Anderson and M. Sterns, "Intermediate oxides of lead," *J. Inorg. & Nuclear Chem,* **11** 272-85 (1959).

24. A. M. Scotch, private communication (2002).

25. J. C. Ho, K. S. Liu, and I. N. Lin, "Study of ferroelectricity in the PMN-PT system near the morphotropic phase boundary.," *J. Mater. Sci.*, **28** [16] 4497-502 (1993).

26. M. Villegas, C. Caballero, M. Kosec, C. Moure, P. Duran, and J. F. Fernandez, "Effects of PbO excess in $Pb(Mg_{1/3}Nb_{2/3})O_3$-$PbTiO_3$ Ceramics: Part I: Sintering and Dielectric Properties," *J. Mater. Res.*, **14** [3] 891-97 (1999).

27. H. M. Jang and K. M. Lee, "Stabilization of perovskite phase and dielectric properties of $Pb(Zn,Mg)_{1/3}Nb_{2/3}O_3$ - $PbTiO_3$ ceramics prepared by excess constituent oxides,," *J. Mater. Res.*, **9** [10] 2634-38 (1994).

28. H. M. Jang and K. M. Lee, "Dielectric and piezoelectric properties of the thermally annealed $Pb(Zn,Mg)_{1/3}Nb_{2/3}O_3$ - $PbTiO_3$ system across the rhombohedral/tetragonal morphotropic phase boundary,," *J. Mater. Res.*, **10** [12] 3185-90 (1995).

29. C. Wagner, "Theory of Precipitate Change by Redissolution (Ostwald Ripening)," *Z. Elektrochem.*, **65** [7/8] 581-91 (1961).

30. J. S. Wallace, J.-M. Huh, J. E. Blendell, and C. A. Handwerker, "Grain Growth and Twin Formation in 0.74 PMN - 0.26 PT," *J. Am. Ceram. Soc.*, **85** [6] 1581-84 (2002).

31. D. J. Rockosi, H.M. Chan, and M. P. Harmer, unpublished work (2002).

32. U.-J. Chung, J.-K. Park, N.-M. Hwang, H.-Y. Lee, and D.-Y. Kim, "Effect of Grain Coalescence on the Abnormal Grain Growth of $Pb(Mg_{1/3}Nb_{2/3})O_3$-$PbTiO_3$ Ceramics," *J. Am. Ceram. Soc.*, **85** [4] 965-68 (2002).

33. M. N. Rahaman, "Ceramic Processing and Sintering," Marcel Dekker, New York, NY (1995).

34. W. Dong, "Microstructure Evolution and Densification of Alumina in Liquid Phase Sintering," Ph.D. dissertation, Lehigh University (2000).

35. H. S. Cannon and F. V. Lenel, "Some Observations on the Mechanism of Liquid Phase Sintering," Plansee Proceedings, F. Beneovsky (ed.), Metallwerk Plansee, Reutte, Austria, 106-121 (1953).

36. V. N. Eremenko, Yu. V. Naidich, and I. A. Lavrinko, "Liquid Phase Sintering," Consultant Bureau, New York, NY, 1970.

37. W. D. Kingery, "Densification during Sintering in the Presence of a Liquid Phase. I. Theory," *J. Appl. Phy.*, **30** [3] 301-06 (1959).

38. W. J. Huppmann, "Sintering in the Presence of a Liquid Phase," Sintering and Catalysis-Material Science Reearch, **10**, 359-378, Plenum Press, New York, NY, 1975.

39. R. M. German, "Liquid Phase Sintering," Plenum Press, New York, NY, (1985).

40. W. D. Kingery, "Densification during sintering in the presence of a liquid phase. I. Theory," *J. Appl. Phys.*, **30** 301-06 (1959).

41. W. J. Huppmann, W. A. Kaysser, D. N. Yoon, and G.Petzow, "Progress in Liquid Phase Sintering," *Powder Metall. Int.* **11** [2] 50-1 (1979).

42. D. S. Wilkinson, "The Mechanisms of Pressure Sintering," Ph.D. dissertation, University of Cambridge (1977).

43. G. C. Kuczynski, "Sintering and Catalysis," Plenum Press, New York, 325-37, (1975).

44. K. S. Churn and D. N. Yoon, "Pore Formation and its Effect on Mechanical Properties in W-Ni-Fe Heavy Alloy," *Powder Met.*, **22** 175-78 (1979).

45. B. Meredith and D. R. Milner, "The Liquid-Phase Sintering of Titanium Carbide," *Powder Met.*, **19** 162-70 (1976).

46. A. J. Ardell, "The Effect of Volume Fraction on Particle Coarsening: Theoretical Considerations," *Acta Metall.*, **20** 61-71 (1972).

47. S. Sarian and H. W. Weart, "Kinetics of Coarsening of Spherical Particles in a Liquid Matrix," *J. Appl. Phys.*, **37** [4] 1675-81 (1966).

48. T. K. Kang and D. N. Yoon, "Coarsening of Tungsten Grains in Liquid Nickel-Tungsten Matrix," *Metall. Trans. A*, **9A** 433-38 (1978).

49. K. C. Kothari, "Densification and Grain Growth during Liquid Phase Sintering of W-Ni-Cu Alloys," *J. less-common Metals*, **13** 457-68 (1967).

50. M.F. Yan, R.M. Cannon, and H.K. Bowen, "Grain Boundary Migration in Ceramics," in Ceramic Microstructure '76. Ed. By R.M. Fulrath and J.A. Pask. Westview Press, Boulder, CO, 1976, p 276-307.

51. R. Watanabe and Y. Musada, "The Growth of Solid Particles in Some Two-Phase Alloys during Sintering in the Presence of a Liquid Phase," *Sintering and Catalysis-Material Science Research*, **10** 389-98 (1975).

52. E.R. Leite, A. Khan, A.M. Scotch, H.M. Chan, and M.P. Harmer, *Sintering: Science, and Technology*, 355-60 (2000).

53. C.V. Thompson, "Secondary grain growth in thin films of semiconductors: theoretical aspects," *J. Appl. Phys.* 58[2], 763-72, (1985).

54. R. C. Weast, M. J. Astle, W. H. Beyer (ed.), *"CRC Handbook of Chemistry and Physics,"* 67th ed. (1986).

55. M. I. Mendelson, "Average Grain Size in Polycrystalline Ceramics," *J. Am. Ceram. Soc*, **52** [8] 443-46 (1969).

56. F. Jorge Alves, "Effect of Liquid Phase on Coarsening Behavior in Porous Single-Phase and Duplex Microstructures, Ph.D. Dissertation, Lehigh University (1997).

57. E. M. Sabolsky, G. L. Messing, S. Trolier-McKinstry, "Kinetics of Templated Grain Growth of $0.65Pb(Mg_{1/3}Nb_{2/3})O_3$-$0.35PbTiO_3$," *J. Am. Ceram. Soc.*, **84** [11] 2507-13 (2001).

58. A. M. Scotch, H. M. Chan, and M. P. Harmer, unpublished work (2002).

59. J. D. French, M. P. Harmer, H. M. Chan, and G. A. Miller, "Coarsening Resistant Dual-Phase Interpenetrating Microstructures," *J. Am. Ceram. Soc.*, **73** [8] 2508-510 (1990).

60. W. A. Kaysser, M. Sprissler, C. A. Handwerker, and J. E. Blendell, "Effect of Liquid Phase on the Morphology of Grain Growth in Alumina," *J. Am. Ceram. Soc.*, **70** [5] 339-43 (1987).

61. J. J. Kim, M. P. Harmer, and T. M. Shaw, "Effect of Liquid Volume Fraction on Coarsening of MgO Grains in Molten $CaMgSiO_4$," unpublished work (1993).

62. E.P. Gorzkowski, P.T. King, H.M. Chan, and M.P. Harmer, unpublished work (2002).

63. L. C. Stearns, "Particle-Inhibited Grain Growth in Al_2O_3-SiC," Ph.D. Dissertation, Lehigh University (1995).

64. Z.-G. Ye, P. Tissot, and H. Schmid, "Pseudo-Binary $Pb(Mg_{1/3}Nb_{2/3})O_3$-PbO Phase Diagram and Crystal Growth of } $Pb(Mg_{1/3}Nb_{2/3})O_3$ [PMN]," *Mat. Res. Bull.*, vol. 25, pp. 739-748 (1990).

65. B. Jaffe, W. R. Cook, Jr., and H. Jaffe, *"Piezoelectric Ceramics,"* Academic Press, London (1971).

66. T. K. Varga and C. Bello, *"Periodic Table of the Elements,"* Papertech Inc., Ontario, Canada (1996).

67. W.D. Kingery, H.K. Bowen and D.R. Uhlmann, "Introduction to Ceramics," 2nd ed., John Wiley and Sons, New York (1976).

68. E. P. Gorzkowski, H. M. Chan, and M. P. Harmer, unpublished work (2002).

69. E. P. Gorzkowski, A. Khan, H. M. Chan, and M. P. Harmer, unpublished work (2002).

3.8 Growth of Lead Magnesium Niobate-Lead Titanate Single Crystals by Seeded Polycrystal Conversion

GROWTH OF LEAD MAGNESIUM NIOBATE-LEAD TITANATE

SINGLE CRYSTALS BY SEEDED POLYCRYSTAL CONVERSION

by

Adam Matthew Scotch

A Dissertation

Presented to the Graduate Committee

of Lehigh University

in Candidacy for the Degree of

Doctor of Philosophy

In

Materials Science and Engineering

Lehigh University

October 2002

Certificate of Approval

Approved and recommended for acceptance as a dissertation in partial fulfillment of the requirements for the degree of Doctor of Philosophy in Materials Science and Engineering.

_12-6-02_
(Date)

Martin P. Harmer
Professor in Charge

Accepted _12-6-02_
(Date)

Special Committee directing the work of Mr. Adam M. Scotch

Martin P. Harmer (Chairman)
Dr. Martin P. Harmer

Helen Chan (Co-Chairman)
Dr. Helen M. Chan

Donald M. Smyth
Dr. Donald M. Smyth

John Blendell
Dr. John Blendell
National Institute of Standards and Technology

To Sara
7

Acknowledgments

Thank you Sara for not giving up hope that I would one day have a real job.

I would like to express my gratitude to my advisor, Dr. Martin P. Harmer, for his support and guidance. Mostly I am grateful that he didn't give up on me after I cast doubts in his mind when I failed to deliver the Ceramographics to the annual meeting my very first year of graduate school. I would also like to thank Dr. Helen M. Chan for not giving up on me after I cast doubts in her mind when I failed to deliver the Ceramographics to the annual meeting my very first year of graduate school. Hopefully, I have made up for that tragedy.

Thank you to my other committee members, Dr. Donald M Smyth, who I pulled out of retirement just so that he could listen to me ramble on about relaxor-based ferroelectric single crystals grown from seeded polycrystalline precursors, and Dr. John Blendell, who I forced to drive up from NIST a few times so that he could listen to me ramble on about relaxor-based ferroelectric single crystals grown from seeded polycrystalline precursors. I am thankful that they didn't know me very well when I failed to deliver the Ceramographics to the annual meeting my very first year of graduate school.

In all seriousness, I do appreciate the thoughtful discussions and comments that they each provided me.

I would like to thank the staff in the department including Arlan Benscoter, Dave

Table of Contents

List of Tables

List of Figures

Abstract

Relaxor-based ferroelectric single crystals of $Pb(Mg_{1/3}Nb_{2/3})O_3$-$PbTiO_3$ [PMN-PT] have been produced via the Seeded Polycrystal Conversion [SPC] technique. Polycrystalline precursors of PMN-PT are converted to single crystals by inducing the boundary of a seed crystal to migrate through a polycrystalline matrix. The quality of PMN-PT single crystals grown by SPC is directly influenced by the microstructure of the polycrystalline precursor. The goal of this work was to examine the factors that controlled the final microstructure of the matrix and grown single crystals and to characterize their effects on properties.

Sintering in oxygen was necessary to obtain fully dense matrix microstructures, which, in turn, produced pore-free single crystals. The primary role of oxygen was to remove insoluble gases before densification began, then to reduce the internal pressure by diffusing out and allowing the pores to close from pressures derived from their own curvatures. The presence of a PbO liquid phase assisted this process by enhancing the densification rate in the early stages of sintering. In contrast, fully-dense, hot-pressed samples of PMN-35PT with excess PbO underwent a de-densification process during the annealing treatments which was attributed to pore formation from internally evolved gases.

Transparent single crystals with maximum strain values of 0.72% at 46 kV/cm, d_{33} ~ 2180 pC/N, and a room temperature dielectric constant of ~5300 were obtained for poled <001> oriented crystals of PMN-30mol.%PT. The dielectric behavior of {001} oriented single crystals was found to be highly dependent on the initial orientation of the

1

seed crystal. For example, {111} seeded crystals grown in oxygen yielded K_{max} values of ~33000, while {001} seeded crystals grown in oxygen had K_{max} values of ~25000. In addition, the T_{max} values were 3 to 5°C higher for crystals grown from {001} seeds, compared to {111} seeds.

CHAPTER 1

INTRODUCTION AND BACKGROUND

1.1 Technological Relevance

<u>Single Crystals of Relaxor Ferroelectrics</u>

Recent advances in the electronic ceramics industry have demonstrated that single crystal ferroelectrics exhibit dramatic improvements in the electromechanical properties compared to their conventional polycrystalline ceramic counterparts. For example, single crystals of the relaxors $Pb(Mg_{1/3}Nb_{2/3})O_3$ (PMN) or $Pb(Zn_{1/3}Nb_{2/3})O_3$ (PZN) with $PbTiO_3$ (PT) near the morphotropic phase boundary possess electric-field induced strains > 0.6%,[1,2] longitudinal coupling coefficients k_{33} > 90%,[3] piezoelectric coefficients d_{33} > 1200 pC/N,[2] and dielectric constants from 1000 to 5000 with low dielectric loss.[2] Consequently, there exists great potential for these single crystal materials to be incorporated into existing devices such as ultrasonic transducers and actuators. The U.S. Navy has recognized that this recent breakthrough points to a revolution in acoustical transduction and has targeted these materials for rapid advancement. The single crystal

3

properties can be exploited for a broad range of applications including naval sonar (i.e. surveillance, tactical, navigation) and medical ultrasonics.

Conventional methods for growing single crystals of relaxor-based ferroelectrics include high temperature solution techniques such as flux, Czochralski, and Bridgman methods. Though suitable for growing bulk single crystals, these techniques have relatively slow growth rates and are not readily transferable to large-scale manufacturing. While the Czochralski and Bridgman techniques have good reproducibility, they require sophisticated (and therefore expensive) equipment. The flux method is a simple, low cost technique, but there are limitations with regard to crystal quality and quantity. The present technique of single crystal growth from polycrystalline precursors is both a potentially more cost-effective method and directly compatible with current manufacturing of polycrystalline components.

1.2   Concept of Seeded Polycrystal Conversion

Lehigh University has pioneered the successful application of seeded polycrystal conversion (SPC) in ferroelectric materials.[4] In the SPC technique, a seed crystal is brought into intimate contact with a polycrystalline ceramic matrix, and single crystal conversion takes place by forcing the crystal boundary to migrate at the expense of the smaller matrix grains. The driving forces for the single crystal boundary migration are differences in local boundary curvature and minimization of overall boundary energy. A schematic of the process is shown in Figure 1.1.

4
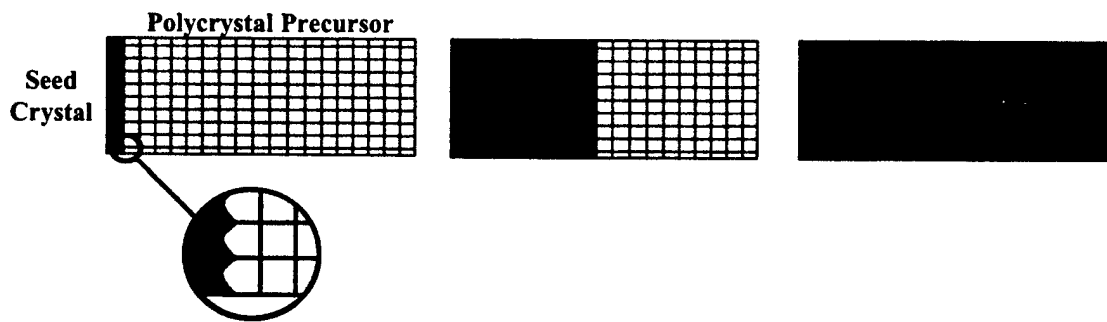
Figure 1.1: Schematic diagram describing the Seeded Polycrystal
Conversion process of growing single crystals.

1.3   Grain Growth Theory

Since the concept of polycrystalline conversion depends on local curvature to drive the migration of the boundary, it is necessary to control the matrix so as to maintain a high driving force. This requires a consideration of some fundamentals of grain growth theory.

The kinetics for grain growth is often expressed as[5]

$$\bar{G}^n - \bar{G}_o^n = K * t \qquad (1)$$

where G is average grain size at time t, G_o is average grain size at time t=0, K is the grain growth constant, and n is the grain growth exponent. More correctly, the normal grain growth rate is given by

$$\frac{d\bar{G}}{dt} = 2v = 2M_b F_b \qquad (2)$$

where v is boundary velocity, M_b and F_b are boundary mobility and driving force, respectively. The velocity of the boundary can also be expressed in terms of atom flux across the boundary, J and the total atomic volume, Ω[6]

$$v \sim \frac{d\bar{G}}{dt} = \Omega J \qquad (3)$$

6

The atom flux is given by

$$J = \frac{D_a}{\Omega kT}\frac{d\mu}{dx} \qquad (4)$$

where D_a is the diffusivity of the rate-limiting ion, k is Boltzmann's constant, and T is temperature. The gradient of the chemical potential, μ represents the driving force, F_b for atomic diffusion across the boundary of thickness dx

$$\frac{d\mu}{dx} = \frac{d}{dx}(\Omega \Delta P) = F_b \qquad (5)$$

The pressure difference across the boundary, ΔP is related to curvature

$$\Delta P = \gamma_b(\frac{1}{r_1} + \frac{1}{r_2}) = \gamma_b(\frac{\alpha}{G}) \qquad (6)$$

where r_1 and r_2 are radii of curvature, γ_b is the boundary energy, α is a geometric constant, and G is the grain size. Combining equations 3-6 yields

$$v \sim \frac{d\overline{G}}{dt} = \frac{D_a}{kT}[\frac{\Omega}{\delta_b}\frac{\gamma_b\alpha}{G}] = M_b\, F_b \qquad (7)$$

Equation 7 represents the velocity of the boundary if the rate controlling mechanism is atomic diffusion across the boundary. This equation demonstrates the significance of a

7

fine grain size for maintaining high boundary velocity. Integration yields parabolic growth kinetics

$$G^2 - G_o^2 = K * t \qquad (8)$$

Considering the presence of a liquid phase during grain growth, the motion of the grain/liquid interface can be controlled by diffusion through the liquid or by the interface reaction (solution/precipitation). When diffusion through a liquid grain boundary phase is the rate-limiting step, the velocity term becomes[7]

$$v = \frac{\theta\ D_l\ C_l\ \Omega}{kT\ G\ \delta_l(G)} \qquad (9)$$

where θ is a geometric constant, D_l is the diffusivity through the liquid, C_l is the grain solubility in the liquid, and $\delta_l(G)$ is the thickness of the liquid film as a function of grain size. For diffusion control through a liquid, the grain size contributes to the velocity in two ways: a curvature controlled driving force and a grain-size dependent film thickness. Integration of Equation 9 produces cubic growth kinetics (n=3).

When the interface reaction is the rate-limiting mechanism, then

$$v = \frac{\eta\ \Gamma\ \Omega\ \gamma_l}{kT\ G} \qquad (10)$$

where η is a constant, γ_l is the interfacial energy of the liquid/grain boundary, and Γ is an

exponential temperature-dependent reaction constant. Integrating Equation 10 yields

parabolic grain growth kinetics (n=2).

1.4 Previous Research

1.4.1 Effect of Excess PbO on PMN-PT Single Crystal Growth

After the initial demonstration of SPC on PMN-PT,[4] work by Khan *et al.*[8] found that

a liquid PbO-based second phase promoted PMN-PT single crystal growth.

Subsequently, Khan and coworkers[9] performed several systematic studies on the effects

of controlled additions of PbO to the PMN-PT polycrystalline precursor, described here.

Flux grown single crystals of PMN-35 mol% (PMN-35PT)* were oriented by Laue

back-reflection. Several (111) plates were cut from the single crystals so that the plate-

normals were in the <111> direction. Individual seeds were embedded in powder

compacts consisting of (A) PMN-35PT + 0 vol.% PbO, (B) PMN-35PT + 1 vol.% PbO,

and (C) PMN-35PT + 5 vol.% PbO. The specimens were subsequently uniaxially hot-

pressed to full density at 900-950°C for 30 min under a pressure of 20 MPa in an air

atmosphere. The center-seeded samples were then pressureless annealed in air at 1150°C

for 10 h. The samples were embedded in powders of the same composition to suppress

---

* Flux grown crystals from S.-E. Park and T. R. Shrout at the Materials Research Laboratory at
The Pennsylvania State University, State College, PA.

9

PbO volatilization. The results are shown in Figure 1.2. No single crystal growth was observed into the PMN-35PT + 0 vol.% PbO matrix. In contrast, moderate (~50 μm) and significant (~1 mm) growth occurred in the samples with 1 vol.% and 5 vol.% PbO, respectively. Clearly, the velocity of the single crystal boundary is dependent on PbO content in the matrix.

If single crystal growth by SPC was largely influenced by boundary curvature (driving force) as previously thought, then the crystal boundary would be expected to migrate into a PMN-35PT + 0 vol.% PbO matrix. Therefore, it was suggested that a PbO liquid film enhances the mobility of the boundary to such a high degree that it overshadows the driving force contribution to the boundary velocity.

In another study, Khan et al.[9] found that the majority of single crystal growth occurred in the early stages of annealing. Figure 1.3 shows the result of a (111) seeded matrix of PMN-35PT + 5 vol.% PbO that was annealed at 1150°C for 0.1, 1, and 10 h (with 5°C/min heating and cooling). It was observed that annealing for longer lengths of time did not significantly advance the crystal boundary. This observation brought to light the fact that the velocity of the single crystal boundary is initially fast, then slows down quickly. This poses a limitation to the SPC single crystal growth process. In order to advance the SPC process, it is necessary to address the issue of what suppresses single crystal boundary migration during the later stages of growth.
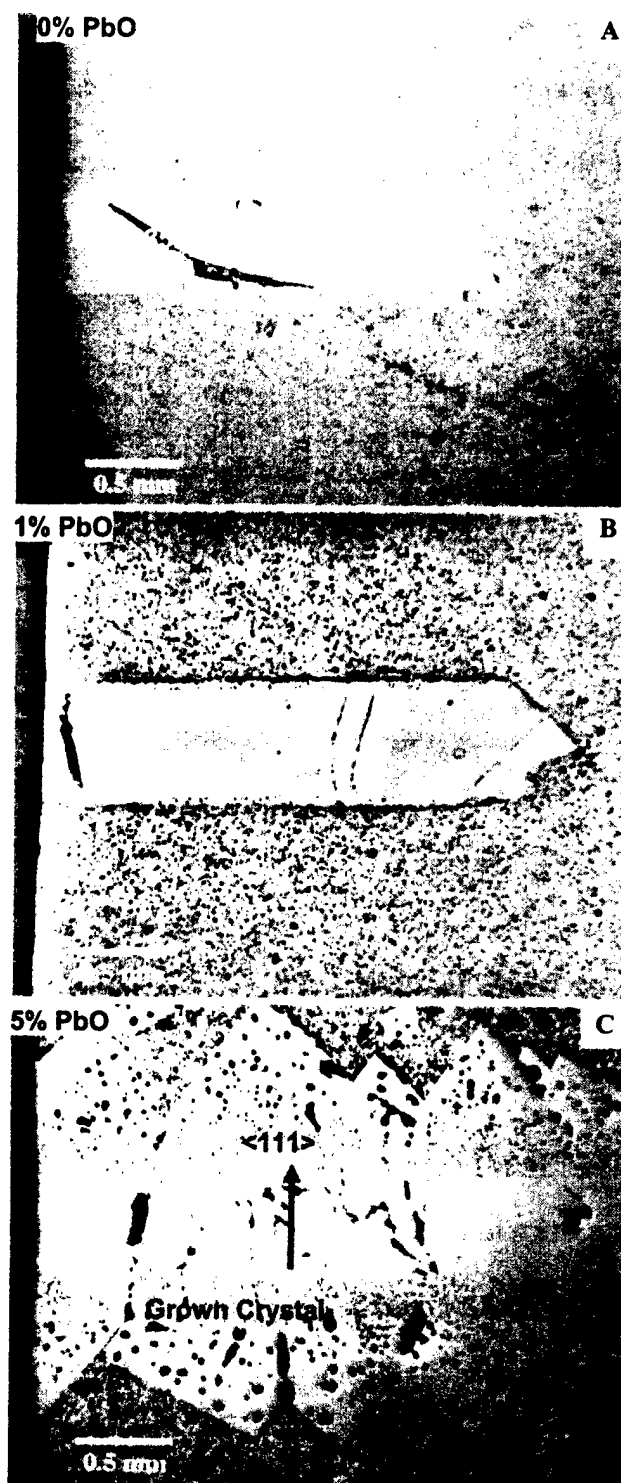
Figure 1.2: Growth from (111) PMN-35PT seed plates into polycrystalline
(A) PMN-35PT + 0 vol.% PbO, (B) PMN-35PT + 1 vol.% PbO, and (C)
PMN-35PT + 5 vol.% PbO, after 1150°C/10h anneal.

11
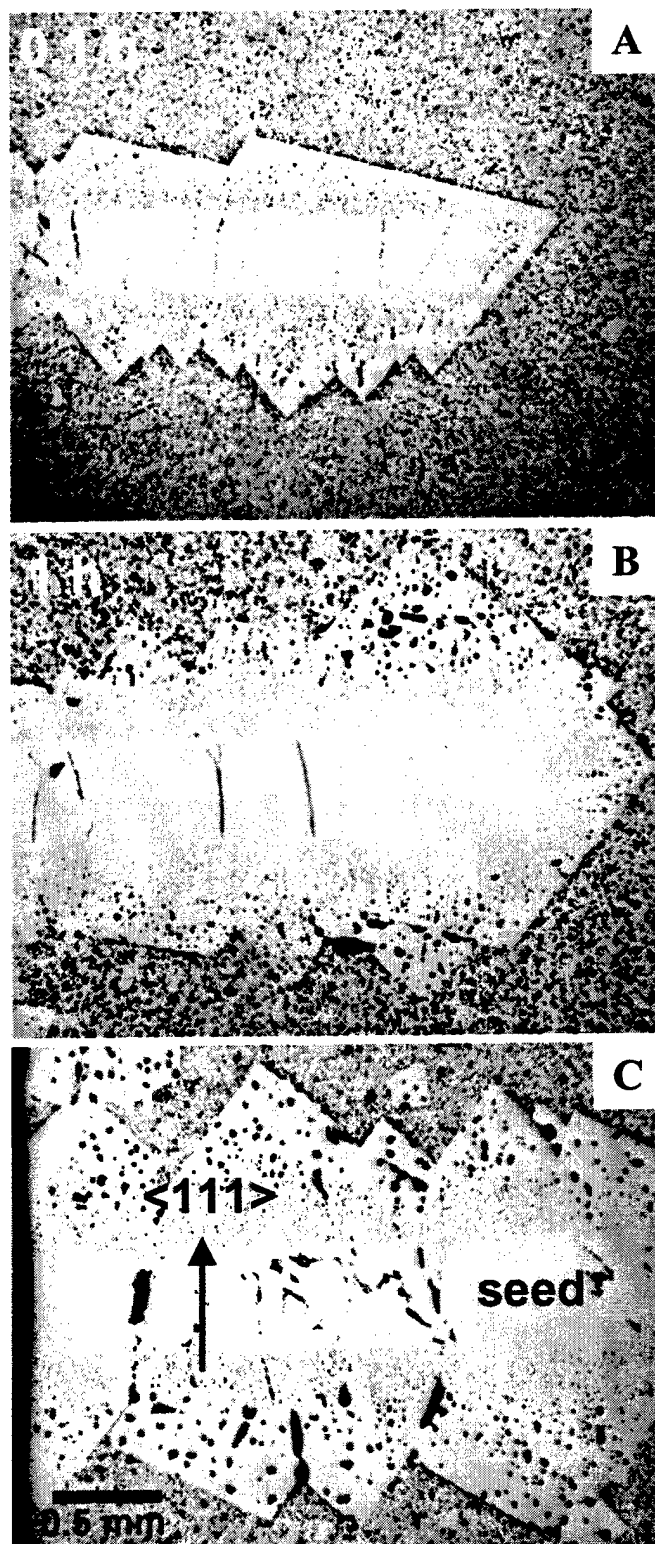
Figure 1.3: Growth from (111) PMN-35PT seed plates into polycrystalline PMN-35PT + 5 vol.% PbO after 1150°C anneal for (A) 0.1 hr, (B) 1 hr, and (C)10 hr.

1.4.2   Effect of Excess PbO on PMN-PT Matrix Grain Growth

Before the issue of decreased crystal boundary velocity is addressed, it is critical to

first evaluate the microstructural development of the polycrystalline matrix.

Khan *et al.*[9] examined the effect of PbO content on the polycrystalline matrix growth

kinetics. Specifically, PMN-35PT compositions containing 0, 1, 1.5, 3 and 5 vol.%

excess PbO were hot-pressed to full density and to the same grain size. These specimens

were then annealed in air at 1150°C for 10 h, packed in powders of like composition to

maintain constant PbO contents during the anneals. The final grain size, like single

crystal growth, was shown to be dependent on PbO content, as shown in Figure 1.4.

Furthermore, the results revealed that small additions of PbO enhanced grain growth up

to a critical maximum of ~3 vol% PbO. Further PbO additions yielded a progressive

decrease in grain growth for the same annealing conditions. Though this grain growth

behavior is unusual, it is not unique. Several other systems show similar trends (ZnO-

Bi_2O_3,[10,11,12] MnZn-ferrites,[13] MgO-V_2O_5[14]).

Later, a more thorough kinetic analysis at 1150°C was done for compositions of

PMN-35PT with 0, 1, and 5 vol.% PbO.[9] These results are summarized in Figures 1.5

and 1.6. PMN-35PT with 0 vol.% PbO additions followed cubic grain growth kinetics, as

seen in Figure 1.6(A). Samples with 1 and 5 vol.% PbO additions both exhibited initial

jumps in grain growth followed by slower cubic growth kinetics, as shown in Figures

1.6(A) and 1.6(B), respectively. The abrupt initial increase in grain growth corresponds

to a microstructural transformation from the as-hot-pressed, equiaxed grains to the

13
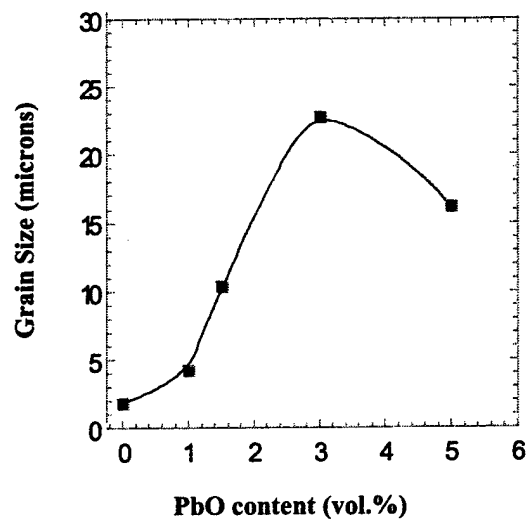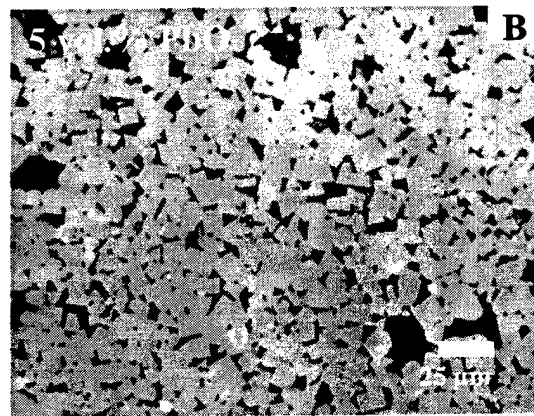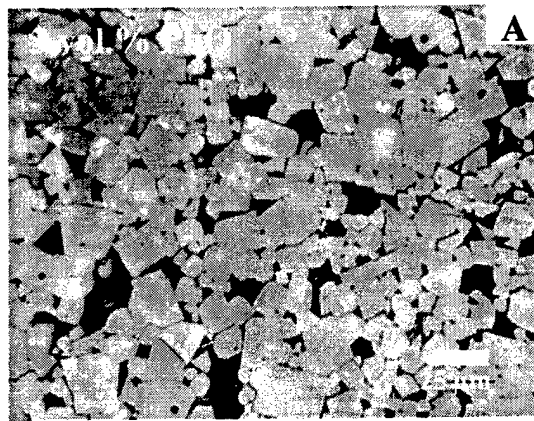
Figure 1.4: Microstructure of polycrystalline PMN-35PT with (A) 3 vol.% PbO
and (B) 5 vol.% PbO additions. PMN-35PT matrix grain size vs. PbO content
(C) reveals a peak in growth kinetics at an intermediate PbO content (peak is at
3vol.% for the PbO content step size studied).

14
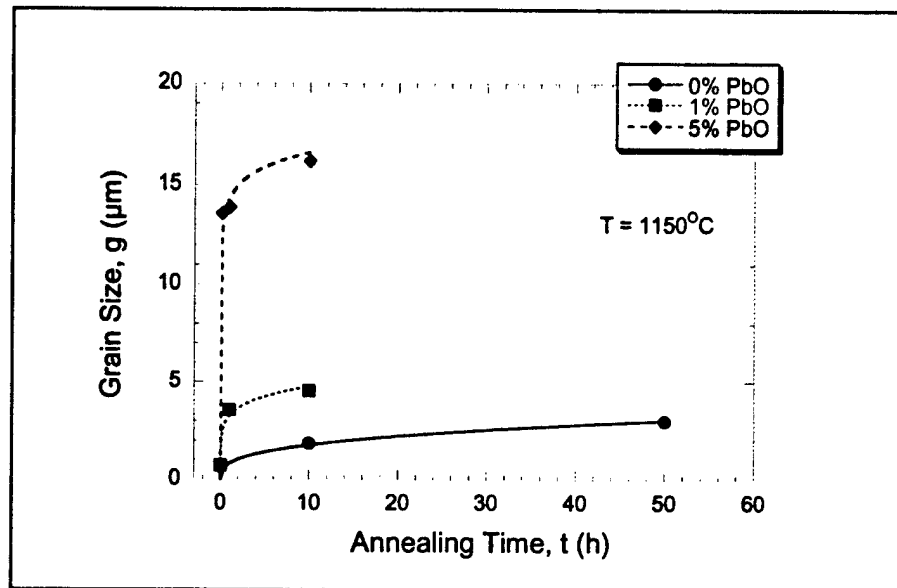
Figure 1.5: Grain size data for PMN-35PT samples with varying PbO contents. Samples were hot-pressed at 900-950°C and annealed in air at 1150°C.
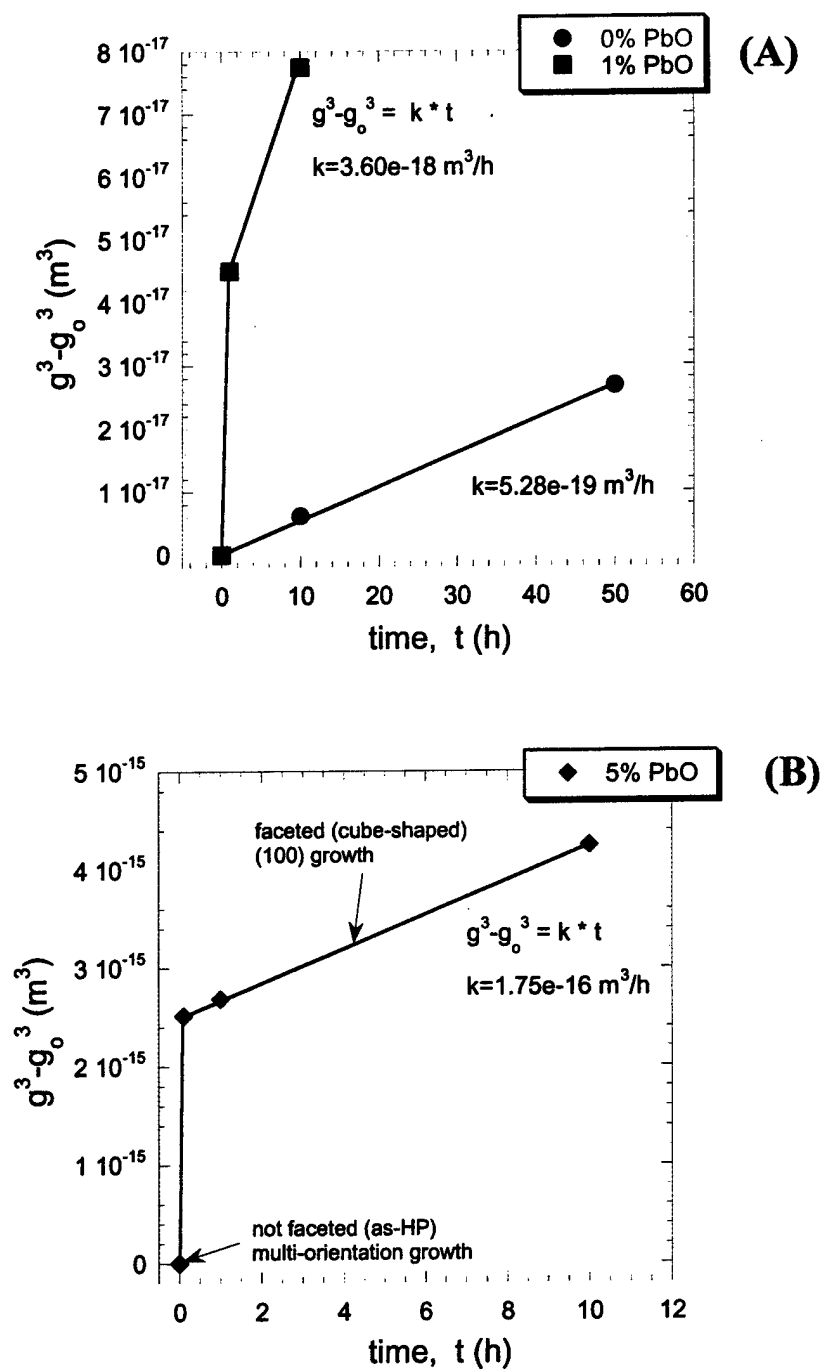
Figure 1.6: Kinetics for grain growth of PMN-35PT with (A) 0 and 1 vol.% PbO and (B) 5 vol.% PbO at 1150°C. Grain growth in the polycrystalline matrix follows cubic kinetics.

annealed, faceted cube-like grains. Grain growth appears to be exceptionally fast until faceting occurs, presumably along (100) faces, when grain growth follows cubic kinetics. It is interesting to point out that this trend parallels the single crystal growth in the <111> direction described earlier (i.e. fast initial crystal growth). Clearly, it can be inferred that the same mechanisms were operating on both matrix grain growth and single crystal growth.

The work of Li et al.,[4] Khan et al.,[8,9] and others at Lehigh have shown an evolution in the microstructure from the as-hot-pressed to the annealed state of PMN-PT materials. The micrographs in Figure 1.7 compare the as-hot-pressed and the annealed microstructures. Table 1.1 summarizes the differences between these starting and final matrix microstructures.

More recently, King et al.[119] confirmed much of the work by Khan et al. with a more thorough kinetic analysis of PMN-35PT with excess PbO contents of 0, 1.5, 3, 4, and 5 vol.%PbO. The grain size data and corresponding grain growth kinetics are shown in Figures 1.8(a) and (b).
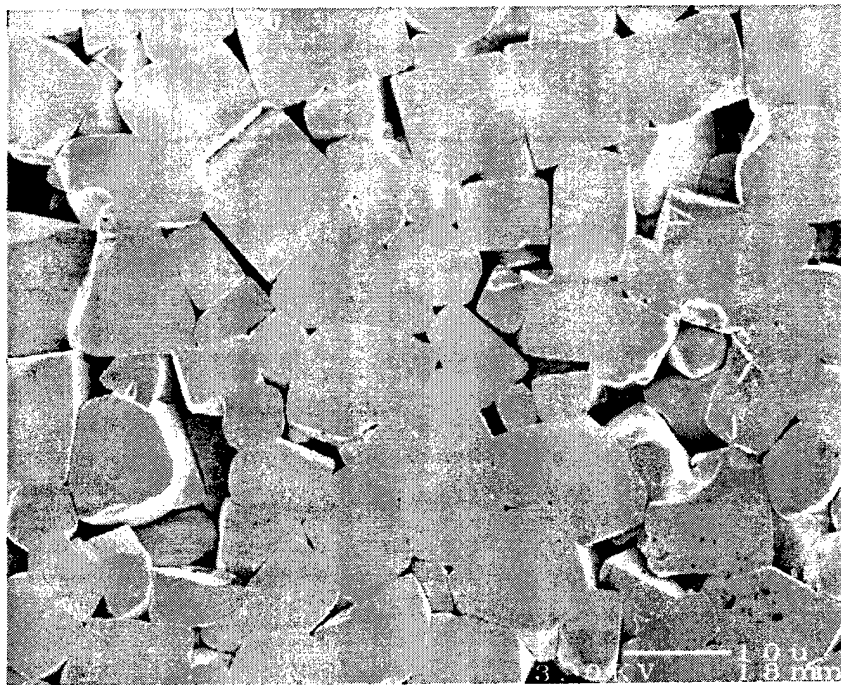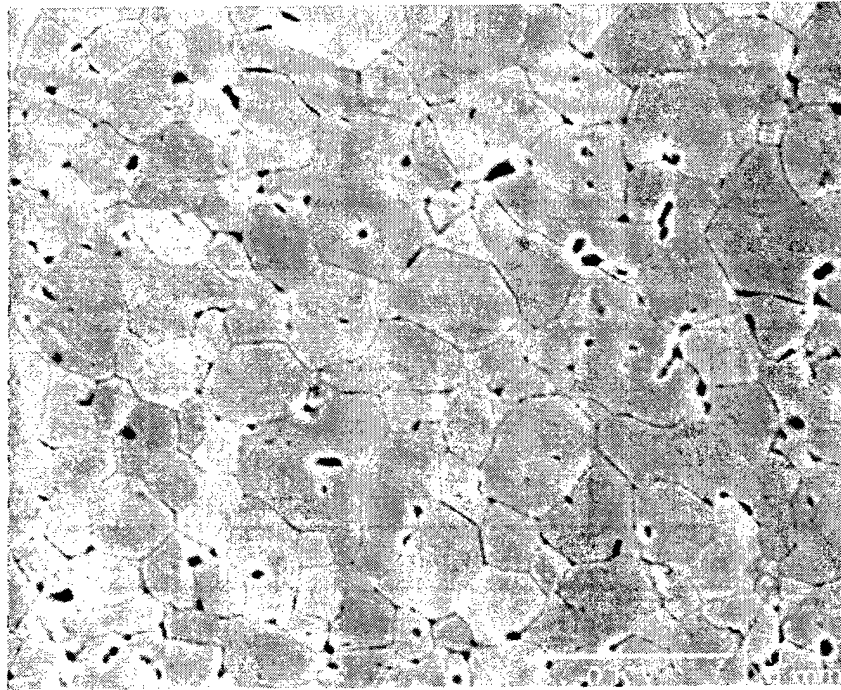
Figure 1.7: Micrographs of PMN-35PT + 5 vol.% PbO after (A) hot-pressing at 900°C and (B) subsequent annealing at 1150°C for 0.1 h. The microstructure evolved during the annealing stage by (i) generating porosity, (ii) increasing grain size, (iii) faceting into cube-like grains. Table 1.1 summarizes these changes.

Table 1.1: Summary of Microstructural Changes in PMN-PT Materials.

Microstructure Element	Initial Microstructure: Hot-Pressed	Final Microstructure: Annealed
Grain Size	Fine grained (~0.7μm)	Coarse grained (~10-20μm)
Abnormal Grains	None	Large (~50μm-1mm)
Grain Shape	Equiaxed	Faceted, cube-like
Liquid phase	Uniformly distributed, constant film thickness	Non-uniformly distributed, liquid pockets
Density	~100% (translucent)	85-96% (opaque)
Porosity	None	In Matrix, Abnormal Grains, Grown Single Crystals
Grain-to-Grain Chemistry	heterogeneous distribution of Mg, Ti, Nb (EDS/STEM)	homogeneous (EDS/SEM)
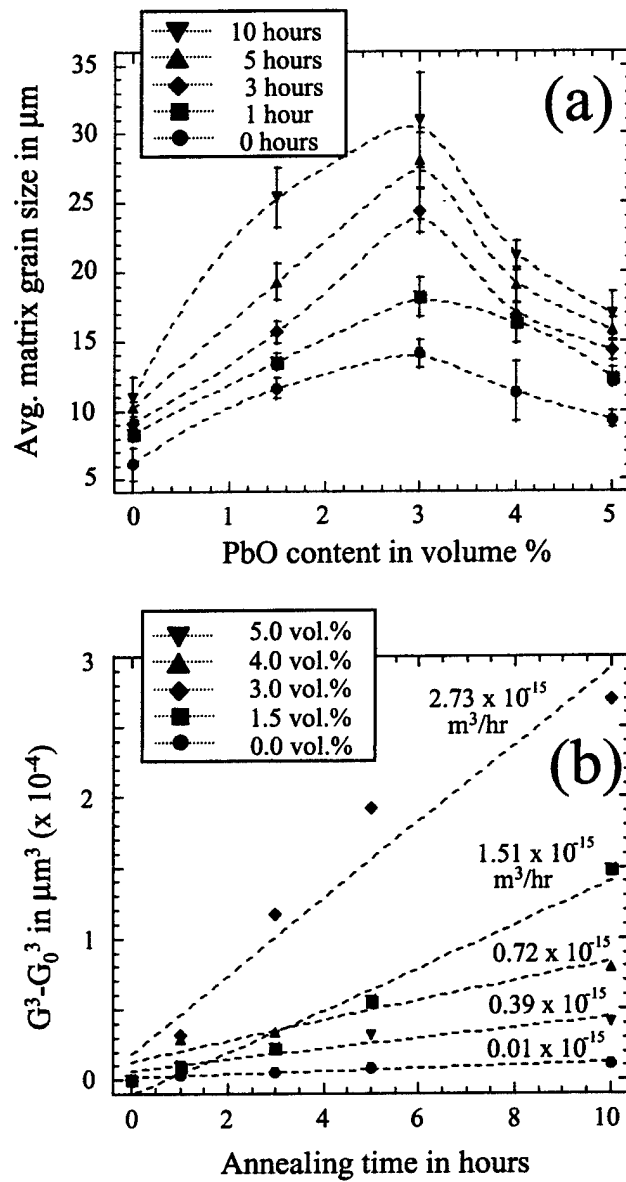
Figure 1.8: (a) Grains size as a function of PbO content for various times and (b) corresponding cubic growth kinetics for matrix grain growth in PMN-35PT with excess PbO at 1150°C. (After King *et al.*[16])

1.5 Research Objectives

The focus of this research was to develop a fundamental understanding of the Seeded Polycrystal Conversion process for growing single crystals. This was accomplished through three primary objectives. First, understand the factors affecting microstructure. Second, adjust the processing parameters to control mictrostucture. Third, characterize the effects of microstructure on properties.

CHAPTER 2

MATRIX AND SINGLE CRYSTAL MICROSTRUCTURE

2.1 Introduction

Single crystal ferroelectrics exhibit dramatic improvements in the electromechanical

properties compared to their conventional polycrystalline ceramic counterparts.[1,2,3]

Consequently, there is great potential for these single crystal materials to be incorporated

into existing devices such as ultrasonic transducers and actuators.

As an alternative to the conventional flux-based techniques for forming single

crystals, initial work established the feasibility of growing relaxor-based ferroelectric

$Pb(Mg_{1/3}Nb_{2/3})O_3$-35mol.%$PbTiO_3$ [PMN-35PT] single crystals by Seeded Polycrystal

Conversion (SPC).[4,8,9,15,16] In this process, a seed crystal is bonded to a polycrystalline

ceramic precursor, and the single crystal boundary is induced to migrate at the expense of

the smaller matrix grains. Maintaining single crystal growth until full conversion of the

polycrystal can only be achieved with an improved fundamental understanding of the

factors that influence the migrating boundary. The most significant parameter is the

addition of a PbO-based liquid phase. It was found that the presence of a liquid phase at

the grain boundaries enhanced the growth rate of the single crystal.[8,9,16] In contrast, little growth was observed in the absence of a liquid.

Although the PbO additions promote single crystal growth, they also enhance matrix grain growth, induce abnormal grain growth, and contribute to the formation of porosity, each of which have the potential to interfere with the migrating boundary. Furthermore, trapped porosity, liquid phase, and other defects can be left behind the migrating boundary, having a detrimental effect on the quality of the final grown single crystal. Although previous work has demonstrated respectable electro-mechanical properties for SPC crystals containing trapped porosity and PbO-based inclusions,[4,8] such crystals can be rather lossy and are more susceptible to dielectric breakdown. Thus, the long-term integrity of the crystals is a concern.

The purpose of the present work was to examine the factors that affected the quality of the SPC-grown PMN-35PT single crystals and to derive an understanding of how the processing parameters may be tailored to control their final microstructures and properties.

2.2 Experimental Procedure

PMN-30PT and PMN-35PT powders (TRS Ceramics) were ball-milled in HDPE bottles with 0, 1.8 and 5 vol.% PbO (Alfa Aesar, puratronic powder) in ethanol for 24 h using 3mm zirconia media (Tosoh). The powders were dried under slight vacuum using a rotoevaporator (Büchi) and subsequently calcined at 450°C for 4 h in air. The calcined

23

powders were crushed with an agate mortar and pestle and passed through a 100-mesh

stainless steel sieve. The mean particle sizes of the powders were determined using a

laser scattering particle size analyzer (Horiba LA-910) with ethanol as the dispersing

agent.

The powders were uniaxially pressed at 67 MPa to form 3 mm x 13 mm ϕ pellets

and subsequently cold isostatically pressed at 345 MPa. In the case of single crystal

growth experiments, oriented {001} and {111} PMN-PT seed crystal plates (Crystal

Associates and Penn State) on the order of 2.5 mm x 2.5 mm x 0.5 mm were embedded in

the center of the pellets prior to pressing.

Specimens were sintered from the green state in both oxygen and air atmospheres

with heating/cooling rates of 5°C/min to 1175°C and hold times of 0 to 12 h. The

samples were enclosed in a platinum foil pouch and embedded in PMN-PT powder with

excess PbO using the double-crucible technique in order to suppress PbO volatilization.

The weight changes were monitored and never exceeded a 2 wt.% loss. It was more

difficult to maintain a constant weight when sintering ~70% dense pellets from the green

state than was previously reported for hot-pressed samples of the same compositions.[9,16]

In order to obtain grown crystals from {001} seeds that were large enough for future

piezoelectric property measurements, the grown crystals from several samples were

etched out of the matrix using a 30% solution of HNO_3 in an ultrasonic bath, cleaned and

re-embedded in fresh powder for subsequent growth cycles. This was required for only

the {001} seeded samples due to the slower planar growth rate in the <001> direction.

The specimens were sectioned, mounted in epoxy, and polished using 9, 3, and 1 μm

diamond paste followed by vibratory polishing overnight with a 1 μm polycrystalline diamond slurry. A finishing polish with 0.05 μm colloidal silica on a vibratory polisher for 1 h often provided enough surface relief to reveal a grain structure. For grain size measurements, the polished samples were either chemically etched using Kroll's reagent (1 vol.% HF + 4 vol.% HNO3 + water) or thermally etched at 850-950°C for 0.5-1 h.

The polished and etched cross-sections were characterized using light optical microscopy (LOM) and scanning electron microscopy (SEM). For LOM analysis, the samples were observed under both bright-field and Nomarski differential interference contrast conditions (Reichert MeF3). For SEM characterization, the specimens were examined uncoated using a 3 kV accelerating voltage with a field-emission gun instrument (JEOL JSM 6300F). Grain size measurements were performed using a computer automated image analysis system (LECO 3001). The average grain size was determined from approximately 200-500 grains per sample by the feret method as previously described.[9,16,17] The values were then multiplied by a geometric factor of 1.56 to convert into three dimensions.[18] Density measurements were measured using the Archimedes method in water containing a small amount of surfactant.

2.3   Results

The SEM micrograph in Figure 2.1(a) demonstrates that the as-milled PMN-35PT + 5 vol.%PbO powder is sub-micron in size. The mean particle size of all milled powders was determined to be ~0.7 μm using a laser scattering technique.

Figures 2.1(b-c) show the matrix microstructures of the oxygen sintered PMN-35PT + 5 vol.%PbO samples for 0, 1, and 12 h hold times, respectively. Note that significant grain growth and densification has occurred by simply heating the sample to 1175°C and cooling, i.e. 0 h hold (Figure 2.1(b)). A grain growth kinetic analysis was performed only for the PMN-35PT + 5 vol.%PbO composition sintered in oxygen. Figure 2.2(a) plots the resultant grain size as a function of time. These data were best fitted to a cubic grain growth law

$$G^3 - G_o^3 = kt$$

where G is grain size at time t, G_o is the initial grain size at time t=0, and k is the growth rate constant. The growth kinetics are conventionally described using a plot of $G^3 - G_o^3$ versus time, where the slope of the best-fit line represents the rate constant, k. As shown in Figure 2.2(b) and Table 2.1, the calculated growth rate constant was 3.6×10^{-16} m³/h with an R^2 of 0.96 for PMN-35PT 5 vol.%PbO samples sintered in oxygen. A better fit was attained by excluding the 0 h sample, yielding a k of 3.3×10^{-16} m³/h and an R^2 of 0.99.

The effect of sintering atmosphere on densification of PMN-35PT with PbO additions is apparent in Figures 2.3(a-d). As seen from the low and high magnification LOM micrographs in Figures 2.3(a) and (b), samples sintered in oxygen achieved a high density of 8.25 g/cc after 4 h at 1175°C. In contrast, samples sintered in an air atmosphere exhibited lower densities, i.e. 7.83 g/cc after 4 h at 1175°C in air. As shown in Figures 2.3(c) and (d), the larger volume fraction of porosity in the air sintered samples
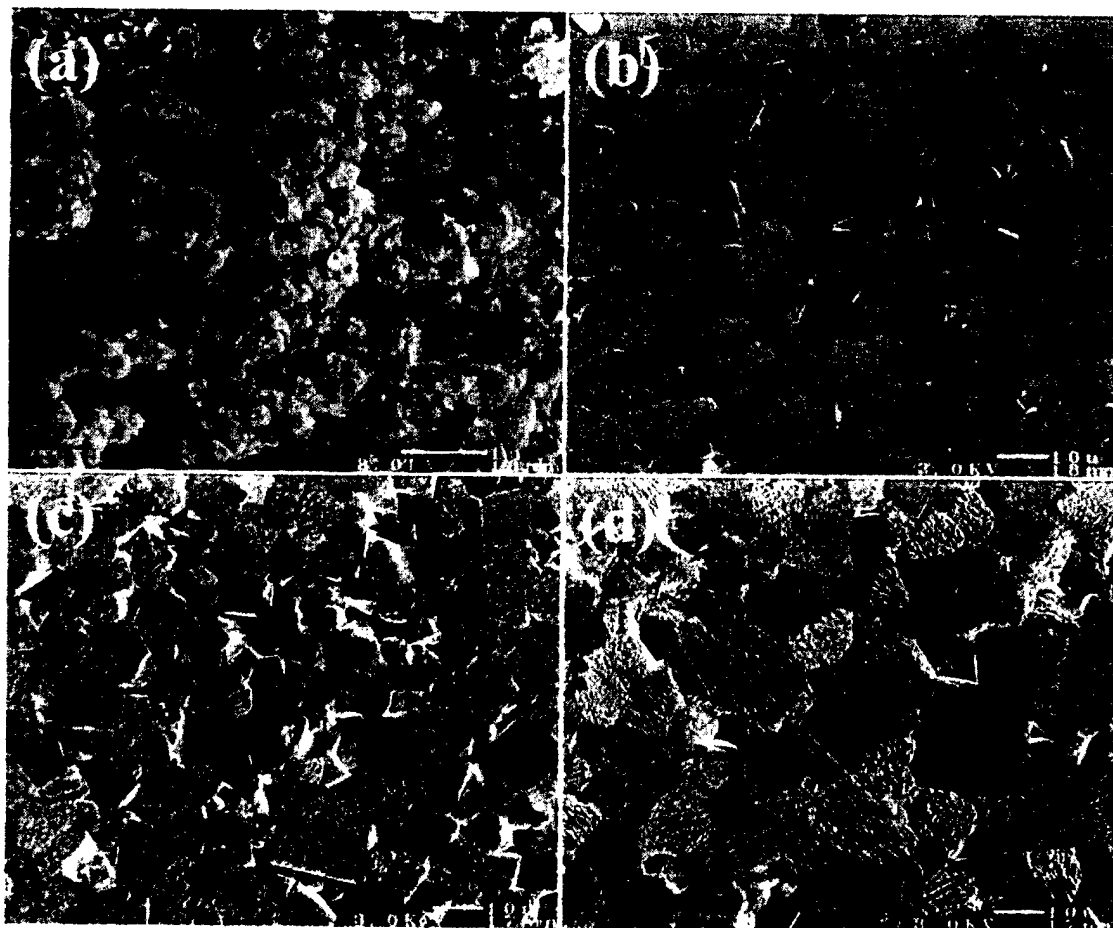
Figure2.1. SEM micrographs of PMN-35PT + 5 vol.%PbO (a) as-milled, and sintered for (b) 0 h, (c) 1 h, and (d) 12 h at 1175°C in oxygen. Sample (b) was chemically etched, while (c) and (d) were thermally etched.
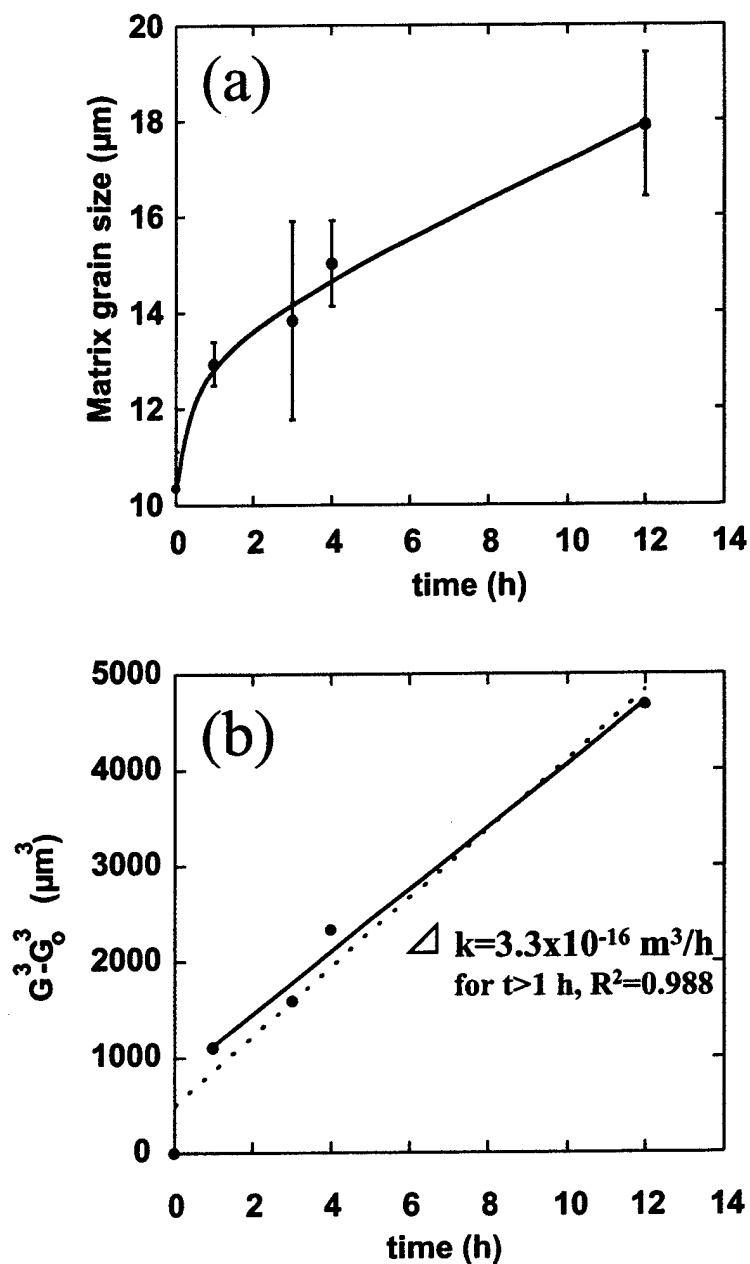
Figure 2.2. Grain growth kinetics of the matrix grains from PMN-35PT + 5 vol.% PbO samples sintered in an oxygen atmosphere at 1175°C for 0 to 12 hours. The data fit a cubic grain growth law with a rate constant of 3.6×10^{-16} m^3/h. The correlation factor, R^2 is 0.961. A better fit is obtained for $t>1$ h, where $k=3.3 \times 10^{-16}$ m^3/h and R^2 is 0.988.
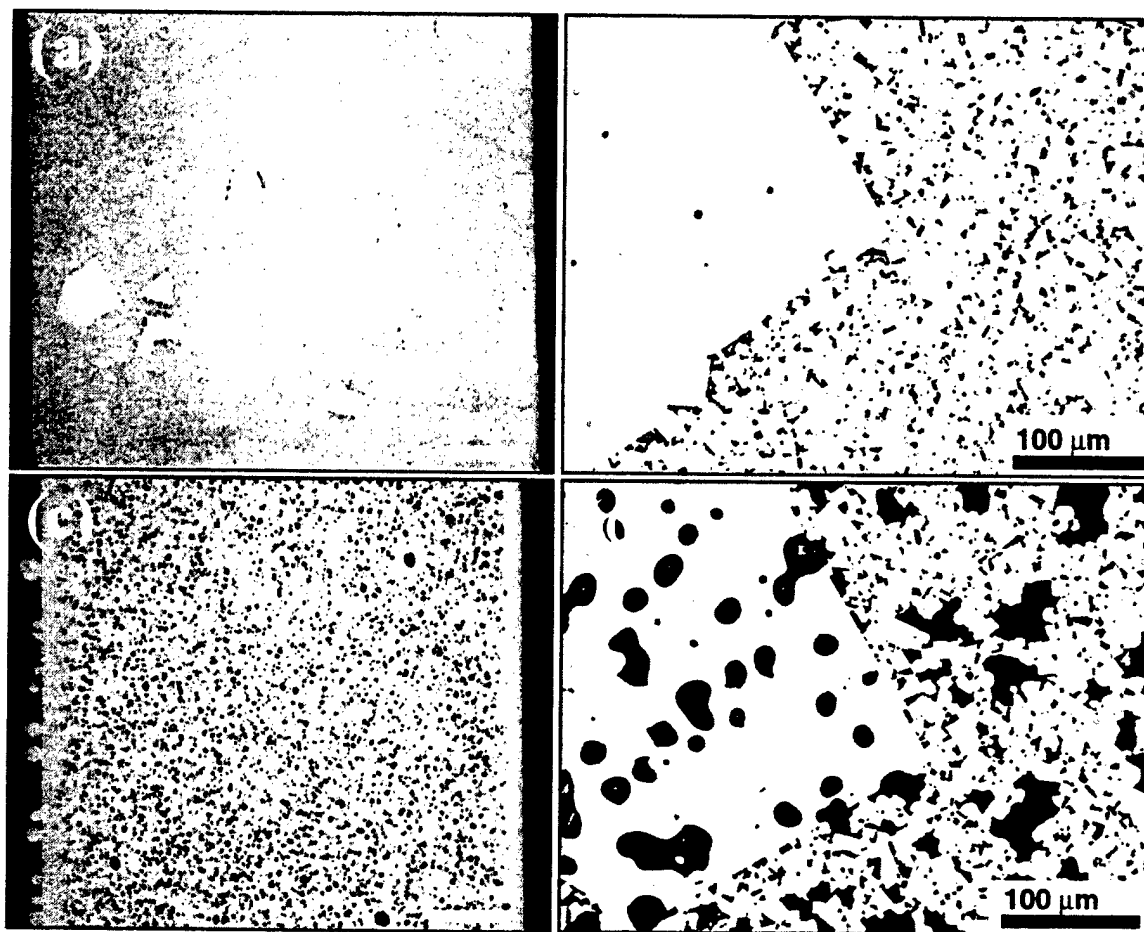
Figure 2.3. LOM micrographs of unseeded PMN-35PT + 5 vol.%PbO sintered at 1175°C for 4 h in (a),(b) oxygen, and (c),(d) air atmospheres. Figures (b) and (d) are higher magnification micrographs showing large abnormal grains which have nucleated from the matrix.

Table 2.1: Comparison of grain growth rate constants for PMN-35PT + 5 vol.% PbO.

Reference	Growth rate constant, $k^{\#}$ (m^3/h)	R^2	time scale (h)	Processing conditions
This work	3.6×10^{-16}	0.96	0-12	sintered in oxygen, 1175°C
	3.3×10^{-16}	0.98	1-12	
Sabolsky *et al.*[27]	5.1×10^{-16}	0.57	0-5	sintered in air, 1150°C*
	2.5×10^{-16}	0.96	0.5-5	
King *et al.*[16]	3.9×10^{-16}	0.90	0-10	hot-pressed + annealed in air, 1150°C
	6.0×10^{-16}	0.98	0-5	

#calculated using conventional cubic growth law, $G^3 - G_o^3 = kt$.
*samples contained 5 wt.% (~4.25 vol.%) PbO.

account for the lower measured densities. Figures 2.3(a-d) also reveal the presence of large (100-300 μm) abnormal grains that have nucleated from the matrix. The abnormal grains were present in both air and oxygen sintered samples and their microstructures were reflections of the surrounding matrices. That is, abnormal grains within the air sintered samples contained trapped porosity while those grains within the oxygen sintered samples did not.

The microstructures of single crystals grown from {111} seed plates embedded in PMN-35PT + 5 vol.%PbO are shown in Figure 2.4. Figures 2.4(a) and (b) show LOM micrographs of {111}-seeded samples that were sintered in oxygen and air, respectively, for 4 h at 1175°C. The arrows indicate the <111> directions of the grown crystals, thus the {111} seed plates are oriented perpendicular to the plane of the paper. As shown, the <111>-grown single crystals exhibited differences in porosity content between oxygen and air sintered samples, similar to the abnormal grains in Figures 2.3(b) and (d). However, the <111>-grown crystals also contained pockets and strings of trapped PbO-based second phase. As observed in Figure 2.5, the amount of this trapped second phase was reduced by lowering the starting PbO content in the matrix to 1.8 vol.%PbO.

The microstructures of single crystals grown from {001} seed plates embedded in PMN-35PT + 5 vol.%PbO and sintered in oxygen and air are presented in Figures 2.6(a) and (b), respectively. The LOM micrographs show the corners of the seed plates and grown single crystals. The arrows indicate the <001> directions. The three growth layers observed in the grown single crystals were the result of three separate sintering cycles where the grown crystals were etched out and re-embedded in fresh powder, as described

in the previous section. The lines of defects present at the seed/grown crystal interface and between the crystal layers in Figure 2.6(a) were small PbO-containing pores.

2.4 Discussion

2.4.1 Matrix Microstructure

2.4.1.1 Grain Growth

For an accurate grain growth analysis on a system containing a low-melting temperature second phase, such as PbO in PMN-35PT, it is necessary that the content of the second phase remains constant over all samples and sintering times. Due to the high volatility of PbO at the sintering temperatures used in the current study, maintaining the liquid phase content was a challenge, especially for long sintering times. The use of the double crucible technique together with packing powders of higher PbO compositions than the sample proved as an effective means to minimize weight loss. This concept was originally advanced for the sintering of Pb(Zr,Ti)O$_3$ (PZT) ceramics.[19,20,21,22,23,24,25]

The measured sample weight losses from green pellets of PMN-35PT + 5 vol.%PbO in this study were higher than previously reported for hot-pressed samples of the same PbO content.[9,16] Due to the low green strength of the unsintered pellets, the samples
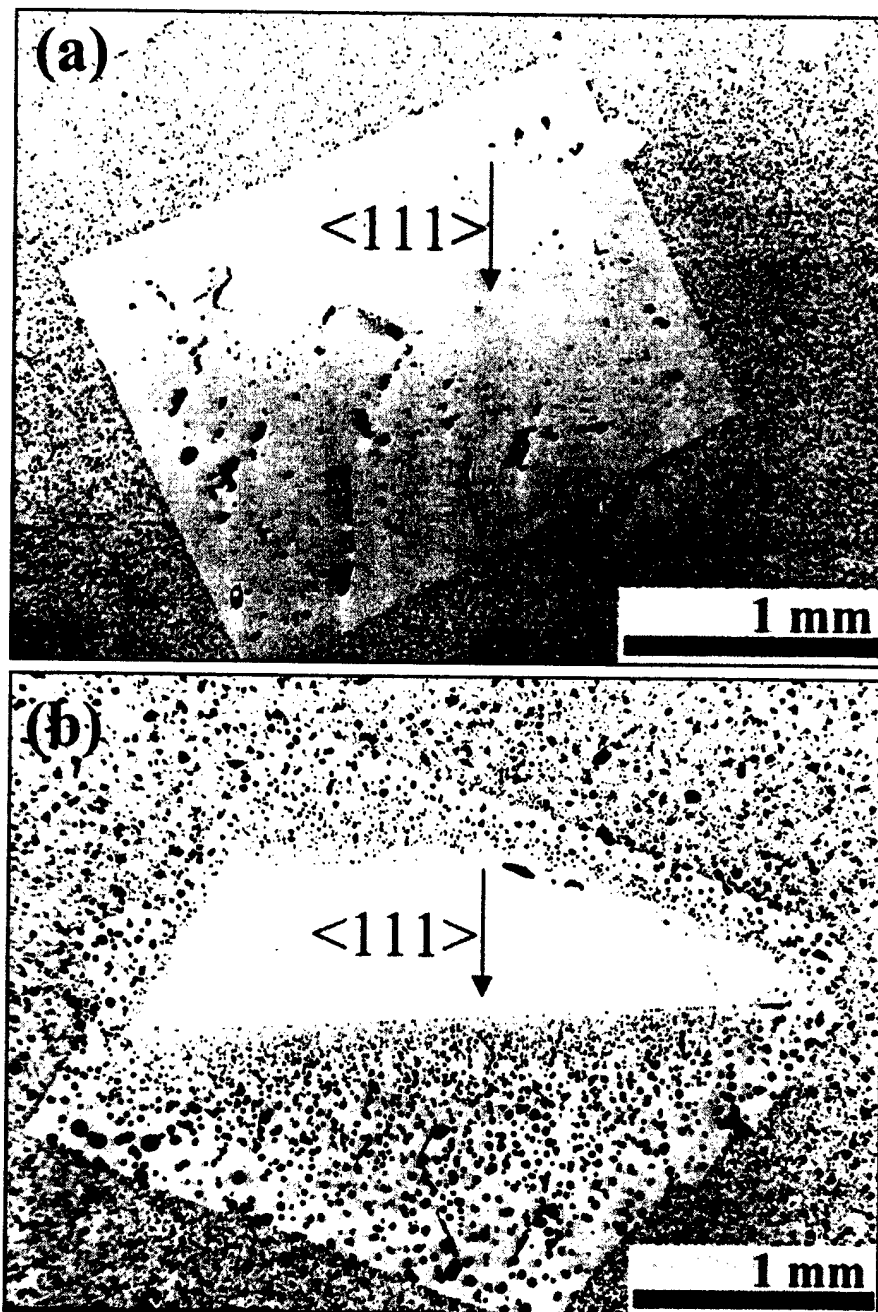
Figure 2.4. LOM micrographs of {111} seeded PMN-35PT + 5 vol.%PbO samples sintered at 1175°C for 4 h in (a) oxygen and (b) air atmospheres. The dark phase in the oxygen-grown crystal in (a) is trapped PbO from the liquid phase. The dark phase in the air-grown crystal is a combination of trapped PbO and porosity.
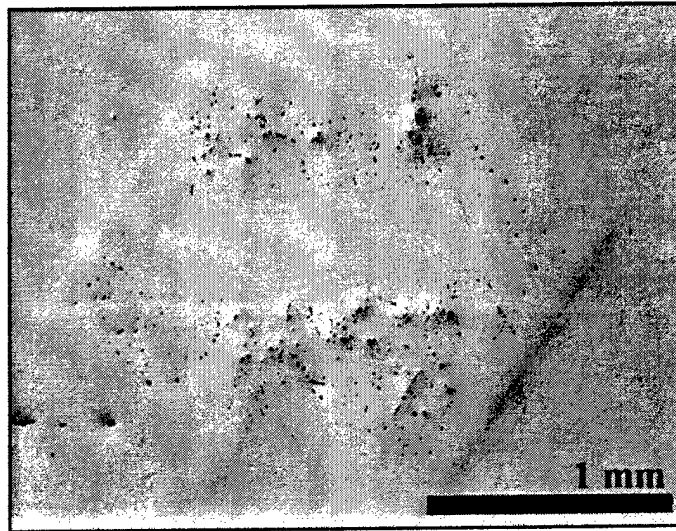
Figure 2.5. LOM micrographs of {111} seeded PMN-35PT + 1.8 vol.%PbO
sample sintered at 1175°C for 4 h in an oxygen atmosphere. Note the reduction in
the amount of trapped PbO compared to Figure 2.4(a).
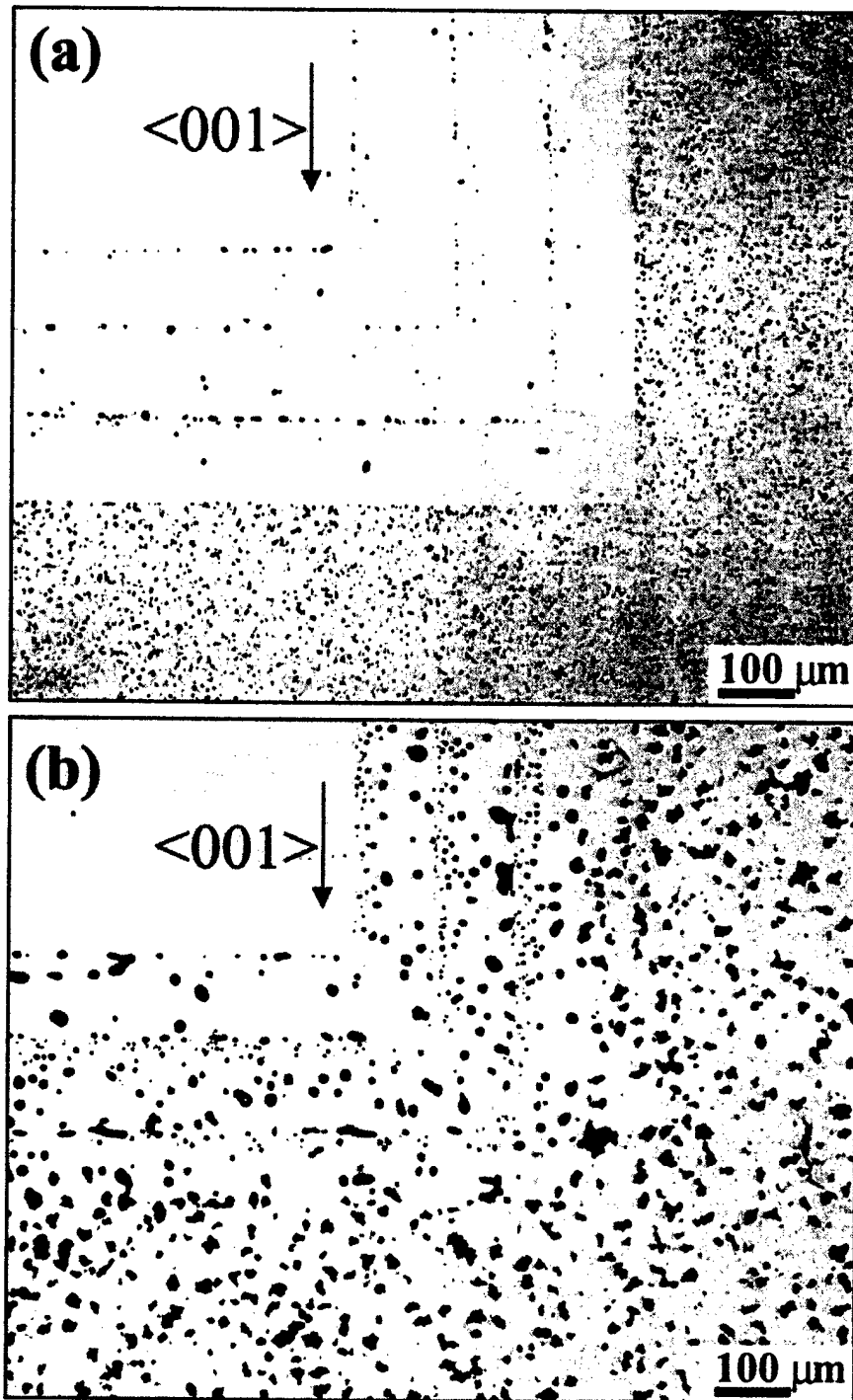
Figure 2.6. LOM micrographs of {001} seeded PMN-30PT + 5 vol.%PbO samples sintered for 3 cycles at 1175°C for 4 h each in (a) oxygen and (b) air atmospheres. After each cycle, the grown crystal was removed from the matrix by a chemical etchant and re-embedded in fresh PMN-30PT + 5 vol.%PbO powder. Note the reduction in the amount of trapped defects in (a) compared to the crystals in (b) and the crystals grown from {111} seed plates in Figure 2.4.

were easily chipped by handling and pieces could flake off when inserted into the Pt foil pouch after the weighing. Consequently, the larger weight losses of some samples may have been artifacts and therefore not true representations of actual PbO loss. Hot-pressed samples were not subject to this problem. However, it could also be argued that the green pellets with their fine particle sizes and low densities had higher surface areas exposed to the atmosphere, thus providing for greater PbO vaporization rates, especially at early times.

As shown from Figures 2.1 and 2.2, PMN-35PT with 5 vol.%PbO underwent significant grain growth during sintering at 1175°C in oxygen. Much of this coarsening occurred during the heating and cooling cycle, since a 0 h hold produced an average grain size of 10.2 μm from an initial starting particle size of 0.7 μm. This was the consequence of a 5°C/min heating and cooling rate which allowed the samples to experience temperatures above the melting point of the PbO for nearly two hours. It is well known that a PbO liquid phase increases both densification and grain growth rates in PMN-PT and other Pb-based perovskites.[9,26] Thus, the elevated rate of densification and grain growth in the present study is due largely to the fine, highly sinterable starting particle size and the PbO second phase. Furthermore, the use of an oxygen sintering atmosphere helped the samples to attain even greater final densities than were achieved by sintering in air. This effect of oxygen will be addressed in the next section.

Figure 2.2(b) plots the grain growth data in the conventional $G^n - G_o^n$ versus time format for PMN-35PT + 5 vol.%PbO samples sintered in oxygen. The data best fit a cubic growth law, where the growth exponent, n=3. The growth rate constant, k was

calculated from the slope as 3.6 x 10^{-16} m³/h (R^2=0.961). This is represented by the dashed line in Figure 2.2(b). A slightly better fit was obtained by excluding the 0 hr point, yielding a k of 3.3 x 10^{-16} m³/h (R^2=0.988), represented by the solid line. The reason for the better fit is because the initially porous samples had to first undergo a densification process in the early stages of the heat treatment and were not yet fully dense by 0 h. By 1 h, the samples achieved full density and behaved as fully dense ceramics, where grain growth and densification were no longer competing events. The grain growth data of Sabolsky et al.[27] showed a similar behavior for PMN-35PT + 5wt.%PbO sintered at 1150°C in air. In that work, rapid grain growth was also observed to occur in the first 1 h, followed by slower kinetics that best fit a cubic growth law for times greater than 0.5 h (R^2=0.957).

Table 2.1 compares the k values calculated in this study with those calculated from raw grain size data reported by King et al.[16] for hot-pressed + air annealed samples and by Sabolsky et al.[27] for air sintered samples of PMN-35PT + PbO. All growth rate constant values were calculated using the conventional cubic growth law described above. As the table shows, the calculated growth rate constants from the present work and from Sabolsky et al. are in very good agreement. This is especially the case after excluding the rapid densification stage in the early part of the heat treatments. Although the lower k value calculated from the Sabolsky et al. data could be attributed to the presence of porosity (as a result of sintering in air) or a slightly lower sintering temperature, the two k values probably fall within experimental errors.

King et al. reported a growth rate constant, k of 3.9 x 10^{-16} m³/h for PMN-35PT + 5

vol.%PbO samples that were initially hot-pressed to full density in air and subsequently annealed in air under pressureless conditions at 1150°C. This is also in good agreement with the present work. It could be argued that once the oxygen sintered samples achieved full density (~1 h), the grain growth behavior paralleled that of the hot-pressed samples which were fully dense from the start. This, coupled with a similar but slightly lower k value for the porous air-sintered samples, would suggest that porosity has a very small effect on the grain growth kinetics of PMN-PT with excess PbO. It should be noted, however, that the hot-pressed samples of King *et al.* underwent a de-densification process during the annealing treatments as the direct result of pore formation from internally evolved gases. This swelling process is described in detail elsewhere[28] and will be discussed in Chapter 5.

As a consequence of the swelling, the hot-pressed and annealed samples contained as much as 10% porosity[16] and were then just as porous as the air sintered samples. With the understanding that the hot-pressed + 10 h annealed sample had the lowest density (and most porosity), and noting from Table 2.1 that the R^2 value of the King *et al.* data was somewhat low at 0.903, a similar approach was taken as before. If the 10 h anneal sample were excluded, the data would better fit a cubic growth law, yielding $R^2=0.975$. The resulting growth rate constant would increase to 6.0 x 10^{-16} m^3/h, nearly twice as high as the k's from the oxygen or air sintered samples of the present work and Sabolsky *et al.* This indicates that starting with an initially fully dense microstructure, as in the hot-pressed case, enhances grain growth by only a factor of two when compared to air or oxygen sintered samples.

2.4.1.2 Effect of Oxygen Atmosphere

As shown in Figure 2.3, the sintering atmosphere had a significant effect on the densification of PMN-35PT. Sintering in oxygen yielded fully dense ceramics, while sintering in air for the same time resulted in porous microstructures, independent of the excess PbO content. This was true even for PMN-35PT samples with 0% excess PbO. This result is consistent with what others have observed for the densification of PZT,[29] (Pb,La)(Zr,Ti)O_3 (PLZT),[22,23,30,31] and Pb(Ni$_{1/3}$Nb$_{2/3}$)O_3-Pb(Zr,Ti)O_3 (PNN-PZT)[32] in oxygen.

In the current work, the density of a PMN-35PT + 5 vol.%PbO sample sintered in air for 4 h at 1175°C was 7.83 g/cc (~96%) (Figure 2.3(c-d)). A sample sintered in oxygen under the same conditions had a density of 8.25 g/cc (Figure 2.3(a-b)), which is greater than the calculated theoretical value of 8.17 g/cc for PMN-35PT + 5 vol.%PbO. The higher than theoretical density values occurred consistently for oxygen sintered samples and will be addressed later.[28]

The existence of abnormal grains in the microstructure of many samples, as seen in Figure 2.3, is related to the presence of excess PbO.[33,34,35] Only those samples containing 5vol.% PbO had abnormal grains, oxygen and air sintered alike. As shown in Figure 2.2(d), any porosity present in the microstructure became entrapped in the abnormal grains as they grew. The abnormal grains in the microstructures of samples sintered in oxygen were clear of porosity. The small defects seen inside the abnormal grain in Figure 2.3(b) are trapped spherical MgO particles which also exist in the matrix and can be

39

found in the air sintered samples as well.

Thermal Decomposition

The differences in the observed microstructures between oxygen and air sintered samples are not surprising when considering the fact that densification of polycrystalline oxide specimens under the atmosphere of a soluble gas (O_2, H_2) is easier than densification under an insoluble gas (N_2, Ar, He).[36] As Moon et al.[32] and Sun et al.[30] point out, however, sintering Pb-based electroceramics is more complicated. Thermal decomposition and evaporation of PbO is known to deteriorate densification in these materials.

The thermal decomposition can be represented as[30,32,37]

$$PbO(s,l) \leftrightharpoons PbO(g) \leftrightharpoons Pb(g) + \tfrac{1}{2}O_2 \tag{1}$$
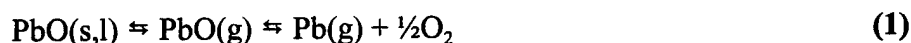
During the final stage of sintering, thermal decomposition increases the pressure inside of a closed pore due to the generation of gas(es). The internal pressure (P_{in}) of a closed pore can therefore be expressed as[30]

$$P_{in} = P_O + P_{therm} - 2\gamma_{sv}/r \tag{2}$$

where P_O is the pressure of trapped insoluble gas, P_{therm} is the pressure induced by thermal decomposition of PbO, γ_{sv} is the grain/vapor interfacial energy, and r is the pore radius. Moon et al.[32] estimated that according to Equation 1, the thermal decomposition of PbO can be suppressed by increasing the partial pressure of O_2.

Northrop,[37] however, performed vaporization studies on hot-pressed PZT and

showed no difference in weight loss between N_2 and O_2 annealing atmospheres. It was concluded that the evaporating species was PbO, not Pb and O_2. Furthermore, mass spectrometric analysis of the vapor phase above PbO[37,38,39] has shown that the vapor composition consists mostly of PbO(g) molecules and its polymers Pb_nO_n(g). Thus, the lead dissociation reaction (right part of Equation 1) does not occur to any great extent and vaporization proceeds by following the reaction

$$nPbO(s,l) \leftrightarrows Pb_nO_n(g)$$
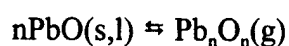
According to this reaction, the vaporization of PbO is not thermodynamically dependent on the partial pressure of O_2. Therefore, an oxygen atmosphere cannot control the decomposition of PbO and thus does not reduce the P_{therm} term of Equation 2.

In any case, the pressure associated with the decomposition of PbO is not high enough to generate porosity on its own, nor increase pore size. The total vapor pressure over liquid PbO has been measured by many authors.[38,40,41] Based on that data, the total pressure over PbO liquid at 1175°C was calculated to be 1.8 kPa. This pressure is insignificant compared to the pressure acting on a pore due to surface energy, i.e. $P=2\gamma/r$. For example, pore sizes of 20, 10, and 1 μm in diameter would produce pressures of 50, 100, and 1000 kPa, respectively. This assumes a surface energy of 0.25 J/m^2, which is a conservatively low estimate. Consequently, the vapor pressure above PbO was not likely to contribute to much of the porosity that existed in PMN-35PT samples that were sintered in air.

Trapped Insoluble Gases

In earlier work on PLZT ceramics, Snow[22] had reported that samples sintered in oxygen were much more dense than those sintered in air. It was postulated that insoluble gases from the air atmosphere (primarily N_2) were trapped inside the closed pores, thus limiting the final density of the air-sintered samples. The author concluded that the oxygen atmosphere was necessary to prevent entrapment of insoluble gases in pores during the early stages of sintering. A subsequent article by the same author[23] reported that PLZT samples containing 6.6 wt.%PbO required only short sintering times (~45 min.) inside a Pt crucible in an oxygen atmosphere to complete densification. The Pt crucible was used to contain the PbO, which aided densification. A second, much longer heat treatment in an alumina crucible in air was used to remove the excess PbO liquid phase before significant grain growth occurred. The switch to air atmosphere did not affect the densification, and the samples achieved transparency.

The detrimental effect of trapped gases on the densification behavior of ceramics was also observed in a more recent study by Dong[42] for liquid phase sintered alumina. In that study, Dong sintered alumina compacts containing up to 20 vol.% calcium aluminosilicate glass in both air and vacuum. The author found the air sintered samples reached a limiting density of 98.5% while the vacuum sintered samples achieved full density. Microstructures of the alumina samples with 20 vol.% glass sintered for 10 hrs at 1600°C in air and vacuum are shown in Figures 2.7(a) and (b), respectively. As shown in Figure 2.7(a), after the final stage of sintering, the air-sintered sample contained

42
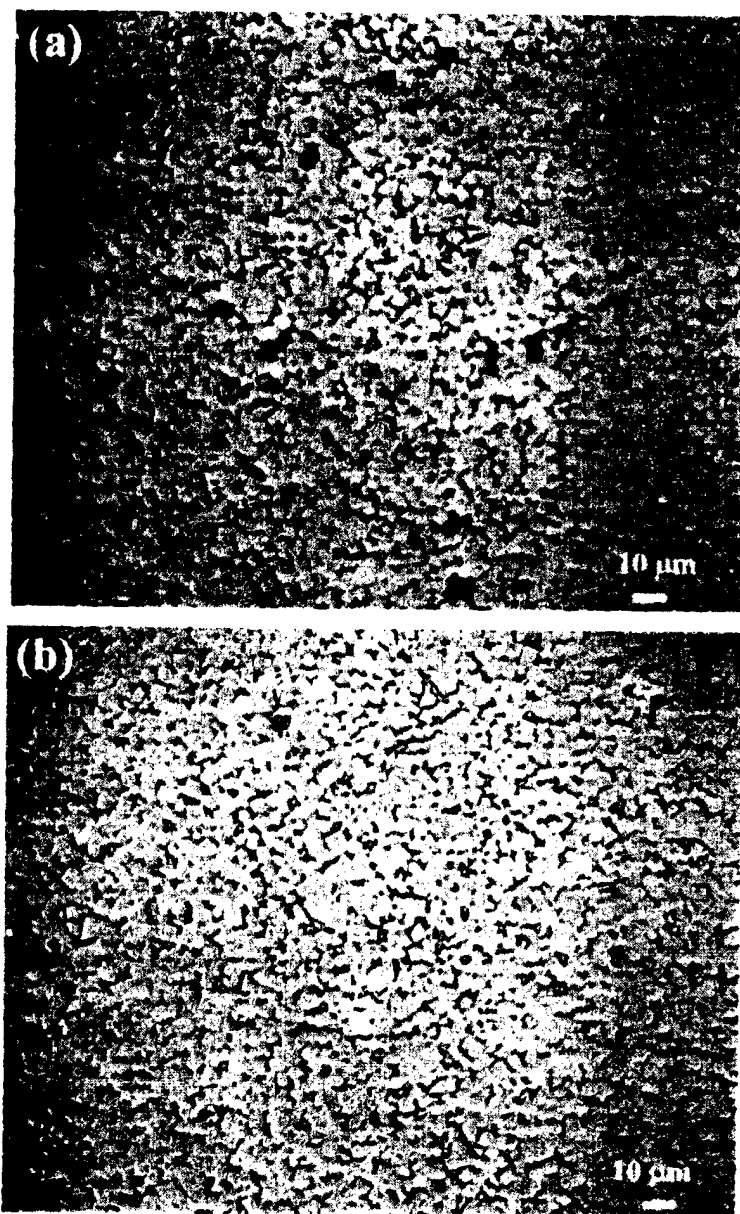
Figure 2.7. Optical micrographs of polished alumina containing 20 vol. % calcium aluminiosilicate glass sintered in (a) air and (b) vacuum, at 1600°C for 10 h (from Dong[47])

residual porosity with pore sizes that were much larger than the matrix grains. In contrast, the vacuum sintered samples contained no porosity, as shown in Figure 2.7(b). It was determined that the porosity remained in the air-sintered samples due to the pressure build-up of trapped gases. By vacuum sintering, these insoluble gases were evacuated from the pores prior to sintering , thus allowing them to be removed.

In the present study of sintering PMN-PT, oxygen was used instead of vacuum to purge out the insoluble gases during the initial stage of sintering. Since oxygen is highly soluble in the perovskite structure of PMN-PT, oxygen was able to diffuse out of the pores, allowing the pores to close during the final stages of sintering.

Large Stable Pores

Kingon et al.[25] found that although excess PbO enhanced the densification rate of PZT during initial and intermediate stages of sintering, the presence of a PbO liquid phase during the final stage of sintering lowered the densification rate. This was attributed to rapid particle rearrangement and solution/precipitation in the early stages, followed by enhanced grain growth. This produced an inhomogeneous final microstructure consisting of localized dense regions and large, stable pores when the sample were sintered in air.

Work of Zhao et al.[43] found that the kinetics of densification to be too slow to ever achieve full density in a large-grained microstructure containing such large pores. It is believed that this was the case in the present study for PMN-35PT + 5 vol.% PbO samples sintered in air. As the final microstructure in Figure 2.3(d) shows, the pore sizes

are much larger than the average grain size. Thus, the pores achieved a thermodynamically stable size and would not allow further densification. The final microstructure of liquid phase sintered alumina from the work of Dong also contained very large pores, as shown in Figure 2.7(a).

This would also help explain the result of Snow.[23] In the case of Snow, the key was to use oxygen and a PbO liquid phase for a short time to enhance densification, then limiting grain growth and pore coarsening in the final stages of sintering by removing the PbO liquid phase.

Dense Surface Layer

The low magnification micrograph in Figure 2.3(c) of a PMN-35PT + 5 vol.%PbO sample sintered in air shows the presence of a dense layer at the surface of the sample. The layer is about 150 μm thick and can be seen on both the left and right sides of the micrograph. Choi et al.[31] observed the same for PLZT ceramics sintered in air. In that work, the authors found the thickness to vary according to a parabolic dependence on time. The dense layer was attributed to enhanced diffusion of atoms due to the formation of lattice vacancies from the vaporization of PbO at the surface. The time dependence was ascribed to the increased diffusion path of PbO to the surface. A similar increase in densification behavior was observed by Kingon et al.[25] for PbO deficient PZT. It was postulated to be the result of oxygen vacancy-limited diffusion.

The dense layer in the present work is not believed to be the result of PbO

evaporation from the surface because of the existence of a PbO liquid phase at the grain boundaries, even at the surface. Instead, the layer is believed to be due to densification associated with the diffusion and release of trapped insoluble gases out of the sample to the surface. The thickness of the layer would grow as the amount of trapped gas is decreased and the pores close. Ultimately, the thickness should vary with the oxygen content in the atmosphere. It could be argued, then that the oxygen sintered sample in Figure 2.3(a-b) contained no porosity because there were no trapped gases from the early stages of sintering to diffuse out of the sample. In fact, Choi *et al.*[31] also observed the layer thickness to vary with the oxygen partial pressure of the sintering atmosphere when comparing samples sintered in Ar, 33% O_2, air, and pure O_2.

Primary Role of Oxygen

It is believed that the primary role of oxygen is to remove insoluble gases before densification begins, then to reduce the internal pressure by diffusing into the lattice or down the grain boundaries, and allowing the pores to close from pressures derived from their own curvatures. This is the case regardless of the amount of excess PbO, including 0 vol.% PbO. If insoluble gases become trapped, high sample densities cannot be achieved because the pores coalesce and coarsen to stable sizes that are not amenable to full densification.

2.4.2 Single Crystal Growth

2.4.2.1 Effect of Atmosphere

As presented in the previous section, sintering PMN-35PT in oxygen yielded fully dense ceramic microstructures, while sintering in air restricted densification and resulted in porous microstructures. The consequences of these contrasting microstructures on the single crystal growth of PMN-35PT by the SPC process are seen clearly in Figure 2.4. The micrographs show PMN-35PT single crystals which have grown from {111} seed crystal plates of similar composition into the polycrystalline matrices. The dark phase in the oxygen-grown crystal in Figure 2.4(a) is a PbO second phase that was trapped behind the fast migrating boundary. The dark phase in the air-grown crystal in Figure 2.4(b) is a combination of trapped PbO and porosity.

As Figures 2.4(a) and (b) suggest, the quality of the grown single crystals is directly influenced by the microstructures of the polycrystalline precursors. Any porosity that existed in the matrix was translated to the grown crystal. Also, large pools of liquid phase accumulated at the interface and could not keep up with the faster moving boundary. Nor could it redistribute itself back into the matrix rapid enough. As a result, large pockets and strings of PbO were left behind the boundary and became entrapped in the crystal.

Since the presence of such defects in the grown crystals would likely be detrimental to the piezoelectric and dielectric properties, it is important to understand the factors that

control the development of the single crystal and matrix microstructures. The previous section addressed the role of oxygen in obtaining fully dense matrix microstructures. Figure 2.4 demonstrates the importance of a dense matrix on single crystal growth. The effects these microstructures have on the properties of PMN-PT single crystals will be addressed in Chapter 3 and in also in a subsequent paper.[44]

2.4.2.2   Effect of PbO Content

Even though the single crystal shown in Figure 2.4(a) was grown in an oxygen atmosphere into a matrix that was fully dense, the resulting microstructure of the grown crystal contained trapped PbO defects. A reduction in the amount of trapped PbO defects was obtained by simply lowering the starting content of the matrix to 1.8 vol.%PbO. Since less PbO liquid phase was present in the matrix, less was available to be trapped in the {111} seeded crystal, as shown in Figure 2.5.

Lowering the PbO content any further would compromise the kinetics of single crystal growth, as previously described by Khan *et al.*[9] and King *et al.*[16] Therefore, reducing the amount of trapped PbO in the grown single crystals would require another means, such as slowing the rate of boundary migration. It should be noted that reducing the amount of excess PbO in the matrix also eliminated the formation of abnormal grains. This result is discussed further in Chapter 4 and in another paper.[33]

2.4.2.3 Effect of Seed Crystal Orientation

Khan *et al.*[8,9] demonstrated that the <111> orientation was the fastest growth direction for single crystals of PMN-35PT. It was also noted that the {111} seeded single crystals grew rapidly until an equilibrium cube shape was attained with low energy {001} faces. Subsequent growth occurred at a much slower rate in the <001> direction. The growth kinetics of {001} seeded single crystals of PMN-35PT was evaluated in a later paper by King *et al.*[16]

Since growth in the <001> direction is much slower than the <111> direction, it was believed that boundary migration would be slow enough to prevent the entrapment of defects in the grown crystals. Figure 2.6 shows the resulting microstructures of PMN-30PT single crystals grown from {001} single crystal plates into matrices of PMN-30PT + 5 vol.%PbO. These crystals were grown in three cycles at 1175°C for 4 h each. After each cycle, the grown crystal was removed from the polycrystalline matrix by chemically etching with 30% HNO_3 in an ultrasonic bath, cleaned, and re-embedded in fresh powder of PMN-30PT + 5 vol.%PbO. The linear growth dimension in the <001> direction was an average of 110 μm after each 4 h growth cycle, regardless of sintering atmosphere. This growth dimension was in excellent agreement with the work of King *et al.* on {001} single crystal growth into hot-pressed PMN-35PT with 5 vol.% PbO.

As in the {111} grown single crystals shown in Figure 2.4 and the abnormal grains in Figures 2.3(b) and (d), the {001} grown single crystals sintered in air contained trapped porosity while those sintered in oxygen did not. As seen in Figure 2.6(a), the {001}

seeded crystal grown in oxygen did not contain large pockets of trapped PbO as before. The oxygen grown crystal was much cleaner. However, it did have small defects that marked the location of the original single crystal/polycrystal interface. These small pores were the result of either poor powder compaction at the seed interface or because the matrix was not fully dense before the crystal boundary started to migrate.

As the micrograph in Figure 2.6(b) shows, the <001> growth direction was still faster than the motion of the pores that existed in the air-sintered matrix. As a result, it became clear that sintering in oxygen is a requirement to obtain high quality, defect-free crystals. Note the pore size gradient within the {001} air-grown crystal in Figure 2.6(b). Since pore size scales with grain size, the trapped porosity reveals the history of matrix grain size as the boundary passed through.

The fact that the {001} single crystals grew the same amount in the presence of porosity (air atmosphere) as they did in the absence of porosity (oxygen atmosphere) is significant. This means that the kinetics of boundary migration (*i.e.* boundary velocity, v) was uninfluenced by porosity and therefore the pore-boundary interaction was minimal. Thus, in the absence of any pore drag effects, it can be deduced that the boundary energy of the {001} plane must be extremely low. Furthermore, pore separation from the boundary also indicates that the boundary mobility of the {001} boundary must be greater than the pore mobility.

2.5 Conclusions

Single crystals of PMN-30PT and PMN-35PT were grown using the Seeded Polycrystal Conversion technique. It was determined that sintering in oxygen was necessary to obtain fully dense matrix microstructures, which, in turn, produced pore-free single crystals. The amount of trapped PbO defects were reduced by lowering the PbO composition to 1.8 vol.% PbO in the matrix. Lowering the single crystal boundary migration rate by changing the seed crystal orientation to {001} produced the cleanest grown crystals when sintered in oxygen.

It was concluded that the role of oxygen in sintering PMN-PT ceramics was to displace insoluble gases such as N_2 prior to the start of densification, then to diffuse into the lattice or down the grain boundaries thereby reducing the internal pressure, and allowing the pores to close from pressures derived from their own curvatures.

CHAPTER 3

MATRIX AND SINGLE CRYSTAL PROPERTIES

3.1 Introduction

Shrout and Park[1,2,3] have reported that single crystal ferroelectrics exhibited dramatic

improvements in electromechanical properties compared to their conventional

polycrystalline ceramic counterparts. Much of that work was based on flux-grown

crystals of $Pb(Mg_{1/3}Nb_{2/3})O_3$-$PbTiO_3$ [PMN-PT] and $Pb(Zn_{1/3}Nb_{2/3})O_3$-$PbTiO_3$ [PZN-PT].

High piezoelectric coefficients of d_{33}>2500 pC/N and strain levels >0.6% were observed

for crystallographically engineered crystals oriented along the non-polar <001> direction.

Comparable results were obtained from single crystals of PMN-PT grown by the Seeded

Polycrystal Conversion (SPC) technique.[4,8] Since the initial work on single crystal

growth by SPC, much progress has been made to advance the understanding of boundary

migration in PMN-PT and other similar systems.[9,15,16,27,34,35,45,46,47,48]

In Chapter 2 and in a previous paper,[45] the present authors examined the effect of

processing variables on the quality of SPC-grown single crystals. Since the quality of the

PMN-PT single crystals was directly influenced by the microstructure of the

polycrystalline precursor, the factors that controlled the final microstructure of the matrix were examined. This was achieved by investigating the grain growth and densification behavior of PMN-35mol.%PT in the presence of a liquid phase. The conditions yielding trapped defects such as porosity and PbO-based second phase were described. It was postulated that such defects that were left behind the migrating boundary would have a detrimental effect on the properties of the final grown single crystal. Although previous work demonstrated respectable electromechanical properties for SPC crystals containing trapped porosity and PbO-based inclusions (*i.e.* 0.5 to 0.7% strain at 35kV/cm),[4,8] such crystals were rather lossy and were more susceptible to dielectric breakdown. Consequently, the long-term integrity of the crystals was a concern.

The purpose of the present work was to determine how the microstructure of single crystals grown under various processing conditions described in Chapter 2 affected the dielectric, piezoelectric and optical properties of PMN-PT.

3.2 Experimental Procedure

PMN-30PT and PMN-35PT single crystals were grown using the Seeded Polycrystal Conversion technique. Seed single crystal plates (Crystal Associates and Penn State) possessing {111} and {001} faces were embedded in powder compacts made from commercially available PMN-PT (TRS Ceramics) milled with various amounts of excess PbO (Alfa Aesar). The seeded polycrystalline precursors were subsequently sintered in both air and oxygen atmospheres at 1175°C for 4 to 12 h. The details of the sample

preparation and single growth techniques employed in this study were described in Chapter 2 and in a previous paper.[45]

After the growth process, the single crystals were extracted from the polycrystalline matrices via chemical etching. A 30% solution of nitric acid in water was used to attack and dissolve the PbO-based grain boundary phase in the matrix. With the aid of an ultrasonic bath, the matrices were broken apart and separated from the single crystals. Single crystal plates with {001} faces were cut from the single crystals using a precision high speed diamond saw (Struers Accutom) and subsequently polished to an 8 μm finish. The seed crystals were carefully removed from the grown single crystals by controlled grinding using a special hand-grinding fixture (South Bay Technologies) and fine SiC papers. The was done in order to characterize the electromechanical behavior of the grown single crystals without contributions from the flux-grown seeds.

The optical transparency of the grown crystals was qualitatively evaluated using light optical microscopy (LOM) at low magnification on a stereo microscope (Olympus).

Prior to electroding, the polished crystals were cleaned with acetone, ethanol, and deionized water then dried. Electrodes were formed on the {001} faces by evaporating a thin layer of chromium followed by a thick layer of gold. The thin Cr layer improved the bond strength of the Au coating.

The dielectric constant K and loss D were measured at frequencies from 1-1000 kHz using an HP 4194A impedance analyzer as a function of temperature. The measurements were acquired upon heating from -50 to 200°C in 1°C steps with 2 min settling times using a computer controlled oven (Delta Design Inc., Model 9010).

Polarization and strain vs. electric-field measurements were acquired simultaneously under applied fields up to 45 kV/cm using a bipolar triangular wave at 0.1 Hz. The computer controlled system was comprised of a modified Sawyer-Tower circuit and a linear variable differential transducer (LVDT) driven by an external synthesizer (HP 3336C) coupled to a lock-in analyzer (Princeton Applied Research, Model 5204). The voltage was supplied by a Trek 610D high voltage amplifier/supply/controller. The samples were immersed in an insulating liquid (Galden HT-200) to prevent arcing.

The grown crystals were poled in the <001> direction under an applied electric field of 35 kV/cm (Trek 610D) for 15 min at room temperature. Unipolar polarization and strain-field measurements were performed on the poled crystals using a triangular wave signal at 0.1 Hz. The unipolar measurements were acquired at least 18 h after initial poling to ensure domain stability. The room temperature dielectric constant K(RT) and loss D(RT) were measured before and after to evaluate the quality of the poling. The piezoelectric coefficients d_{33} were estimated from the slopes of the unipolar strain-field curves. No low-signal resonance measurements were made using the IEEE technique for comparison.

3.3   Results

The low magnification LOM micrographs in Figures 3.1(a) and (b) show the differences in the optical transparency between PMN-30PT crystals grown from {001} seeds in oxygen and air atmospheres, respectively, with 5 vol.%PbO in the matrix. As

seen, the oxygen-grown crystal was completely transparent. Although the air-grown crystal was not transparent, it was translucent. All air-grown crystals had similar optical qualities, regardless of the PT and PbO contents or seed orientation.

Figure 3.2 shows single crystals grown from {111} seeds embedded in PMN-30PT + 5 vol.%PbO. As shown, the crystals were mostly opaque, although they contained a few regions that were somewhat transparent. In addition, the {111} grown crystals in Figure 3.2 were red in color, while those of Figure 3.1 were yellow. The single crystals shown in Figure 3.3 were grown from {001} seed crystals into a PMN-35PT + 5 vol.%PbO matrix. Although obviously transparent, the crystals contained several defects and possessed a milky yellow color with visibly large ferroelectric domains. Figure 3.4 compares crystals grown from {111} seeds into PMN-35PT matrices with (a) 1.8 vol.%PbO and (b) 5 vol.%PbO. The crystals grown with 1.8vol.%PbO were yellow in color and more transparent than the red-colored crystals grown using 5 vol.%PbO in the matrix. Both crystals contained large ferroelectric domains characteristic of tetragonal PMN-PT.

Figures 3.5(a) and (b) show the dielectric behavior at 1 kHz as a function of temperature on heating for grown single crystals of PMN-30PT and PMN-35PT, respectively. The maximum dielectric constant K_{max} was greater for samples grown from {111} seeds compared to {001} grown crystals. Additionally, the dielectric maximum temperature T_{max} was usually higher for single crystals grown from {001} seeds. The K_{max} and T_{max} values are summarized in Table 3.1. All samples were oriented along <001> prior to measurement.
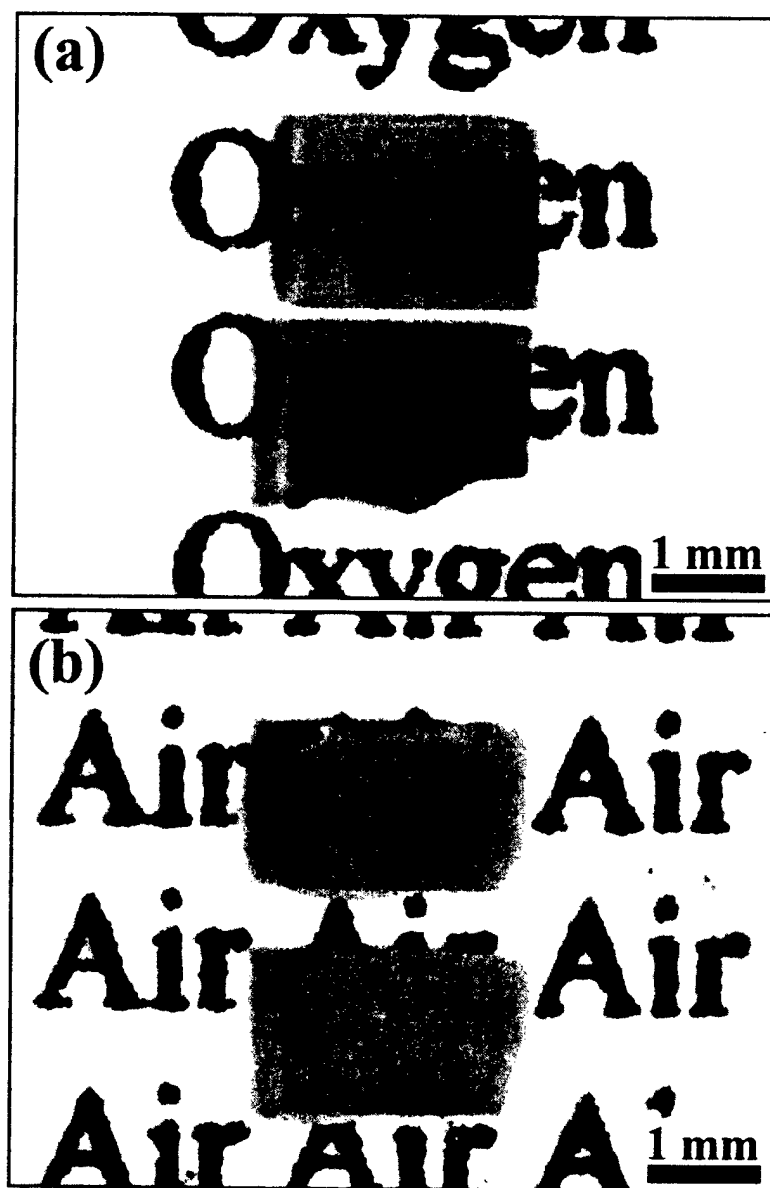
Figure 3.1. Low magnification micrographs of PMN-30PT single crystals grown from {001} seed crystals embedded in PMN-30PT + 5 vol.%PbO. Samples were sintered at 1175°C for 3 cycles of 4 h each in (a) oxygen and (b) air atmospheres.
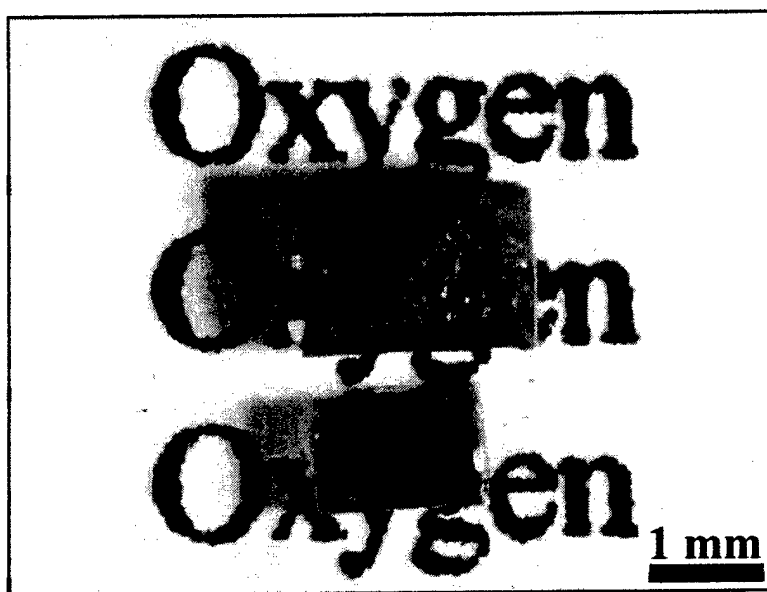
Figure 3.2. Low magnification micrograph of PMN-30PT single crystals grown from {111} seed crystals embedded in PMN-30PT + 5 vol.%PbO. Samples were sintered at 1175°C for 4 h in an oxygen atmosphere.
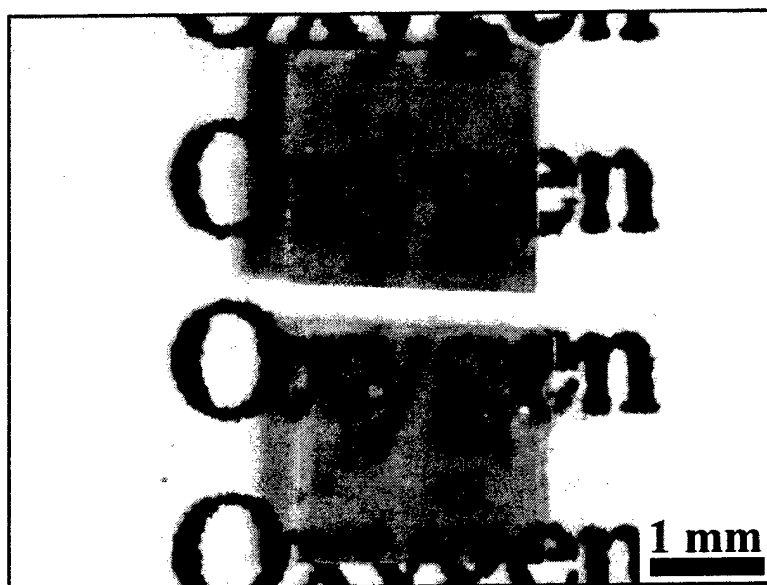
Figure 3.3. Low magnification micrograph of PMN-35PT single crystals grown from {001} seed crystals embedded in PMN-35PT + 5 vol.%PbO. Samples were sintered at 1175°C for 3 cycles at 4 h each in an oxygen atmosphere.
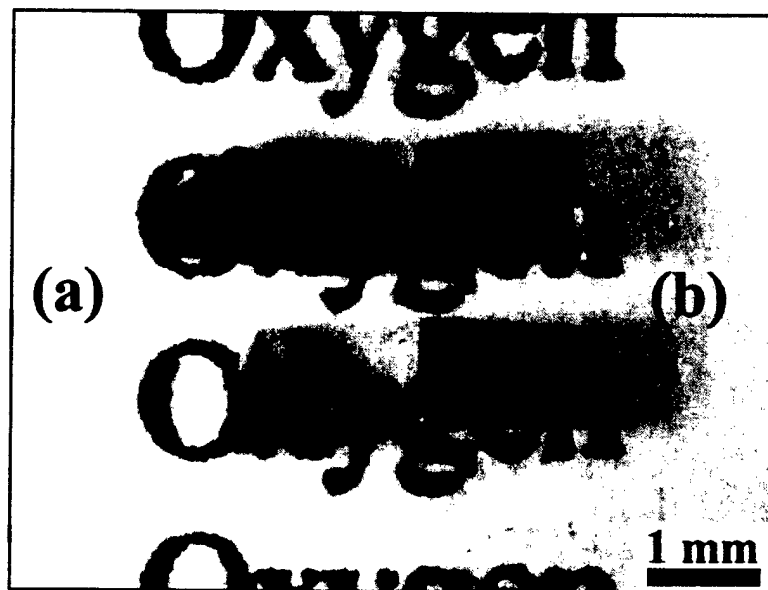
Figure 3.4. Low magnification micrograph of PMN-35PT single crystals grown from {111} seed crystals embedded in PMN-35PT with (a) 1.8 and (b) 5 vol.%PbO. Samples were sintered at 1175°C for 4 h in oxygen atmospheres.
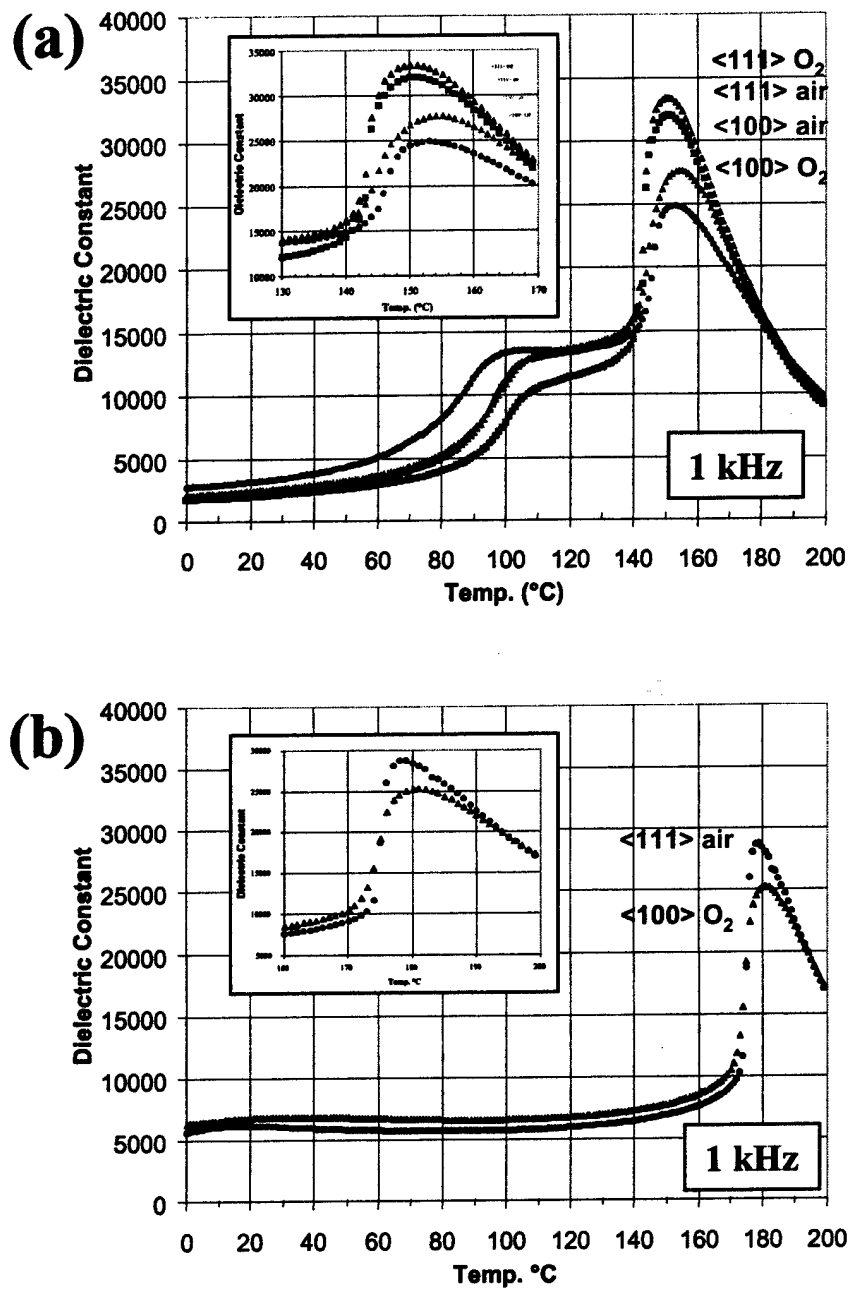
Figure 3.5. Dielectric constant vs. temperature upon heating for unpoled single crystals of (a) PMN-30PT and (b) PMN-35PT grown from {001} and {111} seed crystals in oxygen and air atmospheres at 1175°C.

60
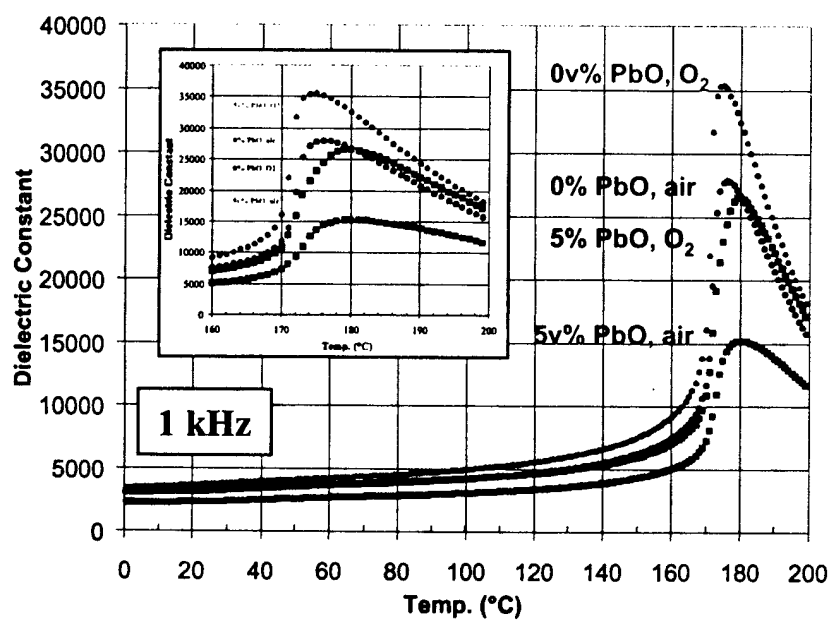
Figure 3.6. Dielectric constant vs. temperature upon heating for unpoled polycrystalline ceramics of PMN-35PT with 0 and 5 vol.%PbO sintered in oxygen and air atmospheres at 1175°C for 4 h.

Table 3.1: Summary of Dielectric Properties of PMN-30mol%PT and PMN-35mol%PT

Single Crystals Grown by Seeded Polycrystal Conversion from {111} and {001} Seed

Crystals in Oxygen and Air Atmospheres.

PT %	Atm	Seed	K (RT) unpoled	D (RT) unpoled	K (RT) poled	D (RT) poled	T_{max}	K_{max}	d_{33}*
30	O_2	{001}	3931	0.024	5316	0.007	153	25019	2180
30	air	{001}	2699	0.020	3641	0.006	155	27595	1860
30	O_2	{111}	2586	0.024	3050	0.012	150	33329	1620
30	air	{111}	2146	0.030	2909	0.016	151	31923	1560
35	O_2	{001}	7074	0.006	1127	0.008	181	25237	300
35	air	{111}	5965	0.007	1283	0.031	178	28684	360

* extracted from slope of low-field region (<10kV/cm) of strain vs. E-field curve

Table 3.2: Summary of Dielectric Properties of PMN-35PT Ceramics With Various PbO

Contents Sintered in Oxygen and Air Atmospheres.

PbO Content (vol.%)	Sinter Atm.	K (RT) unpoled	D (RT) unpoled	K (RT) poled	D (RT) poled	Tmax	K_{max}
0	oxygen	3670	0.017	3636	0.016	175	35317
0	air	3233	0.013	3199	0.013	176	27826
5	oxygen	2934	0.005	2558	0.011	180	26518
5	air	2045	0.007	1805	0.009	180	15146

For comparison with the single crystals, the dielectric behavior as a function of temperature for selected polycrystalline samples of PMN-35PT are shown in Figure 3.6. The T_{max} values were higher and the K_{max} values were lower for samples containing 5 vol.% PbO compared to samples without excess PbO. This is summarized in Table 3.2.

Polarization and strain as a function of E-field (bipolar) for <001> oriented PMN-30PT and PMN-35PT crystals are shown in Figures 3.7 and 3.8, respectively. The remanent polarization P_r for PMN-30PT crystals grown in oxygen and air were 26.3 and 24.8 $\mu C/cm^2$, respectively. The P_r for PMN-35PT crystals grown in oxygen and air were 34.0 and 31.8 $\mu C/cm^2$, respectively. The coercive field E_c for PMN-30PT crystals grown in oxygen and air were 3.3 and 3.7 kV/cm, respectively. The E_c for PMN-35PT crystals grown in oxygen and air were 5.0 and 5.4 kV/cm, respectively.

Table 3.1 also lists the room temperature dielectric constant K(RT) and loss D(RT) for the <001> oriented crystals before and after poling. As seen, the K(RT) increased and the D(RT) decreased upon poling PMN-30PT single crystals. In contrast, the K(RT) decreased significantly and D(RT) increased upon poling the PMN-35PT crystals.

The unipolar strain behavior after poling is shown in Figures 3.9(a) and (b) for PMN-30PT and PMN-35PT single crystals, respectively. The piezoelectric coefficient d_{33} was measured directly from the slope of the strain vs. E-field curve. For PMN-30PT crystals, d_{33} was taken from the slope at low-field values, i.e. <10 kV/cm. For PMN-35PT crystals, d_{33} was taken as the slope after strain saturation, i.e. >30 kV/cm. These values are listed in Table 3.1.

Polarization and strain as a function of E-field (bipolar) for PMN-35PT

63

polycrystalline ceramics are shown in Figures 3.10(a) and (b). The P_r for samples sintered without excess PbO in oxygen and air were 30.6 and 24.5 $\mu C/cm^2$, respectively. The P_r for PMN-35PT + 5vol.%PbO ceramics sintered in oxygen and air were 22.2 and 17.3 $\mu C/cm^2$, respectively. The E_c for all PMN-35PT ceramic samples was 6.1 kV/cm. Unipolar strain curves for sintered ceramics (poled) are shown in Figure 3.11. The d_{33} values for all ceramic samples except the PMN-35PT + 5 vol.%PbO sample sintered in air were 850 pC/N in the low-field region (<10 kV/cm) and 290 pC/N after strain saturation (>30 kV/cm). The PMN-35PT + 5 vol.%PbO sample sintered in air had a d_{33} value of 680 pC/N for low fields.

Figure 3.12 compares the unipolar strain behavior for PMN-30PT and PMN-35PT single crystals grown from {001} seeds in oxygen and PMN-35PT ceramic sintered in oxygen.
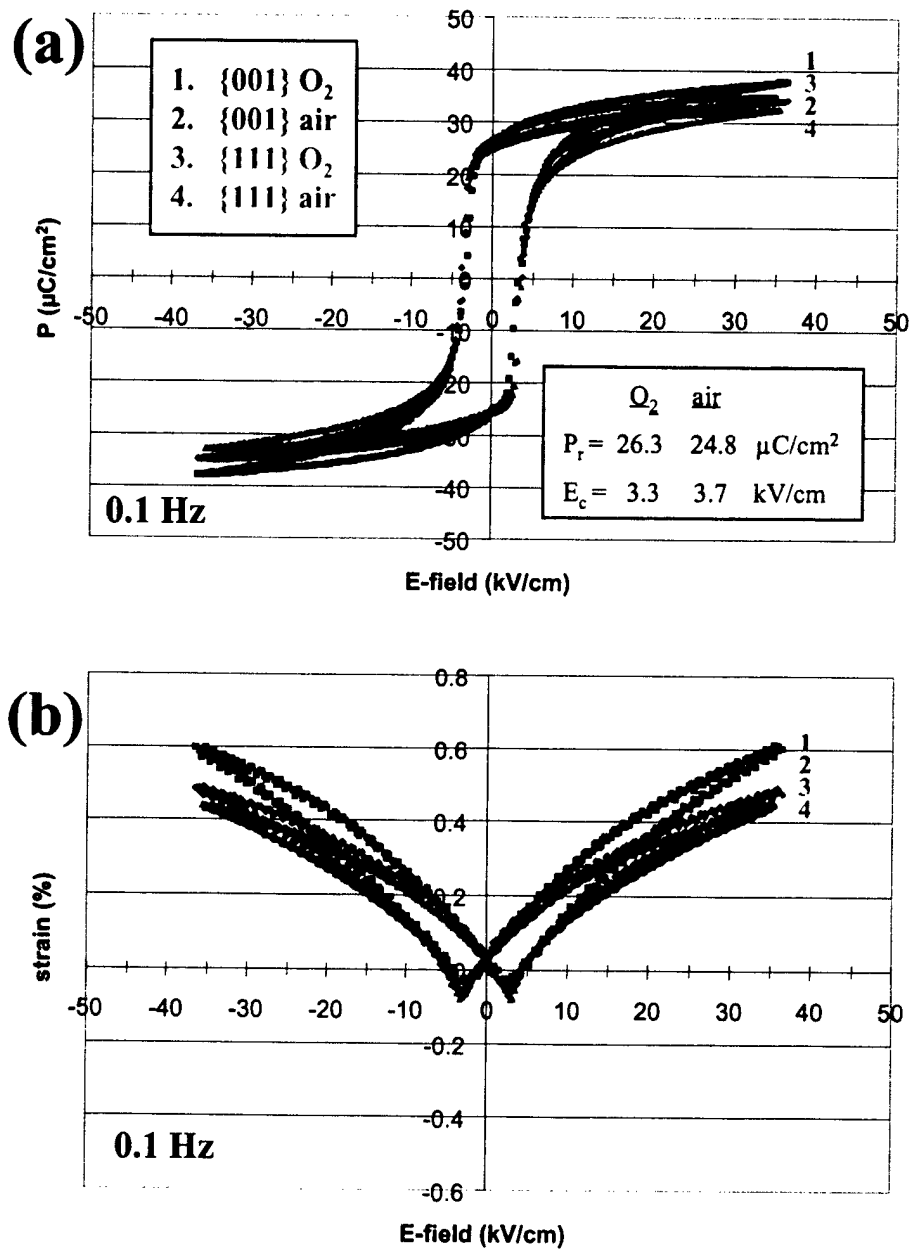
Figure 3.7. (a) Polarization and (b) strain vs. E-field (bipolar) curves for PMN-30PT single crystals grown from {001} and {111} seed orientations in oxygen and air atmospheres at 1175°C.

65

(a)

1. {001} O_2
2. {111} air

	O_2	air	
$P_r=$	34.0	31.8	$\mu C/cm^2$
$E_c=$	5.0	5.4	kV/cm

0.1 Hz

P ($\mu C/cm^2$)

E-field (kV/cm)

(b)

strain (%)

0.1 Hz

E-field (kV/cm)
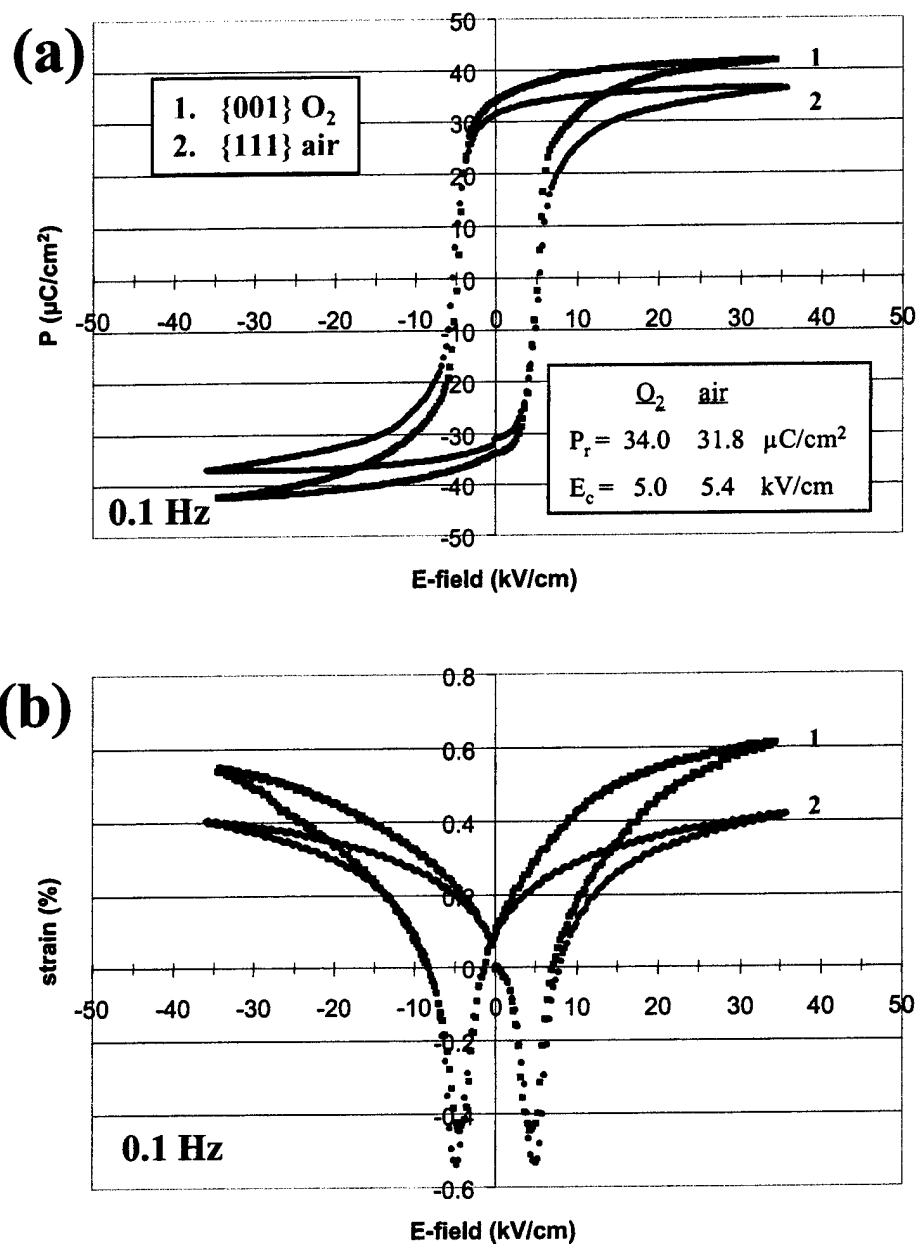
Figure 3.8. (a) Polarization and (b) strain vs. E-field (bipolar) curves for PMN-35PT single crystals grown from {001} and {111} seed orientations in oxygen and air atmospheres at 1175°C.
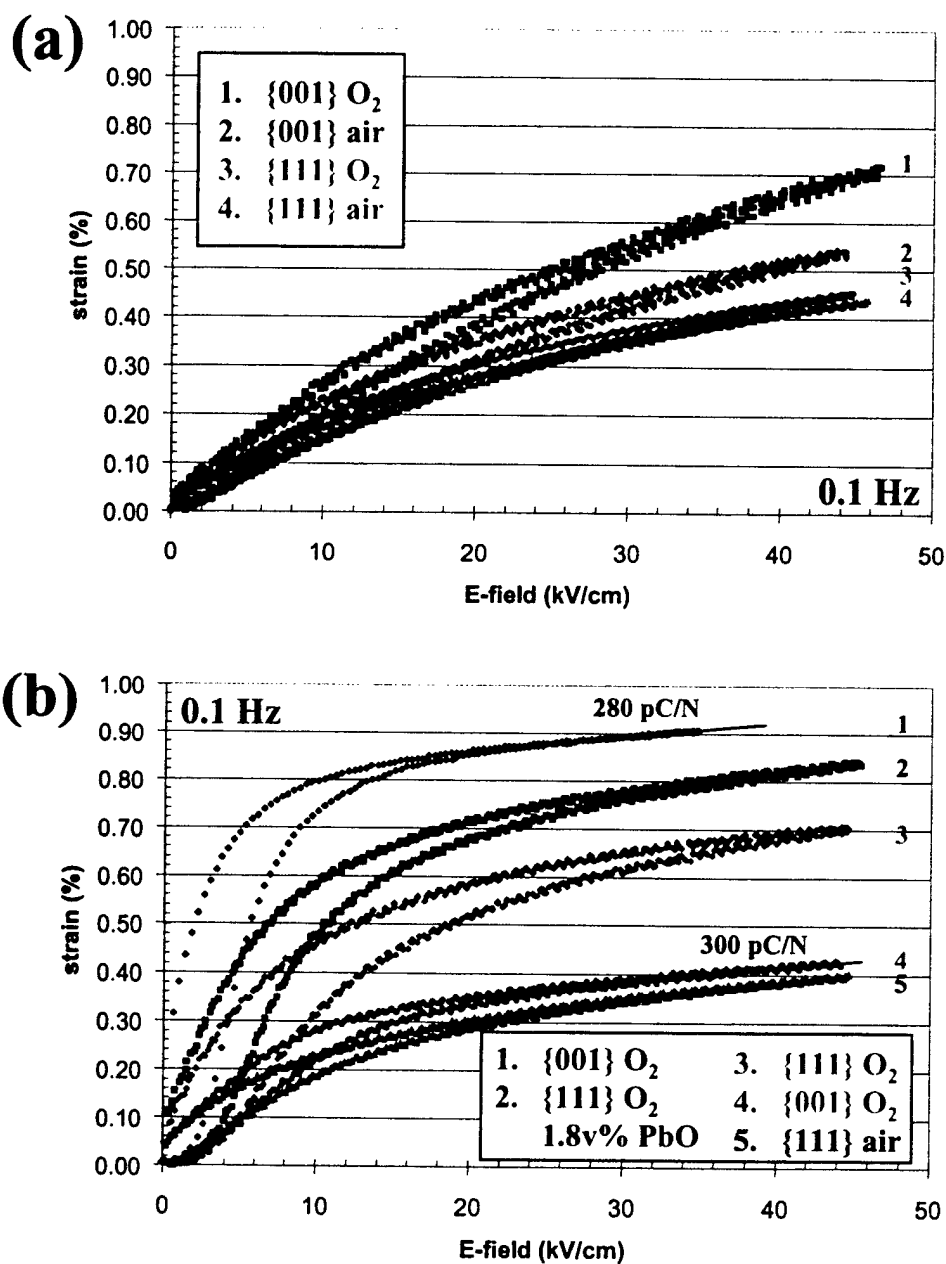
Figure 3.9. Strain vs. E-field (unipolar) curves for (a) PMN-30PT and (b) PMN-35PT single crystals grown from {001} and {111} seed orientations in oxygen and air atmospheres at 1175°C. Samples were poled at 35 kV/cm for 15 min. at R.T.
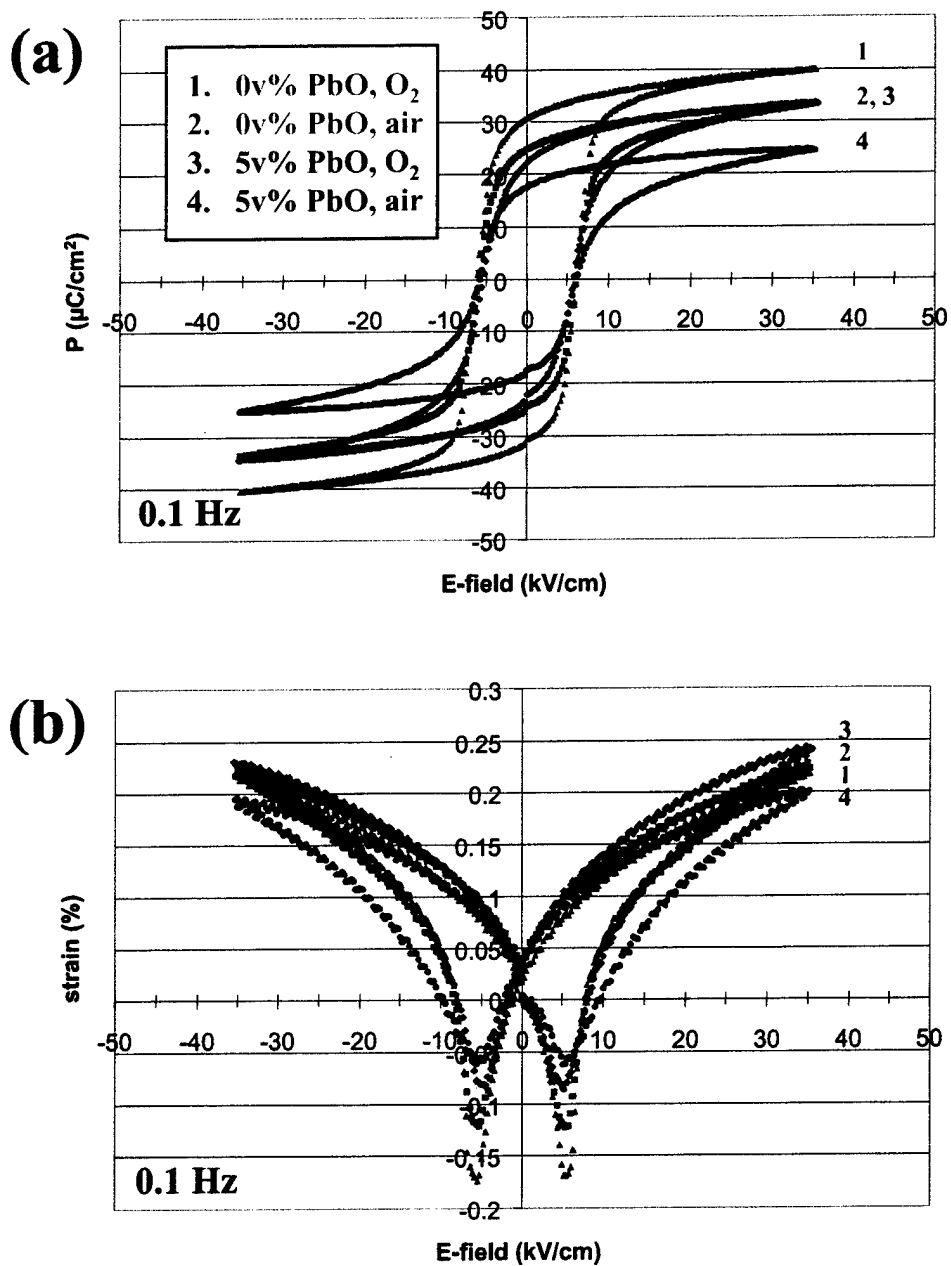
Figure 3.10. (a) Polarization and (b) strain vs. E-field (bipolar) curves for polycrystalline ceramics of PMN-35PT with 0 and 5 vol.%PbO sintered in oxygen and air atmospheres at 1175°C for 4 h.
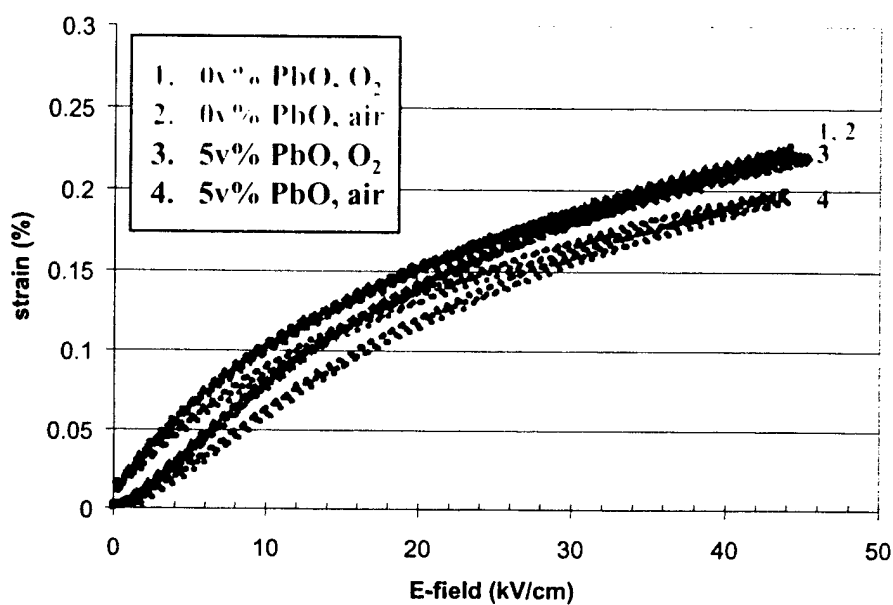
Figure 3.11. Strain vs. E-field (unipolar) curves for polycrystalline ceramics of PMN-35PT with 0 and 5 vol.%PbO sintered in oxygen and air atmospheres at 1175°C for 4 h. Samples were poled at 35 kV/cm for 15 min. at R.T.
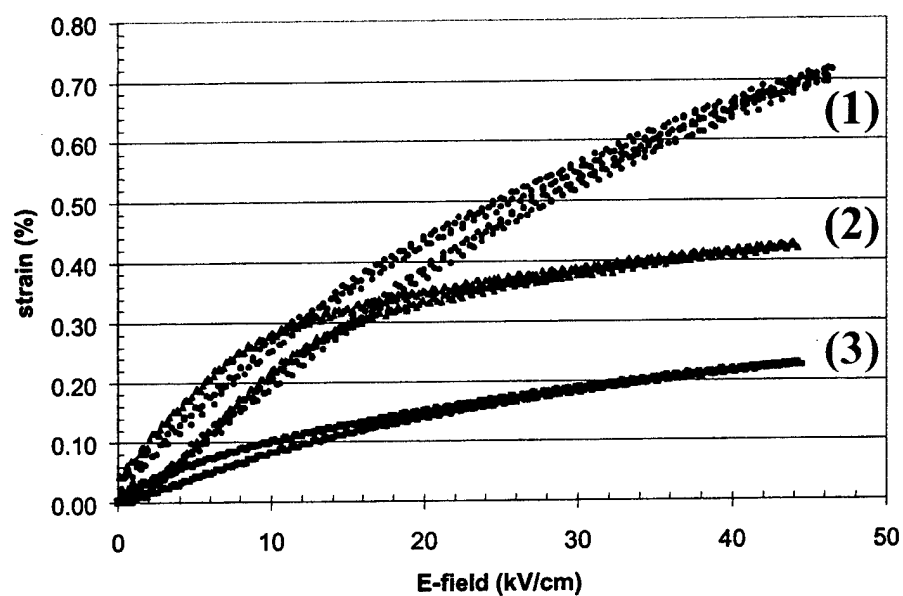
Figure 3.12. Comparison of strain vs. E-field (unipolar) curves for (1) PMN-30PT
and (2) PMN-35PT crystals grown from {001} seeds in oxygen, and (3) PMN-35PT
polycrystal sintered in oxygen without excess PbO. Samples were poled at 35
kV/cm for 15 min. at R.T.

3.4 Discussion

3.4.1 Optical Transparency

The results of the present section supplement the microstructural investigation of SPC-grown single crystals from Chapter 2. As described earlier, it was found that sintering in oxygen with a {001} oriented seed crystal produced the best quality grown single crystals. The crystals were pore-free and clear of any other trapped defects such as a PbO second phase. In contrast, all samples sintered in an air atmosphere yielded porous single crystals. Figures 3.1(a) and (b) of the current study demonstrate the effect of trapped porosity on the optical quality of the single crystals. As expected, the defect-free {001} seeded crystals grown in oxygen were fully transparent (Fig. 1(a)) while the porous crystals grown from both {111} and {001} seeds in air were not (Fig. 1(b)).

Similarly, the crystals grown from {111} seed plates exhibited significant amounts of trapped PbO second phase.[45] This was the result of a fast moving single crystal boundary that swept through the matrix at such a pace that the liquid phase was not allowed to redistribute itself and therefore became entrapped. Sintering in air added trapped porosity as mentioned above. Figure 3.2 shows the macroscopic effect of trapped PbO on single crystals grown from {111} seeds in oxygen. The optical properties of the crystals were affected by the PbO defects, which diffracted the light passing through the crystals, thereby reducing the translucency of the crystals and also providing the red color.

By lowering the initial PbO content in the matrix from 5 vol.% to 1.8 vol.%PbO, the amount of trapped PbO defects were reduced. The result was a much cleaner crystal, as demonstrated in Figure 3.4. The crystals grown from {111} seeds into a matrix containing 1.8vol.%PbO also lacked the red color of the 5 vol.%PbO samples. The samples were not, however, as clear as those of Figure 3.1(a). This was due to the large normal ferroelectric domains that existed as the result of the tetragonal crystal structure for the PMN-35PT composition.

Normal ferroelectric domains were also present in the PMN-35PT crystals grown from {001} seeds, as shown in Figure 3.3. These crystals also contained other visible defects caused by abnormal grains which had formed in the matrix and locally affected boundary migration. As a result, there were either abnormal grains implanted in the surface of the crystals or large depressions left by the abnormal grains after spalling off from the etching operation. Abnormal grains were observed to occur more frequently in matrices of the PMN-35PT composition. It is not clear whether the higher Ti content increased the probability of abnormal grain growth, or if there were other factors involved. This deserves further work in the future.

3.4.2 Dielectric Behavior

The dielectric constant as a function of temperature curves for single crystals of PMN-30PT and PMN-35PT are shown in Figures 3.5(a) and (b), respectively. The K_{max} and T_{max} values are also listed in Table 3.1. Surprisingly, there seemed to be no

discernable effect of sintering atmosphere on the dielectric behavior of the single crystals. Thus, the trapped pores and PbO defects in the crystals had little negative influence on the dielectric behavior. This was not the case for the polycrystalline ceramics, as seen in Figure 3.6 and Table 3.2. For the ceramics, K_{max} dropped significantly with the introduction of porosity into the microstructure as a result of sintering in air. The K_{max} also dropped with the introduction of a PbO second phase. This was expected because lead oxide is a low dielectric constant material.

The difference in behavior stems from the difference in the microstructures between the single crystals and the polycrystalline ceramics. The grain boundaries in the ceramic provided a continuous interconnected network of PbO second phase and porosity, while the defects in the single crystals occurred in mostly discreet, isolated pockets. It is well known that an interconnected second phase of low dielectric material has a greater influence on the dielectric constant of the composite than if it were distributed as isolated phases, especially for low volume fractions.[49]

The dielectric behavior, however, did appear to be drastically affected by the initial orientation of the seed crystal. Given that all crystals were oriented along <001> prior to measurement, these results were not due to the direct effect of crystallographic orientation as previously reported.[50] As indicated in Figures 3.5(a) and (b) and in Table 3.1, the single crystals grown from {111} seeds almost always yielded higher K_{max} and slightly lower T_{max} values than the crystals grown from {001} seeds. This effect is believed to be the indirect result of differences in the single crystal boundary migration rates between the two seed orientations, as explained below.

Recent work by Gorzkowski et al.[51] found the composition of PMN-35PT matrix grains to change over time as grain growth progressed. This change in composition was related to the change in chemistry of the grain boundary liquid phase over time. As a consequence, the Ti concentration in the matrix grains increased with annealing time and possessed a chemical gradient from the core of each grain to the grain boundary. That work was also consistent with the common observations of chemical gradients in single crystals grown by high temperature solution techniques such as flux, Czochralski, and Bridgman methods. The chemical gradients reported by Gorzkowski et al., however, occurred on a much smaller scale and possessed a much narrower compositional gradient, measured by high resolution analytical electron microscopy. The significance of these recent findings on the results of the present work is explained as follows.

In PMN-PT, the boundary migration rate has been shown to be fastest in the <111> direction and slowest in the <001>.[8,9] Thus, in the present study, growth from {001} seed crystals required three times longer than the crystals grown from {111} seeds in order to achieve the crystal dimensions large enough for electromechanical property measurements. As a consequence, and based on the work of Gorzkowski et al., the {001} grown crystals would have migrated through matrices that were effectively higher in Ti concentration than the faster growing {111} seeded crystals. The work of Gorzkowski et al. found the Ti cation ratio to go from 0.35 to 0.38 after 5 h at 1150°C, which certainly would be enough to increase the T_{max} by a few degrees, i.e. from 178 to 181°C for PMN-35PT or from 150 to 155°C for PMN-30PT in the present study.

The dielectric behavior of the polycrystalline ceramics also supports this concept. As

shown in Figure 3.6 and Table 3.2, the measured T_{max} values of PMN-35PT + 5 vol.%PbO were 4 to 5°C higher than those of PMN-35PT sintered without excess PbO. The presence of a grain boundary liquid phase at the sintering temperature not only enhances grain growth,[9,16] but also affects the chemistry of the matrix grains. Following the work of Gorzkowski et al., the addition of excess PbO would promote a change in the Ti concentration of the PMN-PT grains. Thus, the T_{max} would be expected to shift to higher temperatures, as was observed here.

Further, the dielectric constant curves near T_{max} for the {001} grown crystals appear less sharp than for the {111} grown crystals. That is, the crystals grown from {111} seeds seemed to have a more defined K_{max} value than the crystals grown from {001} seeds. This phenomenon is perhaps most clearly seen in the inset of Figure 3.5(b). This is likely the cause of a chemical gradient in the {001} grown crystals. Similar effects of chemical heterogeneity were observed by Leite et al.[52]

The existence of such chemical gradients in the grown crystals should be verified by microscopy techniques similar to that employed by Gorzkowski et al. and will be examined in the future.

3.4.3 Polarization and Strain

Unlike the dielectric behavior, there was a strong effect of sintering atmosphere on the polarization and strain behavior of the SPC-grown crystals. An effect of seed orientation was also observed.

The polarization P vs. E-field (bipolar) curves in Figures 3.7(a) and 3.8(a) show well-saturated, square hysteresis loops which are consistent with reported P-E behaviors of PMN-PT single crystals. As shown, the P_r values were higher for crystals grown in oxygen, which indicates those crystals to have a higher polarizability. Also, the E_c values were slightly lower for the oxygen-grown crystals, indicating the domains were more easily switchable. These were likely due to the fewer defects observed in the oxygen-grown crystals.

The strain vs. E-field (bipolar) curves display the familiar butterfly loops in Figures 3.7(b) and 3.8(b). The bipolar strain behaviors of the PMN-35PT single crystals were much more hysteretic than the PMN-30PT crystals. This was likely due to the differences in the types of domains present in these crystals of two different compositions.

Perhaps the most significant results of the present work were the unipolar strain behaviors of the grown crystals shown in Figures 3.9(a) and (b) for PMN-30PT and PMN-35PT, respectively. As Figure 3.9(a) shows, the PMN-30PT crystal grown from a {001} seed crystal in oxygen yielded a maximum strain of 0.72% at 46 kV/cm. The d_{33} value measured from the slope of the curve was ~2180 pC/N. The maximum strain and d_{33} values decreased with the introduction of defects in the crystals. Thus, the single crystal grown from a {001} seed in an air atmosphere, which contained a significant amount of porosity, had a maximum strain of 0.54% at 44 kV/cm and a corresponding d_{33} value of ~1860 pC/N. For the worst case, the crystal grown in air from a {111} seed, which contained both trapped porosity and PbO second phase, produced a maximum strain value of 0.44% at 45 kV/cm and a d_{33} value of ~1560 pC/N. Consequently, the

76

strain behavior of the SPC-grown single crystals were strongly dependent on the quality of the grown single crystal and were therefore controlled by the sintering atmosphere and seed crystal orientation.

The unipolar strain vs. E-field curves for the PMN-35PT single crystals in Figure 3.9(b) demonstrate large variations in strain behaviors, even for the same processing conditions. For example, both curves (1) and (4) in Figure 3.9(b) represent the strain behavior of single crystals grown from {001} seeds in an oxygen atmosphere. The crystal represented by curve (1) yielded a maximum strain of 0.91% at 35 kV/cm, while that of curve (4) had a strain of only 0.43% at 45 kV/cm. However, much of the strain in curve (1) was due to domain reorientation commonly observed in crystals with a tetragonal crystal structure, such as $BaTiO_3$.[53] The crystal in curve (4) had less of a contribution from domain reorientation. Once both crystals reached strain saturation (>25 kV/cm), their strain vs. E-field behaviors were linear with similar measured d_{33} values of ~280 and 300 pC/N, respectively.

The unstable domain states of the PMN-35PT single crystals prevented any correlations to be made with processing conditions for that composition. The instability of the domains were reflected in the K(RT) and D(RT) values measured for the crystals before and after poling. As shown in Table 3.1, the K(RT) values for the PMN-35PT crystals dropped significantly after poling, while the D(RT) values increased. This occurred consistently for the crystals of that composition. Therefore, it was difficult to achieve and retain well-poled PMN-35PT single crystals with stable domain states.

In contrast, the PMN-30PT single crystals were easily poled and retained their high

quality poled states, as demonstrated by the K(RT) and D(RT) values in Table 3.1.

For comparison with the single crystal properties, bipolar P and strain curves for PMN-35PT polycrystalline ceramics are given in Figures 3.10(a) and (b). Unipolar strain curves are also presented in Figure 3.11. Maximum strain values for the poled ceramics were around 0.22% at 45 kV/cm. Interestingly, the measured d_{33} values after strain saturation (>30 kV/cm) were nearly identical to the PMN-35PT single crystal values, i.e. ~290 pC/N. Therefore, in terms of usable strain, the PMN-35PT single crystals did not offer much of an advantage over their polycrystalline counterparts. The strain behavior of the PMN-30PT SPC-grown single crystals, however, was far superior. This is summarized in Figure 3.12.

3.5 Conclusions

Single crystals of PMN-30PT and PMN-35PT were grown using the Seeded Polycrystal Conversion technique. It was determined that crystal growth from {001} seeds in an oxygen atmosphere produced the highest quality single crystals. Fully transparent PMN-30PT single crystals with maximum strain values of 0.72% at 46 kV/cm, d_{33} ~ 2180 pC/N, and a room temperature dielectric constant of ~5300 were obtained for poled <001> oriented crystals.

The dielectric behavior of SPC-grown single crystals were dependent on the orientation of the seed crystal, with {111} seeded crystals yielding the highest K_{max} values of ~33000. The T_{max} values were 3 to 5°C higher for crystals grown from {001} seeds,

compared to {111} seeded crystals.

In terms of usable strain, SPC-grown single crystals of PMN-35PT did not offer much of an advantage over polycrystalline ceramics of the same composition. Both yielded $d_{33} \sim 300$ pC/N.

CHAPTER 4

ABNORMAL GRAIN GROWTH IN PMN-PT

4.1 Introduction

Previously, relaxor-based ferroelectric $Pb(Mg_{1/3}Nb_{2/3})O_3$-35mol.%$PbTiO_3$ [PMN-35PT] single crystals were grown by Seeded Polycrystal Conversion (SPC).[4,8,9,15,16] In this process, a seed crystal is bonded to a polycrystalline ceramic precursor, and the single crystal boundary is induced to migrate at the expense of the smaller matrix grains. Maintaining single crystal growth until full conversion of the polycrystal can only be achieved with an improved fundamental understanding of the factors that influence the migrating boundary. The most significant parameter is the addition of a PbO-based liquid phase. It was found that the presence of a liquid phase at the grain boundaries enhanced the growth rate of the single crystal.[8,9] In contrast, little growth was observed in the absence of a liquid. Although the PbO additions promoted single crystal growth, they also enhanced matrix grain growth and perhaps more importantly, induced abnormal grain growth.

The purpose of the present work was to examine the factors that induce abnormal

grain growth in PMN-35PT and to determine how the processing parameters may be tailored to restrict their development.

4.2 Experimental Procedure

PMN-35PT powders (TRS Ceramics) were ball-milled in Nalgene bottles with 0, 1.8 and 5 vol.% PbO (Alfa Aesar, puratronic powder) in ethanol for 24 h using 3mm zirconia media (Tosoh). The powders were dried under slight vacuum using a rotoevaporator (Büchi) and subsequently calcined at 450°C for 4 h in air. The calcined powders were crushed with an agate mortar and pestle and passed through a 100-mesh stainless steel sieve. The mean particle sizes of the powders were determined to be ~0.7 μm using a laser scattering particle size analyzer (Horiba LA-910) with ethanol as the dispersing agent.

The powders were uniaxially pressed at 67 MPa to form 3 mm x 13 mm φ pellets and subsequently cold isostatically pressed at 345 MPa.

Specimens were sintered from the green state in an oxygen atmosphere with heating/cooling rates of 5°C/min to temperatures of 975 to1175°C and hold times of 0 to 12 h. The samples were enclosed in a platinum foil pouch and embedded in PMN-PT powder with excess PbO using the double-crucible technique in order to suppress PbO volatilization.

After sintering, cross-sections of the specimens were polished and either chemically etched using Kroll's reagent (1 vol.% HF + 4 vol.% HNO3 + water) or thermally etched

at 850-950°C for 0.5-1 h.

The polished and etched cross-sections were characterized using light optical microscopy (LOM) and scanning electron microscopy (SEM). For LOM analysis, the samples were observed under both bright-field and Nomarski differential interference contrast conditions (Reichert MeF3). Low magnification LOM micrographs were also taken using a stereo microscope (Olympus). For SEM characterization, the specimens were examined uncoated using a 3 kV accelerating voltage with a field-emission gun instrument (JEOL JSM 6300F).

Orientation Image Microscopy (OIM) was performed on the abnormal grains using an automated electron backscatter diffraction (EBSD) acquisition system (TexSEM Laboratories) attached to an environmental SEM (FEI XL-30 ESEM). The system was operated at 20 kV under a chamber atmosphere of 0.1 Torr water vapor to prevent charging and sample drift of the uncoated specimens. A similar procedure was described previously.[54]

Grain size measurements were performed using a computer automated image analysis system (LECO 3001). The average grain size of the abnormal grains was determined by the feret method as previously described.[9,16,17] Due to the large size of the grains, an average of only 15 grains per sample were measured. Although, a statistically accurate kinetic analysis should include at least 300 grains per sample, this would require the analysis of over 20 samples per point (a total of 140 samples for the present work), which was beyond the scope of this study.

To examine the feasibility of reusing the abnormal grains as "seeds", several

abnormal grains were re-embedded in fresh powder compacts of PMN-35PT and re-sintered in oxygen. These seed abnormal grains were originally grown from a PMN-35PT + PbO matrix sintered in air and were extracted from the matrix by chemically etching with 30% HNO_3 and water in an ultrasonic bath. As a consequence of the air sintering atmosphere, the seed abnormal grains were porous,[45] making it easier to distinguish the new growth after re-sintering.

4.3   Results

Low magnification LOM micrographs of PMN-35PT + 5 vol.%PbO sintered in oxygen at 1175°C for 1 and 12 h are shown in Figures 4.1(a) and (b), respectively. The microstructures demonstrate that large abnormal grains nucleate early from the matrix and proceed to grow to sizes exceeding 500 μm.

Figure 4.2 shows an SEM image of an abnormal grain within a matrix of smaller grains after sintering 1 h at 1175°C. The presence of a grain boundary in the center indicated that the abnormal grain consisted of multiple grains and may be a bicrystal. Grain orientation image maps such as that shown in Figure 4.3 confirm the abnormal grains to be mostly bicrystals. The line drawn down the grain boundary between the two crystals in Figure 4.3 was determined to be a Σ3 boundary. Thus, the two grains were misoriented 60° about <111>, the twin orientation relationship. All abnormal grains analyzed contained such a boundary.

Low magnification LOM micrographs of the microstructures for PMN-35PT with 5

and 1.8 vol.% PbO sintered in oxygen for 4 h at 1175°C are shown in Figures 4.4(a) and (b), respectively. Abnormal grains were not present in the sintered samples of PMN-35PT + 1.8 vol.%PbO.

Figures 4.5(a-d) show low magnification LOM micrographs of PMN-35PT + 5 vol.% PbO sintered in oxygen for 4 h at 1025, 1075, 1125, and 1175°C, respectively. No abnormal grains were observed in samples sintered at 975°C. Qualitative observations were made regarding the occurrence of abnormal grain growth in PMN-35PT + 5 vol.%PbO sintered in oxygen for different times and temperatures. The results are presented in the form of a microstructure map in Figure 4.6.

An informal grain growth kinetic analysis was performed for samples of PMN-35PT + 5 vol.% PbO sintered in oxygen at 1175°C. Figure 4.7(a) plots the resultant abnormal grain size as a function of time. These data were best fitted to a cubic grain growth law

$$G^3 - G_o^3 = kt$$

where G is grain size at time t, G_o is the initial grain size at time t=0, and k is the growth rate constant. The growth kinetics are described using a plot of $G^3 - G_o^3$ versus time, as shown in Figure 4.7(b). The calculated growth rate constant was 1.16×10^{-11} m^3/h with an R^2 of 0.972 and is listed in Table 4.1.

Figure 4.8 shows the micrograph of an abnormal grain which was extracted from the matrix and re-embedded in a fresh compact of PMN-35PT + 5 vol.% PbO and sintered for 4 h at 1175°C in oxygen. The dense outer region of the abnormal grain is the new growth from oxygen sintering, while the porous core was the original seed bicrystal from air sintering.
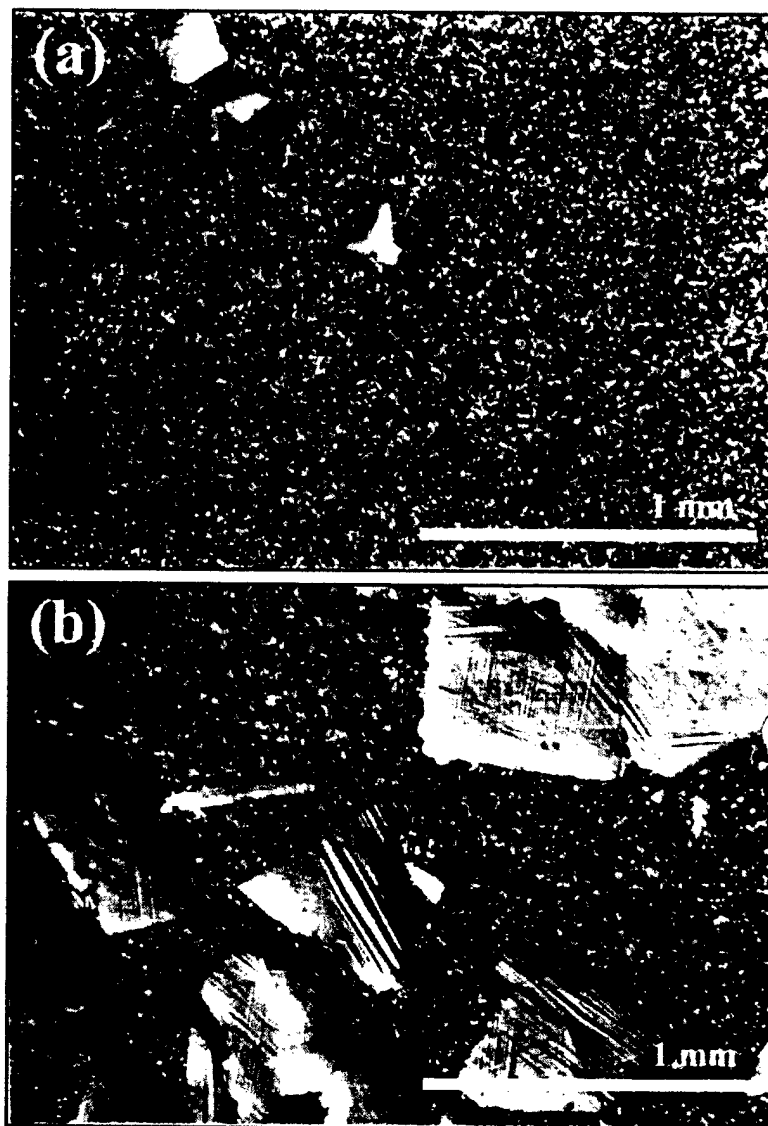
Figure 4.1. LOM micrographs of PMN-35PT + 5 vol.%PbO sintered in oxygen at 1175°C for (a) 1 h and (b) 12 h. The large abnormal grains nucleated from the matrix. Note the ferroelectric domains present in the grains.
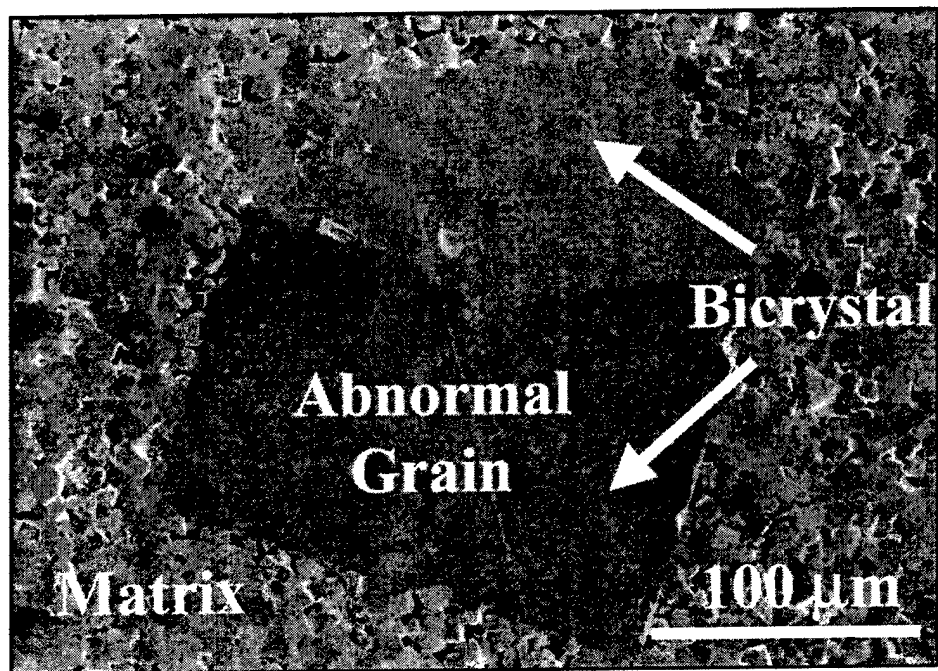
Figure 4.2. SEM micrograph of PMN-35PT + 5 vol.%PbO sintered in oxygen for 1 h at 1175°C. The large abnormal grain is actually a bicrystal.
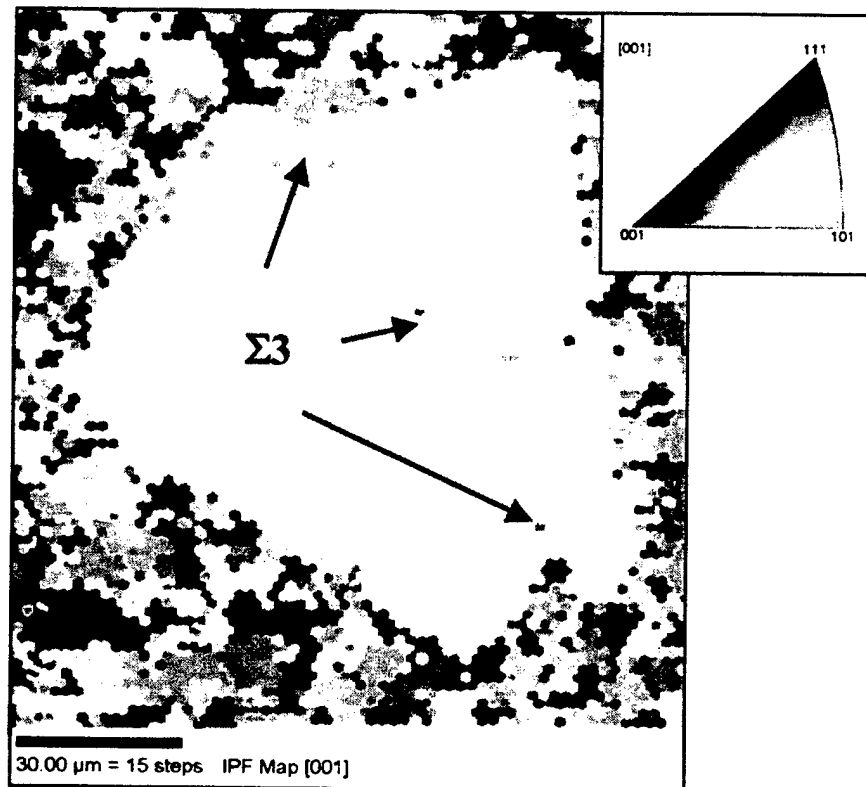
Figure 4.3. Inverse Pole Figure Orientation Image Map (OIM) of an abnormal grain from PMN-35PT + 5 vol.%PbO sintered in oxygen for 1 h at 1175°C. The two grains in the bicrystal are misoriented 60° about <111>, i.e. twin orientation. The line separating the grains denotes a Σ3 grain boundary.

87
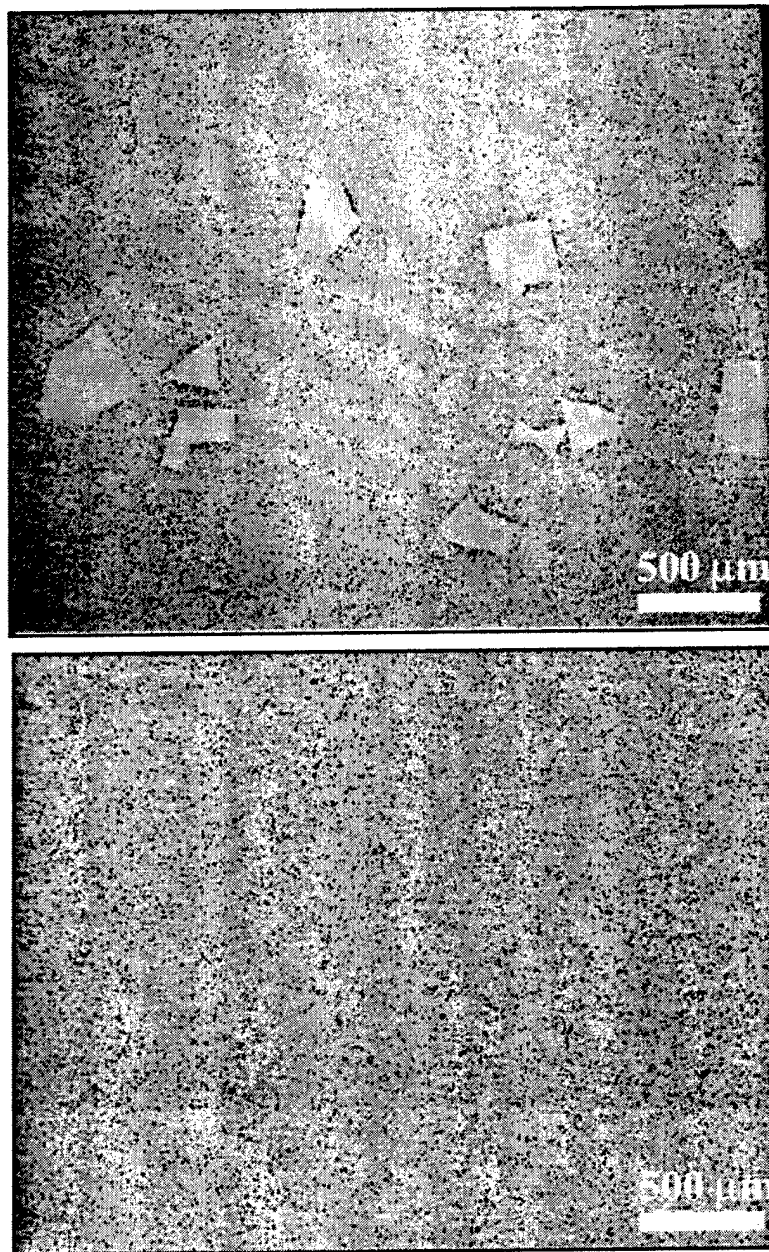
Figure 4.4. Low magnification LOM micrographs of PMN-35PT sintered in oxygen at 1175°C for 4 h with (a) 5 vol.% and (b) 1.8 vol.% PbO. No abnormal grains were observed in (b).
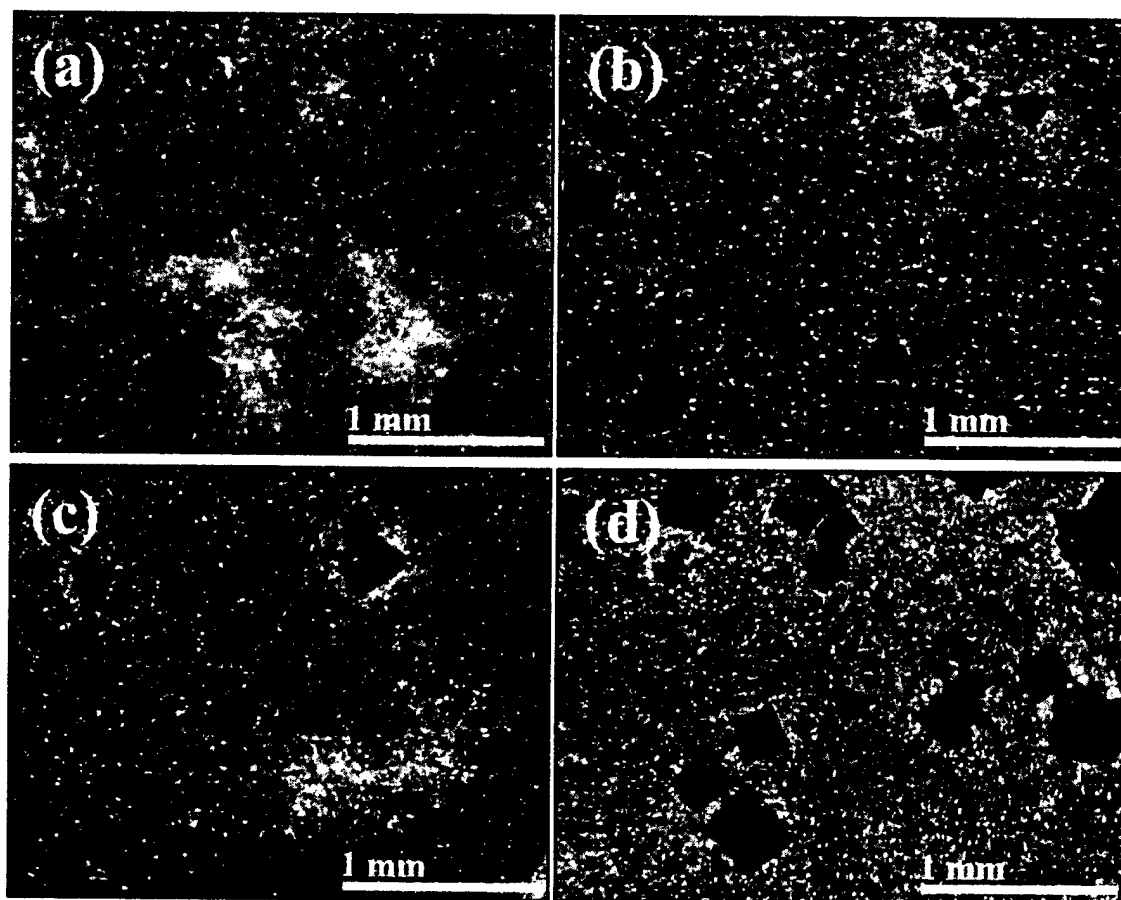
Figure 4.5. Low magnification LOM micrographs of PMN-35PT + 5 vol.%PbO sintered in oxygen for 4 h at (a) 1025°C, (b) 1075°C, (c) 1125°C, and (d) 1175°C. No abnormal grains were observed in samples sintered at 975°C.
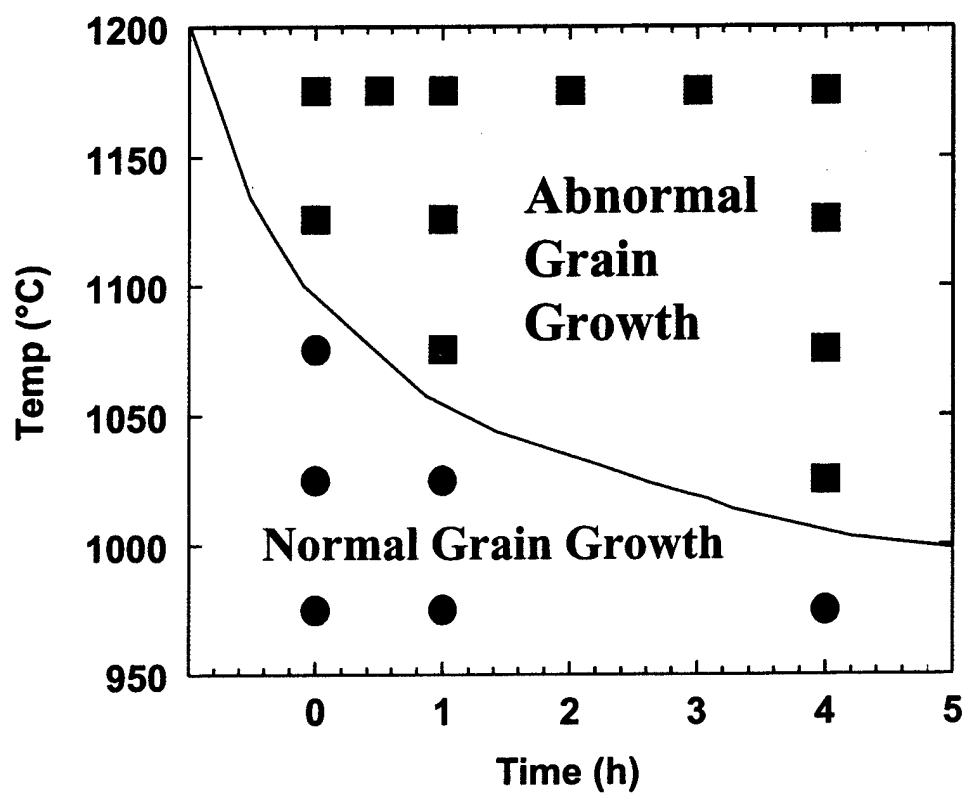
Figure 4.6. Microstructure Map for PMN-35PT + 5 vol.%PbO sintered in oxygen at multiple temperatures and times.
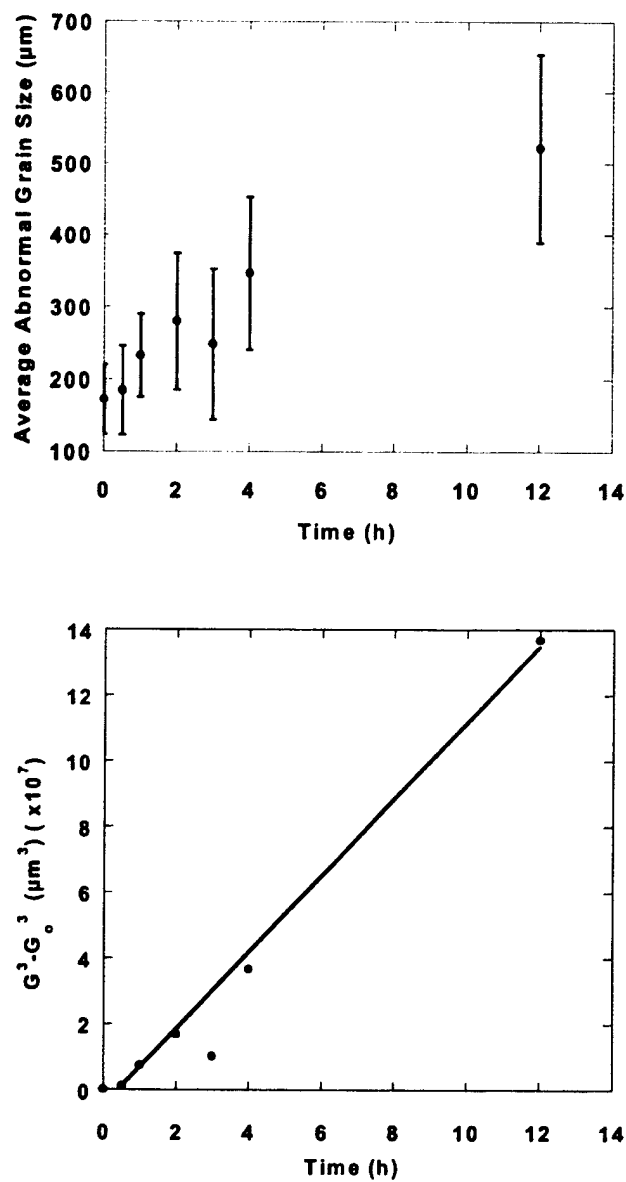
Figure 4.7. (a) Average grain size of the abnormal grains in PMN-35PT + 5 vol.%PbO sintered in oxygen at 1175°C for multiple times; (b) Cubic grain growth kinetics for abnormal grains, k=1.16 x 10^{-11} m³/h (R^2=0.996).

Table 4.1: Comparison of growth rate constants for PMN-35PT + 5 vol.% PbO.

Type of Growth	Growth rate constant, $k^{\#}$ (m^3/h)	R^2	Processing conditions
Abnormal Grain Growth	1.16×10^{-11}	0.97	sintered in oxygen, 1175˚C
Matrix Grain Growth[45]	3.62×10^{-16}	0.96	sintered in oxygen, 1175˚C
{001} Single Crystal Growth[16]	2.18×10^{-11}	0.90	<001> growth from single crystal seed in hot-pressed sample annealed in air, 1150˚C

[#]calculated using conventional cubic growth law, $G^3 - G_o^3 = kt$.
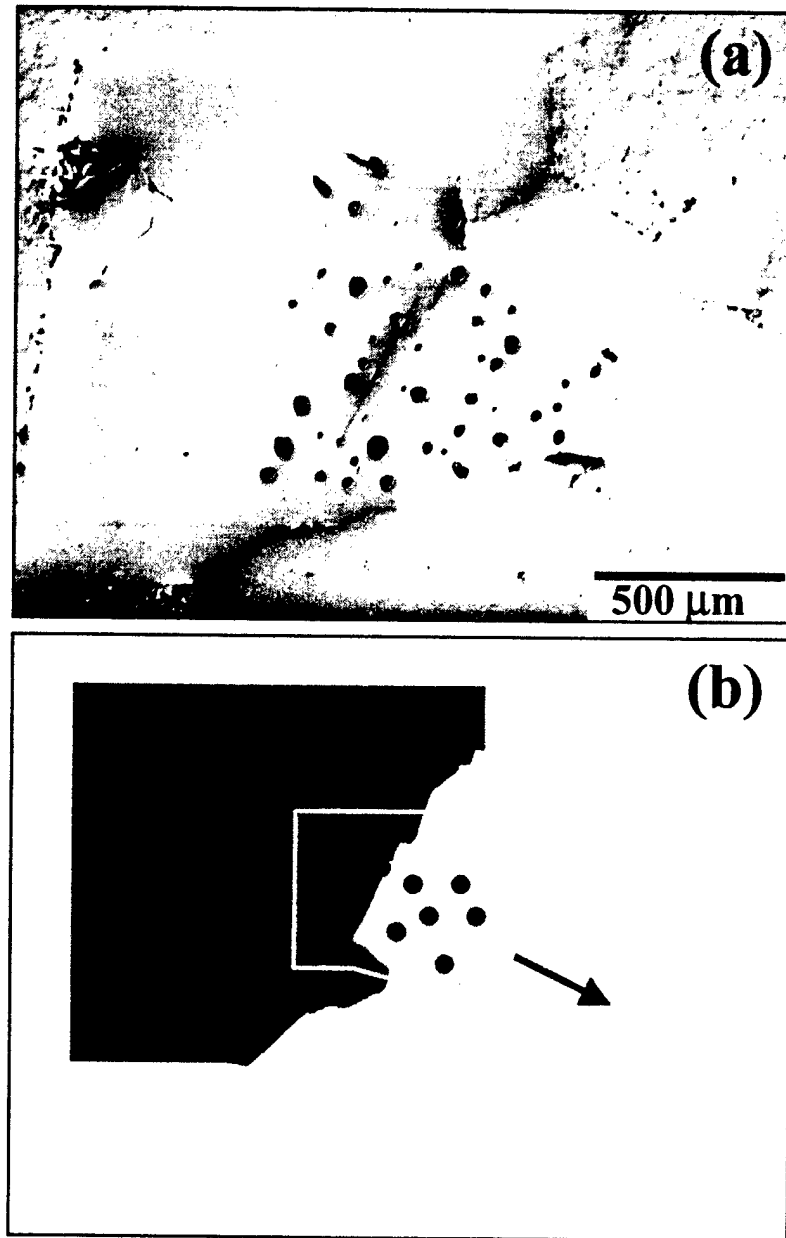
Figure 4.8. (a) LOM micrograph showing crystal growth of a PMN-35PT dense bicrystal from a porous bicrystal "seed" embedded in a PMN-35PT + 5 vol% PbO matrix sintered for 4 hours at 1175°C. (b) Schematic diagram of the embedded bicrystal experiment.

4.4 Discussion

As shown in the previous section, large abnormal grains (>10 times average grain size) have been observed to form in PMN-35PT samples with greater than 1.8 vol% excess PbO. Examples of typical microstructures of PMN-35PT + 5 vol% PbO sintered at 1175°C for 1 and 12 h are shown in Figure 4.1. Note the size of the abnormal grains approach 500-800 μm.

Previously, the origin of these select grains in PMN-PT was not well understood. However, recent work by Wallace *et al.*[34] showed that the abnormal grains in samples containing large amounts of excess PbO (30-70 vol%) were actually bicrystals. Furthermore, it was observed that the bicrystals were in a twin orientation, i.e. rotated 60° about the <111> with respect to each other. The present study verified this result for abnormal grains formed in PMN-PT with much lower PbO contents, as presented in Figures 4.2 and 4.3.

Preliminary evidence was also presented by Wallace *et al.* that indicated these bicrystals formed preferentially in the presence of excess MgO. Though the role of MgO was not examined in this study, many other factors were identified which also induced abnormal grain growth in PMN-PT. The bulk of these were centered around the presence of a PbO liquid phase.

4.4.1   Effect of PbO Content

As shown in Figure 4.4, reducing the PbO content in PMN-35PT from 5 vol.% to 1.8 vol.% PbO eliminated the incidence of abnormal grain growth after sintering at 1175°C in oxygen for all times studied. The matrix grains, however, were similar in size (i.e. ~12-15 μm for 4 h).

It was not surprising that the PbO content affected abnormal grain growth. The amount of excess PbO in the matrix has been shown to affect both the grain growth and single crystal growth kinetics in PMN-PT.[8,9,16] Khan *et al.*[8] first demonstrated that a PbO liquid phase was necessary for single crystal growth from {111} seed crystals. It was surprising, however, that 1.8 vol.% PbO was not high enough to induce abnormal grain growth. In a later study by Khan *et al.*,[9] it was shown that rapid single crystal growth was possible in PMN-35PT for compositions greater than 1 vol.% PbO.

Recently, King *et al.*[16] completed a full kinetic analysis of matrix grain growth and single crystal growth from {001} seed crystals for PMN-35PT with varying amounts of excess PbO. That study reported grain growth rate constants of 1.5×10^{-15} and 3.9×10^{-16} m^3/h for 1.5 and 5 vol.% PbO contents, respectively. Growth rate constants for single crystal growth in the <001> direction were given as 1.6×10^{-11} and 2.2×10^{-11} for 1.5 and 5 vol.% PbO, respectively. Therefore, the 1.8 vol.% PbO content in the present study was clearly high enough for rapid grain growth and single crystal growth to occur.

It is important then to understand how the abnormal grains form in the first place. Since the growth advantage of abnormal grains in PMN-PT has been attributed to the

presence of Σ3 boundaries,[34,35] grain rearrangement might play a role. In liquid phase sintering, the first stage of densification is particle rearrangement.[55,56] The presence of a liquid phase aids this process by lowering the resistence to particle motion. Thus, with the presence of a PbO liquid phase it would be easier for two PMN-PT particles to arrange themselves into a lower energy configuration, such as a Σ3 boundary misoriention. It is believed that the probability of such an event increases with further additions of PbO liquid phase. Two grains which were not close enough to the special Σ3 configuration on their own could easily rearrange themselves if they were surrounded by a pool of liquid. Since the development of abnormal grains in the present study seemed to occur in the early stages of sintering, it was believed that they nucleated as a result of Σ3 boundary formation during the particle rearrangement stage of liquid phase sintering.

King et al.[16] observed abnormal grains in samples that were initially hot-pressed, then annealed. In that study, abnormal grain growth occurred only in those samples with 3 vol.% PbO and greater and for annealing times longer than 5 h. These were also the conditions for which a transition in the grain microstructure was observed to be initiated. This is further support that the abnormal grains were induced by the formation of low energy Σ3 boundaries due to liquid phase assisted grain rearrangement.

4.4.2 Effect of Temperature and Time

As seen from the microstructures in Figure 4.5, there appears to be a temperature dependence of abnormal grain growth in PMN-35PT + 5 vol.% PbO. No abnormal grains

were observed in the sample sintered at 975°C for 4 h, and the size and number of abnormal grains appeared to increase with temperature. The microstructure map in Figure 4.6 also shows there to be a time dependence on abnormal grain growth.

These time and temperature dependencies are simply reflections of the matrix grain growth kinetics. As discussed in the previous section, it is believed that the occurrence of abnormal grain growth is determined by the availability of liquid PbO surrounding the matrix grains. And increasing the amount of liquid available around the matrix grains can be done in two ways. The first is to simply add more liquid, which was addressed above. The second is to increase grain size.

Consider that the thickness of the grain boundary liquid phase increases with increasing grain size as a result of decreased boundary area. Effectively, that means more liquid becomes available as the grains grow. In turn, grain rearrangement becomes easier and the probability of forming Σ3 boundaries is raised. It follows, then, that abnormal grain growth is limited by the kinetics of matrix grain growth. This could explain why abnormal grains were observed to occur at longer times and higher temperatures.

4.4.3 Abnormal Grain Growth Rate

The average abnormal grain size as a function of time is shown in Figure 4.7(a). The values reported represent the size of the abnormal grains measured as bicrystals. It should also be noted that the wide spread in grain size as indicated by the error bars at each point in Figure 4.7(a) was largely due to sectioning effects. A better approach might

have been to etch out grains and measure their size in three dimensions using volume particle analysis techniques.

Due to the large sizes and low numbers of abnormal grains measured per sample, this study was not considered to be an elaborate one and it is acknowledged that further work is required to ensure statistical accuracy of the kinetic data. Still, the data seemed to fit very well to a cubic growth kinetic law, as shown in Figure 4.7(b). The calculated growth rate constant, k was 1.16×10^{-11} m^3/h with a correlation factor, R^2 of 0.972.

The growth rate constant for abnormal grain growth is compared in Table 4.1 with the rate constants measured for matrix grain growth[45] and {001} single crystal growth[16] of the same material. As shown, the growth rate constant for abnormal grain growth was much higher (nearly 5 orders of magnitude) than for matrix grain growth.

In addition, the abnormal grain growth rate agreed very well with the reported single crystal growth rates from {001} seed crystals.[16] The k for abnormal grain growth was slightly lower but still the same order of magnitude as for single crystal growth. This result implies that the abnormal grain bicrystals offer no advantage over conventional seeded single crystal growth. Thus, the role of the Σ3 boundary in the abnormal grains was to offer only a growth advantage over the matrix grains. Further, that growth advantage continued even as the bicrystals grew larger. A more complete analysis of the effect of the Σ3 boundary on growth was done by Rockosi et al.,[57] who compared the growth of large grains with and without Σ3 boundaries in a systematic study.

4.5 Conclusions

Abnormal grain growth was shown to occur in PMN-35PT in the presence of excess PbO in the matrix. It was confirmed that the abnormal grains were bicrystals misoriented 60° about <111>, i.e. the twin relationship.

It was determined that the abnormal grains were the consequence of low energy $\Sigma 3$ boundaries forming due to liquid-phase assisted grain rearrangement. The occurrence of abnormal grains was affected by the inital PbO composition, temperature, and time. It was suggested that abnormal grain growth was also limited by the kinetics of matrix grain growth, which affects the availability of PbO locally surrounding the matrix grains.

The abnormal grain growth rate in PMN-35PT with 5 vol.%PbO was measured to be 5 orders of magnitude faster than that of matrix grain growth, as expected. The presence of the $\Sigma 3$ boundary provides the growth advantage. However, it was also shown that the kinetics for abnormal grain growth wa no faster than conventional seeded single crystal growth in the {001} direction.

CHAPTER 5

SWELLING IN PMN-PT

5.1 Introduction

Since the initial demonstration of single crystal growth of PMN-PT from seeded polycrystalline precursors,[4] a great deal of effort was put forth to try to understand the mechanisms controlling boundary migration in that system. Although there has been a considerable amount of research dedicated to grain boundary migration in general over the past five decades, a fundamental understanding of the process is lacking.[58,59] This is especially the case when trying to relate the effects of a liquid phase to the grain boundary mobility.

The motion of a grain boundary in a pure, single-phase system is governed by the flux of ions across a boundary of only atomic dimensions. This intrinsic migration of the boundary is therefore expected to be very fast.[60] The average grain growth rate would follow parabolic kinetics such that $G^2 - G_0^2 = kt$, where G is the average grain size at time t, G_0 is the starting grain size, and k is the growth rate constant.[61] However, the microstructure development in single phase ceramics rarely follows this kinetic behavior.[7]

Instead, they are often controlled by the presence of one or more extrinsic factors. These include solute or impurity segregation, porosity, and second phase particles, all of which can impair the migration of a boundary by imposing drag forces.[7, 61,62]

The behavior of a grain boundary in the presence of a liquid phase is not as straight forward. Although some of the first models of grain growth with a liquid phase were developed fifty years ago, there still lacks a complete understanding of the role of a liquid on boundary migration in real systems. Experimentally, the relationship between liquid volume fraction and growth rate constant has not been studied extensively, especially using well-controlled microstructures. In PMN-PT, it was found that the addition of a PbO liquid phase enhanced the grain growth rate up to a critical volume fraction beyond which the growth rate decreased.[9,16] There are several other systems reported in the literature that exhibited similar grain growth behaviors with the addition of a small amount of liquid phase. These include Al_2O_3, c-ZrO_2,[63] MgO,[64] ZnO[10,11,12] and Mn-Zn and Li-Zn ferrites.[60,65] In most of these cases, however, the characterized microstructures contained porosity at some point during the grain growth process, whether it existed at the beginning or was generated later. In fact, much of the relevant grain growth data in the literature was the result of liquid phase sintering studies. Consequently, the growth kinetics data were masked by the influence of porosity.

Even in well-designed, critical experiments where every effort is made to ensure that samples begin with very fine-grained, dense microstructures, problems maintaining the density often arise during subsequent heat treatments. For example, Bennison et al.[66] found that the oxidation of ppm levels of C and S impurities was enough to cause

101

significant swelling in hot-pressed Al_2O_3.

As mentioned in section 2.4.1.1, the grain growth kinetics study in the PMN-PT system was also subject to this problem. Fully-dense, hot-pressed samples of PMN-35PT with excess PbO underwent a de-densification process during the annealing treatments which was attributed to pore formation from internally evolved gases.

The purpose of the present study was to examine the cause of de-densification in PMN-PT, to understand the factors promoting pore formation, and to determine the processing conditions required to prevent swelling.

5.2 Experimental Procedure

PMN-35PT powders (TRS Ceramics) were ball-milled with 5 vol.% PbO (Alfa Aesar, puratronic powder) in ethanol for 24 h using 3mm zirconia media (Tosoh). The powders were dried using a rotoevaporator (Büchi) and subsequently calcined at 450°C for 4 h in air. The calcined powders were crushed with an agate mortar and pestle and passed through a 100-mesh stainless steel sieve.

The powders were uniaxially pressed at 67 MPa to form 3 mm thick x 13 mm diameter pellets and subsequently cold isostatically pressed at 345 MPa. In the case of single crystal growth experiments, oriented {001} PMN-PT seed crystal plates (Crystal Associates) on the order of 2.5 mm x 2.5 mm x 0.5 mm were embedded in the center of the pellets prior to pressing.

The green pellets were transferred to an alumina die and hot-pressed for a hold time

of 30 min at a set temperature of 880°C under an applied pressure of 20 MPa in an air atmosphere. The PMN-PT samples were surrounded with coarse (40-50 μm) alumina powder (Aldrich) to prevent the samples from reacting with the die and seizing the punches. The pressure was applied prior to the start of the 5°C/min heating rate and removed after cooling at the same rate to 450°C. The actual temperature observed by the samples inside the die was later measured to be 770 and 830°C at the start and end of the 30 min holds, respectively. Note these temperatures are below the melting temperature of PbO (886°C at standard atmospheric pressure).

The hot-pressed samples were ground with SiC to remove any alumina powder from the surfaces of the samples and quartered using a high-speed diamond saw (Struers Accutom). The samples were subsequently cleaned with ethanol and deionized water, and dried in an oven overnight. The specimens were subsequently placed in a Pt pouch, embedded in powders with like compositions, set in a double crucible arrangement and annealed for various times at 1175°C in air. For comparison, samples of the same composition that were previously sintered to full density in oxygen were also annealed at the same time. The samples were weighed before and after annealing to ensure weight loss was minimized. Density measurements were made using the Archimedes method in water containing a small amount of surfactant.

Cross-sections of the specimens were prepared using standard grinding, polishing, and etching techniques. The microstructures of the samples were examined using scanning electron microscopy (SEM) and light optical microscopy (LOM). The microchemistry of the samples was determined using electron probe microanalysis

(EPMA) (JEOL 733 SuperProbe) and high resolution scanning transmission electron microscopy (STEM) (VG HB 603). The STEM unit was equipped with an X-ray energy dispersive spectrometer (XEDS) for chemical analysis. STEM specimens were prepared using a dual-beam Focused Ion Beam (FIB) instrument (FEI DB235).

A separate study was performed to investigate phase transformations in lead oxide during sample preparation. The same high-purity orthorhombic PbO powder (ortho-PbO) (Alfa Aesar) added to the PMN-PT powders above was characterized using x-ray diffraction (Rigaku) and thermogravimetric analysis (TG) (Netzsch STA-409).

To form the low-temperature stable phase of tetragonal PbO (tetr-PbO), the as-received meta-stable ortho-PbO was mixed in water and heated to 75°C for 3 hours. The slurry was vacuum filtrated and the resulting powder was dried in an oven overnight, followed by a heat treatment at 200°C for 4 h. A similar procedure was reported to induce the orthorhombic to tetragonal phase transformation.[67] The as-received ortho-PbO was also ball-milled in ethanol for 24 h, which was also reported to induce the transformation.[68]

5.3   Results and Discussion

Figure 5.1(a) shows a typical microstructure for an as hot-pressed PMN-35PT + 5vol%PbO sample. After hot-pressing, the average density was 8.21 g/cc. Subsequent pressureless annealing in air produced porous microstructures and corresponding decreases in density. Figure 5.1(b) shows the microstructure of a sample that was

annealed for 10 h in air after hot-pressing, yielding a density of 7.69 g/cc. Figure 5.2 plots the average density of the hot-pressed and annealed samples as a function of annealing time. As shown, there was an initial drop in density by simply heating and cooling the samples (0 h dwell). It is believed that this initial loss of density was due to an instantaneous, gas-evolving event that resulted in the formation of porosity. The density continued to decrease with increased annealing time, probably due to the coarsening of such gas-filled pores. In contrast, samples that were sintered first in oxygen, then annealed in air retained their density, as shown in Figure 5.2. Thus, they did not exhibit the same de-densification behavior.

Based on the work of Bennison et al.,[66] it was thought that the porosity was the result of carbon oxidation from the burnout of organic materials. However, one would have expected pore formation to be enhanced at the surface, as oxygen would need to diffuse in. This was not the case, as shown from the micrograph in Figure 5.3. In fact, the edges of the annealed samples were more dense than the interiors. The microstructure is similar to those discussed previously (Figure 2.3(c)). Recall from section 2.4.1.2 that such a dense surface layer was attributed to the diffusion of trapped gases *out* of the sample. In that case, for air sintering, the trapped gas was believed to be mostly nitrogen.

It is certainly possible that insoluble gases such as nitrogen from the air could have become entrapped in the hot-pressed samples, the gases being compressed at the grain boundaries and triple points by the 20 MPa uniaxial pressure. Subsequent annealing under zero load would then allow the compressed gases to expand and form discrete
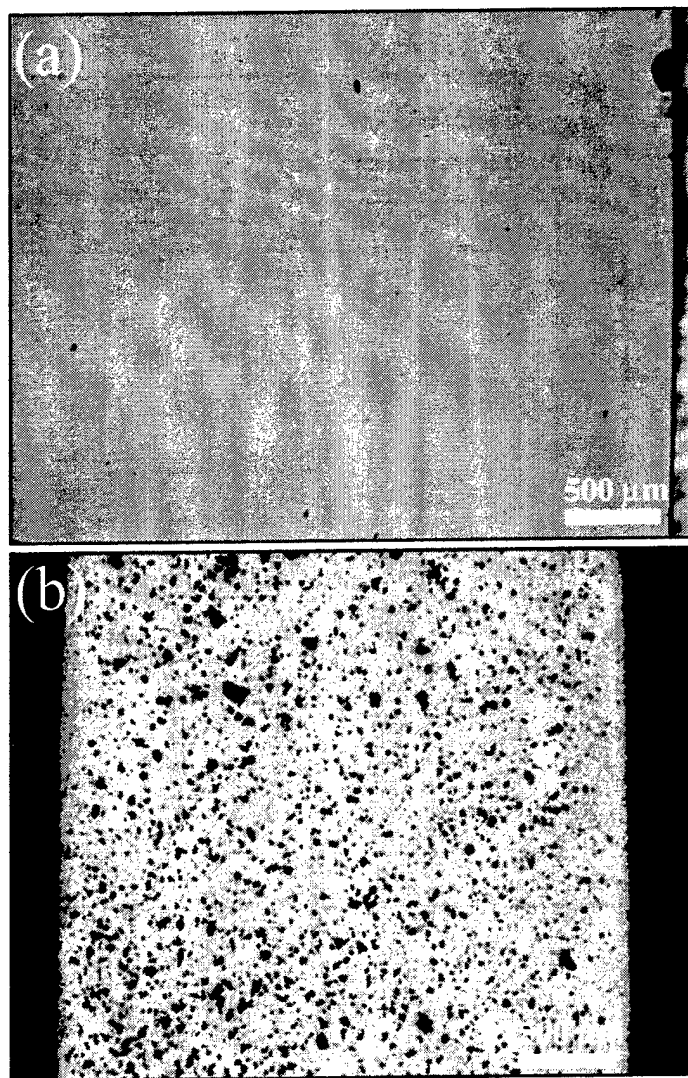
Figure 5.1. Low magnification LOM micrographs of PMN-35PT + 5 vol.%PbO that was (a) hot-pressed in air at 880°C for 30 min at 20 MPa and (b) subsequently annealed in air at 1175°C for 10 h. The dark phase in (b) is porosity.
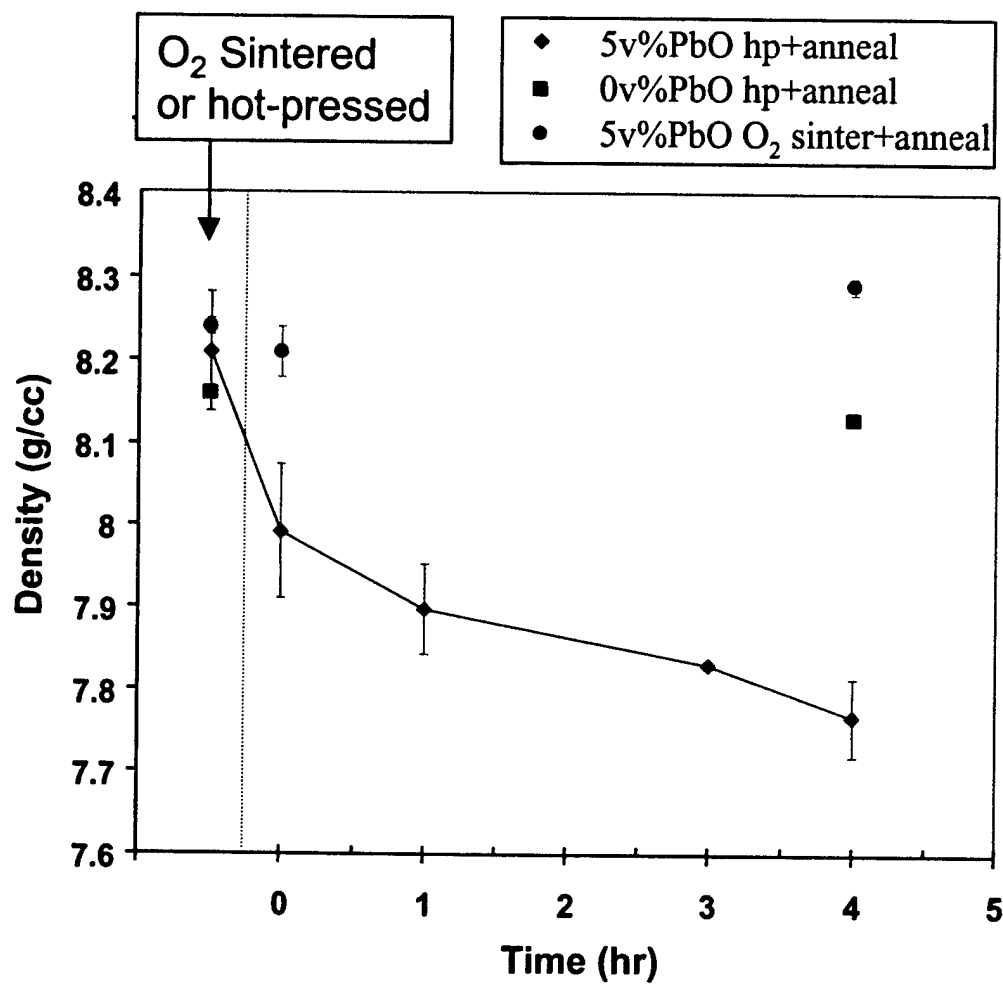
Figure 5.2. Plot of density as a function of time for PMN-35PT samples with 0 and 5 vol.%PbO; samples were either hot-pressed in air and subsequently annealed in air, or sintered in oxygen and subsequently annealed in air.
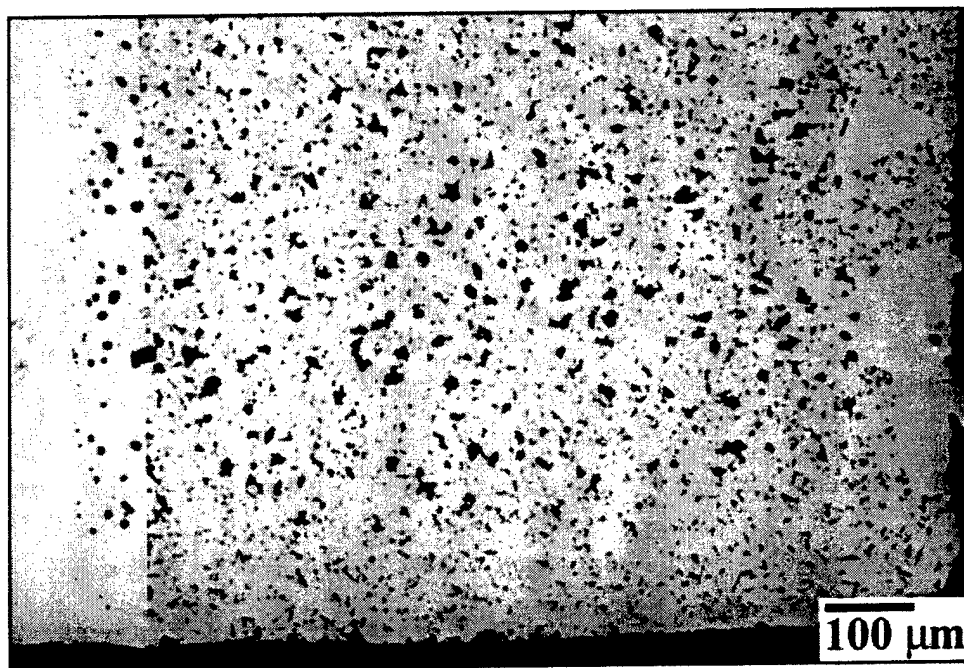
Figure 5.3. Low magnification LOM micrograph of a {001} seeded sample of PMN-35PT + 5 vol.%PbO that was hot-pressed in air at 880°C for 30 min at 20 MPa and subsequently annealed in air at 1150°C for 2 h. Note the edge of the sample was dense, while the core of the sample was porous.

pores. However, pore formation would have been expected to occur for all hot-pressed PMN-PT samples, which was not the case. As Figure 5.2 shows, hot-pressed PMN-35PT with 0% PbO did not exhibit a drop in density upon annealing. This is significant because it also suggests that lead oxide likely plays a major role in the pore formation, the topic of the next section. It is also important to note that the final densities of the hot-pressed + annealed samples which de-densified were lower than the densities of samples sintered in air from the green state (from section 2.4.1.2). This suggests that additional gas was generated in the system after hot-pressing and annealing.

5.3.1 The Role of Lead Oxide

Given the volatile nature of lead oxide at high temperatures, one obvious possibility for gas evolution would be from the vaporization and/or decomposition of PbO. This would follow the following reaction:

$$PbO(s,l) \leftrightarrows PbO(g) \leftrightarrows Pb(g) + \frac{1}{2}O_2$$
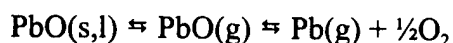
However, as discussed in section 2.4.1.2, the total vapor pressure above PbO liquid at the annealing temperature (1175°C) was calculated to be 1.8 kPa. This pressure on its own is not high enough to counteract the negative pressure due to curvature (on the order of 1 MPa) acting on the pore.

Therefore, decomposition of PbO according to the above reaction is not likely to play a major role in the pore formation in PMN-PT. A more likely decomposition reaction

would be of the form:

$$PbO_{1+x} \rightarrow PbO + x\tfrac{1}{2}O_2(g)$$

That is, an oxygen-rich PbO decomposes to PbO and evolves excess oxygen gas. For example, Pb_3O_4 is a known compound. Its decomposition reaction would follow:

$$Pb_3O_4 \rightarrow 3PbO + \tfrac{1}{2}O_2(g)$$

In the case of a hot-pressed PMN-PT sample with excess PbO, if the lead oxide were in the form of Pb_3O_4 and filled a 1μm pore, then the pressure generated inside the pore from the evolution of oxygen would be on the order of 580 MPa at 650°C. That pressure is certainly large enough to cause pore formation and growth.

5.3.2   Phase Transformations in Lead Oxide

Lead oxide is known to have many forms of higher-order oxides, such as Pb_3O_4 which is the most common and well-documented.[40] Pb_3O_4 is stable for temperatures between 400-650°C and forms readily by heating the low-temperature stable phase of tetr-PbO. Heating Pb_3O_4 above about 650°C, however, results in an abrupt phase transformation to ortho-PbO which is stable until melting at 886°C. Thus,

$$tetr\text{-}PbO \rightarrow Pb_3O_4 \rightarrow ortho\text{-}PbO$$
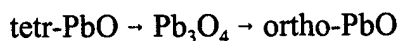
The kinetics of the phase transformations from ortho-PbO back to Pb_3O_4 and tetr-PbO are sluggish and these reactions do not occur readily. In fact, once formed, both ortho-PbO and Pb_3O_4 are very stable (meta-stable) at room temperature. Although Pb_3O_4 will transform to ortho-PbO if heated past 650°C, the meta-stable ortho-PbO phase will

not pass through any phase transformations upon heating from room temperature back to its high-temperature stable state.

It has been reported that ortho-PbO can be forced to transform to tetr-PbO with the addition of (1) mechanical energy (milling)[68,69] or (2) water.[67] This is demonstrated from the XRD patterns in Figure 5.4. As shown in (a), the as-received lead oxide powder was mostly ortho-PbO. Milling the powder for 24 h in ethanol transformed some of the ortho-PbO to tetr-PbO, as pattern (b) shows. Instead, heating the powder in water for only 3 h yielded 100% tetr-PbO, as shown by (c).

Figure 5.4 also confirms that subsequent heat treatments of (c) tetr-PbO at 500 and 675°C yielded (d) Pb_3O_4 and (e) ortho-PbO, respectively. The significance of this is addressed in the next section.

5.3.3 Origins of Pb_3O_4

In the present study, PbO was added to PMN-35PT in the form of ortho-PbO, then milled in ethanol for 24 h, dried, and calcined at 450-500°C for 4 h. In the previous section, it was determined that milling ortho-PbO yielded, at least in part, tetr-PbO. It was also determined that tetr-PbO transformed to Pb_3O_4 upon heating between 400 and 650°C. If follows, then, that the PMN-35PT + PbO powder compacts in the present study probably contained Pb_3O_4 prior to hot-pressing.

In an attempt to alleviate the problem, the pellets were pre-annealed at 700°C for 4 h. That temperature was high enough to transform Pb_3O_4 to ortho-PbO, thereby evolving the

excess oxygen before pore closure. This was verified by TG measurements on tetr-PbO in various atmospheres, as shown in Figure 5.5.

Unfortunately, subsequent hot-pressing and annealing of the pre-treated pellets revealed that the pore formation was not suppressed. The samples swelled just as much as before.

Finally it was deduced that the hot-pressing operation itself induced the PbO phase transformation. This was based on the work of White and Roy[70] who investigated the phase relations in the Pb-O system at high oxygen pressures. Figure 5.6 shows a modified pressure-temperature phase diagram for lead oxide, based on that study. According to the phase diagram, the hot-pressing pressures and temperatures used in the current study fall within the Pb_3O_4 phase field or on the Pb_3O_4-PbO phase boundary. Although it is recognized that there is no direct evidence (*i.e.* XRD pattern) for the existence of such a higher order lead oxide phase in the hot-pressed PMN-PT + PbO samples, there is enough circumstantial evidence to draw the following conclusion. It is believed that the source of the swelling in hot-pressed PMN-PT samples stems from the instantaneous evolution of oxygen as a result of the decomposition of Pb_3O_4. Changing the hot-pressing atmosphere to N_2, Ar, or vacuum would likely eliminate the incidence of de-densification in hot-pressed samples of PMN-PT, which will be investigated in the future.

5.4 Conclusions

Swelling in hot-pressed PMN-PT was determined to be caused by the instantaneous evolution of oxygen as a result of the decomposition of Pb_3O_4. The Pb_3O_4 phase formed during the hot-pressing operation.
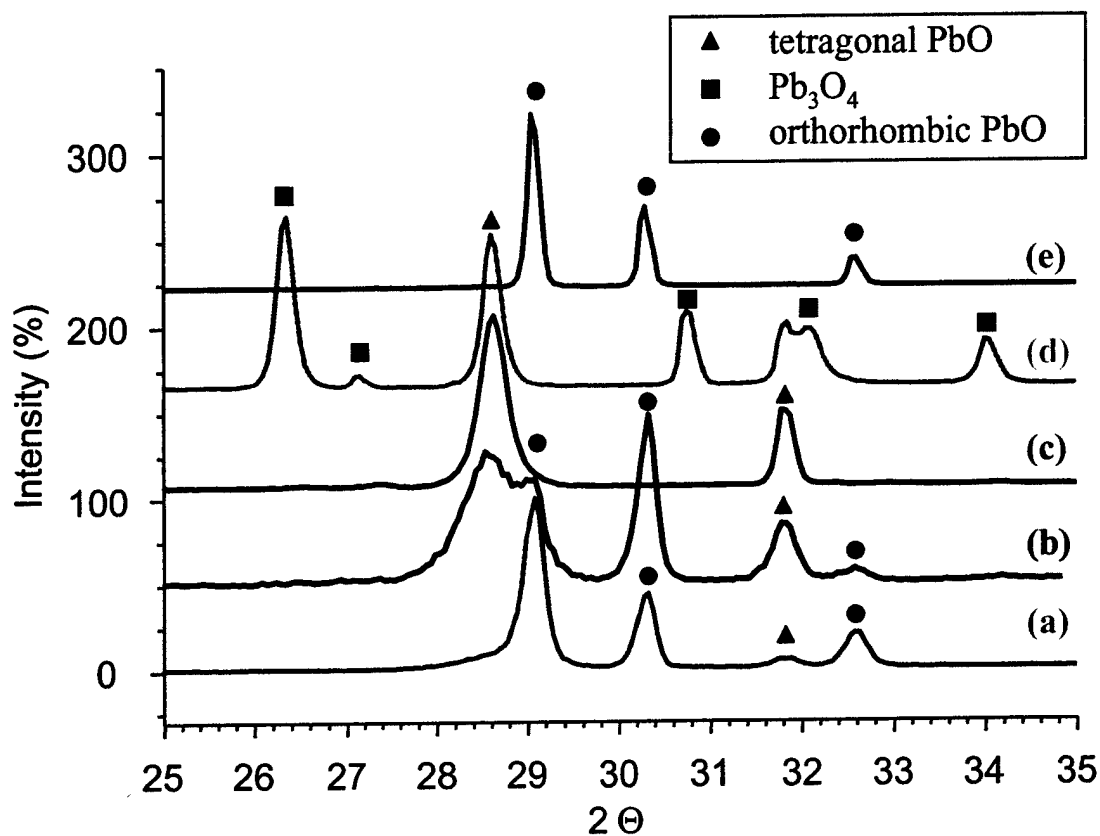
Figure 5.4. X-ray powder diffraction (XRD) patterns for orthorhombic (yellow) PbO (a) as-received, (b) milled in ethanol 24 h, and (c) heated to 75°C in water followed by subsequent annealing at (d) 500°C and (e) 675°C in air for 4 h.
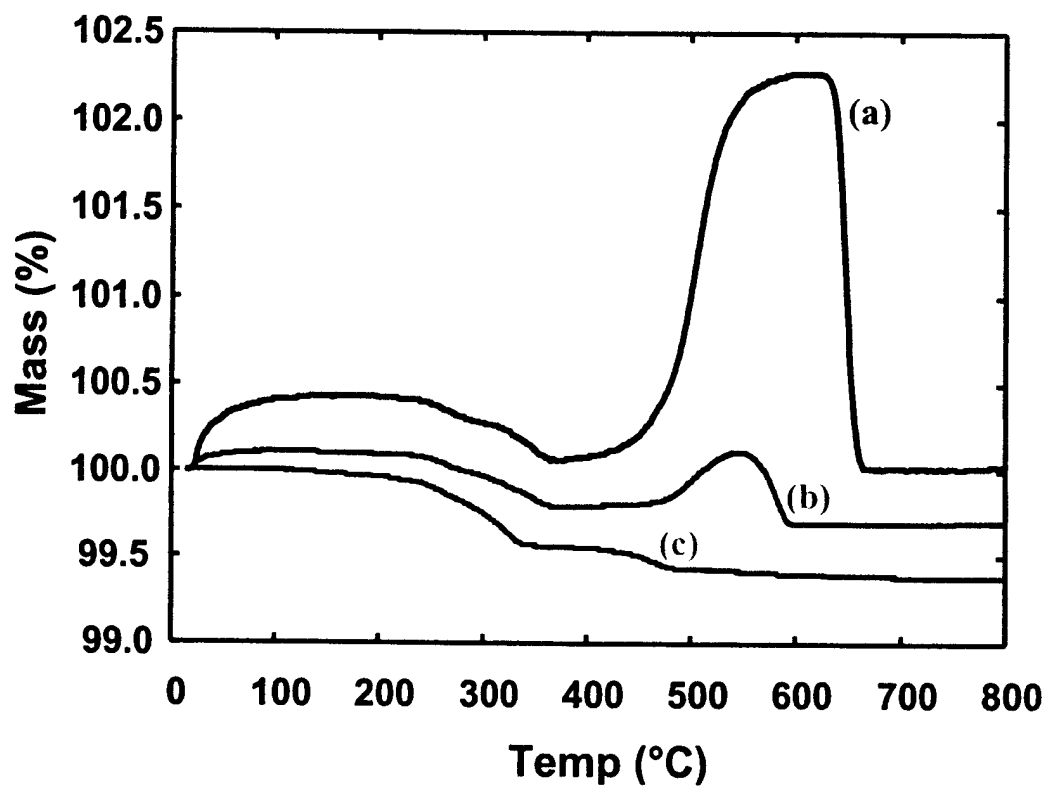
Figure 5.5. Thermogravimetric (TG) measurements describing weight change for tetragonal PbO in (a) oxygen, (b) air, and (c) 150 torr vacuum atmospheres.
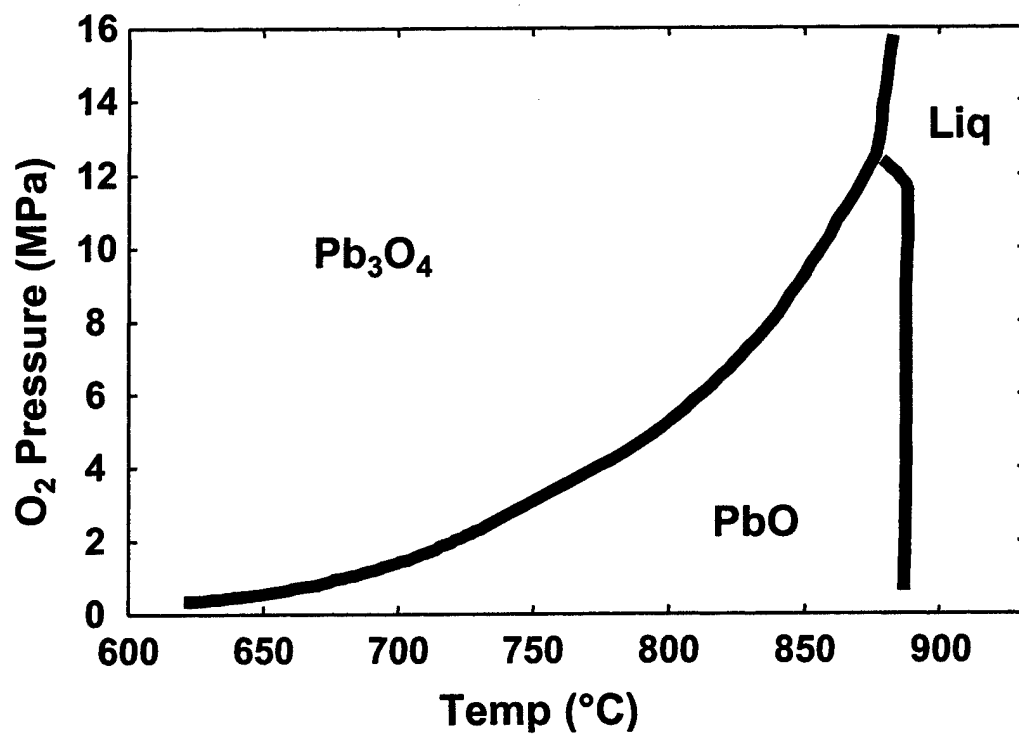
Figure 5.6. Pressure-temperature phase diagram for lead oxide system (after White and Roy).

Suggestions for Future Work

Grain growth kinetics need to be measured for PMN-PT + PbO samples which remain dense after hot-pressing and annealing. This will require the restriction of pore formation caused by evolved gases as discussed in Chapters 2 and 5. It is suggested that the samples be hot-pressed under a low partial pressure of oxygen in order to prevent the formation of higher order lead oxides, such as Pb_3O_4, during the hot-pressing operation. If the PbO second phae does not oxidize during hot-pressing, the excess oxygen cannot evolve during subsequent heating.

The existence of higher order lead oxides in the hot-pressed samples needs to be verified by a diffraction (x-ray, neutron, electron, etc.) technique.

The present study measured the piezoelectric behavior of the grown single crystals using high signals (i.e. high electric fields). It is recommended that future measurements be made using the IEEE standard low signal resonance techniques. This will provide more accurate values of the piezoelectric coefficent, d_{33}.

Finally, abnormal grain growth needs to be examined for earlier times in order to determine the cause of initiation.

References

1. S.-E. Park and T. R. Shrout, "Relaxor-based ferroelectric single crystals for electromechanical actuators," *Mater. Res. Innovations*, **1**, 20-25 (1997).

2. S.-E. Park and T. R. Shrout, "Characteristics of relaxor-based piezoelectric single crystals for ultrasonic transducers," *Proc. IEEE Ultrasonics Symp.*, **2**, 935-42 (1996).

3. S.-E. Park and T. R. Shrout, "Ultrahigh strain and piezoelectric behavior in relaxor based ferroelectric single crystals," *J. Appl. Phys.*, **82** [4], 1804-11 (1997).

4. T. Li, A. M. Scotch, H. M. Chan, M. P. Harmer, S.-E. Park, T. R. Shrout and J. R. Michael, "Single crystals of $Pb(Mg_{1/3}Nb_{2/3})O_3$-35 mol% $PbTiO_3$ from polycrystalline precursors," *J. Am. Ceram. Soc.*, **81** [1] 244-48 (1998).

5. J. Rodel and A. M. Glaeser, "Anisotropy of grain growth in alumina," *J. Am. Ceram. Soc.*, **73** [11] 3292-301 (1990).

6. M. N. Rahaman, Ceramic Processing and Sintering, Marcel Dekker, NY (1995).

7. S.J. Bennison, pp.304-12 in Engineered Materials Handbook, Vol. 4, Ceramics and Glasses, ASM International, Materials Park, OH (1991).

8. A. Khan, F. A. Meschke, T. Li, A. M. Scotch, H. M. Chan, and M. P. Harmer, "Growth of $Pb(Mg_{1/3}Nb_{2/3})O_3$-35 mol% $PbTiO_3$ single crystals from (111) substrates by seeded polycrystal conversion," *J. Am. Ceram. Soc.*, **82** [11] 2958-62 (1999).

9. A. Khan, E. Gorzkowski, A. M. Scotch, E. R. Leite, H. M. Chan, and M. P. Harmer, "Influence of excess PbO additions on {111} single crystal growth of $Pb(Mg_{1/3}Nb_{2/3})O_3$-35 mol% $PbTiO_3$ by seeded polycrystal conversion," submitted to *J. Am. Ceram. Soc.* (2002).

10. T. Senda and R. C. Bradt, "Grain growth in sintered zinc oxide and zinc oxide-bismuth oxide ceramics," *J. Am. Ceram. Soc.*, **73** [1] 106-14 (1990).

11. D. Dey and R. C. Bradt, "Grain growth of zinc oxide during bismuth(III) oxide liquid-phase sintering," *J. Am. Ceram. Soc.*, **75** [9] 2529-34 (1992).

12. J. Kim, T. Kimura, and T. Yamaguchi, "Effect of bismuth oxide content on the sintering of zinc oxide," *J. Am. Ceram. Soc.*, **72** [8] 1541-44 (1989).

13. M. Drofenik, A. Znidarsic, and D. Makovec, "Influence of the addition of Bi_2O_3 on the grain growth and magnetic permeability of MnZn ferrites," *J. Am. Ceram.*

Soc., **81** [11] 2841-48 (1998).

14.   G. C. Nicholson, "Grain growth in magnesium oxide containing a liquid phase," *J. Am. Ceram. Soc.*, **48** [10] 525-28 (1965).

15.   T. Li, S. Wu, A. Khan, A. M. Scotch, H. M. Chan, and M. P. Harmer, "Hetero-epitaxial growth of bulk single crystal $Pb(Mg_{1/3}Nb_{2/3})O_3$-35 mol% $PbTiO_3$ from (111) $SrTiO_3$," *J. Mater. Res.*, **14** [8] 3189-91 (1999).

16.   P. T. King, E. P. Gorzkowski, A. M. Scotch, D. J. Rockosi, H. M. Chan, and M. P. Harmer, "Kinetics of {001} $Pb(Mg_{1/3}Nb_{2/3})O_3$-35 mol% $PbTiO_3$ single crystals grown by seeded polycrystal conversion," submitted to *J. Am. Ceram. Soc.* (2002).

17.   G. S. Thompson, "Kinetic model of particle-inhibited grain growth," Ph.D. dissertation, Lehigh University, Bethlehem, Pa. (2001).

18.   M. I. Mendelson, "Average grain size in polycrystalline ceramics," *J. Am. Ceram. Soc.*, **52** [8] 443-6 (1969).

19.   R. B. Atkin and R. M. Fulrath, "Point defects and sintering of lead zirconate-titanate," *J. Am. Ceram. Soc.*, **54** [5] 265-70 (1971).

20.   R. L. Holman and R. M. Fulrath, "Intrinsic nonstoichiometry in single-phase $Pb(Zr_{0.5}Ti_{0.5})O_3$," *J. Am. Ceram. Soc.*, **55** [4] 192-97 (1972).

21.   R. L. Holman and R. M. Fulrath, "Intrinsic nonstoichiometry in the lead zirconate-lead titanate system determined by Knudsen effusion," *J. Appl. Phys.*, **44** [12] 5227-36 (1973).

22.   G. S. Snow, "Fabrication of transparent electrooptic PLZT ceramics by atmosphere sintering," *J. Am. Ceram. Soc.*, **56** [2] 91-96 (1973).

23.   G. S. Snow, "Improvements in atmosphere sintering of transparent PLZT ceramics," *J. Am. Ceram. Soc.*, **56** [9] 479-80 (1973).

24.   A. I. Kingon and J. B. Clark, "Sintering of PZT ceramics: I, atmosphere control," *J. Am. Ceram. Soc.*, **66** [4] 253-56 (1983).

25.   A. I. Kingon and J. B. Clark, "Sintering of PZT ceramics: II, effect of PbO content on densification kinetics," *J. Am. Ceram. Soc.*, **66** [4] 256-60 (1983).

26.   J. P. Guha, D. J. Hong, and H. U. Anderson, "Effect of excess PbO on the sintering characteristics and dielectric properties of $Pb(Mg_{1/3}Nb_{2/3})O_3$-$PbTiO_3$-based ceramics," *J. Am. Ceram. Soc.*, **71** [3] C152-154 (1988).

27. E. M. Sabolsky, G. L. Messing, and S. Trolier-McKinstry, "Kinetics of templated grain growth of 0.65 Pb(Mg$_{1/3}$Nb$_{2/3}$)O$_3$-0.35 PbTiO$_3$," *J. Am. Ceram. Soc.*, **84** [11] 2507-13 (2001).

28. A. M. Scotch, E. P. Gorzkowski, H. M. Chan, and M. P. Harmer, "Swelling of PMN-PT" in preparation (2002).

29. T. F. Murray and R. H. Dungan, "Oxygen firing can replace hot pressing for PZT," *Ceram. Ind.*, **82** [6] 74-77 (1964).

30. P. Sun, C.-N. Xu, M. Akiyama, and T. Watanabe, "Controlled oxygen partial pressure sintering of (Pb,La)(Zr,Ti)O$_3$ ceramics," *J. Am. Ceram. Soc.*, **82** [6] 1447-50 (1999).

31. J. -J. Choi, J. Ryu, and H. -E. Kim, "Microstructural evolution of transparent PLZT ceramics sintered in air and oxygen atmospheres," *J. Am. Ceram. Soc.*, **84** [7] 1465-69 (2001).

32. J. H. Moon and H. M. Jang, "Effects of sintering atmosphere on densification behavior and piezoelectric properties of Pb(Ni$_{1/3}$Nb$_{2/3}$)O$_3$-PbTiO$_3$-PbZrO$_3$ ceramics," *J. Am. Ceram. Soc.*, **76** [2] 549-52 (1993).

33. A. M. Scotch, H. M. Chan, and M. P. Harmer, "Abnormal grain growth in PMN-PT," in preparation (2002).

34. J. S. Wallace, J. -M. Huh, J. E. Blendell, and C. A. Handwerker, "Grain growth and twin formation in 0.74PMN-0.26PT," *J. Am. Ceram. Soc.*, **85** [6] 1581-84 (2002).

35. U. -J. Chung, J. -K. Park, H.-Y. Lee, and D. -Y. Kim, "Effect of grain coalescence on the abnormal grain growth of Pb(Mg$_{1/3}$Nb$_{2/3}$)O$_3$-35 mol% PbTiO$_3$ ceramics," *J. Am. Ceram. Soc.*, **85** [4] 965-68 (2002).

36. R. L. Coble, "Sintering of alumina: effect of atmospheres," *J. Am. Ceram. Soc.*, **45** [3] 123-27 (1962).

37. D. A. Northrop, "Vaporization of lead zirconate-lead titanate materials: II, hot-pressed compositions at near theoretical density," *J. Am. Ceram. Soc.*, **51** [7] 357-61 (1968).

38. J. Drowart, R. Colin, and G. Exteen, "Mass-spectrometric study of the vaporization of lead monoxide," *Trans. Faraday Soc.,* **61** 1376-83 (1965).

39. E. K. Kazenas and A. A. Petrov, "Thermodynamics of processes of vaporization, dissociation, and gas-phase reactions in vapors over PbO system," *Russian*

Metallurgy, [4] 17-22 (1996).

40. D. Risold, J. -I. Nagata, and R. O. Suzuki, "Thermodynamic description of the Pb-O system," *J. Phase Equilibria*, 19 [3] 213-33 (1998)

41. R. H. Lamoreaux, D. L. Hildenbrand, and L. Brewer, "High-temperature vaporization behavior of oxides II. Oxides of Be, Mg, Ca, Sr, Ba, B, Al, Ga, In, Tl, Si, Ge, Sn, Pb, Zn, Cd, and Hg," *J. Phys. Chem. Ref. Data*, 16 [3] 419-43 (1987).

42. W. Dong, "Microstructural evolution and densification of alumina in liquid phase sintering," Ph.D. dissertation, Lehigh University, Bethlehem, Pa. (2000).

43. J. Zhao and M. P. Harmer, "Effect of pore distribution on microstructure development: II, first- and second-generation pores," *J. Am. Ceram. Soc.*, 71 [7] 530-39 (1988).

44. A. M. Scotch, H. M. Chan, and M. P. Harmer, "Effect of Processing on Properties of PMN-PT single crystals," in preparation (2002).

45. A. M. Scotch, P. T. King, H. M. Chan, and M. P. Harmer, "Effect of Processing on Microstructure of PMN-PT single crystals," in preparation (2002).

46. P. W. Rehrig, G. L. Messing, and S. Trolier-McKinstry, "Templated grain growth of barium titanate single crystals," *J. Am. Ceram. Soc.*, 83 [11] 2654-60 (2000).

47. P. W. Rehrig, S. -E. Park, S. Trolier-McKinstry, G. L. Messing, B. Jones, and T. R. Shrout, "Piezoelectric properties of zirconium-doped barium titanate single crystals grown by templated grain growth," *J. Appl. Phys.*, 86 [3] 1657-61 (1999).

48. E. M. Sabolsky, A. R. James, S. Kwon, S. Trolier-McKinstry, and G. L. Messing, "Piezoelectric properties of <001> textured $Pb(Mg_{1/3}Nb_{2/3})O_3$-$PbTiO_3$ ceramics," *Appl. Phys. Lett.*, 78 [17] 2551-53 (2001).

49. J. Chen and M. P. Harmer, "Microstructure and dielectric properties of lead magnesium niobate-pyrochlore diphasic mixtures," *J. Am. Ceram. Soc.*, 73 [1] 68-73 (1990).

50. T. R. Shrout, Z. P. Chang, N. Kim, and S. Markgraf, "Dielectric behavior of single crystals near the (1-x) $Pb(Mg_{1/3}Nb_{2/3})O_3$-(x)$PbTiO_3$ morphotropic phase boundary," *Ferrelectrics Letters*, 12 63-69 (1990)

51. E. P. Gorzkowski, M. Watanabe, H. M. Chan, M. P. Harmer, "Microanalysis of PMN-35PT," unpublished work (2002).

52. E. R. Leite, A. M. Scotch, A. Khan, T. Li, H. M. Chan, M. P. Harmer, S. -F. Liu, and S. -E. Park, "Chemical heterogeneity in PMN-35PT ceramics and effects on dielectric and piezoelectric properties," accepted to *J. Am. Ceram. Soc.* (2002).

53. S. Wada, S. Suzuki, T. Noma, T. Suzuki, M. Osada, M. Kakihana, S. -E. Park, L. E. Cross, and T. R. Shrout, "Enhanced piezoelectric property of barium titanate single crystals with engineered domain configurations," *Jpn. J. Appl. Phys.*, **38** Pt. I [9b] 5505-11 (1999).

54. A. Khan, D. T. Carpenter, A. M. Scotch, H. M. Chan, and M. P. Harmer, "Electron backscatter diffraction analysis of $Pb(Mg_{1/3}Nb_{2/3})O_3$-35 mol% $PbTiO_3$ single crystals grown by seeded polycrystal conversion," *J. Mater. Res.*, **16** [3] 694-700 (2001).

55. W. D. Kingery, H. k. Bowen, and D. R. Uhlmann, Introduction to Ceramics, John Wiley & Sons, N.Y. (1976).

56. R. M. German, Liquid Phase Sintering, Plenum Press, N.Y. (1985).

57. D. J. Rockosi, "Growth from twinned and untwinned PMN-35PT single crystals," unpublished work (2002).

58. G. Gottstein, D.A. Molodov, and L.S. Shvindlerman, "Grain boundary mobility in metals: the current status," pp. 373-86 in Grain Growth in Polycrystalline Materials III: Third International Conference on Grain Growth, 1998.

59. V.J. Keast and D.B. Williams, "Grain boundary chemistry," *Current Opinion in Solid State and Materials Science*, **5** 23-30 (2001).

60. M.F. Yan and D.W. Johnson, Jr., "Impurity-induced exaggerated grain growth in Mn-Zn ferrites," *J. Am. Ceram. Soc.*, **61** [7-8] 342-49 (1978).

61. R.J. Brook, "Controlled grain growth," pp. 331-64 in Treatise on Materials Science and Technology, Vol. 9, Academic Press, N.Y. (1976).

62. M.F. Yan, R.M. Cannon, and H.K. Bowen, "Grain boundary migration in ceramics," pp. 276-307 in Ceramic Microstructures '76, Westview Press, Boulder, Colorado (1977).

63. F.J.L. Alves, "Effect of liquid phase on coarsening behavior in porous single-phase and duplex microstructures," Ph.D dissertation, Lehigh University, Bethlehem, Pa. (1997).

64. S. Ramamurthy, M.P. Mallamaci, C.M. Zimmerman, C.B. Carter, P.R. Duncombe, and T.M. Shaw, "Microstructure of polycrystalline MgO penetrated

by a silicate liquid," *J. Microscopy Society of America*, **2** [3] 113-28 (1996).

65. Y.S. Cho, D.T. Hoelzer, V.L. Burdick, and V.R.W. Amarakoon, "Grain boundaries and growth kinetics of polycrystalline ferrimagnetic oxides with chemical additives," *J. Appl. Phys.*, **85** [8] 5220-22 (1999).

66. S. J. Bennison and M. P. Harmer, "Grain growth and cavity formation in MgO-doped Al2O3," pp. 171-83 in Advances in Ceramics, Vol. 6. Character of Grain Boundaries. Edited by M. F. Yan and A. H. Heuer. American Ceramic Society, Columbus, OH (1983).

67. C. A. Sorrell, "PbO transformation induced by water," *J. Am. Ceram. Soc.*, **55** [1] 47 (1972).

68. V. V. Zyryanov, "Mechanically induced phase transformations in PbO," *Inorganic Materials*, **33** [10] 1039-45 (1997).

69. M. Senna and H. Kuno, "Polymorphic transformation of PbO by isothermal wet ball-milling," *J. Am. Ceram. Soc.*, **54** [5] 259-62 (1971).

70. W. B. White and R. Roy, "Phase relations in the system lead-oxygen," *J. Am. Ceram. Soc.*, **47** [5] 242-49 (1964).

Vita

Adam Matthew Scotch was born on June 28, 1974 to Charles Bernard and Diana Lee Scotch in Medina, Ohio. He has two older sisters, Denise and Wendy. He grew up in the small, rural town of Homerville, Ohio where his family owned and operated an RV Campground for 17 years. For all but the last two years of high school, Adam attended school in the Black River School District. After that, he went to Buckeye High School, from where he graduated. Adam first learned of Lehigh by reading Lee Iacocca's autobiography. Out of curiosity, he visited the school as a junior in high school and fell in love with Lehigh. He knew he wanted to be an engineer at an early age, but thought electrical engineering was the field to pursue. It was Arlan Benscoter who ultimately drew Adam into materials science. He was a work-study student for Arlan for all 4 years at Lehigh. After graduating with a B.S. in MS&E in 1996, Adam married the love of his life, Sara Krystene, a chemical engineer whom he met at Lehigh. Three years later, they had their first child, Aaron Charles in 1999, then Hanna Krystene in 2001. After more than six years of pursuing a Ph.D., Adam will graduate so that he can come home for supper and "eat together like a family." He will work at the National Institute of Standards and Technology in Gaithersburg, MD as an NRC post-doctoral fellow for 2 years.

4. PERSONNEL

Faculty:

Prof. Martin P. Harmer, Principal Investigator
Prof. Helen M. Chan, Co-Principal Investigator

Post-Doctoral Research Associates:

Suxing Wu

Graduate Students:

Adam M. Scotch
Edward P. Gorzkowski
Patrick T. King
Derrick J. Rockosi

5. PUBLICATIONS

1. A. Khan, D.T. Carpenter, A.M. Scotch, H.M. Chan, and M.P. Harmer, "Electron Backscatter Diffraction Analysis of PMN-35mol%PT Single Crystal Grown by Seeded Polycrystal Covnersion," *J. Mater. Res.*, **16** [3] 694-700 (2001).

2. E.R. Leite, A. Khan, A.M. Scotch, T. Li, H.M. Chan, M.P. Harmer, S.-F. Liu, and S.-E. Park, "Chemical Heterogeneity in PMN-35PT Ceramics and Effects on Dielectric and Piezoelectric Properites," to be published in *J. Am. Ceram. Soc.* (2002).

6. PRESENTATIONS

1. A. M. Scotch, "Single Crystal Ferroelectrics from Polycrystalline Precursors," IBM Graduate Student Seminar, Lehigh University, February 20, 2001.

2. M.P. Harmer, H.M. Chan, S. Wu, A.M. Scotch, E. P. Gorzkowski, P. T. King, D. J. Rockosi, " Processing and Application of Solid State Converted High Strain Undersea Transmitter Materials," DARPA/ONR Joint Review Meeting, Arlington, VA., April 10, 2001.

3. M.P. Harmer, H.M. Chan, S. Wu, A.M. Scotch, E. P. Gorzkowski, P. T. King, D. J. Rockosi, "Growth of Single Crystal Ferroelectrics by Seeded Polycrystal Conversion," AFOSR Review Meeting, Arlington, VA., April 11, 2001.

4. A.M. Scotch, E. P. Gorzkowski, P. T. King, D. J. Rockosi, S. Wu, M.P. Harmer, H.M. Chan, "Effect of Microstructural Variables on Single Crystal Growth of PMN-PT by Seeded Polycrystal Conversion," 103rd Annual Meeting of the American Ceramic Society, Indianapolis, IN, April 23, 2001.

5. (Invited) M.P. Harmer, "More Maps, Myths, and Marvels," Special Symposia in Honor of Prof. Arthur Heuer, 103rd Annual Meeting of the American Ceramic Society, Indianapolis, IN, April 23, 2001.

6. (Invited) H.M. Chan, M.P. Harmer, S. Wu, A.M. Scotch, E. P. Gorzkowski, P. T. King, D. J. Rockosi, " Growth of Single Crystal PMN-35PT Using the Solid State Conversion Technique of Seeded Polycrystal Conversion," 103rd Annual Meeting of the American Ceramic Society, Indianapolis, IN, April 23, 2001.

7. H.M. Chan, M.P. Harmer, A. Khan, S. Wu, A.M. Scotch, E. P. Gorzkowski, P. T. King, D. J. Rockosi, " Single Crystal Growth of PMN-PT by Seeded Polycrystal Conversion," U.S. Navy Meeting on Acoustic Transduction Materials and Devices, Baltimore, MD, May 15, 2001.

8. M.P. Harmer, H.M. Chan, S. Wu, A.M. Scotch, E. P. Gorzkowski, P. T. King, D. J. Rockosi, " Single Crystal Relaxor Ferroelectrics by Seeded Polycrystal Conversion," ONR PiezoCrystals Workshop, Washington, D.C., July 26, 2001.

9. E. P. Gorzkowski, A.M. Scotch, P. T. King, D. J. Rockosi, S. Wu, M.P. Harmer, H.M. Chan, "Effect of Microstructural Variables on Single Crystal Growth of PMN-PT by Seeded Polycrystal Conversion," Gordon Research Conference on Solid State Studies in Ceramics, Meriden, NH, August 12, 2001.

10. P. T. King, A.M. Scotch, E. P. Gorzkowski, D. J. Rockosi, S. Wu, M.P. Harmer, H.M. Chan, "Geometric Characterization of PMN-PT Single Crystals Grown by Seeded Polycrystal Conversion," Gordon Research Conference on Solid State Studies in Ceramics, Meriden, NH, August 12, 2001.

11. M.P. Harmer, H.M. Chan, A.M. Scotch, E. P. Gorzkowski, P. T. King, D. J. Rockosi, "Single Crystal Ferroelectrics from Polycrystalline Precursors," U.S./Japan Meeting on Dielectric and Piezoelectric Ceramics, Providence, RI, September 26-29, 2001.

12. E. P. Gorzkowski, "Effect of Liquid Phase Chemistry on Single Crystal Growth of PMN-PT by Seeded Polycrystal Conversion," IBM Graduate Student Seminar, Lehigh University, October 2, 2001.

13. E. P. Gorzkowski, H.M. Chan, and M.P. Harmer, "Effect of Liquid Phase Chemistry on Single Crystal Growth of PMN-PT by Seeded Polycrystal Conversion," 104th Annual Meeting of the American Ceramic Society, St. Louis, MO (April 2002).

14. E. P. Gorzkowski, P. T. King, A.M. Scotch, D. J. Rockosi, H.M. Chan, and M.P. Harmer, "Effect of Mircostructural Variables on Single Crystal Growth of PMN-PT by Seeded Polycrystal Conversion," 104th Annual Meeting of the American Ceramic Society, St. Louis, MO (April 2002).

15. P. T. King, H.M. Chan, and M.P. Harmer, "Effect of PbO on Growth Kinetics of {001} Oriented PMN-35PT Single Crystals Produced by Seeded Polycrystal Conversion," 104th Annual Meeting of the American Ceramic Society, St. Louis, MO (April 2002).

16. D. J. Rockosi, H.M. Chan, and M.P. Harmer, "Growth from Twinned and Untwinned Abnormal Grains of PMN-35PT in a Matrix Containing PbO Additions," 104th Annual Meeting of the American Ceramic Society, St. Louis, MO (April 2002).

17. (Invited) H.M. Chan, M.P. Harmer, E. P. Gorzkowski, P. T. King, D. J. Rockosi, A. M. Scotch, "Critical Issues in Single Crystal Growth of PMN-PT by Seeded Polycrystal Conversion," IFFF 2002: International Joint Conference on the Applications of Ferroelectrics, May 29, 2002

18. H.M. Chan, M.P. Harmer, E. P. Gorzkowski, P. T. King, D. J. Rockosi, A. M. Scotch "Microstructural Analysis of PMN-PT Single Crystals Grown by Seeded Polycrystal Conversion," U.S. Navy Meeting on Acoustic Transduction Materials and Devices, Baltimore, MD, May 14, 2002.

19. E. P. Gorzkowski, P. T. King, A.M. Scotch, D. J. Rockosi, M.P. Harmer, and H.M. Chan, "Effects of Interfacial Chemistry on Single Crystal Growth of PMN-PT," Gordon Research Conference on Solid State Studies in Ceramics, Meriden, NH, August 2002.

20. D. J. Rockosi, E. P. Gorzkowski, P. T. King, A.M. Scotch, M.P. Harmer, and H.M. Chan, "Growth from Twinned and Untwinned Abnormal Grains of PMN-35PT in a Matrix Containing PbO Additions," Gordon Research Conference on Solid State Studies in Ceramics, Meriden, NH, August 2002.

21. M.P. Harmer, H.M. Chan, A. M. Scotch, E. P. Gorzkowski, P. T. King, and D. J. Rockosi, "Single Crystal Ferroelectrics from Polycrystalline Precursors," PiezoCrystals Workshop Washington DC, January 29, 2003

22. E. P. Gorzkowski, A.M. Scotch, M. P. Harmer, and H. M. Chan, "Critical Microstructural Variables of Seeded Polycrystal Conversion of PMN-PT," 105th Annual Meeting of the American Ceramic Society, Nashville, TN (April 2003).

23. D. J. Rockosi, H.M. Chan, and M.P. Harmer, "Abnormal Grain Growth of $PbMg_{1/3}Nb_{2/3}O_3$-35PbTiO$_3$ with Excess PbO," 105th Annual Meeting of the American Ceramic Society, Nashville, TN (April 2003).

7. HONORS/AWARDS

1. P. T. King, 1st Place in Undergraduate Category in the Ceramographic Competition at the 103rd Annual Meeting of the American Ceramic Society, Indianapolis, IN, April 23, 2001.

2. D. J. Rockosi, 3rd Place in Undergraduate Category in the Ceramographic Competition at the 103rd Annual Meeting of the American Ceramic Society, Indianapolis, IN, April 23, 2001.

3. E. P. Gorzkowski and A. M. Scotch, 1st Place in the Graduate Student Poster Contest at the 103rd Annual Meeting of the American Ceramic Society, Indianapolis, IN, April 23, 2001.

4. E. P. Gorzkowski, 1st Place in Microanalysis Category in the Ceramographic Competition at the 104th Annual Meeting of the American Ceramic Society, St. Louis, MO, April, 2002.

5. E. P. Gorzkowski , 3rd Place in the Graduate Student Poster Contest at the Gordon Research Conference, Meriden, NH, August, 2002.

6. E. P. Gorzkowski, 1st Place in Light Optical Microscopy Category in the Ceramographic Competition at the 105th Annual Meeting of the American Ceramic Society, Nashville, TN, April, 2003.

7. D. J. Rockosi, 2nd Place in Combined Techniques Category in the Ceramographic Competition at the 105th Annual Meeting of the American Ceramic Society, Nashville, TN, April, 2003.